GEOLOGICA ULTRAIECTINA

Mededelingen van de
Faculteit Aardwetenschappen der
Rijksuniversiteit te Utrecht

No. 105

DYNAMICS OF LITHOSPHERIC EXTENSION: A MODELING STUDY

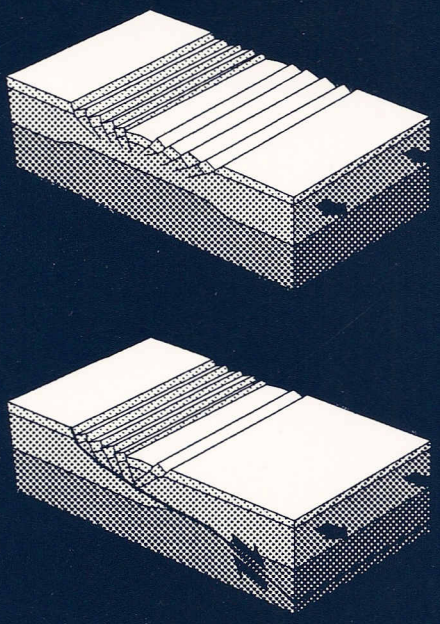

ROB GOVERS

GEOLOGICA ULTRAIECTINA

Mededelingen van de
Faculteit Aardwetenschappen der
Rijksuniversiteit te Utrecht

No. 105

DYNAMICS OF LITHOSPHERIC EXTENSION: A MODELING STUDY

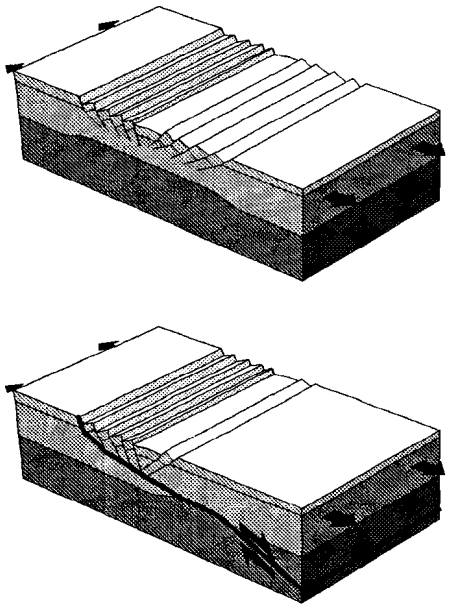

ROB GOVERS

CIP-GEGEVENS KONINKLIJKE BIBLIOTHEEK, DEN HAAG

Govers, Robertus Mathias Adolphus
Dynamics of lithospheric extension: a modeling study /
Robertus Mathias Adolphus Govers. - Utrecht: Faculteit Aardwetenschappen der
Rijksuniversiteit Utrecht. - (Geologica Ultraiectina, ISSN 0072-1026; no. 105)
Proefschrift Rijksuniversiteit Utrecht. - Met lit. opg. - Met samenvatting
in het Nederlands.
ISBN 90-71577-57-0
Trefw.: aardkorst/tektoniek/geofysica.

Dynamics of lithospheric extension: a modeling study

De dynamica van lithosfeer-extensie:
een modelstudie

(met een samenvatting in het Nederlands)

PROEFSCHRIFT

TER VERKRIJGING VAN DE GRAAD VAN DOCTOR
AAN DE RIJKSUNIVERSITEIT TE UTRECHT,
OP GEZAG VAN DE RECTOR MAGNIFICUS PROF. DR J.A. VAN GINKEL,
INGEVOLGE HET BESLUIT VAN HET COLLEGE VAN DEKANEN
IN HET OPENBAAR TE VERDEDIGEN OP
WOENSDAG 26 MEI 1993 DES NAMIDDAGS TE 12.45 UUR

DOOR

ROBERTUS MATHIAS ADOLPHUS GOVERS

GEBOREN OP 10 JUNI 1961 TE TILBURG

PROMOTOR: PROF. DR M.J.R. WORTEL
PROMOTOR: PROF. DR N.J. VLAAR

The research described in this thesis was carried out at the:

Department of Geophysics
Institute of Earth Sciences
Utrecht University
Budapestlaan 4
3584 CD Utrecht
The Netherlands

Contents

Chapter 1

Chapter 2

Chapter 3

Chapter 4

Chapter 5

Chapter 6

Chapter 7

Chapter 8

Chapter 1

Introduction

The theory of plate tectonics gives a good first order description of the kinematics of the outer shell of the earth. Massive amounts of evidence show that this shell consists of large rigid plates moving with relative velocities which are accommodated along plate boundaries. After the concept of plate tectonics had generally been accepted in the late sixties, it was recognized that the plates are not completely rigid and that intraplate deformation was an important second order deviation from the original plate tectonics theory. Attempts were made to make a smaller subdivision of rigid domains ("microplates"), but apart from giving a better fit to surface velocity data, little insight was gained from this. Deformation of the plates is an important ingredient of a continuously changing face of the earth.

Internal deformation occurs predominantly within continental parts of the plates. Oceanic lithosphere exhibits a more rigid behavior with deformation localized along its plate boundaries. Thickening and mountain building associated with colliding oceanic and continental plates typically occurs on the continental side of the subduction zone, not on the oceanic side. Extension and rift formation is mostly confined to continental lithosphere. The Rhine Graben, the East African Rift Zone and the North Sea are well-known examples of extended regions in interior parts of the continental lithosphere. Basins on the continental side of plate boundaries are, for instance, the Aegean Sea and the Basin and Range Province.

This thesis focuses on extension of continental lithosphere. In the geological history, oceanic ridges have been subducted or have become inactive. For a continued operation of plate tectonics new ridges were necessary. Typically, oceanic ridges form by spreading and breakup of continental lithosphere. Extension does not necessarily lead to continental breakup; many sedimentary basins on the continental lithosphere have been formed as a result of subsidence after extension. The economic importance of sedimentary basins is enormous; most of the hydrocarbon reserves are located within sedimentary basins. Understanding the mechanisms of continental extension therefore has both scientific and economic significance.

KINEMATICS OF EXTENSION

Extension and sedimentary basin formation is accompanied by vertical surface movements. Historically, it was this aspect of sedimentary basins that was actively studied and for which explanations were sought. A typical Neptunian theory of the seventeenth century was proposed by Steno (1669), who suggested that karst formation processes were the cause of vertical movements. Hutton (1788) established the operation of the sedimentary cycle and, after introduction of the concept of isostasy (Airy, 1855; Pratt, 1855) it was recognized that thermal processes and density changes associated with phase changes (e.g. Bowie, 1927) might well produce vertical movements on the order of kilometers, and depressions where sediments could be deposited in. The first significant study in the modern plate tectonics era in this respect was done by Sleep (1971), who incorporated the thermal decay with time of basin subsidence. Sleep proposed that erosion of a thermally uplifted bulge was the cause of subsequent basin formation. The weak point of this model was a lack of observations in support of massive erosion before subsidence. A very important study was that of Şengör and Burke (1978), who recognized two end-members of rifting: "active" rifting, in which rifting is a result of mantle convection, and "passive" rifting, in which rifting is a response to intraplate stresses resulting from plate boundary processes. A feature common to most rifts is volcanism, and Şengör and Burke (1978) identified the expected sequence of events for active rifting as doming-volcanism-rifting, and as rifting-volcanism for passive rifting. They concluded that, at present, passive rifting is "by far more widespread" than active rifting.

McKenzie (1978) published "some remarks on the development of sedimentary basins". In his model he investigated the thermal and subsidence evolution of lithosphere that had been uniformly thinned (Figure 1). Thinning is assumed to occur by pure shear (i.e. coaxial deformation), and the model has become known as the "pure shear model" or "stretching model". With his pure shear model, McKenzie did not propose a physical mechanism for continental extension, but a description of a geometry that did explain observations of heat flow and subsidence data in many sedimentary basins. On the basis of geological observations in the Basin and Range Province, Wernicke (1981) proposed that extension of continental lithosphere occurs on a single, gently dipping, lithosphere-cutting fault[1] (Figure 2). Thinning occurs by simple shear along a fault with a normal sense of movement, and this model is often referred to as the "normal simple shear model" or "simple

1. I will use the term "fault" in a very loose way as a zone in which deformation is localized to some extent. In this definition, deformation may occur by both brittle and by ductile processes.

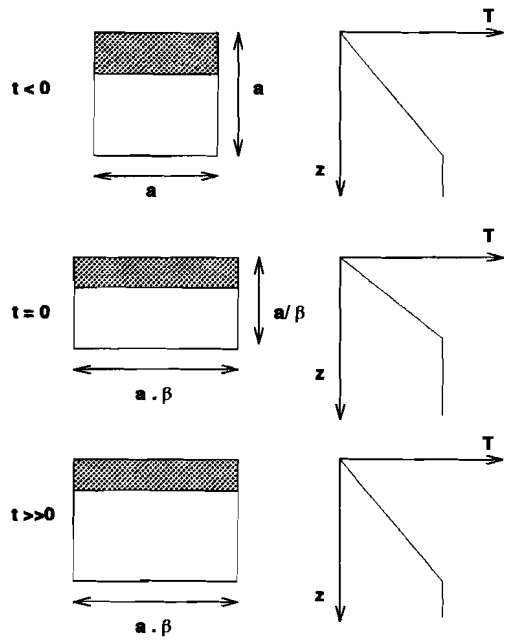

Fig. 1. *The pure shear model, or stretching model (McKenzie, 1978a). At* $t = 0$*, continental lithosphere is extended by a factor* β*. Initially, the lithosphere was in thermal equilibrium, but after stretching the geotherm has advected. Subsequent cooling is put forward as an explanation of the thermal subsidence observed in sedimentary basins.*

shear model". Like the pure shear model, the simple shear model has a descriptive nature and is not a mechanism of extension. Before turning to dynamical models and mechanisms of continental extension, the pure shear and simple shear model will be described more extensively, together with the observations in support of each of the models. We will discuss the results from studies that aimed at discriminating pure shear from simple shear models on the basis of observations.

Pure shear model

The pure shear model was originally proposed by Artemjev and Artyushkov (1971) for the Baikal Rift (see also Salveson, 1978). McKenzie's (1978) extension of the model reconciled observations of post-rifting thermal decay with its tectonic origin. In his model, McKenzie quantitatively explained the subsidence and heat flow following a tectonic phase of instantaneous and uniform thinning. Given the conceptual simplicity of the pure shear model and its good fit to observations of subsidence and heat flow, the model has become very popular (Sclater and Christie,

1980; Le Pichon and Sibuet, 1981; Barton and Wood, 1984; and numerous other papers).

Subsequent studies have investigated the sensitivity of the results to various model assumptions. For instance, Jarvis and McKenzie (1980) focused on the effects of finite stretching rates. They concluded that the instantaneous stretching is a good approximation if the extension phase lasts less than 20 Ma (million years). Issler and Beaumont (1987) investigated the thermal blanketing effect of the sedimentary basin fill. The essentially one-dimensional stretching model was generalized to two dimensions, to investigate the effects of lateral heat conduction (Steckler, 1981; Cochran, 1983; Alvarez *et al.*, 1984) from beneath the basin center to the colder flanks. Lateral heat conduction was put forward as an explanation for the often very impressive rift shoulders that flank major rift zones. Other mechanisms to explain the flank uplifts associated with lithospheric extension were proposed; magma intrusions (McKenzie, 1984), secondary convection (Steckler, 1985; Keen, 1985; Buck, 1986; Moretti and Froidevaux, 1986) and erosion (Garfunkel, 1988). A simple physical explanation for rift shoulder uplifts was given by Braun and Beaumont (1989c), who do not assume, like in the original stretching model, that syn-tectonic uplifts are completely locally compensated. They showed that the lithosphere retains some flexural strength during rifting and rift flank uplifts are caused by residual buoyancy forces.

Simple shear model

Wernicke (1981) proposed that crustal extension in the Basin and Range Province of the western United States is predominantly accommodated along one, or a few, gently dipping normal faults. These detachment faults penetrate the continental crust and "perhaps the mantle". Lithospheric extension accommodated along a gently dipping fault provides a simple mechanism to exhume lower crustal rocks which are observed in metamorphic core complexes. In metamorphic core complexes, lower crustal rocks have been dragged from beneath extended upper crustal rocks along gently dipping normal faults of large areal extent (Crittenden *et al.*, 1980). The pertinent observations which form the basis of the simple shear model are; (1) slip along dominant faults is of normal type, indicating that they accommodate extension, (2) lower block rocks are largely undeformed and (3) very large amounts of fault slip have been accommodated. Reflection profiling data in the Sevier Desert area (Utah, Western United States) (Allmendinger *et al.*, 1983; see also Allmendinger *et al.*, 1987) show a single, gently dipping reflector that can be traced to a depth of 12 to 15 km. Normal offsets along the interpreted fault are about 30 to 60 km. A last argument in favor of the simple shear model is (4) the observation of pronounced asymmetries in half-graben complexes.

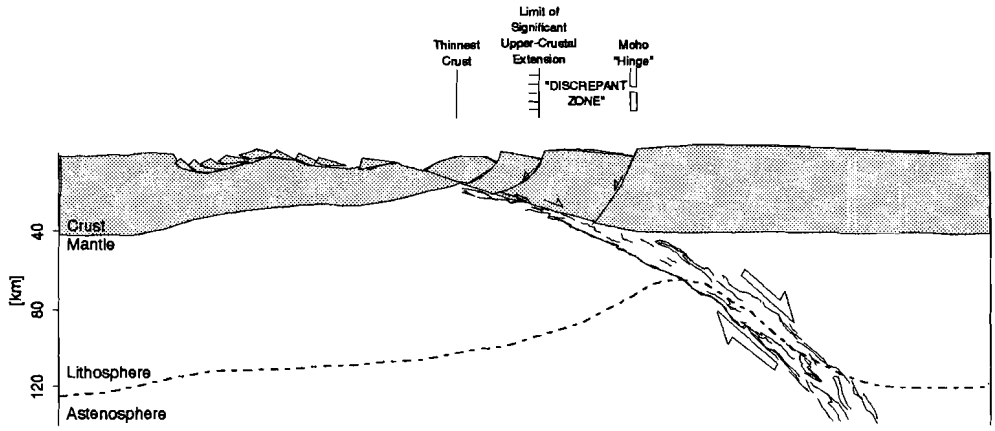

Fig. 2. *The normal simple shear model, or detachment model (Wernicke, 1985).*

Wernicke (1985) introduced the concept of "discrepant zones" (Figure 2) to shed light onto the downward continuation of crustal detachments into the mantle. By comparing Moho depths obtained from seismic and gravity data with surface observations of extension, Wernicke noted that, in the Basin and Range, there is a horizontal offset (a discrepant zone) between the point of onset of Moho uplift and the location where significant crustal thinning starts. Discrepant zones in the Basin and Range can be up to 100 km wide and are an important indication for mantle thinning that is laterally offset from crustal thinning as a result of a whole lithosphere-cutting fault. Wernicke (1985) proposed that the asymmetric uplift pattern in the Basin and Range Province and the Red Sea rift zone, and the occurrence of volcanism on only one side of the Red Sea rift are caused by a lithosphere-cutting detachment fault.

The simple shear model has been applied in many sedimentary basins and at passive continental margins. Beach (1986) proposed that extension in the North Sea Basin is accommodated along a major detachment. In the Aegean Sea, Lister *et al.* (1984) find geological evidence in support of the detachment model. Many of the structural features of passive continental margins could be explained in terms of a simple shear model by Lister *et al.* (1986).

From a study in actively extending regions, Jackson (1987) concluded that fault planes that dip less than 30^o are seismically inactive in most cases. This observation was confirmed by a regional seismicity study in the Basin and Range Province by Arabasz and Julander (1986). Apparently, these observations are inconsistent with the simple shear model, which requires significant extension along gently dipping faults. One solution is that the fault plane rotates during extension (Jackson,

1987; Wernicke and Axen, 1988) and becomes inactive. Wernicke and Axen (1988) noted, however, that there is evidence for gently dipping faults which are still active. On the basis of paleomagnetic data, Livaccari *et al.* (1993) showed that footwall blocks which are now exposed in metamorphic core complexes in the Basin and Range Province, did not undergo significant amounts of tilting. They concluded that the master detachment fault was active as a low-angle extensional structure. Another, yet simpler solution is that detachment faults are very weak features. Given the large amount of strain that is accommodated along detachment faults, strain softening processes are very likely to occur.

Mixed models

One of the major assumptions in McKenzie's (1978) pure shear model, that the strain during extension and rifting is uniform with depth, was questioned immediately after the model was proposed. Sclater and Christie (1980) and Royden and Keen (1980) found evidence that crustal extension and initial subsidence are much less than that predicted by the pure shear model on the basis of thermal subsidence. In other words, the thermal subsidence is greater than that predicted from the observed crustal extension. To account for these observations, a two-layer model was proposed with less crustal thinning than mantle thinning. Differential thinning of crust and mantle would be accommodated by slip along the Moho, which was presumed to be the brittle-ductile transition (Royden and Keen, 1980; Hellinger and Sclater, 1983; Rowley and Sahagian, 1986; Gans, 1987).

In concert with Kusznir and Mathews (1988), Kusznir and Egan (1989) argued that no seismic reflection study establishes a fault which unequivocally passes continuously into the mantle. Therefore, they investigated the uplift and sedimentation signals of a continental extension model in which the crust deforms by simple shear along a fault and by pure shear in the ductile mantle (see also Lister and Davis, 1989).

The simple shear model of Wernicke (1981) and the pure shear model of McKenzie (1978) represent end-members on a scale of shear localization; in the simple shear model the strain is completely localized along a lithosphere-cutting fault, in the pure shear model the strain is completely uniform with depth. The multiple layer stretching models and mixed simple/pure shear models are intermediate derivatives.

Discrimination studies

After the pure shear model and the simple shear model had been proposed, workers started to classify specific basins as due to either pure shear or to simple shear. For instance, Beach (1986) concluded from seismic reflection data that the dominant mode of extension in the North Sea Basin is simple shear. Barton and Wood (1984) explained the subsidence data in the North Sea Basin in terms of the pure shear model. Furlong and Londe (1986) were amongst the first to recognize the need for data on the basis of which the two models could be discriminated. They investigated the thermal, gravity and uplift consequences of both pure and simple shear models, to find that, more than 15 Ma after an extension phase, none of these geophysical signals are sufficiently different to be useful as a discriminating tool (see also, Kusznir *et al.*, 1987; Buck *et al.*, 1988; Voorhoeve and Houseman, 1988; Wang *et al.*, 1989; White, 1989). The work of Ruppel *et al.* (1988) and Issler *et al.* (1989) indicated that P-T-*t* data, sedimentary data and fission track data might be used to discriminate between basin forming mechanisms in older basins. In younger basins, surface uplift, heat flow and maturation data could be useful.

An integral part of extension is that rocks are brought to shallower depths and, if the ascent is rapid enough, may (partially) melt as a result of decompression. Volcanism and magmatic activity are therefore associated with most extended terrains. Buck *et al.* (1988) concluded that the simple shear model is less efficient at generating melts than the pure shear model. The reason for this discrepancy is that in the pure shear model, rocks rise with higher vertical velocities than in the simple shear model at an equivalent extension rate. Latin and White (1990) quantitatively investigated adiabatic decompression melting in both the simple shear and the pure shear model. Based upon compiled, experimental batch-melting results (McKenzie and Bickle, 1988; Furlong and Fountain, 1986), their calculations indicated that it is very difficult to reconcile the observed amount and composition of magma in the North Sea with a simple shear mechanism. Also, the location of magmatic activity was concluded to disagree with a detachment model origin.

PHYSICAL MECHANISMS OF EXTENSION

The first study that addressed the dynamical characteristics of extension models was done by England (1983) (see also the modification to England's model proposed by Sawyer (1985)). A one-dimensional uniform stretching model was used to quantify the forces required to initiate and maintain extension. In order to relate strains to stresses and forces, a rheology had to be assumed in these studies (as well as in any other dynamical model). Sawyer (1985) concluded that extension is hardly ever self-limiting and that all reasonable extension rates can lead to oceanization.

These studies have been very significant in that they established the idea that extension and rifting are not necessarily preceded by a thermal pulse or any other process that considerably reduces the lithospheric strength, in accordance with the findings of Şengör and Burke (1978). Force modeling studies (Richter and McKenzie, 1978; Lister, 1975) and subsequent stress modeling (Wortel and Cloetingh, 1981; Cloetingh and Wortel, 1985) had shown that stresses of hundreds of MPa's are possible in the lithosphere. In chapter 2 of this thesis it will be shown that large magnitude stresses in oceanic plates are consistent with observations of seismicity. Driving forces for continental extension are therefore, in principle, available from lithospheric processes alone. This result is very important in subsequent chapters of this thesis, when quantitative models of continental extension are investigated. The results from chapter 2 put upper limits on the magnitude of in-plane force boundary conditions that are applied in later chapters.

It has long been recognized (e.g. Love, 1911; Artyushkov, 1973; Fleitout and Froidevaux, 1982) that thickened continental crust, although in isostatic equilibrium, is not in mechanical equilibrium, in that it is in a state of tension. Observations of normal faulting in highly (>3 km) elevated mountain belts (e.g. Dewey, 1988; Mercier *et al.*, 1987) support this argument. Potential energy increase as a mechanism for subsequent extension has been suggested for the Altiplano in the Andes (Dewey, 1988), for the Tibetan Plateau (England and McKenzie, 1982; Mercier *et al.*, 1987), the Aegean Sea in the Mediterranean (McKenzie, 1972; Berckhemer, 1977; Le Pichon, 1983) and for the Basin and Range Province in the western United States (Coney, 1987; Wernicke *et al.*, 1987; Sonder *et al.*, 1987). Houseman and England (1986) presented a quantitative analysis of the effect of variations of the normal stress, associated with hot rising jets or sheets in the sub-lithospheric mantle, which acts on the base of continental lithosphere. Their two-dimensional model predicts instantaneous extension in the lithosphere as a result of impinging buoyant plumes. The potential energy increase of lithosphere that is uplifted by the mantle plumes drives extension. Another source for a potential energy increase and subsequent extension was suggested by McKenzie (1978b), who proposed that (parts of) the mantle may detach from the lithosphere during thickening, and sink into the hotter, less dense asthenosphere. Supporting evidence for this mechanism was found by Houseman *et al.* (1981) from numerical convection experiments. Sonder *et al.* (1987) and Braun and Beaumont (1989b) quantitatively modeled post-detachment uplift and subsequent extension to explain observations of a time lag (Wernicke *et al.*, 1987) between the end of continental thickening and the onset of significant extension in the Basin and Range Province.

Mechanisms controling the style of continental extension

A realistic assessment of the physical conditions which determine whether continental extension will occur by pure shear or by simple shear is made in very few papers in the contemporary literature. Away from plate boundaries, total strain rates tend to be uniform with depth (Kusznir and Bott, 1977; chapter 3). It is shown in chapter 3 of this thesis that this result is not sensitive to the distribution with depth of plate boundary end loads. In other words, in the absence of significant mechanical heterogeneities, the normal mode of intraplate deformation as a result of in-plane forces is pure shear.

Straightforward application of concepts from rock mechanics suggests that faults initiate in steeply dipping orientations in lithosphere in in-plane tension. This inference clearly disagrees with the observed low angle dip of detachments in extensional terrains. The suggestion that these faults would form at steeper dips and subsequently rotate during extension (Jackson, 1987) is consistent with rock mechanical arguments. However, the metamorphic grade of exhumed lower block rocks is relatively constant in the Basin and Range, and precludes a steep origin of detachment faults (Lister and Davis, 1989). Also, on the basis of paleomagnetic data, Livaccari *et al.* (1993) showed that denudated footwall blocks in the Basin and Range Province did not tilt by significant amounts. Given the evidence in support of (at least) crustal scale asymmetric extension, the natural question which arises is how extension according to the simple shear model is physically possible. It is the subject of this thesis to identify the physical conditions under which asymmetric behavior might be promoted.

Initiation of lithosphere-scale faults

Previous studies (Yin, 1987; Yin, 1989; Spencer and Chase, 1989) showed that stress trajectories in elastic bodies that are subject to combinations of stress boundary conditions, are consistent with the low-angle nature of detachment faults. Their choice for an elastic rheology was motivated by the large stresses that can be supported near brittle-ductile transitions. For a more realistic rheology, it can be expected that the upper crust, lower crust and mantle are decoupled by weak zones to some degree at specific geothermal gradients. In these cases, the results of Yin (1987; 1989) and Spencer and Chase (1989) can be interpreted to apply to these layers individually. However, the relevance of their models in the context of whole-lithosphere deformation is more difficult to determine.

In an equally simplified rheological model, Melosh (1990) showed that principal stress trajectories flatten out in a low-viscosity layer beneath a strong layer containing a (steeply dipping) normal fault. He argued that Yin (1989) and Spencer and

Chase (1989) need to invoke boundary conditions that derive from hidden sources, but in his model, Melosh (1990) invokes a disputable end load; basically, he assumes that the upper and lower crust ride along on an extending upper mantle. It is therefore clear from the onset that shear between crust and mantle is required.

One mechanism for initiation of lithosphere scale asymmetric behavior would be that the lithospheric mantle and crust would boudinage during stretching (Martinod and Davy, 1992). Thinned zones in the crust and mantle would be horizontally offset and link up into dipping zones of localized deformation. In chapter 4, this mechanism is investigated in the context of continental lithosphere that is thermally and mechanically close to equilibrium. Another mechanism for initiating lithosphere scale asymmetries, which is studied in chapter 4, is a dramatic viscosity decrease as a result of strain weakening. It is concluded that neither mechanism will lead to strain localization and initiation of lithosphere scale detachment faults in continental lithosphere that is thermally and mechanically close to equilibrium.

Pre-existing weak zones

It has been argued by various authors (e.g., Wilson, 1966; McConnell, 1972; Sykes, 1978; White *et al.*, 1986; Wernicke and Tilke, 1989) that once lithosphere-scale faults or weak zones have been established, they will be re-activated in subsequent tectonic phases. Most continental breaks tend to follow pre-existing weak trends, like suture zones and young orogenic belts. Older and stronger cratons are mostly unaffected by orogenic phases. Wilson (1966) noted that the Iapetus-Atlantic Ocean closed and subsequently opened along approximately the same suture line. The current pattern of rifting in East Africa follows Pre-Cambrian mobile belts (McConnell, 1972). In the Basin and Range Province it has been found that successive detachments which are observed at the surface, branch off from a master detachment fault at depth (Lister and Davis, 1989). This observation suggests that a gently dipping detachment fault, rooted in strong parts of the continental crust, controls the evolution of the extending crust. This is consistent with the view that major faults splay to the surface from dislocations in strong levels of the lithosphere. More generally, in case of lithosphere-scale simple shear deformation, a low angle fault rooted in the strongest part of the lithosphere directly beneath the Moho, is considered likely to initiate an asymmetric mode of deformation. Wernicke and Tilke (1989) noted that "Once a structural asymmetry is established in the initial phase of rifting, it seems likely that it is expressed in some way throughout the extensional history of the system". Braun and Beaumont (1989a) and Dunbar and Sawyer (1989) investigated the style of extension in continental lithosphere containing offset pre-existing weakness zones in the crust and mantle. They concluded that the weak lower crust may act as a level of décollement between crust

and mantle, along which horizontally offset mantle and crustal weaknesses may link up.

Pre-existing weaknesses, whether related to earlier faults or perhaps to lithological heterogeneity, might indeed control the initiation of detachment faults. However, there is no evidence that this is always so; in regions where evidence exists for asymmetric extension, there is not always evidence for initiation along pre-existing weaknesses. Also, an explanation of detachment faults in terms of pre-existing weaknesses disregards the possible relation between a pre-extension thickening period and subsequent asymmetric extension, as was suggested by Coney (1987) for the Basin and Range Province. A similar relation might exist between thickening related to the Alpine closing of the Tethys Sea and subsequent asymmetric extension in the Aegean Sea of Greece (Lee and Lister, 1992). The work presented in chapters 4, 5, 6 and 7 focuses on the initial stages of continental extension, when the conditions for subsequent symmetric or asymmetric behavior are created. Rather than investigating the effects of pre-existing weaknesses, I investigate the influence of various tectonic scenarios on the evolution of continental lithosphere not containing large scale defects or lateral inhomogeneities. In chapter 5, I investigate whether continental collision, magma intrusions and mantle-lithosphere interaction generate conditions which lead to initiation of lithosphere scale faults. It is concluded that continental thickening and delamination of lithospheric mantle create conditions that are favorable for subsequent asymmetric extension on zones of localized deformation in some cases. Chapter 6 presents a more detailed evaluation of the physical mechanisms underlying asymmetric extension following a collision phase. In this chapter, parameters are identified that control the style of continental extension. In the last chapter, chapter 7, delamination of continental mantle is investigated as a mechanism for subsequent extension in greater detail than was possible in chapter 5.

FORWARD MODELING

The work presented in chapters 3, 4, 5, 6 and 7 is based upon numerical models that predict the evolution of the continental lithosphere from assumed initial and boundary conditions. These physical models[2] make predictions of data (e.g. surface uplift, heat flow) instead of starting with observations to match some model to, i.e. instead of "inverting" data. The significance of investigating physical models is not

2. In the literature, the term "physical model" is typically used for experiments on scale models of earth processes, e.g. sandbox models. I use the term "physical models" in a more general sense for describing both numerical and "real world" models that are used to simulate some physical process.

always clearly understood. The classical approach in earth sciences has been to do observations, sometimes followed by construction of a conceptual model. This approach to understanding the processes that have created and modified the earth to its present day state, is not typical to earth sciences. Specific to earth sciences, however, is the lack of data which are relevant for understanding even the most basic processes. For instance, understanding the driving forces of plate tectonics has been a hot topic since this theory was postulated.

Data are incomplete as a result of the difficulty to do observations at depth and in the past. Some physical quantities, as measured at the earth surface, cannot uniquely be inverted to physical properties at depth. For example, gravity data can not uniquely be converted to density distributions in the earth. Even worse is that some quantities cannot be measured at all, in that they do not generate signals that can be observed at the earth surface. The grain size of a rock in situ, for instance, is an important rheological parameter that cannot be measured from the surface.

The present day state of the earth is the result of the evolution of a system with a memory. Observations from which the physical state of the earth can be deciphered are therefore crucial for our understanding of processes occurring in the earth. The second law of thermodynamics implies that all natural processes are dissipative and irreversible. Overprinting processes obscure the data and the past state of the earth cannot be uniquely be determined from them.

This problem of data obviously is reflected in conceptual models that are constructed from the data. The more incomplete the data, the more models can be constructed from them (non-uniqueness). The fact that both the simple shear model and the pure shear model have been used to describe the strain beneath the North Sea Basin is a fine example of non-uniqueness. Physical modeling is an important tool for accepting or rejecting particular conceptual models; through physical models, it can be tested whether a conceptual model is physically plausible. As a result of the strong temperature dependence of the rheology of continental rocks, the response of the lithosphere system to driving forces is very complicated. Only through studies of physical models it is possible to get insight into processes which are the cause of particular observations.

A field geologist might not easily agree with my previous statement on the lack of sufficient data, as he is confronted with enormous amounts of data available in exposed rocks. A geological map resulting from field observations is, by necessity, a selection and summary of available data (and therefore a conceptual model). Separating important observations from observations of secondary importance is a difficult and time-consuming task. A prime goal of physical models is that they provide realistic cartoons of lithospheric evolution, which can be discriminated on the basis of particular types of data. For instance, uplift rates of a mantle delamination

model probably are very different from uplift rates associated with continental collision. As the surface heat flow signal (at least initially) is very similar in these two cases, there is more sense in trying to extract uplift rates from, for instance, sedimentary data than to measure the surface heat flow. Likewise, physical models may guide the field geologist in judging the importance of a particular observation and even draw his attention to types of data he did not consider before.

Physical models can be used to simulate experiments which cannot be done in the laboratory; first, because numerical models may span millions of years on human life timescales and second, because physical conditions can be simulated that are not achievable in the laboratory. Knowledge from different disciplines is integrated into a physical model and the model results are predictions of observations which are relevant for these disciplines. For instance, ideas about sediment transport may be integrated with notions of the rheology of continental rocks to predict infill patterns of sedimentary basins forming over an extending lithosphere.

REFERENCES

Airy, G.B., On the computation of the effect of the attraction of mountain-masses, as disturbing the apparent astronomical latitude of stations in geodetic surveys, *Phil. Trans., 145,* 101-104, 1855.

Allmendinger, R.W., J.W. Sharp, D. Von Tish, L. Serpa, S. Kaufman, J. Oliver, and R.B. Smith, Cenozoic and Mesozoic structure of the eastern Basin and Range Province, Utah, from COCORP seismic reflection data, *Geology, 11,* 532-536, 1983.

Allmendinger, R.W., T.A. Hauge, E.C. Hauser, C.J. Potter, S.L. Klemperer, K.D. Nelson, P. Knuepfer, and J. Oliver, Overview of the COCORP 40 °N Transect, Western United-States: the fabric of an orogenic belt, *Geol. Soc. Am. Bull., 98,* 308-319, 1987.

Alvarez, F., J. Virieux, and X. Le Pichon, Thermal consequence of lithosphere extension over continental margins: the initial stretching phase, *Geophys. J. R. astron. Soc., 78,* 389-411, 1984.

Arabasz, W.J., and D.R. Julander, Geometry of seismically active faults and crustal deformation within the Basin and Range-Colorado Plateau transition in Utah, *Geol. Soc. Am. Bull., 208,* 43-74, 1986.

Artemjev, M.E., and E.V. Artyushkov, Structure and isostasy of the Baikal rift and the mechanism of rifting, *J. Geophys. Res., 76,* 1,197-1,211, 1971.

Artyushkov, E.V., Stresses in the lithosphere caused by crustal thickness inhomogeneities, *J. Geophys. Res., 78,* 7,675-7,708, 1973.

Barton, P., and R. Wood, Tectonic evolution of the North Sea basin: crustal stretching and subsidence, *Geophys. J. R. astron. Soc., 79,* 987-1,022, 1984.

Beach, A., A deep seismic reflection profile across the northern North Sea, *Nature, 232,* 53-55, 1986.

Berckhemer, H., Some aspects of the evolution of marginal seas deduced from observations in the Aegean region, in *International symposium on the structural history of the Mediterranean basins, Split (Yugoslavia),* edited by B. Biju-Duval and L. Montadert, pp.

303-313, Technip, Paris, 1977.
Bowie, W., *Isostasy*, 275 pp., E.P. Dutton and Company, New York, 1927.
Braun, J., and C. Beaumont, Dynamical models of the role of crustal shear zones in asymmetric continental extension, *Earth Planet. Sci. Lett., 93*, 405-423, 1989a.
Braun, J., and C. Beaumont, Contrasting styles of lithospheric extension: implications for differences between Basin and Range Province and rifted continental margins, in *Extensional tectonics and stratigraphy of the North Atlantic Margins*, edited by A.J. Tankard and H.R. Balkwill, pp. 53-79, Am. Ass. Petr. Geol. Mem. 46, 1989b.
Braun, J., and C. Beaumont, A physical explanation of the relation between flank uplifts and the breakup unconformity at rifted continental margins, *Geology, 17*, 760-764, 1989c.
Buck, W.R., Small-scale convection induced by passive rifting: the case for uplift of rift shoulders, *Earth Planet. Sci. Lett., 77*, 362-372, 1986.
Buck, W.R., F. Martinez, M.S. Steckler, and J.R. Cochran, Thermal consequences of lithospheric extension: pure and simple, *Tectonics, 7*, 213-234, 1988.
Cloetingh, S.A.P.L., and M.J.R. Wortel, Regional stress field of the Indian plate, *Geophys. Res. Lett., 12*, 77-80, 1985.
Cochran, J.R., Effects of finite rifting times on the development of sedimentary basins, *Earth Planet. Sci. Lett., 66*, 289-302, 1983.
Coney, P.J., The regional tectonic setting and possible causes of Cenozoic extension in the North Americal Cordillera, in *Continental extensional tectonics, 28*, edited by M.P. Coward, J.F. Dewey and P.L. Hancock, pp. 177-186, Geological Society of London Special Publication, 1987.
Crittenden, M.D., P.J. Coney, and G.H. Davis (eds.), *Tectonic significance of metamorphic core complexes of the North American Cordillera*, Mem. Geol. Soc. Am., 153, 1980.
Dewey, J.F., Extensional collapse of orogens, *Tectonics, 7*, 1,123-1,139, 1988.
Dunbar, J.A., and D.S. Sawyer, How preexisting weaknesses control the style of continental breakup, *J. Geophys. Res., 94*, 7,278-7,292, 1989.
England, P.C., Constraints on extension of continental lithosphere, *J. Geophys. Res., 88*, 1,145-1,152, 1983.
England, P.C., and D.P. McKenzie, A thin viscous sheet model for continental deformation, *Geophys. J. R. astron. Soc., 70*, 295-321, 1982.
Fleitout, L., and C. Froidevaux, Tectonics and topography for a lithosphere containing density heterogeneities, *Tectonics, 1*, 21-56, 1982.
Furlong, K.P., and D.M. Fountain, Continental crustal underplating: thermal considerations and seismic-petrologic consequences, *J. Geophys. Res., 91*, 8,285-8,294, 1986.
Furlong, K.P., and M.D. Londe, Thermal-mechanical consequences of Basin and Range extension, *Geol. Soc. Am. Bull., 208*, 23-30, 1986.
Gans, P.B., An open-system, two-layer crustal stretching model for the eastern Great Basin, *Tectonics, 6*, 1-12, 1987.
Garfunkel, Z., Relation between continental rifting and uplifting: evidence from the Suez rift and northern Red Sea, *Tectonophysics, 150*, 33-49, 1988.
Hellinger, S.J., and J.G. Sclater, Some comments on two-layer extension models for the evolution of sedimentary basins, *J. Geophys. Res., 88*, 8,251-8,269, 1983.
Houseman, G.A., and P.C. England, A dynamical model of lithosphere extension and sedi-

mentary basin formation, *J. Geophys. Res., 91,* 719-729, 1986.
Houseman, G.A., D.P. McKenzie, and P. Molnar, Convective instability of a thickened boundary layer and its relevance for the thermal evolution of continental convergent belts, *J. Geophys. Res., 86,* 6,115-6,132, 1981.
Hutton, J., Theory of the earth; or an investigation of the laws observable in the composition, dissolution, and restoration of land upon the globe, *Trans. Soc. Edinburgh, 1,* 1788.
Issler, D., and C. Beaumont, Thermal and subsidence history of the Labrador and West Greenland continental margins, in *Sedimentary Basins and Basin-Forming Mechanisms,* edited by C. Beaumont and A.J. Tankard, pp. 45-69, Can. Soc. Pet. Geol. Mem. 12, 1987.
Issler, D., H. McQueen, and C. Beaumont, Thermal and isostatic consequences of simple shear extension of the continental lithosphere, *Earth Planet. Sci. Lett., 91,* 341-358, 1989.
Jackson, J.A., Active normal faulting and crustal extension, in *Continental extensional tectonics, 28,* edited by M.P. Coward, J.F. Dewey and P.L. Hancock, pp. 3-18, Geological Society of London Special Publication, 1987.
Jarvis, G.T., and D.P. McKenzie, Sedimentary basin formation with finite extension rates, *Earth Planet. Sci. Lett., 48,* 42-52, 1980.
Keen, C.E., The dynamics of rifting: deformation of the lithosphere by active and passive driving mechanisms, *Geophys. J. R. astron. Soc., 80,* 95-120, 1985.
Kusznir, N.J., and M.M.P. Bott, Stress concentration in the upper lithosphere caused by underlying visco-elastic creep, *Tectonophysics, 43,* 247-256, 1977.
Kusznir, N., and S.S. Egan, Simple-shear and pure-shear models of extensional sedimentary basin formation: application to the Jeanne d'Arc, Grand Banks of Newfoundland, in *Extensional tectonics and stratigraphy of the North Atlantic Margins,* edited by A.J. Tankard and H.R. Balkwill, pp. 305-322, Am. Ass. Petr. Geol. Mem. 46, 1989.
Kusznir, N., and D.H. Mathews, Deep seismic reflections and the deformational mechanisms of the continental lithosphere, *J. Petrol., Special Lithosphere Issue,* 63-87, 1988.
Kusznir, N.J., G.D. Karner, and S. Egan, Geometric, thermal and isostatic consequences of detachment in continental lithosphere and basin formation, in *Sedimentary basins and basin forming mechanisms,* edited by C. Beaumont and A.J. Tankard, pp. 101-116, Can. Soc. Petrol. Geol. Mem. 12, 1987.
Latin, D., and N. White, Generating melt during lithospheric extension: pure shear vs. simple shear, *Geology, 18,* 327-331, 1990.
Le Pichon, X., Land-locked oceanic basins and continental collision: the eastern Mediterranean as a case example, in *Mountain building processes,* edited by K. Hsü, pp. 201-211, Acad. Press, London, 1983.
Le Pichon, X., and J.-C. Sibuet, Passive margins: a model of formation, *J. Geophys. Res., 86,* 3,708-3,720, 1981.
Lee, J., and G.S. Lister, Late Miocene ductile extension and detachment faulting, Mykonos, Greece, *Geology, 20,* 121-124, 1992.
Lister, C.R.B., Gravitational drive on oceanic plates caused by thermal contraction, *Nature, 257,* 663-665, 1975.
Lister, G.S., and G.A. Davis, The origin of metamorphic core complexes and detachment faults formed during Tertiary continental extension in the northern Colorado River re-

gion, U.S.A., *J. Struct. Geol., 11,* 65-94, 1989.
Lister, G.S., G. Banga, and A. Feenstra, Metamorphic core complexes of Cordilleran type in the Cyclades, Aegean Sea, Greece, *Geology, 12,* 221-225, 1984.
Lister, G.S., M.A. Etheridge, and P.A. Symonds, Detachment faulting and the evolution of passive continental margins, *Geology, 14,* 246-250, 1986.
Love, A.E.H., *Some problems of geodynamics,* Cambridge Univ. Press, London, 1911.
Martinod, J., and P. Davy, Periodic instabilities during compression or extension of the lithosphere 1. Deformation modes from an analytical perturbation method, *J. Geophys. Res., 97,* 1,999-2,014, 1992.
McConnell, R.B., Geological development of the rift system of eastern Africa, *Geol. Soc. Am. Bull., 83,* 2,549-2,572, 1972.
McKenzie, D.P., Active tectonics of the Mediterranean region, *Geophys. J. R. astron. Soc., 30,* 109-185, 1972.
McKenzie, D.P., Some remarks on the development of sedimentary basins, *Earth Planet. Sci. Lett., 40,* 25-32, 1978a.
McKenzie, D.P., Active tectonics of the Alpine-Himalayan belt: the Aegean Sea and surrounding regions, *Geophys. J. R. astron. Soc., 55,* 217-254, 1978b.
McKenzie, D.P., A possible mechanism for epeirogenic uplift, *Nature, 307,* 616-618, 1984.
McKenzie, D.P., and M.J. Bickle, The volume and composition of melt generated by extension of the lithosphere, *J. Petrol., 29,* 625-679, 1988.
Melosh, H.J., Mechanical basis for low-angle normal faulting in the Basin and Range province, *Nature, 343,* 1990.
Mercier, J.-L., R. Armijo, P. Tapponier, E. Carey-Gailhardis, and H.T. Lin, Change from Late Tertiary compression to Quaternary extension in southern Tibet during the India-Asia collision, *Tectonics, 6,* 275-304, 1987.
Moretti, I., and C. Froidevaux, Thermomechanical model of active rifting, *Tectonics, 5,* 501-511, 1986.
Pratt, J.H., On the attraction of the Himalaya mountains, and of the elevated regions beyond them, upon the plumb-line in India, *Phil. Trans., 145,* 53-100, 1855.
Richter, F.M., and D.P. McKenzie, Simple plate models of mantle convection, *J. Geophys. Res., 44,* 441-456, 1978.
Rowley, D.B., and D. Sahagian, Depth-dependent stretching: a different approach, *Geology,* 32-35, 1986.
Royden, L., and C.E. Keen, Rifting processes and thermal evolution of the continental margin of eastern Canada determined from subsidence curves, *Earth Planet. Sci. Lett., 51,* 343-361, 1980.
Ruppel, C., L. Royden, and K.V. Hodges, Thermal modeling of extensional tectonics: application to pressure-time histories of metamorphic rocks, *Tectonics, 7,* 947-957, 1988.
Salveson, J.O., Variations in the geology of rift basins - a tectonic model (abstract), *Proceedings of the Rio Grande Symposium,* pp. 82-86, Santa Fe, October 8-17, 1978.
Sawyer, D.S., Brittle failure in the upper mantle during extension of continental lithosphere, *J. Geophys. Res., 90,* 3,021-3,025, 1985.
Sclater, J.G., and P.A.F. Christie, Continental stretching: an explanation for the post-Mid-Cretaceous subsidence of the central North Sea Basin, *J. Geophys. Res., 85,* 3,711-3,739,

1980.
Şengör, A.M.C., and K. Burke, Relative timing of rifting and volcanism on earth and its tectonic implications, *Geophys. Res. Lett., 5,* 419-421, 1978.
Sleep, N.H., Thermal effects of the formation of Atlantic continental margins by continental break up, *Geophys. J. R. astron. Soc., 24,* 325-350, 1971.
Sonder, L.J., P.C. England, B.P. Wernicke, and R.L. Christiansen, A physical model for Cenozoic extension of western North America, in *Continental extensional tectonics, 28,* edited by M.P. Coward, J.F. Dewey and P.L. Hancock, pp. 187-201, Geological Society of London Special Publication, 1987.
Spencer, J.E., and C.G. Chase, Role of crustal flexure in initiation of low-angle normal faults and implications for structural evolution of the Basin and Range Province, *J. Geophys. Res., 94,* 1,765-1,775, 1989.
Steckler, M.S., The thermal and mechanical evolution of Atlantic-type continental margins, PhD thesis, Columbia University, New York, 261 pp., 1981.
Steckler, M.S., Uplift and extension of the Gulf of Suez: indications of induced mantle convection, *Nature, 317,* 135-139, 1985.
Steno, N., *De solido intra solidum naturaliter contento dissertationis prodromus,* Florence, Italy, 1669.
Sykes, L.R., Intraplate seismicity, reactivation of preexisting zones of weakness, alkaline magmatism, and other tectonism postdating continental fragmentation, *Rev. Geophys., 16,* 621-688, 1978.
Voorhoeve, H., and G. Houseman, The thermal evolution of lithosphere extending on a low-angle detachment, *Basin Resarch, 1,* 1-9, 1988.
Wernicke, B., Low-angle normal faults in the Basin and Range Province: nappe tectonics in an extending orogen, *Nature, 291,* 645-648, 1981.
Wernicke, B., Uniform-sense normal simple shear of the continental lithosphere, *Can. J. Earth Sci., 22,* 108-125, 1985.
Wernicke, B., and G.J. Axen, On the role of isostasy in the evolution of normal fault systems, *Geology, 16,* 848-851, 1988.
Wernicke, B., and P.G. Tilke, Extensional tectonic framework of the U.S. Central Atlantic passive margin, in *Extensional tectonics and stratigraphy of the North Atlantic Margins,* edited by A.J. Tankard and H.R. Balkwill, pp. 7-21, Am. Ass. Petr. Geol. Mem. 46, 1989.
Wernicke, B., R.L. Christiansen, P.C. England, and L.J. Sonder, Tectonomagmatic evolution of Cenozoic extension in the North American Cordillera, in *Continental extension tectonics, 28,* edited by M.P. Coward, J.F. Dewey and P.L. Hancock, pp. 203-221, Geological Society of London Special Publication, 1987.
White, N.J., The nature of lithospheric extension in the North Sea, *Geology, 17,* 111-114, 1989.
White, S.H., P.G. Bretan, and E.H. Rutter, Fault-zone reactivation: kinematics and mechanisms, *Phil. Trans. R. Soc. London (A), 317,* 81-97, 1986.
Wilson, J.T., Did the Atlantic close and then re-open?, *Nature, 211,* 676-681, 1966.
Wortel, M.J.R., and S.A.P. Cloetingh, On the origin of the Cocos-Nazca spreading center, *Geology, 9,* 425-430, 1981.
Yin, A., Origin of regional, rooted low-angle normal faults: a mechanical model and its tec-

tonic implications, *Eos Trans. AGU, 68*, 1,449, 1987.
Yin, A., Origin of regional, rooted low-angle normal faults: a mechanical model and its tectonic implications, *Tectonics, 8*, 469-482, 1989.

Chapter 2

Stress magnitude estimates from earthquakes in oceanic plate interiors †

R. Govers, M.J.R. Wortel, S.A.P.L. Cloetingh and C.A. Stein

In this chapter, seismicity data will be used to put constraints on the magnitude of stresses in interior parts of oceanic plates. Oceanic intraplate stresses are guided to continental parts of the plates. Therefore, the results of this chapter put an upper bound on inplane forces which will be applied on continental stretching models in subsequent chapters.

ABSTRACT

We propose a method to estimate stress magnitudes in oceanic plate interiors from focal depths and focal mechanisms. Using a depth-dependent rheology, we show it is possible to estimate the differential stress ($\sigma_1 - \sigma_3$), averaged over some reference lithospheric thickness. The resolving power of the method is investigated by evaluating the effect of uncertainties in parameters that are involved in the analysis. We apply the method to the Central Indian Ocean, where intraplate seismicity is high. From well-studied earthquakes we estimate differential stresses of the order of hundreds of megapascals. This result is consistent with the high level of stress that was found from numerical model calculations by Cloetingh and Wortel (1985,

---

† This chapter has been published as: Govers, R., M.J.R. Wortel, S.A.P.L. Cloetingh and C.A. Stein, Stress magnitude estimates from earthquakes in oceanic plate interiors, *J. Geophys. Res.*, *97*, 11,749-11,759, 1992.

1986). From the few intraplate events in the Pacific plate, we also estimate differential stresses in this area.

INTRODUCTION

Earthquakes relax stresses within the lithosphere, and therefore information on the stress distribution at the hypocenter is contained in seismograms. The relevance of intraplate stresses in the context of plate dynamics is an important motivation to study earthquakes in the interior parts of the plates. Directions of principal stresses are generally derived from focal mechanisms, either directly from P and T axes or via the criterion of Raleigh *et al.* (1972) if one of the nodal planes can be identified as the fault plane. The general consistency of stress trajectories obtained from focal mechanism data and their good agreement with stress orientations derived from various other indicators show that such directions have a regional significance (Zoback *et al.*, 1989). However, a more complete specification of the stress field also requires magnitude information.

We propose a method to estimate differential stress magnitudes in oceanic plate interiors. By relating focal depth and focal mechanism information to a depth-dependent rheology, it will be shown that we can estimate the differential stress level in the lithosphere where an earthquake occurs. Hence, starting from high-quality seismological data and a model for the rheology of the lithosphere (which involves several assumptions and simplifications), we derive estimates for the stress level in the lithosphere. Composition and temperature structure within the lithosphere need to be known well enough to obtain a good approximation of the strength distribution with depth. Compared with continental lithosphere, oceanic lithosphere is therefore more suited for application of the method, although no principal objections exist to using it in continental areas. In this paper we focus on estimating differential stress magnitudes in oceanic plate interiors. Well-resolved earthquake depths are a prerequisite for the method, so that intraplate earthquakes that have been the subject of depth relocation studies provide the best data for estimating stress magnitudes in oceanic plates.

The high seismicity in the Central Indian Ocean (e.g., Wiens and Stein, 1983, 1984; Bergman and Solomon, 1984, 1985) makes this area very well suited for studying the relation between seismicity and differential stress magnitudes. In a force modeling study of the Indian plate, Cloetingh and Wortel (1985, 1986) calculated stresses in the Central Indian Ocean that are very high (several hundreds of megapascals) in comparison with studies by Richardson *et al.* (1979) and Richardson (1987, 1989). In agreement with Cloetingh and Wortel's results, Zuber (1987) and McAdoo and Sandwell (1985) found that hundreds of megapascals stresses are required to explain the gravity highs in the Central Indian Ocean that are attributed

to basement undulations as a result of lithospheric buckling. We will test whether Cloetingh and Wortel's stress results are approximately an order of magnitude too high, as suggested by Richardson (1987, 1989). Therefore, at stages in the analysis when assumptions need to be made, we will adopt those assumptions which (1) are considered to be realistic and (2) give low-end differential stress estimates. Finally, we will estimate differential stress magnitudes for the Pacific Ocean from its seismicity, which is significantly lower than in the Central Indian Ocean.

RHEOLOGY

In relating the depth of an oceanic intraplate earthquake to the stress field in the lithosphere, the rheology model adopted strongly affects the inferred differential stress values. In this section we briefly describe the rheology model adopted in this paper. Brittle deformation in oceanic lithosphere is expected to occur at shallow depth. We assume that the strength $(\sigma_1 - \sigma_3)$ in the brittle regime is described by Byerlee's (1978) law. At deeper levels deformation occurs by temperature-activated ductile flow, controlled by creep of olivine (Goetze and Evans, 1979; Kirby and Kronenberg, 1987).

Brittle Strength

The strength of brittle rock is to a first approximation insensitive to temperature and is mainly pressure-controlled. The stress required for initiation of slip on precut rock faces was found by Byerlee (1978) to be insensitive to rock type. A linear frictional law provides a useful approximation of brittle strength in the lithosphere, particularly at effective pressures above approximately 100 MPa, where the initial surface roughness has little or no effect on friction (Byerlee, 1978).

An estimate of the pore fluid pressure at the fault surface is required to calculate the brittle strength with Byerlee's law. Fluid pressures may range from zero to superlithostatic and are not known in general. Lacking detailed information on pore fluid pressure distributions in the seismic source regions, we assume that the pore fluid pressure is hydrostatic. As the mantle source region for the growth of oceanic lithosphere is very likely to be extremely depleted in volatile elements (Anderson, 1989), very little water is available for building substantial fluid pressures in subcrustal oceanic lithosphere (Dixon *et al.*, 1988). Ophiolitic rocks show evidence of hot water percolation in the crust, where an open system of pores is likely to exist. Therefore, fluid pressures probably are close to hydrostatic in the upper 5-10 km and subhydrostatic in the rest of the oceanic lithosphere. Our assumption of hydrostatic pore fluid pressure therefore yields a lower limit to the brittle strength and is consistent with our approach of getting low-end stress estimates, within the limits

of (what we consider to be) realistic assumptions.

The brittle strength ($\sigma_1 - \sigma_3$) depends on which of the principal stresses is vertical. We adopt the convention that compression is positive and that $\sigma_1 \geq \sigma_2 \geq \sigma_3$. If σ_3 is vertical, the resistance of preexisting faults to sliding is largest ("compression" curve in Figure 1). If σ_1 is vertical the brittle strength is smallest ("tension" branch in Figure 1). If both σ_1 and σ_3 are horizontal, the brittle strength may vary between these two extremes (Turcotte and Schubert, 1982; Sibson, 1974).

Ductile Rheology

Recent laboratory data have modified the depth-dependent strength model of Goetze and Evans (1979) only slightly, the main difference being the incorporation of "wet" deformed olivine, i.e., olivine containing trace amounts of water (Chopra and Patterson, 1981; Tsenn and Carter, 1987). Steady state flow laws for olivine are now well established under both anhydrous conditions and in the presence of water. The creep stress for olivine under conditions that favor dislocation processes may be represented by a powerlaw. Under conditions of low temperatures and high stress the powerlaw breaks down to exponential behavior (Goetze and Evans, 1979; Tsenn and Carter, 1987). In the present study we used a powerlaw flow law for "wet" olivine with an average grain size of 1 mm and an exponential law with data from Tsenn and Carter (1987). As argued in our discussion on pore fluid pressures, we do not actually expect the oceanic lithosphere to be wet but use the present flow law in order to get a lower bound on the stress magnitude.

Oceanic geotherms are a function of lithospheric age. Temperature profiles in oceanic lithosphere are calculated using Crough's (1975, 1977) boundary layer model with a constant basal heat flux and a temperature at the base of the lithosphere of 1300°C. The basal heat flux is selected on the basis of a fit to bathymetry and heat flow data (Parsons and Sclater, 1977). Lithospheric age is estimated from the magnetic anomaly map of Larson *et al.* (1985) and the geomagnetic time scale of Harland *et al.* (1982).

FOCAL MECHANISMS

Constraints on Brittle Strength From Vertical Slip Components

If a vertical cross section of brittle rock, deforming by plane strain, is subjected to a horizontal in-plane stress, faults exhibit normal slip in response to tensile stress and reverse slip due to compressive stress. As the brittle strength is weaker in tension than in compression, one could infer whether to use the "tension" or "compression" branch (Figure 1) from the vertical slip component. However, if stresses and strains are three-dimensional, the relation between vertical slip components and

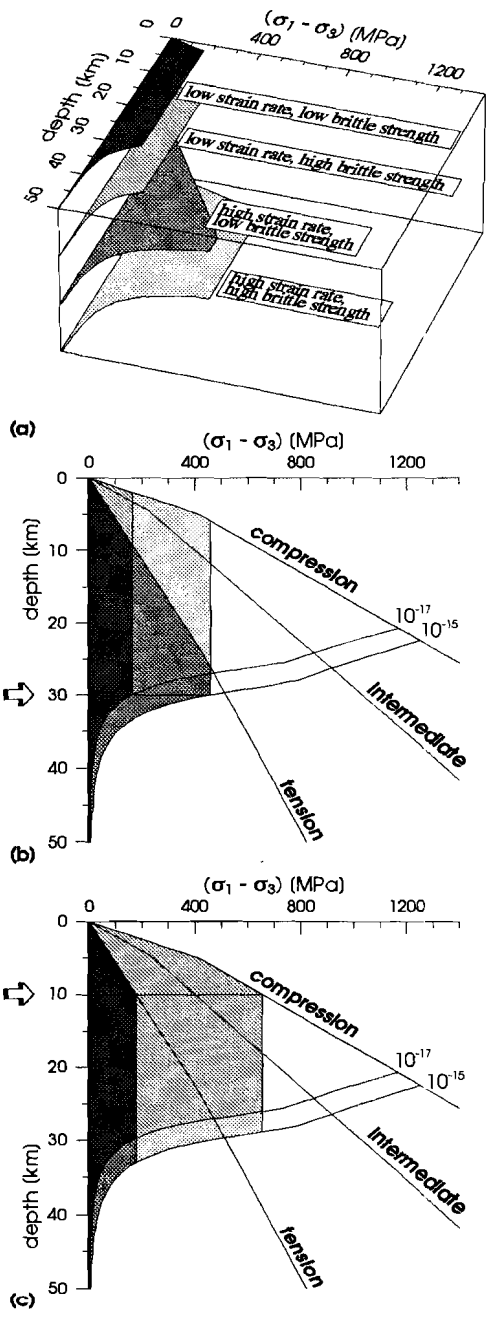

Fig. 1. *Relationship between focal depth of an intraplate earthquake and the stress distribution. (a) Three-dimensional image showing how Figures 1b and 1c are built up by stacking overlapping surfaces that have been calculated for various assumptions on brittle strength and strain rate. (b) Plan view of top surface of Figure 1a. Various strength envelopes are shown for oceanic lithosphere (age 53 Ma). Brittle strength branches labeled "compression," "intermediate," and "tension" are calculated for various principal stress orientations from Byerlee's (1978) law with hydrostatic pore pressure. The ductile strength (flow stress) is shown for strain rates of* 10^{-15} s^{-1} *and* 10^{-17} s^{-1}. *The differential stress* $(\sigma_1 - \sigma_3)$ *has reached the strength locally at the focal depth of 30 km (indicated by arrow), where ductile behavior is predicted. The depth-dependent stress distribution* $(\sigma_1 - \sigma_3)(z)$ *is found by assuming that the stress in weaker parts of the lithosphere has reached the strength, whereas stronger parts elasticly support a stress that is (at least) equal to the stress at the focal depth. Shaded surfaces are a measure of the (average) differential stress (equation (1)). The sensitivity of the average differential stress to assumptions on brittle strength and strain rate is shown by areas of different grey tones. (c) Earthquake with focal depth at 10 km, where brittle behavior is expected. The sensitivity to strain rate is seen to be relatively small for a brittle event. Both ductile and brittle earthquakes are very sensitive to the selection of one of the brittle branches.*

brittle strength is unclear.

The minimum shear stress required for initiation of slip on preexisting faults is described by Byerlee's (1978) law, whereas new faults will be created at higher shear stresses described by Coulomb's (1773) law. Byerlee's law predicts the most favorable fault plane orientation as well as the minimum shear stress that is required for initiation of slip (see Turcotte and Schubert, 1982). However, if this particular fault is not present, the strength of the system is higher. Preexisting faults that are less favorably oriented might become activated at higher stress magnitudes.

We have used a three-dimensional numerical model, employing Byerlee's and Coulomb's laws, to determine bounds on the brittle strength from vertical slip components (Appendix A). We conclude that if the focal mechanism solution indicates a reverse slip component, the brittle strength is limited by "compression" and "intermediate" branches in Figure 1. In case of a normal slip component, the brittle strength ranges from "intermediate" to "tension". Strike-slip faulting does not provide any constraint on the brittle strength.

The sign of the vertical slip component is identical on both nodal planes (see Appendix B). Therefore, putting limits on the brittle strength by using vertical slip components does not depend on a proper selection of fault plane and auxiliary plane.

Earthquakes in Ductile Lithosphere

It will become clear in the next section where we explain how to infer differential stresses from earthquakes, that even if events occur in ductile rock, stress estimates would be more accurate if we could limit the range of brittle strengths in the same way we did for brittle earthquakes. Several models have been proposed to explain the occurrence of seismic slip at depths where crystal-plastic processes are thought to occur (we will refer to these earthquakes as "ductile events"). Sibson (1980) suggests that brittle frictional sliding within the ductile regime may occur due to compositional differences. Variation of unstable to stable frictional slip on deeply penetrating faults is suggested by Tse and Rice (1986) to explain the occurrence of ductile earthquakes. Instability caused by injection of fluids into shear zones and fault gouges, for instance by dehydration reactions, has been put forward by Raleigh and Paterson (1965) and analyzed by Shimamoto (1985). Finally, creep instability, i.e., catastrophic strain softening due to an increase in strain rate or temperature (Orowan, 1960; Griggs and Baker, 1968; Hobbs *et al.*, 1986; Ogawa, 1987), has been put forward to explain ductile earthquakes. The seismic radiation pattern of most ductile earthquakes cannot be distinguished from that of a brittle shear fracture. Currently, it is impossible to select one of the proposed models on the basis of seismic or rheological data.

In the previous section we discussed how the vertical slip component of a brittle earthquake can be used to tighten the range of brittle strengths that are used to estimate upper and lower bounds to the differential stress. The well-established mechanism of brittle earthquakes was a principal ingredient in this discussion. For ductile earthquakes the mechanism is unknown, so that we consider it unwarranted to attribute significance to the vertical slip component inferred from a double couple representation of the source. Therefore, if a seismic event occurs at a depth where rocks are deforming ductily, we take the full range of brittle strengths into account to estimate the differential stress ("tension" to "compression" branches in Figure 1).

DIFFERENTIAL STRESS

The method is designed to yield a measure of stress magnitude that is directly comparable with results from modeling studies. Principal stress magnitudes inferred from modeling generally constitute averages over some (elastic) reference thickness L_{ref} (in the present study we used L_{ref}=100 km). This reference thickness has no physical meaning and is only used to facilitate comparison of stresses derived from force modeling studies with stresses estimated from earthquakes. The average differential stress is defined as

$$\overline{(\sigma_1 - \sigma_3)} = \frac{1}{L_{ref}} \int_{z=0}^{L} (\sigma_1 - \sigma_3)\, dz \qquad (1)$$

L is the thermally defined, age dependent thickness of the lithosphere, i.e., the depth of the 1300°C isotherm in Crough's (1975; 1977) model. Bending stresses in the interior parts of the plate are assumed to be negligible.

Method Description

To calculate the average differential stress at an epicentral site, we note that the strength at the focal depth has been exceeded locally (see Figure 1). No major strength discontinuities occur within oceanic lithosphere, so it is a reasonable assumption that stresses are distributed evenly over the lithospheric thickness. Weak parts of the lithosphere reach their strength at low stresses, stronger parts deform elasticly until stresses increase sufficiently to cause deformation either by flow or by fault slip. We conclude that the strength curve provides an upper limit for differential stresses at depths where the strength is less than that at the focal depth. The differential stress in the "elastic core", i.e., the strong part of the lithosphere where stress is supported elasticly, is at least equal to the stress level at the focal depth (Wortel, 1986; Wortel and Vlaar, 1988). After integration of the depth-

dependent differential stress and scaling by L_{ref} we obtain $\overline{(\sigma_1 - \sigma_3)}$. In the following we will refer to the average differential stress as "differential stress".

Sensitivity of Results to Input Parameters

Our results are sensitive to two different types of parameters: variables related to the method, that cause uncertainties in the rheology model, and "observational" pa rameters, like focal depth and lithospheric age. Relevant method-related parameters affecting the depth-dependent rheology model are the pore fluid pressure, the assumed strain rate, and the brittle strength.

The effect of decreasing the pore fluid pressure is that the brittle strength and, therefore, our stress estimates increase. As discussed before, we aim at getting a lower bound to differential stresses, within the limits of (what we consider to be) realistic assumptions. We therefore did not include pore pressures smaller than hydrostatic in our calculations.

Figure 1 displays the sensitivity of differential stress to brittle strength and strain rate for a ductile and a brittle event. In Figure 1, hatched areas are a measure of differential stress. The effect of varying the strain rate between 10^{-15} s^{-1} and 10^{-17} s^{-1} can be significant for ductile earthquakes (Figure 1*b*). The stress in the elastic core is strongly affected, so that the differential stress is sensitive to a change in strain rate. From Figure 1*c* it is clear that stresses calculated from events in the brittle part of the lithosphere are relatively insensitive to changes in strain rate.

Both for brittle and for ductile earthquakes the differential stress is very sensitive to the selected brittle strength. In the absence of constraints on the vertical slip component, upper and lower bounds to the differential stress are calculated from "compression" and "tension" strength branches, respectively. Figures 2*a* and 2*b* show upper and lower bounds as a function of focal depth and lithospheric age, for a strain rate of 10^{-16} s^{-1}. A measure of the resolution that can be obtained with our method is the difference between upper and lower bounds to the differential stress (Figure 2*c*). In older lithosphere we observe differences of several hundreds of megapascals between minimum and maximum differential stresses. Figure 2*c* can be used to estimate what can be gained by improving the focal depth accuracy after an approximate focal depth range has been determined: an estimated earthquake depth of 20 ± 10 km in 90 Ma lithosphere does not require additional waveform modeling to resolve differential stresses much better. However, if the observed focal depth is 40 ± 10 km, it is worthwhile to try to improve the depth accuracy.

If the focal mechanism has a normal slip component the upper bound to the differential stress is not calculated from the "compression" brittle strength but from the "intermediate" strength branch (Figure 1). The lower bound to the differential

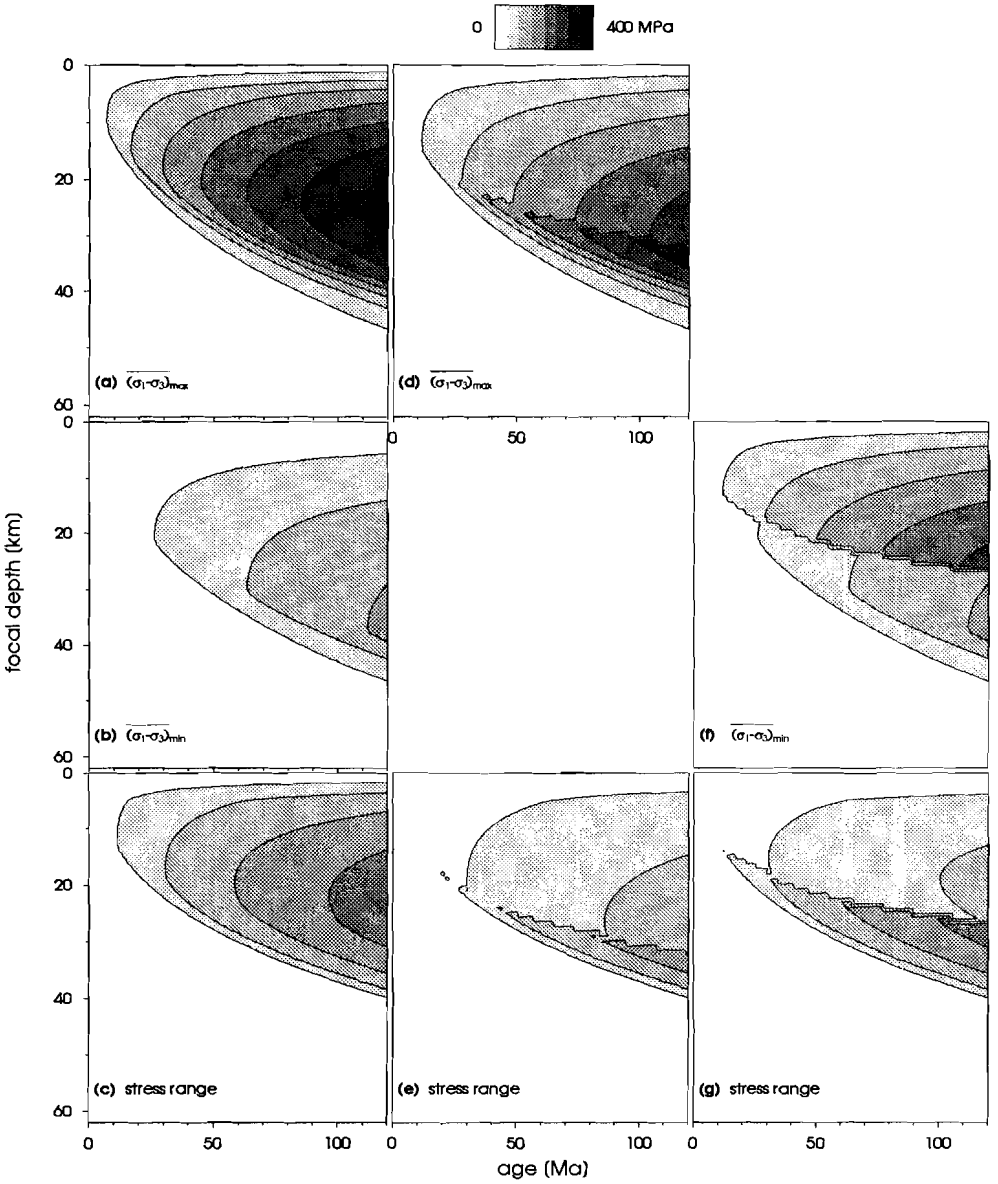
0
400 MPa
focal depth (km)
0
20
40
60
(a) $\overline{(\sigma_1-\sigma_3)}_{max}$
(d) $\overline{(\sigma_1-\sigma_3)}_{max}$
(b) $\overline{(\sigma_1-\sigma_3)}_{min}$
(f) $\overline{(\sigma_1-\sigma_3)}_{min}$
(c) stress range
(e) stress range
(g) stress range
0
50
100
age (Ma)

Fig. 2. *Differential stress as a function of age and focal depth, for a strain rate of* 10^{-16} s^{-1}: *(a) for maximum brittle strength in case of reverse slip or strike slip mechanism, (b) for minimum brittle strength in case of normal slip or strike slip mechanism, (c) difference between maximum and minimum stress, a measure for method accuracy, if no constraints on the vertical slip components are available, (d) for maximum brittle strength in case of a normal slip event, and (e) difference between maximum and minimum stress (minimum in Figure 2b). Note that the the lower ductile part is not affected by the normal slip constraint, (f) for minimum brittle strength in case of reverse slip, and (g) difference between maximum and minimum stress for focal mechanism with a reverse slip component (maximum differential stress in Figure 2a).*

stress again follows from using the "tension" brittle strength (Figure 2*b*). Comparing Figures 2*d* and 2*a*, we observe a significant reduction of the maximum differential stress for those focal depths that are in the brittle lithosphere. The exclusion of focal mechanism information for ductile events results in a discontinuity of calculated stresses at the brittle-ductile transition. The reduction of the maximum differential stress clearly improves the resolution of differential stress estimates for brittle events, as can be seen from comparing Figures 2*e* and 2*c*.

In case of reverse slip the "intermediate" in stead of "tension" branch is used to calculate the minimum differential stress. The upper bound to the differential stress follows from the "compression" brittle strength (Figure 2*a*). Figures 2*f* and 2*g* show minimum stress and stress resolution as a function of age and focal depth, assuming that the fault slip has a reverse component. Again, reduction of the range of brittle strengths improves the resolution significantly.

DIFFERENTIAL STRESS IN THE CENTRAL INDIAN OCEAN

The Central Indian Ocean, with its high intraplate seismicity, provides an excellent opportunity to study the relation between earthquakes and the level of intraplate stress. An important motivation to study intraplate stress fields is to improve our understanding of the dynamics of plate motion. With this goal in mind Richardson *et al.* (1979) performed numerical calculations of the stress field in all major plates. Subsequently, Wortel and Cloetingh (1981, 1983, 1985) performed a similar type of numerical modeling, with some important new aspects in their force modeling procedure. In contrast with the earlier models the ridge push was not represented as a line force but as an integrated pressure gradient (Lister, 1975) distributed over all contributing parts of the lithosphere. The slab pull was incorporated as an age-dependent force giving rise to significant lateral variations in the forces representing the subduction process. Whereas the force modeling for the Nazca plate (Wortel and Cloetingh, 1983, 1985) yielded stress values in agreement with Richardson *et al.*'s (1979) models, a later application of the same modeling to

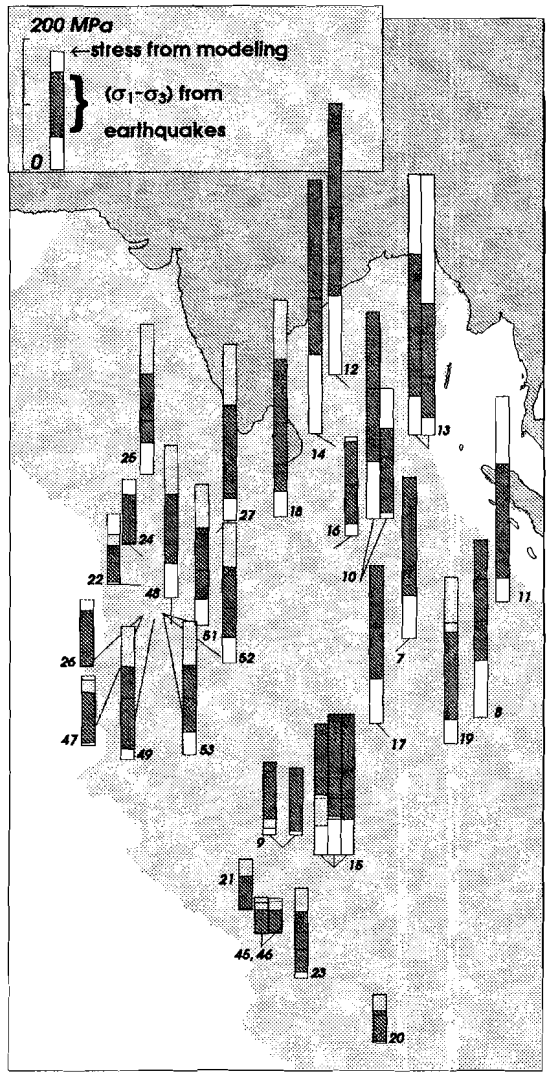

Fig. 3. *Differential stresses in the Central Indian Ocean at epicentral locations of events listed in Table 1. Thin solid lines from the base of the columns end at epicentral locations. The height from the base of a column is a measure of the differential stress magnitude. Stress magnitudes constitute averages over a reference value (100 km) of the plate thickness. In each column, the darkest grey band corresponds to the uncertainty in the inferred differential stress. The uncertainty increases for most events if the vertical slip component is neglected; in this case the light grey band plus the dark grey band correspond to the range of inferred differential stresses. The thick horizontal line in (or at the top of) the column corresponds with the differential stress calculated by Cloetingh and Wortel (1985, 1986).*

the Indo-Australian plate (Cloetingh and Wortel, 1985, 1986) resulted (Figure 3) in a significantly higher stress level than in the study by Richardson *et al.* (1979) (see also Richardson (1987, 1989)). This difference stems from a difference in modeling procedure. Richardson *et al.* (1979) made a variable parameter study of the various plate tectonic forces involved. Cloetingh and Wortel (1985, 1986) treated the driving forces (ridge push and slab pull) as known forces, which could be cal-

culated from kinematic parameters (relative motion along convergent plate boundaries) and the age of the lithosphere involved, and derived the magnitudes of the resistive forces from the equation representing the balance of torques of all forces acting on the plate.

In view of the relevance of such discrepancies for ongoing and future numerical modeling we address this issue by investigating the information which the unusually high seismic activity in the Central Indian Ocean (e.g., Wiens and Stein, 1983, 1984; Bergman and Solomon, 1984, 1985) provides concerning the level of intraplate stress. Previously, only the orientations of the principal stress directions have been used to test the results of stress modeling. For the Central Indian Ocean, good agreement was found between calculated orientations and focal mechanism data (Cloetingh and Wortel, 1986; Bergman, 1986). Also the orientations of observed long wavelength basement undulations appear to be consistent with the calculated stress orientations (Stein *et al.*, 1989; Petroy and Wiens, 1989).

Large ($m_b \geq 4.9$) oceanic intraplate earthquakes in the Central Indian Ocean have been the subject of seismological waveform modeling studies by various authors. The earthquakes for which adequate information on depth and focal mechanism were available are listed in Table 1. The focal depth accuracy for shallow teleseismic earthquakes is discussed for various methods by Stein and Wiens (1986). Depth relocation methods like long-period *P* waveform modeling (Wiens and Stein, 1983), Rayleigh waveform modeling with additional long-period *P* waveform modeling for shallow events (Wiens and Stein, 1984) and body waveform inversion (Bergman and Solomon, 1984, 1985) all are estimated to have a 2-km accuracy. Pre-WWSSN data, relocated with *P*, *SH*, Rayleigh and Love waveform modeling techniques (Wiens, 1986) have 5-km accuracies. Depth phase identifications from short-period *P*/*pwP*/*pP* arrivals (Stein and Weissel, 1990) are assigned a 5-km accuracy. Vertical slip components are considered significant if the slip direction makes an angle with the strike of more than 10^o.

For all these events the differential stress is estimated, first without focal mechanism information taken into account and next with inclusion of such information (see Table 1). The results are displayed in Figure 3 in combination with the numerical model values obtained by Cloetingh and Wortel (1985, 1986). Figure 3 clearly demonstrates what was already apparent from Figures 2*c*, 2*e* and 2*g*, namely, that hypocentral depth alone does not provide a firm constraint on the level of differential stress. If, however, reliable information on the vertical slip components of an event is available, the large contribution of the brittle slope variation to the uncertainty of the integrated differential stress can be reduced.

Gravity highs attributed to 200-km wavelength basement undulations as a result of lithospheric buckling have been observed in the region between 18°S and 10°N

TABLE 1. Central Indian Ocean Intraplate Earthquake Data

Event[a]	Date	Latitude °N	Longitude °E	Depth[b], km	Vertical Component[c]	Age, Ma	References[d]
7	May 25, 1964	-9.1	88.9	17 ± 2	SS	58 ± 2	BS85
8	October 31, 1965	-14.2	95.3	24 ± 2	SS	65.5 ± 0.5	WS83
9	September 14, 1968	-24.4	80.4	3 ± 2	SS	31 ± 3	BS85
				4 ± 2	T		BS85
10	October 10, 1970	-3.6	86.2	27 ± 2	SS	73 ± 9	BS85
				39 ± 2	T		BS85
11	June 26, 1971	-5.2	96.9	29 ± 2	T	52.5 ± 0.5	BS85
12	November 24, 1972	11.7	85.3	27 ± 2	T	116 ± 14	BS85
13	April 7, 1973	7.0	91.3	13 ± 2	SS	75 ± 7	BS85
				6 ± 2	SS		BS85
14	August 30, 1973	7.2	84.3	27 ± 2	T	109 ± 7	BS85
15	June 25, 1974	-26.0	84.3	23 ± 2	T	42.5 ± 3.5	BS85
				18 ± 2	T		BS85
				13 ± 2	T		BS85
16	August 3, 1978	-0.9	84.2	39 ± 2	T	80.5 ± 2.5	WS83
17	December 2, 1981	-15.7	88.4	23 ± 2	T	50 ± 5	BS85
18	April 23, 1967	1.6	80.2	32 ± 5	T	83 ± 6	SW90
19	June 3, 1978	-16.2	93.0	11 ± 5	T	65 ± 3	SW90
20	October 8, 1968	-39.9	87.7	11 ± 2	N	7.5 ± 2.5	WS84
21	November 2, 1976	-29.4	77.7	14 ± 2	N	9 ± 2	WS84
22	March 31, 1970	-3.8	69.7	12 ± 2	N	8.5 ± 2.5	WS84
23	September 19, 1975	-34.7	81.9	19 ± 2	N	20.5 ± 3.5	WS84
24	November 17, 1973	-1.6	69.8	19 ± 2	N	13 ± 2	WS84
25	December 12, 1981	5.0	70.2	15 ± 2	N	46 ± 7	BS84
26	October 2, 1957	-6.3	69.7	14 ± 5	SS	12 ± 3	W86
27	Februari 29, 1944	0.3	75.4	10 ± 5	T	76 ± 3	W86
45	December 19, 1965	-32.2	78.9	13 ± 2	N	5.5 ± 1.5	WS84
46	Februari 17, 1966	-32.2	78.9	11 ± 2	N	5.5 ± 1.5	WS84
47	April 25, 1970	-6.3	69.8	15 ± 2	N	12 ± 3	WS84
48	November 30, 1983	-6.8	72.0	16 ± 2	N	49 ± 7	WS84
49	September 12, 1965	-6.5	70.8	18 ± 2	N	30 ± 12	BS84
51	November 10, 1967	-6.0	71.3	18 ± 2	N	36 ± 11	BS84
52	November 11, 1967	-6.0	71.4	17 ± 2	N	36 ± 11	BS84
53	March 2, 1968	-6.1	71.4	13 ± 2	N	36 ± 11	BS84

[a] Numbers 7-27 refer to Cloetingh and Wortel (1986), numbers 45-53 have been added to their list.
[b] Depth from top of crust.
[c] SS, strike slip; T, thrust; N, normal.
[d] BS85, Bergman and Solomon (1985); WS83, Wiens and Stein (1983); SW90, Stein and Weissel (1990); WS84, Wiens and Stein (1984); W86, Wiens (1986); BS84, Bergman and Solomon (1984).

and 80°E and 100°E. Earthquakes 7, 10, 16, and 18 all occur near highs, so that the effect of flexural bending stresses in this compressive region would be to reduce stresses at the top and increase stress near the bottom of the lithosphere. Differential stress estimates in this region are very high, and the contribution of superimposed flexural bending stresses to the average differential stress generally is not large. More particularly, the stress found from event 7 probably is a lower estimate, and the stress from event 16 is estimated too high. Stresses from the other events are hardly affected by bending stresses, since their epicenters are in the flanks of the buckles. Bathymetric loading by the Chagos-Laccadive Ridge and Ninetyeast Ridge also might cause bending stresses. These would affect the stresses estimated from event 7, 17, 26, and 47-53.

Comparison of Cloetingh and Wortel's (1985, 1986) numerical model values (horizontal bars) with the differential stress ranges in Figure 3 indicates that for events 22, 24, 26, 45, 46, and 47, all near the ridge, the model values are somewhat too high. Only for events 11 and 13 the model values greatly exceed the inferred stress ranges. These events are near the Sumatra-Nicobar-Andaman trench system. All model values for the Central Indian Ocean (with the minor exceptions of one of the events of 10, and 19) fall clearly within the stress ranges. The model values for events 15, 18, and 27 are even near the minima of the seismicity derived stress ranges. We particularly note the good agreement for the high stress values of events 12 and 14.

Since our method yields low-end estimates of the differential stress, our results are more in agreement with those of Cloetingh and Wortel (1985, 1986) than with stress levels found by Richardson (1987, 1989), which are about an order of magnitude lower.

PACIFIC PLATE STRESSES

Seismicity in the Pacific plate is less abundant than in the Indian plate and focal depth and focal mechanism constraints are relatively poor compared to Indian Ocean data. Table 2 is a selection of $m_b \geq 4.8$ events we made from World Stress Map data. Figure 4 shows results of differential stress computations from focal depth and focal mechanism.

The highest stresses are estimated for the Samoa-Gilbert-Ralik area from event 6, 7, and 8. Okal *et al.* (1986) note teleseismically recorded swarms of intraplate seismicity ($4.0 \leq m_b \leq 6.0$) in this region and attribute them to large-scale deformation. However, nearby seamounts probably cause bending stresses so that differential stresses derived from these events do not reflect the intraplate stress field.

Stein (1979) studied event 3 in the northwest of the Pacific and concluded that the epicenter occurred on Emperor Trough, a dead spreading center that has also

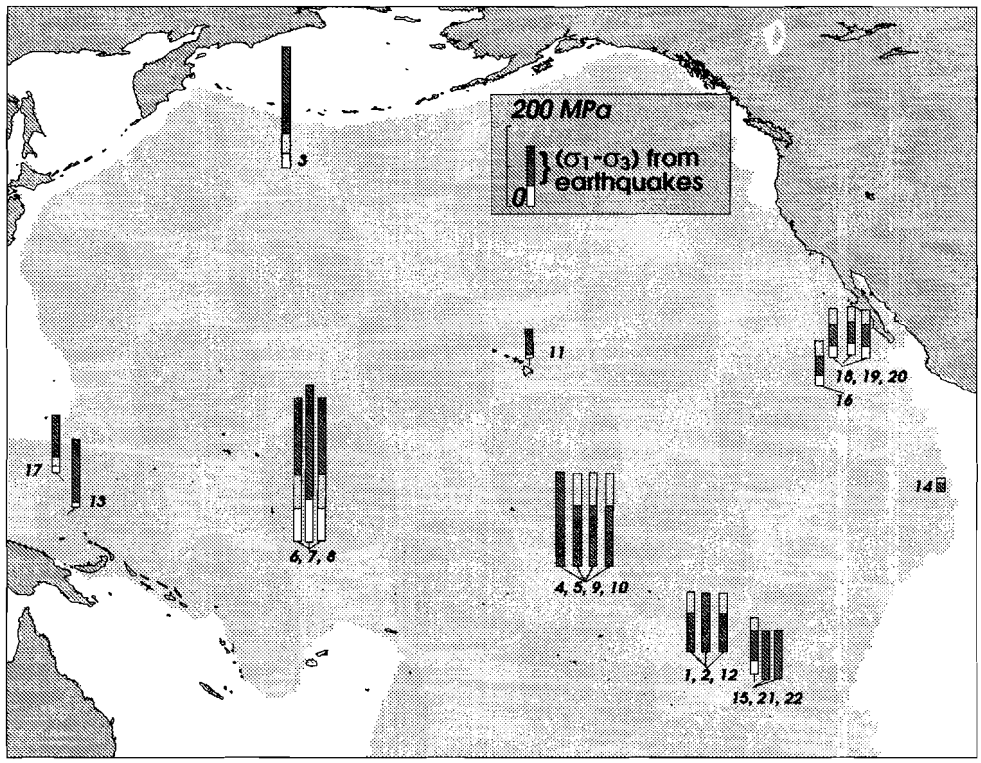

Fig. 4. *Differential stresses in the Pacific intraplate area at epicentral locations of events listed in Table 2. Columns have the same meaning as in Figure 3.*

been active as a transform fault between Kula and Pacific plates (Larson and Chase, 1972; Hilde *et al.*, 1976). Due to the large uncertainties in lithospheric age and focal depth, the difference between maximum and minimum estimated stresses is large. The Caroline plate, north of New Guinea, has been proposed by Weissel and Anderson (1978) to be subducting under the Pacific plate at the Mussau Trench. The epicenter of event 17 lies on the proposed Caroline-Pacific plate boundary and might not be a true intraplate event.

The magnitude of intraplate stresses in the Pacific plate east of 170°W appears to be lower than in the west. The strongest constraint on intraplate stresses in the southeast Pacific comes from event 15. Other earthquakes in this area have less well resolved focal depths. Differential stresses southwest of Baja California also indicate that differential stresses in the eastern Pacific do not exceed the 100 MPa level. Earthquakes in the eastern Pacific that are related to bending stresses due to

TABLE 2. Pacific Intraplate Earthquake Data

Event	Date	Latitude °N	Longitude °E	Depth}[a], km	Vertical Component[b]	Age, Ma	Reference[c]
1	March 6, 1965	-18.4	-132.8	5 ± 5	N	34 ± 1	O80
2	September 18, 1966	-18.4	-132.9	5 ± 5	N	34 ± 1	O80
3	April 28, 1968	44.8	174.6	10 ± 5	T	90 ± 10	S
4	July 29, 1968	-7.5	-148.3	5 ± 5	SS	89 ± 5	O80
5	August 6, 1969	-7.6	-148.1	5 ± 5	N	89 ± 5	O80
6	Januari 7, 1982	-3.4	177.6	15 ± 3	T	122 ± 3	LO, D83
7	Februari 15, 1982	-3.5	177.5	21 ± 3	SS	122 ± 3	LO, D83
8	March 16, 1982	-3.3	177.5	15 ± 3	T	122 ± 3	LO, D83
9	Januari 19, 1973	-7.6	-148.2	5 ± 5	N	89 ± 5	O80
10	Januari 19, 1973	-7.6	-148.1	5 ± 5	N	89 ± 5	O80
11	April 26, 1973	20.1	-155.2	45 ± 2	N	90 ± 5	B86, B, U
12	May 25, 1975	-18.4	-133.0	5 ± 5	SS	34 ± 1	O80
13	August 30, 1976	1.0	147.6	26 ± 2	SS	34 ± 3	B86, WS83
14	October 29, 1975	4.1	-103.5	9 ± 2	N	3 ± 1	WS84
15	July 31, 1983	-20.1	-126.9	17 ± 2	N	22 ± 2	WS84, D84, O84
16	June 30, 1945	16.6	-115.8	12 ± 2	N	16 ± 1	WO
17	August 20, 1968	5.4	147.1	6 ± 3	T	34 ± 3	B86, BS
18	October 5, 1984	20.1	-116.0	13 ± 2	N	18 ± 1	WO, D85
19	December 2, 1984	20.4	-115.8	15 ± 2	N	18 ± 1	WO, D85
20	May 28, 1986	20.0	-115.9	15 ± 2	N	18 ± 1	WO, D87
21	Januari 5, 1978	-20.9	-126.9	5 ± 5	T	23 ± 1	O80
22	July 25, 1978	-20.8	-126.9	5 ± 5	T	23 ± 1	O80

[a] Depth from top of crust.

[b] SS, strike slip; T, thrust; N, normal.

[c] B86, Bergman (1986); BS, Bergman and Solomon (1980); B, Butler (1982); D83, Dziewonski *et al.* (1983); D84, Dziewonski *et al.* (1984); D85, Dziewonski *et al.* (1985); D87, Dziewonski *et al.* (1987); LO, Lay and Okal (1983); O84, Okal (1984); O80, Okal *et al.* (1980); S, Stein (1979); U, Unger and Ward (1979); WO, Wiens and Okal (1987); WS83, Wiens and Stein (1983); WS84, Wiens and Stein (1984).

seamount loads are event 1, 2, and 12 (Okal *et al.*, 1980) and event 11 near Hawaii (e.g., Watts *et al.*, 1985).

DISCUSSION

Strength on Different Time Scales

Jeffreys (1959) observed that high, uncompensated mountain ranges can be supported by the lithosphere and inferred that the strength of the lithosphere must be hundreds of megapascals. Laboratory experiments on both brittle as ductile rocks showed that the lithosphere is indeed capable of bearing stresses of large magnitude on long time scales (Byerlee, 1978; Goetze, 1978). It was noted by Chinnery (1964) that the stress drop in an earthquake is 2 orders of magnitude lower. Thus, if the stress drop is taken to be a measure of strength, the strength on short time scales ("seismic strength") seems to be much lower than the strength on geological time scales ("tectonic strength"). The question arises whether we can use long-term strength envelopes to infer stress magnitudes from earthquakes? While further insight into this aspect has to be gained, we adopt the hypothesis concerning the relation between stress, strength (rheology), and earthquake generation proposed by Wortel (1986). Recognizing that parts of the lithosphere in which the strength is low and where the stress is at or near the strength (comparable with the near-surface part of the oceanic lithosphere) earthquake generation is not observed, he postulated that seismic activity occurs when and where the width (or depth interval) of the anelasticly deforming region increases at the expense of the "elastic core", in other words, when and where the stress reaches the strength for the first time. It was shown that this hypothesis adequately accounts for the distribution of seismic activity in subducting lithosphere (Wortel, 1986; Wortel and Vlaar, 1988). In this hypothesis the seismic stress drop does not reflect the absolute level of stress but rather a stress adjustment to the equilibrium tectonic stress. Consequently, the seismic strength can be higher than the tectonic strength and earthquakes are envisaged to relax stresses that exceed the long-term strength. The stress drops involved are low, so the long-term strength envelope yields a good approximation of the stresses at the hypocenter.

Nonequilibrium Stress Distribution

In our analysis we assumed that ductile rocks in the "elastic core" are able to support stresses elasticly on geologic time scales. If, however, ductile rock is subject to differential stresses it will show some elastic deformation, transient creep and eventually steady state creep. In steady state, the strain rate has equilibrated to the imposed stress. Therefore stress distributions like in Figure 1 cannot represent equilibrium, since ductile rock will eventually support a stress that is equal to the flow stress (the stress we previously named "strength") at some strain rate.

It is clear that the time required for establishing an equilibrium is a (highly non-linear) function of boundary conditions and rheology. Probably, the stresses in the strongest layers will not change very rapidly with time, since their viscosity is very high. Therefore, the "elastic core" can be interpreted as a depth interval where creep in the ductile rocks very slowly alters the stress. We note that there is a great need for a dynamic approach to investigate the stress distribution with depth as it develops with time, if lithosphere is subjected to a stress boundary condition.

Brittle Strength

Our assumptions are aimed at getting a low-end estimate of the differential stress in oceanic lithosphere. However, the brittle strength inferred from Byerlee's (1978) relation is thought to be exceptionally high by a number of authors (Haimson and Doe, 1983; Zoback and Mastin, 1986). In spite of the possible shortcomings we consider Byerlee's law to be the most suitable quantitative description available at present. Most likely, deviations from the assumed brittle strength are most pronounced near the brittle-ductile transition, and our method is not very sensitive to them.

Focal Depth

Many of the reported depths in Tables 1 and 2 are centroid depths. The centroid depth is the average depth of the fault plane and is therefore not necessarily equal to the initiation depth, the hypocenter. The difference in depth between hypocenter and centroid can be up to 5 km, depending on the wavelengths that were used in determining the centroid depth, the spatial source function asymmetry, the fault plane orientation, and the fault plane dimensions. In our analysis we assumed that hypocentral depth and centroid depth are equal.

CONCLUSIONS

The main objective of the current paper is to investigate the possibility of extending our knowledge of the intraplate stress field with magnitudes. Our present knowledge of lithospheric rheology required to relate intraplate deformation (earthquakes) to stress limits the accuracy of inferred stress magnitudes. Therefore, efforts to make the accuracy of focal depths better than 2 km are not expected to contribute to our knowledge of intraplate stress magnitudes. If the vertical slip component is not well constrained by the focal mechanism, if the faulting is pure strike-slip, or if an earthquake occurs in ductile lithosphere, the uncertainty in differential stresses is large. If the focal mechanism is known with confidence, tighter bounds can be placed on the stress magnitude.

Numerical calculations of the stress field in the Central Indian Ocean by Richardson *et al.* (1979) and Cloetingh and Wortel (1985, 1986) yield order of magnitude differences. From our analysis we find that seismicity data require a stress level comparable with that calculated by Cloetingh and Wortel (1985, 1986). Stress levels about an order of magnitude lower, as advocated by Richardson (1987, 1989) are less in agreement with differential stresses found in this study.

APPENDIX A

We investigate the relation between the vertical slip component of an earthquake and the brittle strength. Obviously, both are related by the stress field; slip occurs in the direction of maximum resolved shear stress if the strength is exceeded.

In general, the brittle strength according to a linear friction law can be written in terms of the difference between maximum and minimum principal stresses

$$(\sigma_1 - \sigma_3) = \frac{2 S_0}{\sqrt{1+\mu^2}} + \frac{2 \mu (q - \lambda)}{\sqrt{1+\mu^2}} \sigma_v$$

$$q = \frac{\sigma_1 + \sigma_3}{2 \sigma_v} \quad , \quad \frac{\sqrt{1+\mu^2} + \lambda \mu}{\sqrt{1+\mu^2} + \mu} \leq q \leq \frac{\sqrt{1+\mu^2} - \lambda \mu}{\sqrt{1+\mu^2} - \mu}$$

cohesion S_0, coefficient of friction μ, overburden load σ_v, and pore fluid coefficient $\lambda = P_f/\sigma_v$. We assume that one of the principal stress directions is vertical and equal to the overburden pressure. Upper and lower limits to the brittle strength and q correspond to in-plane compression and in-plane tension, respectively, or more precisely, correspond to vertical σ_3 and σ_1. Therefore, if we would know the principal stress directions at the epicenter, we could select a single brittle strength curve to estimate differential stress. Unfortunately, focal mechanism solutions only give principal deformation quadrants, not principal stress directions.

To determine the relation between focal mechanism and applied stress, we performed a number of synthetic tests. For various three-dimensional stress fields we calculated the orientations of preexisting fault planes on which the conditions for slip are met; that is, the threshold value of shear stress has been reached or exceeded according to Byerlee's law. Horizontal stresses are limited by the failure strength of brittle rock, which was calculated by Coulomb's (1776) law.

Figure A1 shows a typical result of our modeling. Three basic response types are indicated; if horizontal tectonic stresses (σ_x and σ_y) are small deformation is elastic. If stresses increase slip on preexisting faults (if present) may occur. If stresses cannot be accommodated on preexisting faults, new ones may be created at even

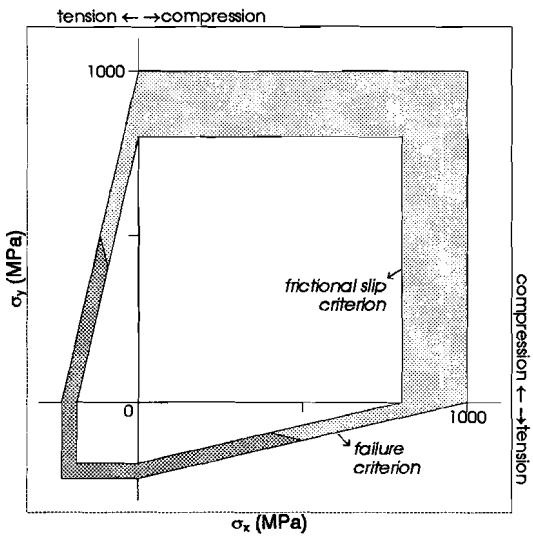

Fig. A1. *Vertical fault slip component as a function of horizontal stresses σ_x and σ_y. The grey shaded areas indicate stresses at which slip along pre-existing faults can take place. At lower stresses, in the internal part of the figure, the deformation is purely elastic. The failure criterion puts an upper bound to the stress level that can be reached. In the light grey shaded area the predominant vertical component is reverse slip. In the dark grey area normal slip is observed. The shape of the figure is invariant to depth; the figure simply shrinks or expands at smaller or greater depths (numbers on the axes correspond to a depth of 13 km).*

higher stresses. Faulting types typical for particular stresses may be recognized (Anderson, 1951; Sibson, 1974); if both horizontal stresses are compressive mainly reverse faults become activated. Normal faulting typically occurs in response to horizontal tensile stresses. The switch of slip with normal component to slip with reverse component occurs approximately midway the transitional domain where σ_2 is vertical.

From our synthetic experiments we conclude that if a focal mechanism has a significant reverse component, the brittle strength is bounded by "compression" and "intermediate" curves in Figure 1. If a normal slip component has been observed, the brittle strength lies between "tension" and "intermediate" curves. A mechanism with a pure strike-slip character does not give any constraints on the brittle strength, so that the full strength range has to be taken into account.

APPENDIX B

Given the orientations of unit length **T**, **P**, and **B** axes we will show that the vertical slip component on both nodal planes has the same sign. Let **X** be north, **Y** east, and **Z** vertically downward. To specify the orientation of a particular vector, we use angles ϕ and δ. ϕ is the angle between the projection of the vector on the horizontal **X**-**Y** plane and the **X** axis, measured clockwise. δ is the clockwise angle between the horizontal projection of the vector and the vector itself. **P**, **T**, and **B** axes are typically given in lower hemisphere stereographic coordinates, so that $\delta \in [0, \pi/2]$ and $\phi \in [0, 2\pi]$.

We define a matrix R that rotates **X** to the **B** axis (ϕ_B, δ_B):

$$R = \begin{pmatrix} \cos\phi_B \cos\delta_B & -\sin\phi_B & -\cos\phi_B \sin\delta_B \\ \sin\phi_B \cos\delta_B & \cos\phi_B & -\sin\phi_B \sin\delta_B \\ \sin\delta_B & 0 & \cos\delta_B \end{pmatrix}$$

If we let R^{-1} work on **T** axis (ϕ_T, δ_T) and **P** axis (ϕ_P, δ_P), both $\mathbf{P}' = R^{-1}\,\mathbf{P}$ and $\mathbf{T}' = R^{-1}\,\mathbf{T}$ will lie in the Y-Z plane. We now define a third angle γ, to specify the angle in the Y-Z plane between the $\mathbf{P}'$ or $\mathbf{T}'$ axis and Z. We consider two cases: $\mathbf{T}'$ closest to the vertical, i.e., $\gamma_T \in [-\pi/4, \pi/4]$, and $\mathbf{P}'$ closest to the **Z** axis.

If $\mathbf{T}'$ is closest to the vertical in the system of north directing **B** axis, we define a second rotation matrix

$$V = \begin{pmatrix} 1 & 0 & 0 \\ 0 & \cos\gamma_T & -\sin\gamma_T \\ 0 & \sin\gamma_T & \cos\gamma_T \end{pmatrix}$$

so that $\mathbf{T}' = R\,V\,\mathbf{T}''$. $\mathbf{T}''$ is the vertical unit vector. Slip vectors in the system of vertical $\mathbf{T}''$ axis and north directing $\mathbf{B}'$ axis are $S'_1 = (0, \frac{1}{2}\sqrt{2}, -\frac{1}{2}\sqrt{2})$ and $S'_2 = (0, -\frac{1}{2}\sqrt{2}, -\frac{1}{2}\sqrt{2})$. Slip vectors in the original system of **P**, **B**, and **T** axes can be calculated from

$$S_1 = R\,V\,S'_1$$

$$S_2 = R\,V\,S'_2$$

Evaluation of the vertical slip components in the original system of **P**, **B**, and **T** axes yields

$$S_1^z = -\frac{1}{2}\sqrt{2}\cos\delta_B\,(\cos\gamma_T - \sin\gamma_T)$$

$$S_2^z = -\frac{1}{2}\sqrt{2}\cos\delta_B\,(\cos\gamma_T + \sin\gamma_T)$$

for $\gamma_T \in [-\pi/4, \pi/4]$. For the given range of γ_T, both vertical slip components have the same sign.

By the same approach it can be shown that if the $\mathbf{P}'$ axes is closest to the vertical in the system of north directing **B** axis we have

$$S_1^z = \frac{1}{2}\sqrt{2}\cos\delta_B\,(\cos\gamma_P - \sin\gamma_P)$$

$$S_2^z = \frac{1}{2}\sqrt{2}\cos\delta_B\,(\cos\gamma_P + \sin\gamma_P)$$

for $\gamma_P \in [-\pi/4, \pi/4]$, so that both vertical slip components have either dip-slip or thrust components.

Acknowledgments

During this research, R.G. was financially supported by AWON, the Earth Science branch of the Netherlands Organization for Scientific Research (NWO). M.J.R.W. and S.A.P.L.C. received partial support from NATO grant 0148/87.

REFERENCES

Anderson, D.L., *Theory of the Earth*, 366 pp., Blackwell Scientific, Boston, Mass., 1989.

Anderson, E.M., *The Dynamics of Faulting and Dyke Formation With Applications to Britain*, Oliver and Boyd, Edinburgh, 1951.

Bergman, E.A., Intraplate earthquakes and the state of stress in oceanic lithosphere, *Tectonophysics*, *132*, 1-35, 1986.

Bergman, E.A., and S.C. Solomon, Oceanic intraplate earthquakes: Implications for local and regional intraplate stress, *J. Geophys. Res.*, *85*, 5389-5410, 1980.

Bergman, E.A., and S.C. Solomon, Source mechanisms of earthquakes near midocean ridges from body waveform inversion: Implications for the early evolution of oceanic lithosphere, *J. Geophys. Res.*, *89*, 11,415-11,441, 1984.

Bergman, E.A., and S.C. Solomon, Earthquake source mechanisms from body waveform inversion and intraplate tectonics in the northern Indian Ocean, *Phys. Earth Planet. Inter.*, *40*, 1-23, 1985.

Butler, R., The 1973 Hawaii earthquake: A double earthquake beneath the volcano Mauna Kea, *Geophys. J.R. Astron. Soc.*, *69*, 173-186, 1982.

Byerlee, J.D., Friction of rocks, *Pure Appl. Geophys.*, *116*, 615-626, 1978.

Chinnery, M.A., The strength of the Earth's crust under horizontal shear stress, *J. Geophys. Res.*, *69*, 2085-2089, 1964.

Chopra, P.N., and M.S. Patterson, The experimental deformation of dunite, *Tectonophysics*, *42*, 75-110, 1981.

Cloetingh, S.A.P.L., and M.J.R. Wortel, Regional stress field of the Indian plate, *Geophys. Res. Lett.*, *12*, 77-80, 1985.

Cloetingh, S.A.P.L., and M.J.R. Wortel, Stress in the Indo-Australian plate, *Tectonophysics*, *132*, 49-67, 1986.

Coulomb, C.A., Sur une application des règles de Maximis et Minimis a quelques problèmes de statique relatifs à l'Architecture, *Acad. R. Sci. Mem. Math. Phys. divers savans*, *7*, 343-382, 1773.

Crough, S.T., Thermal model of oceanic lithosphere, *Nature, 256*, 388-390, 1975.
Crough, S.T., Approximate solutions for the formation of the lithosphere, *Phys. Earth. Planet. Inter., 14*, 365-377, 1977.
Dixon, J.E., E. Stolper, and J.R. Delaney, Infrared spectroscopic measurements of CO_2 and H_2O in Juan de Fuca Ridge basaltic glasses, *Earth Planet. Sci. Lett., 90*, 87-104, 1988.
Dziewonski, A.M., A. Friedman, D. Giardini, and J.H. Woodhouse, Global seismicity of 1982: Centroid moment tensor solutions for 308 earthquakes, *Phys. Earth Planet. Inter., 33*, 76-90, 1983.
Dziewonski, A.M., J.E. Franzen, and J.H. Woodhouse, Centroid moment tensor solutions for July-September, 1983, *Phys. Earth Planet. Inter., 34*, 1-8, 1984.
Dziewonski, A.M., J.E. Franzen, and J.H. Woodhouse, Centroid-moment tensor solutions for October-December 1984, *Phys. Earth Planet. Inter., 39*, 147-156, 1985.
Dziewonski, A.M., G. Ekström, J.E. Franzen, and J.H. Woodhouse, Centroid-moment tensor solutions for April-June 1986, *Phys. Earth Planet. Inter., 45*, 229-239, 1987.
Goetze, C., The mechanisms of creep in olivine, *Philos. Trans. R. Soc. London, Ser. A, 288*, 99-119, 1978.
Goetze, C., and B. Evans, Stress and temperature in the bending lithosphere as constrained by experimental rock mechanics, *Geophys. J.R. Astron. Soc., 59*, 463-478, 1979.
Griggs, D.T., and D.W. Baker, The origin of deep focus earthquakes, in *Properties of Matter Under Unusual Circumstances*, edited by H. Mark and S. Fernback, pp. 23-42, John Wiley, New York, 1968.
Haimson, B.C., and T.W. Doe, State of stress, permeability and fractures in the Precambrian granite of northern Illinois, *J. Geophys. Res., 88*, 7355-7371, 1983.
Harland, W.B., A.V. Cox, P.G. Llewellyn, C.A.G. Pickton, A.G. Smith, and R. Walters, *A Geologic Time Scale*, Cambridge University Press, New York, 1982.
Hilde, T.W., N. Isezaki, and J.M. Wageman, Mesozoic seafloor spreading in the North Pacific, in *The Geophysics of the Pacific Ocean Basin and Its Margin, Geophys. Monogr. Ser.*, vol. 19, edited by G.H. Sutton, M.H. Manghnani, and R. Moberly, pp. 205-226, AGU, Washington, D.C., 1976.
Hobbs, B.E., A. Ord, and C. Teyssier, Earthquakes in the ductile regime?, *Pure Appl. Geophys., 124*, 309-336, 1986.
Jeffreys, H., *The Earth*, Cambridge University Press, New York, 1959.
Kirby, S.H., and A.K. Kronenberg, Rheology of the lithosphere: Selected topics, *Rev. of Geophys., 25*, 1219-1244, 1987.
Larson, R.L., and C.G. Chase, Late Mesozoic evolution of the western Pacific Ocean, *Geol. Soc. Am. Bull., 83*, 3627-3643, 1972.
Larson, R.L., W.C. Pitman III, X. Golovchenko, S.C. Cande, J.F. Dewey, W.F. Haxby, and J.C. LaBreque, *The Bedrock Geology of the World*, W.H. Freeman, New York, 1985.
Lister, C.R.B., Gravitational drive on oceanic plates caused by thermal contraction, *Nature, 257*, 663-665, 1975.
Lay, T., and E.A. Okal, The Gilbert Islands (Republic of Kiribati) earthquake swarm of 1981-1983, *Phys. Earth Planet. Inter., 33*, 284-303, 1983.
McAdoo, D.C., and D.T. Sandwell, Folding of oceanic lithosphere, *J. Geophys. Res., 90*, 8563-8569, 1985.
Ogawa, M., Shear instability in a viscoelastic material as the cause of deep focus earthquakes, *J. Geophys. Res., 92*, 13,801-13,810, 1987.

Okal, E.A., Intraplate seismicity of the southern part of the Pacific plate, *J. Geophys. Res.*, *89*, 10,053-10,071, 1984.

Okal, E.A., J. Talandier, K.A. Sverdrup, and T.H. Jordan, Seismicity and tectonic stress in the south central Pacific, *J. Geophys. Res.*, *85*, 6479-6495, 1980.

Okal, E.A., D.F. Woods, and T. Lay, Intraplate deformation in the Samoa-Gilbert-Ralik area: A prelude to a change of plate boundaries in the southwest Pacific?, *Tectonophysics*, *132*, 69-77, 1986.

Orowan, E., Mechanism of seismic faulting, *Mem. Geol. Soc. Am.*, *79*, 323-345, 1960.

Parsons, B., and J.G. Sclater, An analysis of the variation of ocean floor bathymetry and heat flow with age, *J. Geophys. Res.*, *82*, 803-827, 1977.

Petroy, D.E., and D.A. Wiens, Historical seismicity and implications for diffuse plate convergence in the Northeast Indian Ocean, *J. Geophys. Res.*, *94*, 12,301-12,319, 1989.

Raleigh, C.B., and M.S. Paterson, Experimental deformation of serpentinite and its tectonic implications, *J. Geophys. Res.*, *70*, 3965-3985, 1965.

Raleigh, C.B., J.H. Healy, and J.D. Bredehoeft, Faulting and crustal stress at Rangely, Colorado, in *Flow and Fracture of Rocks, Geophys. Monogr. Ser.*, vol. 16, edited by H.C. Heard, I.Y. Borg, N.L. Carter, and C.B. Rayleigh, pp. 275-284, AGU, Washington, D.C., 1972.

Richardson, R.M., Modeling the tectonics of the Indo-Australian plate, *Eos Trans. AGU*, *68*, 1466, 1987.

Richardson, R.M., The origin of the intraplate stress field, paper presented at 28th International Geological Conference, Washington D.C., 1989.

Richardson, R.M., S.C. Solomon, and N.H. Sleep, Tectonic stress in the plates, *Rev. Geophys.*, *17*, 981-1019, 1979.

Shimamoto, T., The origin of large or great thrust-type earthquakes along subducting plate boundaries, *Tectonophysics*, *119*, 37-65, 1985.

Sibson, R.H., Frictional constraints on thrust, wrench and normal faults, *Nature*, *249*, 542-544, 1974.

Sibson, R.H., Transient discontinuities in ductile shear zones, *J. Struct. Geol.*, *2*, 165-171, 1980.

Stein, C.A., and J.K. Weissel, Constraints on the Central Indian Basin thermal structure from heat flow, seismicity, and bathymetry, *Tectonophysics*, *176*, 315-332, 1990.

Stein, C.A., S.A.P.L. Cloetingh, and M.J.R. Wortel, Seasat-derived gravity constraints on stress and deformation in the northeastern Indian Ocean, *Geophys. Res. Lett.*, *16*, 823-826, 1989.

Stein, S., Intraplate seismicity on bathymetric features: The 1968 Emperor Trough earthquake, *J. Geophys. Res.*, *84*, 4763-4768, 1979.

Stein, S., and D.A. Wiens, Depth determination for shallow teleseismic earthquakes: methods and results, *Rev. Geophys.*, *24*, 806-832, 1986.

Tse, S.T., and J.R. Rice, Crustal earthquake instability in relation to the depth variation of friction slip properties, *J. Geophys. Res.*, *91*, 9452-9472, 1986.

Tsenn, M.C., and N.L. Carter, Upper limits of power law creep of rocks, *Tectonophysics*, *136*, 1-26, 1987.

Turcotte, D.L., and G. Schubert, *Geodynamics: Applications of Continuum Physics to Geological Problems*, 448 pp., John Wiley, New York, 1982.

Unger, J.D., and P.L. Ward, A large, deep Hawaiian earthquake — The Honomu, Hawaii

event of April 26, 1973, *Bull. Seismol. Soc. Am.*, *69*, 1771-1782, 1979.
Watts, A.B., U.S. ten Brink, P. Buhl, and T.M. Bocher, A multi-channel seismic study of lithospheric flexure across the Hawaiian-Emperor seamount chain, *Nature*, *315*, 105-111, 1985.
Weissel, J.K., and R.N. Anderson, Is there a Caroline plate?, *Earth Planet. Sci. Lett.*, *41*, 143-158, 1978.
Wiens, D.A., Historical seismicity near Chagos: A complex deformation zone in the equatorial Indian Ocean, *Earth Planet. Sci. Lett.*, *76*, 350-360, 1986.
Wiens, D.A., and E.A. Okal, Tensional intraplate seismicity in the east-central Pacific, *Phys. Earth Planet. Inter.*, *49*, 264-282, 1987.
Wiens, D.A., and S. Stein, Age dependence of oceanic intraplate seismicity and implications for lithospheric evolution, *J. Geophys. Res.*, *88*, 6455-6468, 1983.
Wiens, D.A., and S. Stein, Intraplate seismicity and stresses in young oceanic lithosphere lithospheric evolution, *J. Geophys. Res.*, *89*, 11,442-11,464, 1984.
Wortel, M.J.R., Deep earthquakes and the thermal assimilation of subducting lithosphere, *Geophys. Res. Lett.*, *13*, 34-37, 1986.
Wortel, M.J.R., and S.A.P.L. Cloetingh, On the origin of the Cocos-Nazca spreading center, *Geology*, *9*, 425-430, 1981.
Wortel, M.J.R., and S.A.P.L. Cloetingh, A mechanism for fragmentation of oceanic plates, *AAPG Mem.*, *34*, 793-801, 1983.
Wortel, M.J.R., and S.A.P.L. Cloetingh, Accretion and lateral variations in tectonic structure along the Peru-Chile Trench, *Tectonophysics*, *112*, 443-462, 1985.
Wortel, M.J.R., and N.J. Vlaar, Subduction zone seismicity and the thermo-mechanical evolution of downgoing lithosphere, *Pure Appl. Geophys.*, *128*, 625-659, 1988.
Zoback, M.D., and L. Mastin, Implications of wellbore breakouts for the state of stress at mid-crustal depths in the Kola Peninsula ultradeep borehole, *Eos Trans. AGU*, *67*, 382, 1986.
Zoback, M.L., et al., Global patterns of tectonic stress, *Nature*, *341*, 291-298, 1989.
Zuber, M.T., Compression of oceanic lithosphere: An analysis of intraplate deformation in the Central Indian Basin, *J. Geophys. Res.*, *92*, 4817-4825, 1987.

Chapter 3

Extension of laterally homogeneous continental lithosphere due to inplane forces

INTRODUCTION

To study the response of continental lithosphere to various driving forces we have to consider the effect of thermal structure, boundary conditions and rheology. We employ a numerical method to solve the governing differential equations, because this allows accurate calculation of stresses, strains, temperatures, etc. in irregular, non-homogeneous and deformable bodies with non-linear rheologies. This chapter is divided into three parts. The first part covers the flow laws which are used to model the rheological behavior of lithospheric materials. It is imperative to consider the limitations of the rheological laws we adopt in our models in view of their prominent effect on the results of our modeling. The second part involves a brief description of the numerical method which is employed to solve the differential equations that govern the evolution of stresses, strains and temperatures with time. There are no analytical models available for the evolution of stresses in two-dimensional structures with rheologies which are more complex than linear elastic or linear viscous. A comparison can, however, be made with the numerical model of Kusznir [1982] in which laterally homogeneous lithosphere is subject to a constant in-plane force. This is done in the third part, which begins with a description of the approximations and approaches that are made in Kusznir's model. A comparison will be made with the results of Kusznir and Park [1987], who apply Kusznir's model to continental lithosphere. In the discussion special emphasis will be put on the relation between the numerical time step size and the extremely low viscosities in some parts of the lithosphere.

RHEOLOGY OF CONTINENTAL LITHOSPHERE

In our model calculations we approximate the rheology of the lithosphere as a combination of elastic, viscous and visco-plastic behavior (Figure 1). We will show in the next paragraph how an empirical steady-state flow law results in an effective viscosity η_{eff} and how brittle strength relates to the plastic yield criterion Y. In this paragraph we discuss the limitations and uncertainties in the underlying empirical flow laws. This discussion is far from complete; a comprehensive overview is given by Carter and Tsenn [1987]. Our purpose is to stress that empirical flow laws are only approximate descriptions of the material behavior at geological strain rates.

Accurate knowledge of the flow properties of continental rocks is hampered by three classes of sources for uncertainties. First, the chemical constitution of the lithosphere is only known to a first approximation. It is to be expected that, with time, the distribution of material heterogeneities will be revealed with seismic techniques, but, in view of the sensitivity of some rheological properties to minute amounts of inclusions (e.g. Chopra and Patterson, 1984), spatial resolution will never allow us to pinpoint the flow behavior of a volume of rock at depth.

The second class of sources for uncertainties in rheological laws includes variables that relate to physical state. These include pressure, temperature, and variables that are a function of deformation and initial "state", like grain size, dislocation density, contact surface roughness, crack tip shape, etc.. Brittle strength is first-order sensitive to the effective pressure as a function of depth, i.e. the difference between lithostatic and pore fluid pressure. The distribution of the lithostatic pressure with depth is fairly well constrained. The pore fluid pressure however depends strongly on the permeability and on the availability of a fluid phase, both of which are largely unknown. The pore fluid pressure can range from zero to superlithostatic in general. Carter and Tsenn [1987] conclude that water is generally available in the continental crust and that regions of very low effective pressures are fairly common. However, Brace and Kohlstedt [1980] conclude that the permeability in the upper 5-8 km of the continental crust is high, so that pore fluid pressures would be hydrostatic in the upper crust. Estimates of geotherms are mainly based upon model predictions, thermometry and relatively few well temperatures. These methods all have their restrictions and the derived geotherms are fairly rough estimates, especially at greater depths. Microstructural variables can be very important physical parameters. For instance, when deformation occurs by Nabarro-Herring or Coble creep, the flow stress is controlled by grain size. Order of magnitude changes in flow stress can be expected from variations in grain size. Grain sizes can range from a few centimeters to a few microns, but the actual distribution of grain size with depth is largely unknown.

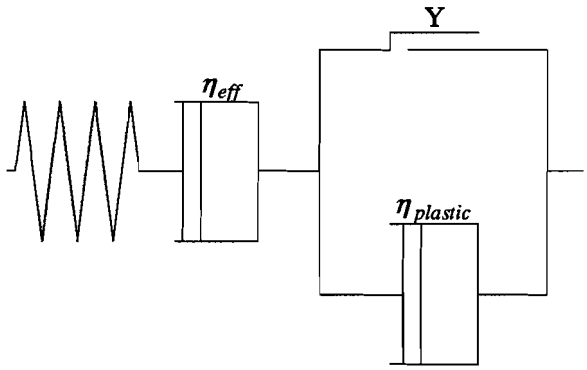

Fig. 1. *Model for the rheology of continental lithosphere.*

The third class of sources for uncertainties in the model flow laws relate to the experimental conditions. As Ranalli [1987, p.304] summarizes it: 'Problems of extrapolation are central to the application of rheology to geodynamics'. From experiments on brittle rocks at pressures up to 600 MPa ($\approx$ 20 km) and temperatures up to 200 °C, Byerlee [1978] derives a linear relation between strength and pressure. The validity of this relation below depths of 5 km is questioned by various authors (see Carter and Tsenn, 1987 and references therein). In the ductile field, flow laws derived from laboratory experiments of practical duration (i.e. strain rates $> 10^{-8}$ s^{-1}) are extrapolated to geological strain rates (typically $< 10^{-13}$ s^{-1}). Extrapolations of grainsize-sensitive flow laws suffer from an even greater uncertainty (Paterson, 1987; Carter and Tsenn, 1987). Extrapolation of brittle and ductile flow laws gives a "brittle-ductile transition" depth at which very high stresses can be supported. The brittle-transition peak is considered te be an artefact by many authors (Carter and Kirby, 1978; Kirby, 1983; Scholz, 1988); exhumed rocks deformed in a brittle-transition zone show evidence for concurrent brittle and ductile deformation. Despite the importance of these zones, where most of the lithospheric stresses are supported, quantitative relations for the semi-brittle and low-temperature semi-ductile fields are not available.

In summary, the chemical and physical conditions in the lithosphere are only roughly known. As a result, there are large discrepancies between flow laws for the upper crust, the lower crust and mantle. The empirical flow laws we use as a basis for our model calculations are approximate descriptions of the material behavior at geological strain rates.

FINITE ELEMENT APPROACH

Governing equations

In most tectonic problems accelerations can be neglected, and the mechanical equilibrium equations govern the motion of particles in a continuous body

$$\nabla \cdot \boldsymbol{\sigma} + \rho \boldsymbol{X} = 0 \tag{1}$$

where $\boldsymbol{\sigma}$ is the Cauchy stress tensor, ρ mass density and X body force (see the list of symbols at the end of this thesis). Equations (1) can be rewritten in a more suitable form, when supplemented with the constitutive equations. We model the rheology of the lithosphere as a combination of elasto-visco-plasticity and non-linear visco-elasticity (Figure 1)

$$\dot{\boldsymbol{\varepsilon}} = \boldsymbol{D}^{-1}\dot{\boldsymbol{\sigma}} + \boldsymbol{V}\boldsymbol{\sigma} + \boldsymbol{P}\boldsymbol{\sigma} \tag{2}$$

A dot indicates a derivative with respect to time, $\dot{\boldsymbol{\varepsilon}}$ is the strain rate tensor, $\boldsymbol{D}$ the elasticity tensor, which is a function of the Young's modulus E and Poisson's ratio ν (Jaeger and Cook, 1976), $\boldsymbol{V}$ the viscosity matrix, which is a function of the effective viscosity η_{eff} and $\boldsymbol{P}$ is the plastic viscosity matrix, which depends on the brittle strength. The effective viscosity of rocks is strongly temperature controlled (Goetze, 1978), so that the system of partial differential equations (1)-(2) needs to be supplemented with the heat equation

$$\rho C_p \frac{\partial T}{\partial t} = \nabla \cdot (\boldsymbol{k}\nabla T) + H + \boldsymbol{\sigma} \cdot \dot{\boldsymbol{\varepsilon}} \tag{3}$$

where C_p is the specific heat at constant pressure, T is temperature, t time, $\boldsymbol{k}$ the conductivity tensor and H the heat production per unit volume. The terms on the right hand side of (3) depend on geometry, so that the system of equations (1)-(3) is fully coupled. In most tectonic problems, however, equations (1)-(2) and (3) can be solved sequentially as changes in geometry and temperature are small on time scales of the order of thousands of years. It is clear that the time step size in the numerical solution of the system of partial differential equations (1)-(3) needs to be small enough to satisfy this "uncoupling" requirement.

The finite element method of solution is selected, since it allows accurate calculation of stresses, strains, temperatures, etc. in irregular, non-homogeneous and deformable bodies with complex and non-linear rheologies. An extensive body of literature exists on the finite element method for the mechanical equilibrium and heat equations. Zienkiewicz [1977] and Desai and Abel [1972] give an excellent introduction to the finite element method. We have employed the TECTON finite element program (Melosh and Raefsky, 1980) for the solution of the mechanical equi-

librium equations. This program was extended to solve the heat equation in two dimensions.

The mechanical equilibrium equation is solved by minimizing the potential energy functional that is related to equations (1). A displacement method is used to establish the finite element equations. Displacement shape functions are linear in isoparametric quadrilateral and triangular elements, so that stresses and strains are constant in each element. The solution to the elasto-visco-plastic and non-linear visco-elastic creep is achieved by an implicit (tangential) algorithm (Hughes and Taylor, 1978; Melosh and Raefsky, 1980). In the Appendix we discuss the relation between time step size and stability, accuracy and oscillation limit for this algorithm.

For solution of the heat equation we select linear shape functions for nodal temperatures. Temperature solutions are forwarded with time through an implicit algorithm.

Gravity and isostatic rebound forces

McGarr [1988] argues that a hydrostatic stress is the only likely stress state in the absence of applied tectonic forces. Numerical experiments by Braun [1988] indicate that the tectonic history of continental lithosphere determines its state of stress even after hundreds of million years (Ma). The nature and the duration of a particular tectonic event both have impact on the state of stress. Long or repeated phases of tectonic activity facilitate the achievement of an equilibrium hydrostatic stress state. The best estimate that can be made for the state of stress prior to a new tectonic event is to assume an equilibrium hydrostatic stress.

The hydrostatic stress in most of the continental lithosphere is larger in magnitude than the deviatoric stresses that drive deformation. It seems therefore reasonable to remove the hydrostatic pressure from equations (1). In the "density-stripping" method (Braun, 1988; Williams and Richardson, 1991) the hydrostatic pressure $\rho g d$ (gravitational acceleration g, depth d) is replaced by restoring pressures at compositional boundaries. Braun [1988] shows that removing the hydrostatic pressure from the equilibrium equations is equivalent to making the equations homogeneous. Consider a situation (Figure 2) where $Z=0$ is the original horizontal interface between two halfspaces of constant density, ρ_1 and ρ_2. The original configuration is assumed to be in equilibrium. The interface is deformed to new configuration z. Let capitals $\boldsymbol{X}=(X, Y, Z)$ describe the original coordinates and $\boldsymbol{x}=(x, y, z)$ the final, deformed configuration. If we assume plane strain conditions, the equations of static equilibrium (1) in the deformed configuration are

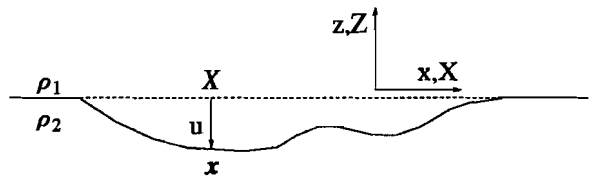

Fig. 2. *A flat surface separates two half spaces with constant densities, ρ_1 and ρ_2. This surface is displaced by an amount u from its initial position $\boldsymbol{x}$ to a final position $\boldsymbol{X}$.*

$$\begin{aligned}
\frac{\partial \sigma_{xx}}{\partial x} + \frac{\partial \sigma_{xz}}{\partial z} &= 0 \\
\frac{\partial \sigma_{yy}}{\partial y} &= 0 \\
\frac{\partial \sigma_{zz}}{\partial z} + \frac{\partial \sigma_{xz}}{\partial x} &= -\rho_1 g H(Z) - \rho_2 g H(-Z)
\end{aligned}$$

where $H(Z)$ is the Heavyside function. The body force works to restore the original equilibrium situation. We require continuity of the normal stress through the boundary $Z = 0$:

$$\sigma_n(Z = 0^+) = \sigma_n(Z = 0^-)$$

which is equivalent to continuity of the vertical stress if the interface slope is hardly changed by deformation (i.e. $|du/dx| \ll 1$):

$$\sigma_{zz}(Z = 0^+) = \sigma_{zz}(Z = 0^-)$$

Define a new stress tensor $\bar{\sigma}$:

$$\bar{\sigma}_{ij} = \sigma_{ij} + \rho_1 g z H(Z)\delta_{ij} + \rho_2 g z H(-Z)\delta_{ij}$$

where $\boldsymbol{\delta}$ is the Kronecker delta function. With the new definition of the stress tensor the equilibrium equations become homogeneous:

$$\begin{aligned}
\frac{\partial \bar{\sigma}_{xx}}{\partial x} + \frac{\partial \bar{\sigma}_{xz}}{\partial z} &= 0 \\
\frac{\partial \bar{\sigma}_{yy}}{\partial y} &= 0 \\
\frac{\partial \bar{\sigma}_{zz}}{\partial z} + \frac{\partial \bar{\sigma}_{xz}}{\partial x} &= 0
\end{aligned}$$

The continuity condition becomes

$$\bar{\sigma}_n(Z = 0^+) - \rho_1 g z|_{Z=0^+} = \bar{\sigma}_n(Z = 0^-) - \rho_2 g z|_{Z=0^-}$$

or

$$\bar{\sigma}_n(Z = 0^+) = \bar{\sigma}_n(Z = 0^-) - (\rho_2 - \rho_1) g u$$

because $z|_{Z=0^+} = z|_{Z=0^-} = u$. It can be shown that the constitutive equations still hold for the newly defined stress tensor $\bar{\sigma}$. In the last equation we observe the restoring stress that is to be applied to a density contrast surface that is displaced over a vertical distance u. Forces equivalent to displacement can very conveniently be incorporated in a finite element procedure. This is done by adding vertical elastic springs along density interfaces, which comes down to modifying diagonal elements of the stiffness matrix (see Williams and Richardson [1991] for a very elaborate description of this procedure).

In this very simple model we did not consider the effect of body forces arising from density changes. Density changes can result from local heating, chemical reactions or phase transitions. These body forces are perturbations of the hydrostatic field and can therefore be incorporated in the model as real body forces without leading to unstable results (Braun, 1988). In the next section we show how we calculate the body force contribution from a change in temperature.

If the slope of a density interface does not change very much as a result of deformation, the density stripping method is a good approximation to a full stress description. As it is assumed that initially the whole lithosphere is in hydrostatic equilibrium, the restoring pressures relate to the initial depth of a density interface. Modeling a thickened lithosphere that has not reached this equilibrium state requires the use of additional forces.

Thermo-mechanical coupling forces

Loads resulting from density changes due to thermal expansion and thermal stresses need to be added as body forces in the mechanical equation. The body force resulting from a change in density is

$$g \int_{V_e} \alpha \rho \Delta T \, dV_e$$

(volumetric expansion coefficient α, element volume V_e). Pressure variations due to thermal expansion (thermal stresses) are calculated from

$$\int_{V_e} \boldsymbol{B}^T \boldsymbol{D} \Delta \boldsymbol{\varepsilon} \, dV_e$$

$\boldsymbol{B}^T$ is the transpose of the matrix relating strain and displacements, $\boldsymbol{\varepsilon}$ denotes strain.

$$\Delta \boldsymbol{\varepsilon} = (\Delta \varepsilon_{xx} \;\; \Delta \varepsilon_{zz} \;\; \Delta \varepsilon_{xz}) = \alpha \Delta T (1 \; 1 \; 0)$$

Constitutive equations for elasto-viscous creep

In the plane strain approximation, the constitutive equations for nonlinear elasto-viscous creep can be written

$$\begin{aligned}
\dot{\varepsilon}_{xx} &= \frac{(1+\nu)}{E}[(1-\nu)\dot{\sigma}_{xx} - \nu\dot{\sigma}_{zz}] + \frac{(\sigma_E/\eta_{eff})^{n-1}}{4\eta_{eff}}[\sigma_{xx} - \sigma_{zz}] \\
\dot{\varepsilon}_{zz} &= \frac{(1+\nu)}{E}[(1-\nu)\dot{\sigma}_{zz} - \nu\dot{\sigma}_{xx}] - \frac{(\sigma_E/\eta_{eff})^{n-1}}{4\eta_{eff}}[\sigma_{xx} - \sigma_{zz}] \\
\dot{\varepsilon}_{xz} &= \frac{(1+\nu)}{E}\dot{\sigma}_{xz} + \frac{(\sigma_E/\eta_{eff})^{n-1}}{2\eta_{eff}}\sigma_{xz}
\end{aligned} \tag{4}$$

or, in shorthand

$$\dot{\boldsymbol{\varepsilon}} = \boldsymbol{D}^{-1}\dot{\boldsymbol{\sigma}} + \dot{\boldsymbol{\varepsilon}}^{vp}$$

power n, visco-plastic strain rate $\dot{\boldsymbol{\varepsilon}}^{vp}$, and the effective shear stress (Ranalli, 1987);

$$\sigma_E = \left(\frac{1}{2}\sigma'_{ij}\sigma'_{ij}\right)^{\frac{1}{2}} = \left[\left(\frac{\sigma_{xx} - \sigma_{zz}}{2}\right)^2 + \sigma_{xz}^2\right]^{\frac{1}{2}}$$

(primes denote deviatoric tensor).

Effective viscosities in (4) will be selected on the basis of empirical steady state flow laws derived from laboratory experiments. Typically, a uniaxial shortening experiment on a cylindrical sample results in a flow law

$$\dot{\varepsilon}_1 = A(\sigma_1 - \sigma_2)^n \exp\left(-\frac{Q_{pl}}{RT}\right)$$

with experimental pre-exponent A, power law activation energy Q_{pl} and universal

gas constant R. In our finite element models, stresses and strain rates are not uniaxial, so we need to translate the experimental result to a law that is valid for more general stresses and strain rates. The resulting flow law should reflect the mechanical properties of the material and should therefore be insensitive to coordinate transformation. As a consequence, the general flow law will be expressed in terms of invariants of the stress and strain rate tensors. We assume that the material is incompressible and that the mechanical properties of the sample are isotropic. Assuming incompressibility is another way of saying that a purely isotropic stress does not induce ductile flow. This assumption is supported by experimental results. Experiments on single crystals (e.g. Durham and Goetze, 1977; Darot and Gueguen, 1981) indicate that the mechanical behavior of individual minerals can be anisotropic. Experiments performed on rock samples with sizes that are large compared to the grain size of the rock forming minerals will average out crystal anisotropy if the minerals don't have a strong preferred orientation. Preferred orientation developing during deformation can induce mechanical anisotropy, but this effect is typically limited to a factor of 10 in strain rate (Franssen and Spiers, 1990). The generalized law that relates deviatoric strain rate components with stress components that follows from this specific experimental setup is

$$\dot{\varepsilon}_{ij} = A_{pl} \exp\left(-\frac{Q_{pl}}{RT}\right)\sigma_E^{n-1} \qquad A_{pl} = 3^{\frac{1+n}{2}} \cdot \frac{1}{2} \cdot A$$

By comparing the elasto-viscous strain rates in (4) with the above expression we arrive at

$$\eta_{eff} = (2A_{pl})^{-1/n} \exp\left(\frac{Q_{pl}}{nRT}\right)$$

Time behavior of non-Newtonian flow

In the previous paragraph we derived an expression for the effective viscosity in the non-linear stress-strain rate equations (4). To appreciate the difference between Newtonian and non-linear viscosities it is useful to investigate the time behavior for a simple experiment. We will derive a time constant for relaxation of a step displacement in a way that is similar to Melosh and Raefsky [1983].

For a material deforming by plane strain, the elastic strain due to a step displacement at $t = 0$ is

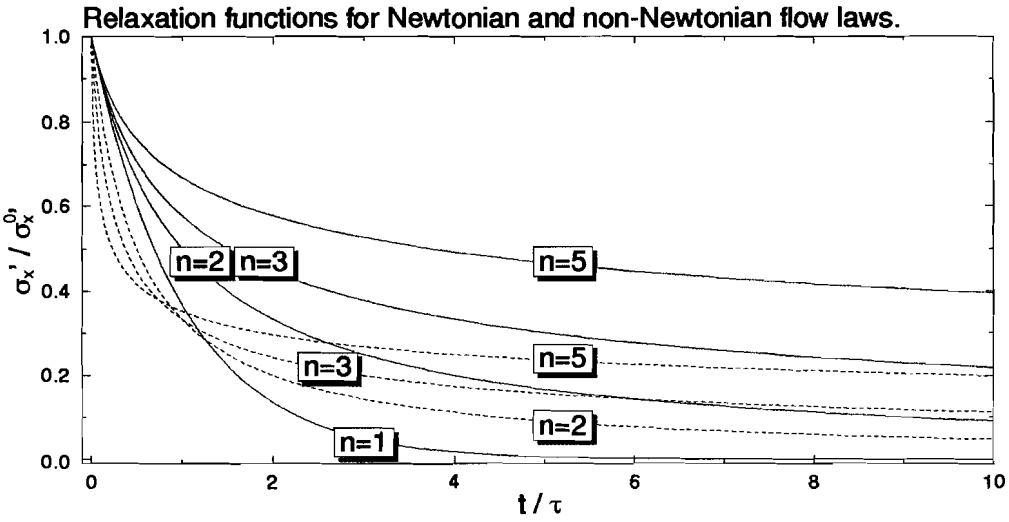

Fig. 3. *Characteristic stress decay behavior for various non-linear rheologies.*

$$\varepsilon_{xx} = \frac{1+\nu}{E}\left[(1-\nu)\sigma^0_{xx} - \nu\sigma^0_{zz}\right]$$
$$\varepsilon_{zz} = \frac{1+\nu}{E}\left[(1-\nu)\sigma^0_{zz} - \nu\sigma^0_{xx}\right]$$
$$\varepsilon_{xz} = \frac{1+\nu}{E}\,\sigma^0_{xz}$$

(initial stresses σ^0_{xx}, σ^0_{zz} and σ^0_{xz}). At $t>0$ the total strain rates (the sum of elastic and visco-plastic strain rates)

$$\dot{\varepsilon}^t_{ij} = \dot{\varepsilon}^e_{ij} + \dot{\varepsilon}^{vp}_{ij}$$

are approximately zero, as the decrease in the elastic stored energy with time is approximately equal to the total dissipation due to permanent strain deformation mechanisms. Therefore, at later times

$$0 = \frac{1+\nu}{E}\left[(1-\nu)\dot{\sigma}_{xx} - \nu\dot{\sigma}_{zz}\right] + \frac{(\sigma_E/\eta_E)^{n-1}}{4\eta_E}(\sigma_{xx} - \sigma_{zz})$$

$$0 = \frac{1+\nu}{E}\left[(1-\nu)\dot{\sigma}_{zz} - \nu\dot{\sigma}_{xx}\right] - \frac{(\sigma_E/\eta_E)^{n-1}}{4\eta_E}(\sigma_{xx} - \sigma_{zz})$$

$$0 = \frac{1+\nu}{E}\dot{\sigma}_{xz} + \frac{(\sigma_E/\eta_E)^{n-1}}{2\eta_E}\sigma_{xz}$$

The differential equations can solved by standard techniques, giving for $n > 1$

$$\left.\begin{aligned}\sigma'_{xx} &= \sigma^0_{xx}\left(\frac{t}{\tau_n}(n-1)+1\right)^{\frac{-1}{n-1}}\\ \sigma'_{xz} &= \sigma^0_{xz}\left(\frac{t}{\tau_n}(n-1)+1\right)^{\frac{-1}{n-1}}\end{aligned}\right\} \quad \tau_n = \frac{2(1+\nu)\eta_E^n}{E(\sigma_E^0)^{n-1}}$$

(σ_E^0 is the effective shear stress at $t = 0$, τ_n the non-Newtonian relaxation time). For comparison, in the Newtonian case, stresses decrease by an exponential law with relaxation time τ:

$$\left.\begin{aligned}\sigma'_{xx} &= \sigma^0_{xx}\exp\left(\frac{-t}{\tau}\right)\\ \sigma'_{xz} &= \sigma^0_{xz}\exp\left(\frac{-t}{\tau}\right)\end{aligned}\right\} \quad \tau = \frac{2(1+\nu)\eta}{E}$$

The relaxation behavior for the Newtonian and the non-linear rheology can be described as the initial stress times a time function. Figure 3 displays time characteristics for various stress exponents. Solid curves show the time behavior for $\tau_n = \tau$, i.e. $\eta = \eta_E/(\sigma_E/\eta_E)^{n-1}$. The dashed curves in Figure 3 show the effect of doubling the initial stress. The behavior displayed in the dashed curves is typical for realistic parameter values. In comparison with the Newtonian case, the stress drop shortly after $t = 0$ is larger in the nonlinear case, but at a few times the relaxation time the Newtonian stress residue is much smaller than in the non-linear case. This effect becomes stronger with increasing power n.

Brittle strength

At low pressure and temperature, rocks deform by brittle failure and slip on discrete faults. Brittle behavior is approximated by continuum deformation by elasto-visco-plastic flow of a Von Mises material. Viscous flow thus occurs if, at some depth, the stress exceeds the local yield strength criterion Y, which is defined by

$$Y = \sigma_E^2 + f \cdot p$$

(pressure p; the pressure is assumed to be insensitive to tectonic driving stresses). The parameter f -which has the dimension of stress- is selected so that the brittle strength is that of Byerlee [1978], modified to include a hydrostatic pore fluid pressure. The rate of viscous flow after the yield strength has been exceeded is controlled by the viscosity $\eta_{plastic}$ (Fig. 1). Experiments with $\eta_{plastic}$ indicate that its exact value is unimportant as long as it is selected at the lower end of the range of viscosities η_{eff} that are used to model power law flow in the rest of the model. In fact, modeling brittle deformation as elasto-visco-plastic and not as elasto-plastic was selected for programming convenience; the difference between the two approaches disappears with decreasing viscosity $\eta_{plastic}$.

BENCH MARK: IN-PLANE EXTENSION OF CONTINENTAL LITHOSPHERE

No analytical models are available for non-homogeneous models with non-linear rheologies to compare the results of the finite element procedures with. A comparison can however be made with a model derived by Kusznir [1982] for calculating the stress distribution with depth and time in lithosphere that is subject to an in-plane force. Kusznir and Park [1987] apply this model to continental lithosphere in extension. We show results of a finite element model that is designed to mimic a model of Kusznir and Park [1987].

The approach Kusznir [1982] makes in his model and the approximations that are involved will first be discussed. Next, we show that the accuracy of the finite element results degrades as a result of very low viscosity layers in the continental lithosphere. The overall accuracy can be improved by putting a lower limit to the viscosities. Differences between the finite element result and the result of Kusznir and Park [1987] are discussed. The model of Kusznir [1982] basically is one-dimensional. In the last section we investigate the validity of his model in a two-dimensional geometry. The rationale for doing this is that the assumptions made by Kusznir do not allow vertical gradients in strain, a basic requirement for lithosphere scale faults to be operative. As such, the last section can be regarded as a step to the next chapters, where we investigate conditions for initiation of lithosphere scale detachment surfaces.

The Kusznir model

In the model of Kusznir [1982] a horizontal force F_x is applied uniformly in the horizontal x-direction (y is the perpendicular horizontal direction, z depth) This force is kept constant with time, i.e.

$$\int_0^L \sigma_x \mathrm{d}z = F_x = \text{constant}$$

(lithospheric thickness L) Differentiation with respect to time gives

$$\sigma_x(L,t)\frac{\partial L}{\partial t} + \int_0^{L(t)} \frac{\partial \sigma_x}{\partial t}\,\mathrm{d}z = 0$$

At this point several assumptions are introduced:

1. The lithospheric thickness L does not vary with time. As a result of this, the above equation reduces to

$$\int_0^L \dot{\sigma}_x \mathrm{d}z = 0$$

2. The total horizontal strain rate is uniform with depth.
3. It is assumed that no strain occurs in the y-direction (plane strain) and
4. that the vertical stress arising from the applied force is zero (plane stress).

Finally, Kusznir [1982] arrives at equations for the temporal and spatial variations of stress

$$\sigma_x = \int_0^t \left(\frac{1}{L} \int_0^L \frac{E}{(1-\nu^2)} \frac{\sigma_x(2-\nu) - \sigma_y(1-2\nu)}{6\eta_{eff}} \mathrm{d}z \right) \mathrm{d}t' - \frac{1}{L} \int_0^L \sigma_x^0 \cdot \mathrm{d}z + \sigma_x^0$$

$$\sigma_y = \int_0^t \left(\nu\dot{\sigma}_x - E\frac{(2\sigma_y - \sigma_x)}{6\eta_{eff}} \right) \mathrm{d}t' + \sigma_y^0 - \nu\sigma_x^0$$

where $\sigma_x^0 = \sigma_x(t=0)$ and $\sigma_y^0 = \sigma_y(t=0)$. These equations are solved with a finite difference method by Kusznir.

The second assumption, that the total horizontal strain rate is uniform with depth, is not obvious. Imagine a two-dimensional model of a cross-section of a lithospheric plate. The model has a large horizontal extent and in-plane forces of equal magnitude pull on the plate boundaries. For symmetry reasons the horizontal strain rate in the vertical center of the model, midway the two end loads, needs to be constant with depth. Away from the symmetry center, however, it is not clear *a*

priori how the horizontal strain rate behaves. Kusznir [1982] motivates this assumption stating that the lithospheric layers are "welded together". We will address this point again in the last section.

Conceptually a uniform, constant in-plane force is difficult to establish exactly in a finite element procedure; At each time step the stresses in a column are integrated with depth to 'measure' the force. As long as the geotherm of the lithosphere is stable and deformation is small, we are measuring the relaxation of the end load. If stress relaxation has occurred, one can opt for re-loading to the required level in a uniform manner, consistent with the initial uniform loading condition. Alternatively, one can restore the uniform force by adding a load proportional to the amount of relaxation has that has occurred. The first option leads to smaller changes of the horizontal strain rate with depth than the second.

Another problem related to maintaining a constant in-plane force is that changes in temperature and deformation lead to additional horizontal force contributions that cannot easily be separated from the in-plane force component. Monitoring the in-plane force in a part of the model that is relatively stable is the most simple solution to this.

The plane strain assumption in the model of Kusznir [1982] is a classical one in geology and geophysics and applies well to structures that have a very long and relatively constant y-dimension. The plane stress assumption is typically used for plate-like structures. Here the argument is typically that the vertical stresses at the top and bottom of the plate disappear and can therefore not be very large in the interior. Note, however, that thinning of a 100 km thick lithospheric plate by 1% can cause buoyancy forces equivalent to 30 MPa deviatoric vertical stress. The assumption of no vertical stress is therefore only valid if deformation is very small.

Extension model 1

Figure 4 shows the finite element grid and the initial steady-state geotherm of Model 1. The thermal structure remains constant over the 10 Ma modeling time. Table 1 lists the rheological and thermal properties of the model. A uniform force of 10^{12} Nm^{-1} is built up in the first 10 years. The horizontal deviatoric stresses near the symmetry center of the model ($x=0$) are integrated to monitor the net horizontal force at each time step and, if necessary, the force is updated by adding a uniform load. Deviations of the horizontal force remain within 0.1 %.

Figure 5 displays the horizontal stress σ_x, strain rate $\dot{\varepsilon}_x$, the ratio of the time step size at the oscillation limit Δt_{Osc} to the actual time step size, and the ratio of the time step size that is required for a modal accuracy of 1%, Δt_{Acc}, to the actual time step size. These quantities are measured near the symmetry axis of the model. The time step sizes in this model are $\Delta t = 1$ year (yr) for $t \in [0, 10^3$ yr], $\Delta t = 10$ yr for t

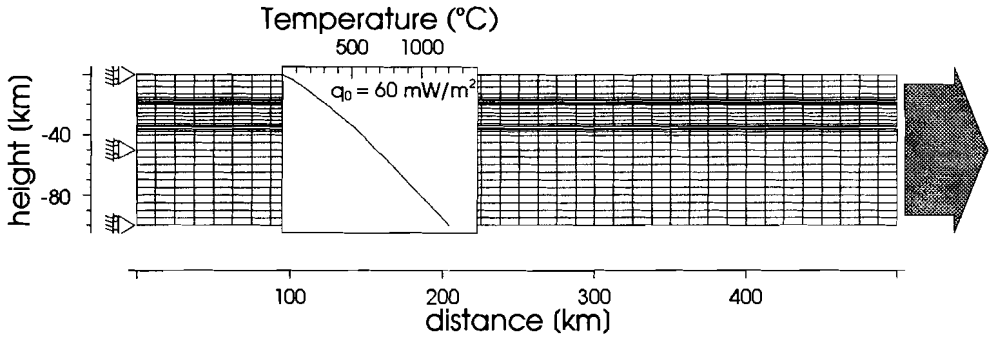

Fig. 4. *Mesh definition, mechanical boundary conditions and initial geotherm for continental extension models*

Table 1a. Rheological data.

		n	Q_{pl} kJ/mole	A_{pl} $Pa^{-n}s^{-1}$
Upper crust	Wet quartzite[1)]	2.44	159.8	$4.3562 \cdot 10^{-19}$
Lower crust	Plagioclase[2)]	3.2	238.5	$1.0348 \cdot 10^{-22}$
Mantle	Dry olivine[3)]	3	440.9	$3.15 \cdot 10^{-13}$

[1)] Koch et al. [1980], [2)] Shelton and Tullis [1981],
[3)] Goetze [1978] (modified, see text).

Table 1b. Thermal data.

	H $\mu W/m^2$	$k_x = k_z$ $W/m/K$	C_p $m^2/s^2/K$	α K^{-1}
Upper 8 km of crust	3	2.5	1300	$3.2 \cdot 10^{-5}$
Rest of Upper crust	0.25	2.5	1300	$3.2 \cdot 10^{-5}$
Lower crust	0.1	2.5	1300	$3.2 \cdot 10^{-5}$
Mantle	0	3.2	1300	$3.2 \cdot 10^{-5}$

$\in (10^3$ yr, 10^4 yr], $\Delta t = 100$ yr for $t \in (10^4$ yr, 0.1 million year], $\Delta t = 1000$ yr for $t \in$ (0.1 Ma, 1 Ma], and $\Delta t = 10^4$ yr for $t \in$ (1 Ma, 10 Ma].

At $t = 10^3$ yr the initially uniform force has redistributed by viscous flow in the most fluid layers in the lowermost part of the lithosphere. As the horizontal instantaneous total strain rate is measured near the symmetry axis of the model it is ex-

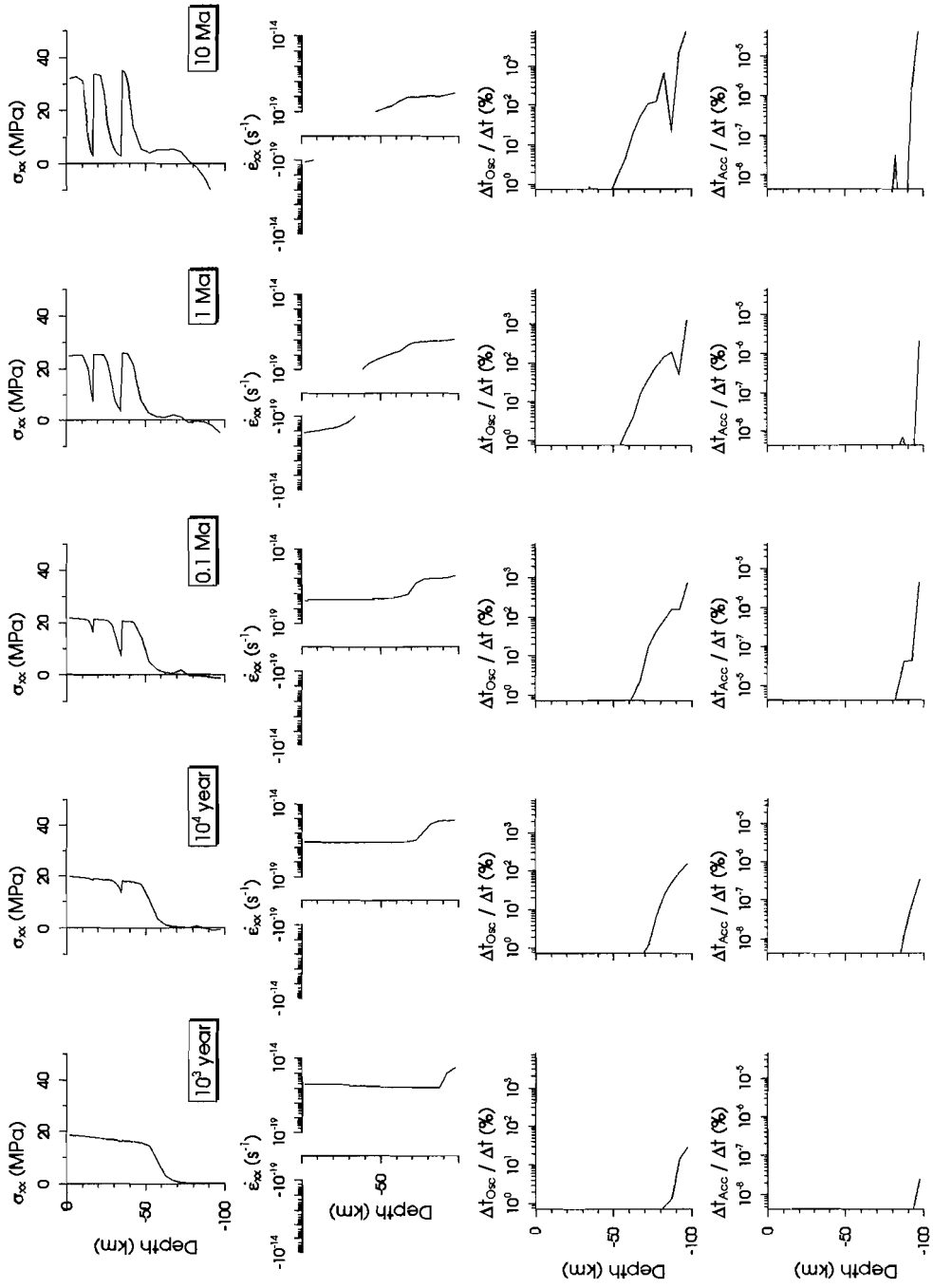
10³ year
10⁴ year
0.1 Ma
1 Ma
10 Ma
σxx (MPa)
0
20
40
Depth (km)
0
-50
-100
ε̇xx (s⁻¹)
-10⁻¹⁴
-10⁻¹⁹
10⁻¹⁹
10⁻¹⁴
Δt_Osc / Δt (%)
10⁰ 10¹ 10² 10³
Δt_Acc / Δt (%)
10⁻⁸ 10⁻⁷ 10⁻⁶ 10⁻⁵
10⁻⁵ 10⁻⁷ 10⁻⁶ 10⁻⁵

Fig. 5. *Extension model 1. Each column displays (from top to bottom) the horizontal stress, horizontal strain rate, oscillation limit percentage and the modal error percentage at a specific time.*

---

pected not to vary with depth. Clearly, this is not the case; in the most fluid layers the strain rate is about 1-2 orders of magnitudes higher than in the rest of the model. Here the oscillation limit ratio is greater than 100%, i.e. the time step size taken in the modeling is greater than that was required for oscillatory behavior not to occur. The modal error percentage stays well below 10^{-4} and is therefore not a problem.

An important observation can be made from the results at $t = 10^3$ yr. In our calculations we use a Crank-Nicholson (implicit) time marching scheme to forward the mechanical solutions in time. It was shown by Cormeau [1975] that this algorithm is stable at all time step sizes. From our result it is clear, however, that stability of the time marching scheme does not mean that the results are accurate. Some notion of the accuracy at a particular step size is required. The oscillation limit and modal error will prove to be important tools in judging the accuracy of the model results.

At $t = 10^4$ yr, 0.1 Ma, 1 Ma and 10 Ma the horizontal stress redistributes further, and the rheological layering of the lithosphere becomes apparent as the classical Christmas-tree stress profile emerges. At $t = 10$ Ma a bulge in the lower half of the stress profile has shown up, although the material viscosity is very low here. This is, again, the result of cumulative inaccuracies at the highest modes, as may be clear from inspecting the corresponding oscillation percentage figure (note that we are showing the *instantaneous* time step limit percentages). Although we might not be very much interested in these very fluid layers from a geophysical point of view, as there is virtually no stress supported there, inaccuracies in these layers do in fact decrease the stresses in the more viscous layers in which we would like to have accurate results.

Making the numerical time step size smaller is one way of increasing the accuracy. Apart from giving practical problems with the large amount of computer time that would be required, this is also not a very appealing method; it would give more accurate results in a part of the model that is most affected by interaction with the mantle, which we do not model anyway. As there is no point in modeling the deformation of these layers very accurately as long as processes in the mantle are not taken into account, we set a lower limit to the viscosity in the most fluid layers to get more accurate results in the regions we are interested in. Effectively, the strains in the lowest part of the lithosphere will be underestimated, but, as a result of im-

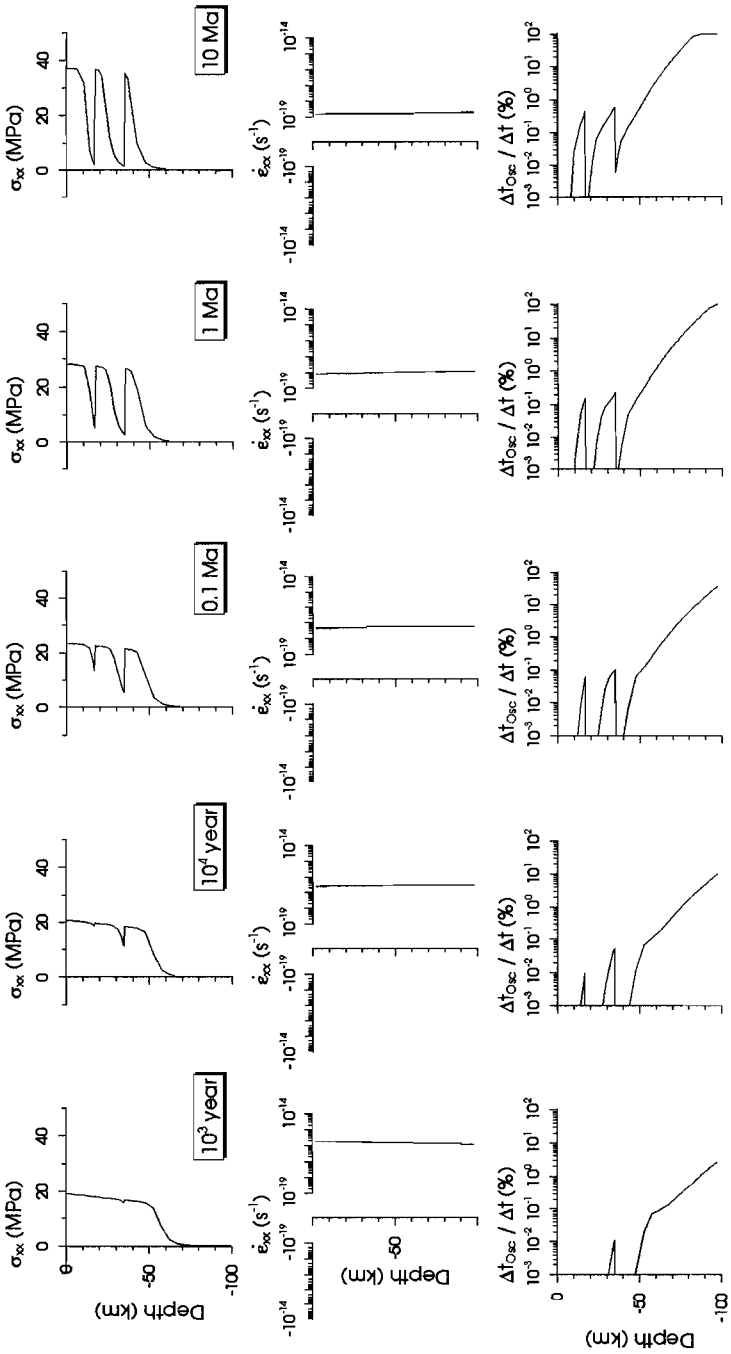
10 Ma
1 Ma
0.1 Ma
10⁴ year
10³ year
σxx (MPa)
ε̇xx (s⁻¹)
Δt_Osc / Δt (%)
Depth (km)

Fig. 6. *Extension model 2. Each column displays (from top to bottom) the horizontal stress, horizontal strain rate and oscillation limit percentage at a specific time.*

proved accuracy, the predicted stresses will be low. The viscosity minimum will be estimated from the time step size via the relations we derived in the Appendix for the oscillation limit and modal error. In our models we check the influence on the results of using a viscosity minimum by decreasing the time step size.

Extension model 2

In the next model we retain all the parameter values of the previous model, with the exception that we put a lower limit to viscosities as discussed above. Figure 6 shows horizontal stress, strain rate and time step variables at the symmetry axis. The overall pattern of development of the stress envelope (solid lines in the Figure) is similar to that of Figure 5. However, the 'mantle stress bulge' in the lower half of the model does not develop, and the peak stress in especially the upper crust is higher. Strain rates are constant in that part of the model where the oscillation limit ratio stays below 10%; we interpret that this is the part of the model where the results are accurate. Experiments indicate that it is very well possible to get constant strain rates with depth by increasing the lower viscosity limit, i.e. by decreasing the range of viscosities and making the model stiffer. This will, however, increase the stress bearing capacity of the lower lithosphere, so that the peak stresses in the crust and mantle directly beneath the Moho decrease. The criteria for the minimum viscosity carefully balance between too small minimum viscosities and too large viscosities, both which give more inaccurate results in the stronger parts of the lithosphere in which we are interested.

In Figure 7 the evolution of the horizontal stress as a function of depth is shown. The results of Kusznir and Park [1987] are indicated by fat solid lines. Thin lines with box and circle symbols are the results of our finite element modeling, without and with isostatic restoring forces respectively. In most of the lithosphere the results are approximately the same, except for the mantle region from the Moho to 60 km depth.

We have performed a few tests to explain this discrepancy; reducing the time step size to decrease the minimum viscosity and increasing the mesh density. None of these gave different results.

Next, we investigate if the assumptions made by Kusznir [1982] in the formulation of the model cause the discrepancy. One of the assumptions is that the vertical stress σ_z is zero. From the finite element results we find that indeed vertical stresses are very small (< 0.25 MPa), even if we include isostatic rebound forces. There-

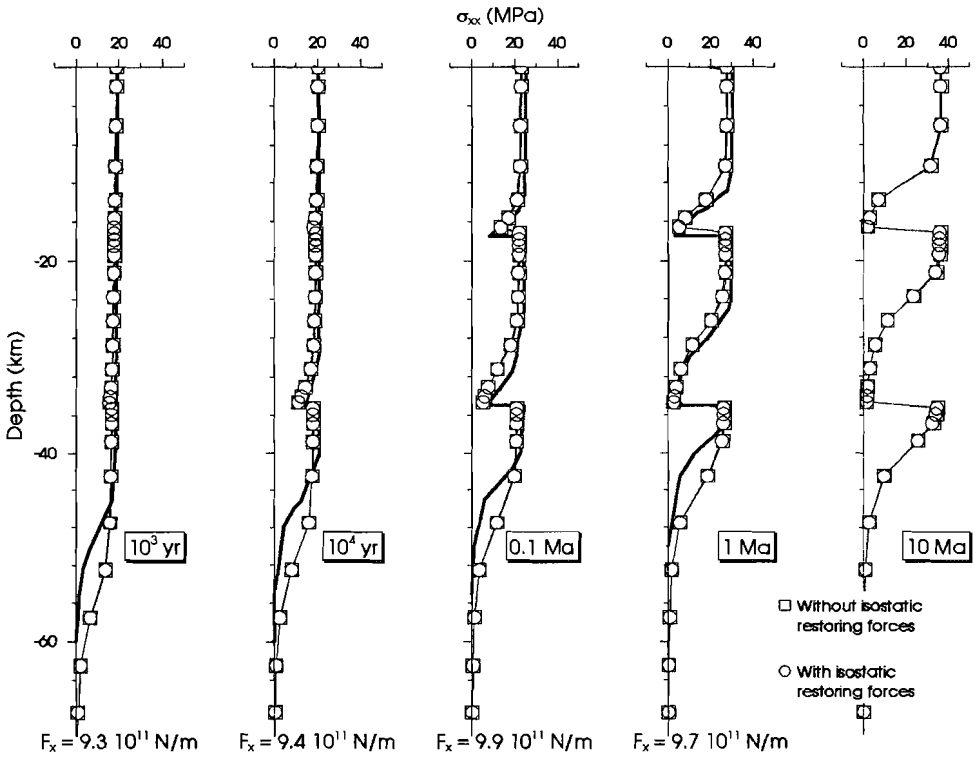

Fig. 7. *Comparison between Extension model 2, with and without isostatic restoring forces, and the results of Kusznir and Park [1987]. F_x is the total horizontal force derived from the results of Kusznir and Park.*

fore, this assumption is not violated in our models. One other assumption made by Kusznir, that the in-plane force F_x is constant, is investigated in Figure 7. Integrating the stress profiles of Kusznir and Park [1987] with depth we calculate the F_x at each time step. We observe that the actual horizontal force is always less than 10^{12} N/m, up to 7% at 1000 year.

Another source for discrepancies could obviously be parameter values that are different. As relaxation of stresses is quicker in the mantle part of the lithosphere of their models, possible candidates would be a higher geothermal gradient and different rheological parameters. In their model Kusznir and Park incorporate a change in the rheological law to a "Dorn creep" description above a transition stress of 200 MPa. It is clear from Figure 7 that 200 MPa stresses never occur in their model, so this cannot be the cause of their less viscous mantle. The activation

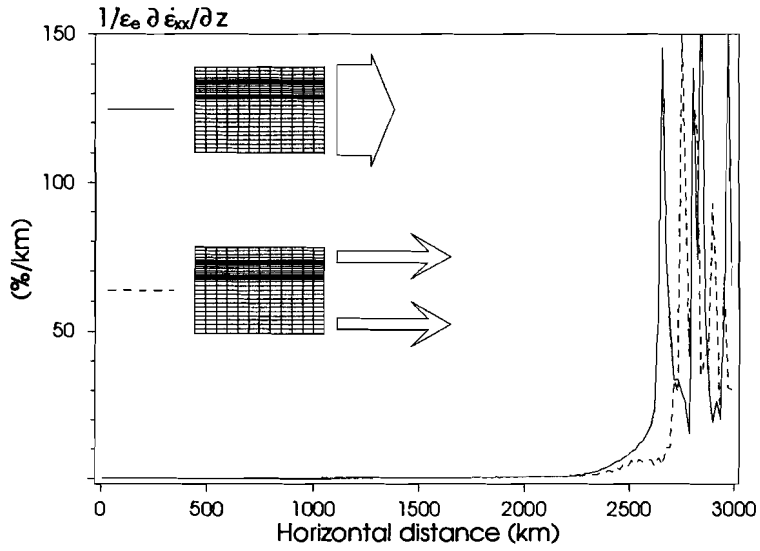

Fig. 8. *Validity of the constant horizontal strain rate gradient assumption. End loads are applied at* $x = 3000$ *km.*

energy for power law creep in olivine is reported by Goetze [1978] to be 510.4 kJ/mole. Referring to Goetze's paper, Kusznir and Park [1987] use an activation energy of 440.9 kJ/mole. The finite element results that are shown in Figure 7 have been calculated with an activation energy of 440.9 kJ/mole. Would we use the original value for Q_{pl}, the mantle in our calculations would become even stronger and the discrepancy with Kusznir and Park's results larger. If Kusznir and Park [1987] used the uni-axial rheological parameter A (see the "Constitutive equations for elasto-viscous creep" section) instead of effective parameter $A_{pl} = 4.5 \cdot A$, their effective viscosity η_{eff} would be 1.651 times the viscosity we used. The discrepancy would therefore become larger if we would perform the calculations with a viscosity based on uni-axial parameters.

In summary, a good agreement between the results of Kusznir and Park [1987] and our finite element calculations is found in most of the model. We have however difficulty matching the results in the mantle part of the lithosphere. Careful consideration of sources for discrepancies did not make clear what exactly causes these differences.

Validity of the uniform strain rate assumption

How well does Kusznir's [1982] assumption of a horizontal strain rate that is uniform with depth apply away from the vertical center of the model? To answer this question, we ran two very long models (3000 km). In the first model a uniform end load ($F_x = 10^{12}$ N/m) is applied. In the second we apply an equal total force, but it is distributed differently; only the upper and lower 15 km of the lithosphere are stressed in this case. We do not believe that either of the two models represents realistic loading characteristics. The models are solely intended to monitor the sensitivity of strain rates to different load distributions.

The normalized horizontal strain rate gradient ($\dot{\varepsilon}_E^{-1}\, \partial \dot{\varepsilon}_{xx}/\partial z$) can be seen as the deviation of the horizontal strain rate from being constant with depth. Figure 8 displays the maximum normalized strain rate gradient within a lithospheric column as a function of the horizontal position of that column. It can be seen that for both models the deviation is less than 10% per kilometer at a distance greater than 500 km from the plate boundary ($x = 3000$ km). We conclude that the distribution of the end load is insignificant within the inner part of the lithospheric plate, where the uniform horizontal strain rate assumption applies well.

DISCUSSION AND CONCLUSIONS

In this chapter we have given an introduction to the numerical method that is employed in this thesis. The effective viscosities that are used to study the evolution of continental lithosphere are based on results from experimental studies. We emphasize that these empirical rheological laws have mostly been established under experimental conditions that are completely different from natural conditions. Therefore, the flow laws should be regarded as rough indications of the response of lithospheric materials to stress.

We show that extremely low viscosities in the mantle part of continental lithosphere yield inaccurate results in stronger parts of the lithosphere, in which we are interested. By putting a lower limit to the viscosities the overall numerical results become more accurate, at the expense of (strongly) underestimating the strains in the least viscous layers. The minimum viscosity limit is derived from the numerical time step size. Model calculations at decreased time step size are therefore required in order to check the dependence of the results in "interesting areas" on the viscosity minimum.

Since there are no appropriate analytical models to test our finite element code against, we investigate a model for extension of continental lithosphere to make a comparison with a model that was derived by Kusznir [1982] and that was used by Kusznir and Park [1987]. Good agreement with the results of Kusznir and Park

[1987] is found, with exception of the 30 km beneath the Moho, where the fit is poor. Careful investigation of these discrepancies could not elucidate the sources for the differences.

We conclude from our modeling that the assumptions made by Kusznir [1982] are justified in a non-deforming, laterally homogeneous, thermally stable continental lithosphere that is subject to an in-plane force. We find that the assumption of a horizontal strain that is uniform with depth applies well in regions more than 500 km away from plate boundaries, independent of how the end load is distributed with depth. This conclusion is relevant as a step to the next chapters, in which we investigate the conditions that facilitate initiation of lithosphere scale faults. It is impossible for detachments to be operative in the absence of horizontal strain rate gradients with depth. We conclude that initiation of lithosphere-cutting detachment faults is unlikely in a laterally homogeneous and thermally stable continental lithosphere that is subject to an in-plane force only.

APPENDIX A. STABILITY, OSCILLATION AND ACCURACY IN QUASI-STATIC VISCO-ELASTIC FINITE ELEMENT ANALYSIS

Introduction

Several publications on the subject of numerical stability of algorithms for the solution of quasi-static elasto-viscous finite element equations have seen the light in the past (Cormeau, 1975; Hughes and Taylor, 1978). Numerical stability is shown to be unconditional in some implicit algorithms and to be limited by the time step size in other implicit algorithms and explicit algorithms. Hughes (1987) proves that this family of implicit and explicit algorithms converges. We apply these results to the specific algorithms used in the TECTON finite element code (Melosh and Raefsky, 1980).

In section (1) we will state the relevant equations for quasi-static elasto-viscous flow. In section (2) a short description of explicit and implicit time-stepping algorithms is introduced. Section (3) summarizes the stability analysis of Cormeau (1975) and Hughes and Taylor (1978). Convergence is proved in section (4) and the oscillation limit is derived. In this section the modal error is introduced, a quantity that will prove to give some insight in the accuracy of the solutions. In section (5) an upper bound to maximum eigenvalues are derived from the constitutive equations. Finally, in section (6) we show how a lower limit to effective viscosities is estimated from the numerical time step size.

(1) Problem statement

Let Ω be a bounded region in $\mathbf{R}^3$ with a piecewise smooth boundary. Vector and tensor fields on Ω are written in standard cartesian tensor notation, e.g. u_i is the ith component of the displacement vector. A comma is used to denote differentiation with respect to the cartesian coordinates, a superposed dot indicates time differentiation and the summation convention is employed for repeated indices. A general point in Ω is denoted $\boldsymbol{x}$ and t denotes time.

The equations under consideration are

$$\sigma_{ij,\,j} + X_i = 0 \tag{A1.1}$$

the equilibrium equations, where σ_{ij} is the stress tensor and X_i denotes the given body force,

$$\dot{\sigma}_{ij} = \boldsymbol{D}\,(\dot{\varepsilon}_{ij} - \dot{\varepsilon}_{ij}^{vp}) \tag{A1.2}$$

the constitutive equations, where $\boldsymbol{D}$ is the matrix of elastic properties, $\dot{\varepsilon}_{ij}$ is the total strain rate tensor and $\dot{\varepsilon}_{ij}^{vp}$ is the visco-plastic strain rate tensor,

$$\varepsilon_{ij} = \frac{1}{2}\,(u_{i,\,j} + u_{j,\,i}) \tag{A1.3}$$

(strain tensor ε_{ij}, displacements u_i),

$$\dot{\varepsilon}_{ij}^{vp} = \beta_{ij}(\sigma_{kl}) \tag{A1.4}$$

i.e., visco-plastic strain rates are given functions of the components of the stress tensor.

The quasi-static initial-boundary-value problem consists of finding a displacement field $u_i(\mathbf{x}, t)$ and stress field $\sigma_{ij}(\mathbf{x}, t)$ which satisfy equations (A1.1) to (A1.4) for all $\mathbf{x}\in\Omega$ and $t\in[0, T]$, $T > 0$, such that

$$\left.\begin{aligned} u_i(\mathbf{x}, 0) &= u_{0i}(\mathbf{x}), && \mathbf{x}\in\Omega \\ \sigma_{ij}(\mathbf{x}, 0) &= \sigma_{0ij}(\mathbf{x}), && \mathbf{x}\in\Omega \\ u_i(\mathbf{x}, t) &= g_i(\mathbf{x}, t), && \mathbf{x}\in\delta\Omega_1, \quad t\in[0, T] \\ n_j(\mathbf{x})\sigma_{ij}(\mathbf{x}, t) &= h_i(\mathbf{x}, t), && \mathbf{x}\in\delta\Omega_2, \quad t\in[0, T] \end{aligned}\right\} \tag{A1.5}$$

where u_{0i} and σ_{0ij} are the given initial data, g_i and h_i are the given boundary condition data, $\mathbf{n}$ is the outward normal vector to $\delta\Omega$ and $\delta\Omega_1$ and $\delta\Omega_2$ are subregions of $\delta\Omega$ so that $\delta\Omega_1 \cup \delta\Omega_2 = \delta\Omega$ and $\delta\Omega_1 \cap \delta\Omega_2 = \emptyset$. σ_{0ij} should equilibrate X_i at $t = 0$, and the boundary and initial data should be compatible.

(2) Algorithms

Bold-printed symbols denote vector or matrix entities, indices relate to time. The standard variational approach of establishing the finite element equations for (A1.1)-(A1.4) by the displacement method (see, for example Zienkiewicz, 1977) amounts to obtaining solutions to

$$\int_{\Omega} \boldsymbol{B}^T \boldsymbol{\sigma}_n \, \mathrm{d}\Omega = \boldsymbol{F}_n \tag{A2.1}$$

$\boldsymbol{B} = \boldsymbol{B}(\mathrm{x})$ is the strain-displacement matrix, $\boldsymbol{\sigma}_n = \boldsymbol{\sigma}(\mathrm{x}, t_n)$ and $\boldsymbol{F}_n = \boldsymbol{F}(t_n)$ is the global force vector.

$$\boldsymbol{\sigma}_{n+1} - \boldsymbol{\sigma}_n = \boldsymbol{DB}(\boldsymbol{u}_{n+1} - \boldsymbol{u}_n) - \Delta t_{n+1} \boldsymbol{D}\boldsymbol{\beta}(\boldsymbol{\sigma}_{n+\alpha}) \tag{A2.2}$$

where Δt_{n+1} is the time step size in the forthcoming time step and

$$\boldsymbol{\sigma}_{n+\alpha} = (1-\alpha)\boldsymbol{\sigma}_n + \alpha \boldsymbol{\sigma}_{n+1} \tag{A2.3}$$

Table A1. Explicit algorithm

1. Initialization: Set $n=0$ and $\boldsymbol{\varepsilon}_0^{vp} = \mathbf{0}$, form stiffness matrix $\boldsymbol{K}$ and $\boldsymbol{F}_0$ and compute elastic solution $\boldsymbol{u}_0 = \boldsymbol{K}^{-1}\boldsymbol{F}_0$ and $\boldsymbol{\sigma}_0 = \boldsymbol{DBu}_0$.
2. Determine next time step size Δt_{n+1} and define $\boldsymbol{\varepsilon}_{n+1}^{vp} = \boldsymbol{\varepsilon}_n^{vp} + \Delta t_{n+1}\boldsymbol{\beta}_n$.
3. Form $\boldsymbol{F}_{n+1}$.
4. Solve $\boldsymbol{K}\boldsymbol{u}_{n+1} = \int_{\Omega} \boldsymbol{B}^T \boldsymbol{D}\boldsymbol{\varepsilon}_{n+1}^{vp} \mathrm{d}\Omega + \boldsymbol{F}_{n+1}^{imposed}$ for displacements $\boldsymbol{u}_{n+1}$
5. $\boldsymbol{\sigma}_{n+1} = \boldsymbol{D}(\boldsymbol{B}\boldsymbol{u}_{n+1} - \boldsymbol{\varepsilon}_{n+1}^{vp})$
6. set n to $n+1$. If $\sum_{i=1}^{n} \Delta t_i < T$ goto 2, otherwise stop

Nonlinearities, which, in general, necessitate use of iteration, enter through $\boldsymbol{\beta}$. Table A1 summarizes the main steps of the explicit (Euler) solution algorithm that was developed and successfully employed by Zienkiewicz and Cormeau (1974). The advantages of this algorithm are that it is concise, simply coded and that the stiffness matrix $\boldsymbol{K}$ is factored once and for all. The main disadvantage is the rather stringent stability condition on the time step (see Section 3).

In table A2 the main steps of the implicit method (tangential, Newton-Raphson)

Table A2. Implicit algorithm

Defining $S = D^{-1}$, β' is the Jacobian matrix formed by differentiating β with respect to components of σ_n and $\alpha \in [0, 1]$:

1. Initialization: Set $n=0$ and $\varepsilon_0^{vp} = \mathbf{0}$, form K and F_0 and compute elastic solution $u_0 = K^{-1}F_0$ and $\sigma_0 = DBu_0$.
2. Determine next time step size Δt_{n+1}
3. Form $F_{n+1} = \int_\Omega B^T(S + \alpha\Delta t_{n+1}\beta_n')^{-1}(\Delta t_{n+1}\beta_n)\mathrm{d}\Omega + F_{n+1}^{imposed}$
   and $K_{n+1} = \int_\Omega B^T(S + \alpha\Delta t_{n+1}\beta_n')^{-1}B\mathrm{d}\Omega$
4. Solve $K_{n+1}\delta u_{n+1} = F_{n+1}$
5. $\delta\sigma_{n+1} = (S + \alpha\Delta t_{n+1}\beta_n')^{-1}(\beta\delta u_{n+1} - \Delta t_{n+1}\beta_n)$.
6. Update $u_{n+1} = u_n + \delta u_{n+1}$
   and $\sigma_{n+1} = \sigma_n + \delta\sigma_{n+1}$
7. set n to $n+1$. If $\sum_{i=1}^{n} \Delta t_i < T$ goto 2, otherwise stop

are summarized. It will be shown that for appropriate values of α the algorithm is unconditionally stable, but the price we pay is that K needs to be reformulated and factored more often, generally a time-consuming task.

(3) Stability analysis

It will become clear later, when we give the full constitutive expressions, that we can write

$$\beta(\sigma) = \Gamma(\sigma)\sigma$$

A very important result established by Cormeau (1975) is that the finite element equations (A2.1) are equivalent to solving a system of non-linear first order ordinary differential equations of the form

$$\dot{\bar{\Sigma}} = \bar{S}\bar{C}\bar{\Gamma}\bar{\Sigma} - \bar{\Xi} \tag{A3.1}$$

with compound vectors and matrices denote complete sets of integrating point values:

$$\bar{\Sigma} = (\sigma_1^T, \sigma_2^T, \cdots \sigma_G^T)^T$$

$$\bar{\Gamma} = \begin{pmatrix} \Gamma_1 & & 0 \\ & \ddots & \\ 0 & & \Gamma_G \end{pmatrix} \quad \bar{C} = \begin{pmatrix} c_1 I & & 0 \\ & \ddots & \\ 0 & & c_G I \end{pmatrix} \quad \bar{D} = \begin{pmatrix} D_1 & & 0 \\ & \ddots & \\ 0 & & D_G \end{pmatrix}$$

$$\bar{S} = \overline{DB} K^{-1} \overline{B}^T \overline{D} - \overline{DC}^{-1}$$

$$\dot{\bar{\Xi}} = \overline{DB} K^{-1} \dot{\bar{F}}$$

$$\bar{B} = (B_1^T, B_2^T, \cdots B_G^T)^T$$

$$\overline{E^{vp}} = (\varepsilon_1^{vp^T}, \varepsilon_2^{vp^T}, \cdots \varepsilon_G^{vp^T})^T = \overline{\Gamma\Sigma}$$

Subscripts (1, 2, ..., G) refer to integration points, c_i are positive weights associated with the integrating rule. The system of differential equations (A3.1), together with initial conditions, determines a unique stress history $\bar{\Sigma}(t)$ under the sole assumption that it be Lipschitzian (i.e. that a finite time increment yields a finite stress increment) (Cormeau, 1975).

We will invoke the following hypotheses in the stability analysis:

- $\bar{S}$ is symmetric, negative semi-definite (eigenvalues ≤ 0) (Cormeau, 1975).
- $\bar{\Gamma}$ is symmetric, positive semi-definite (eigenvalues ≥ 0). It will be shown that this is true for the constitutive equations we will be using.
- $F = 0$, i.e. we will look only at relaxation behavior!

Let

$$\bar{L} = \bar{C}\bar{\Gamma}$$

From the hypothesis it follows that $\bar{L}$ is symmetric positive definite.

In terms of the quantity $\bar{\Sigma}$, the algorithm of table A2 amounts to solving the following equation

$$\bar{\Sigma}_{n+1} = \bar{\Sigma}_n + \Delta t_{n+1} \bar{S} \bar{L}_{n+\alpha} \bar{\Sigma}_{n+\alpha} \tag{A3.2}$$

where $\bar{\Sigma}_{n+\alpha} = (1-\alpha)\bar{\Sigma}_n + \alpha\bar{\Sigma}_{n+1}$, etc. The numerical stability of a difference marching scheme is the property of the method by which

(i) the accumulated truncation error vanishes

(ii) the accumulated roundoff error remains bounded in the limit after an infinite number of time steps.

Hughes and Taylor (1978) propose the following stability condition

$$\|\bar{\Sigma}_{n+1}\|_{n+\alpha} \leq \|\bar{\Sigma}_n\|_{n+\alpha}$$

for each $n = 0, 1, 2, \ldots$, where the norm $\| \|_{n+\alpha}$ is defined by

$$\|X\|^2_{n+\alpha} = X^T \bar{L}_{n+\alpha} X$$

By considering the eigenvalue problem that is associated with (A3.2) it is shown that this stability criterion yields a useful measure of stability. Consider the eigenvalue problem

$$(\bar{L}_{n+\alpha} \bar{S} \bar{L}_{n+\alpha} - \lambda^i \bar{L}_{n+\alpha}) \phi^i = 0 \tag{A3.3}$$

By virtue of the properties of $\bar{S}$ and $\bar{L}$, the eigenvectors constitute a complete, orthogonal set and the eigenvalues are real and satisfy $\lambda^i \leq 0$. The inner product can be used to scale the eigenvectors such that $\phi^{iT} \bar{L}_{n+\alpha} \phi^i = \delta^{ij}$. Employing these properties, stresses can be developed from their modal components:

$$\left.\begin{aligned} \bar{\Sigma}_n &= \sum_i (\bar{\Sigma}^i_n \phi^i) \\ \bar{\Sigma}_{n+1} &= \sum_i (\bar{\Sigma}^i_{n+1} \phi^i) \end{aligned}\right\} \tag{A3.4}$$

Multiplying (A3.2) by $\phi^{iT} \bar{L}_{n+\alpha}$ and employing (A3.4), results in modal equations

$$\bar{\Sigma}^i_{n+1} = \bar{\Sigma}^i_n + \Delta t_{n+1} \lambda^i \bar{\Sigma}^i_{n+\alpha} \tag{A3.5}$$

or, more conveniently,

$$\bar{\Sigma}^i_{n+1} = A^i \bar{\Sigma}^i_n$$

with

$$A^i = \frac{1 + \Delta t_{n+1}(1-\alpha)\lambda^i}{1 - \Delta t_{n+1} \alpha \lambda^i}$$

Thus, if $|A^i| \leq 1$, then each modal component $|\bar{\Sigma}_{n+1}| \leq |\bar{\Sigma}_n|$. Since $\phi^{iT} \bar{L}_{n+\alpha} \phi^i = \delta^{ij}$

$$\begin{aligned} \|\bar{\Sigma}_{n+1}\|^2 &= \sum_i (\bar{\Sigma}^i_{n+1} \phi^i)^2 = \sum_i (A^i \bar{\Sigma}^i_n \phi^i)^2 \\ &\leq \sum_i (\bar{\Sigma}^i_n \phi^i)^2 = \|\bar{\Sigma}_n\|^2 \end{aligned}$$

by Parseval's inequality. If $\alpha \geq 1/2$, $|A^i| \leq 1$ for all time step sizes, i.e. the algorithm is *unconditionally stable*. If $\alpha < 1/2$ the requirement $|A^i| \leq 1$ restricts the time step size to

$$\Delta t_{n+1} \leq \frac{2}{(1-2\alpha)\lambda}$$

where $\lambda = \max_i |\lambda^i|$. In practice, these requirements prove to be stringent (Hughes and Taylor, 1978).

(4) Convergence

Convergence can be seen from the following. If we replace in (A3.5) model stresses by their exact values we obtain an expression of the form

$$\bar{\Sigma}(t_{n+1}) - \bar{\Sigma}(t_n) - \Delta t \lambda^i \bar{\Sigma}(t_{n+\alpha}) = \Delta t \cdot \tau(t_n)$$

We will prove that $|\tau(t_n)| \leq c\Delta t^k$, for all $t \in [0, T]$, where c is a constant independent of Δt and $k = 1$ in general, except if $\alpha = \frac{1}{2}$ in which case $k = 2$.

Proof. We expand $\bar{\Sigma}(t_{n+1})$ and $\bar{\Sigma}(t_n)$ about $t_{n+\alpha}$ in a finite Taylor series expansion.

$$\begin{aligned}
\Delta t \cdot \tau(t_n) &= \bar{\Sigma}(t_{n+\alpha}) + (1-\alpha)\Delta t \partial_t \bar{\Sigma}(t_{n+\alpha}) + \frac{((1-\alpha)\Delta t)^2}{2} \partial_t^2 \bar{\Sigma}(t_{n+\alpha}) \\
&\quad + \frac{((1-\alpha)\Delta t)^3}{3!} \partial_t^3 \bar{\Sigma}(t_{n+\alpha}) - \bar{\Sigma}(t_{n+\alpha}) + \alpha \Delta t \partial_t \bar{\Sigma}(t_{n+\alpha}) \\
&\quad - \frac{(\alpha \Delta t)^2}{2} \partial_t^2 \bar{\Sigma}(t_{n+\alpha}) + \frac{(\alpha \Delta t)^3}{3!} \partial_t^3 \bar{\Sigma}(t_{n+\alpha}) - \Delta t \lambda \bar{\Sigma}(t_{n+\alpha}) + O(\Delta t^4) \\
&= \Delta t(\partial_t \bar{\Sigma}(t_{n+\alpha}) - \lambda \bar{\Sigma}(t_{n+\alpha})) + \frac{(1-2\alpha)\Delta t^2}{2} \partial_t^2 \bar{\Sigma}(t_{n+\alpha}) \\
&\quad + \frac{(3\alpha^2 - 3\alpha + 1)\Delta t^3}{6} \partial_t^3 \bar{\Sigma}(t_{n+\alpha}) + O(\Delta t^4)
\end{aligned}$$

And, since we were trying to solve the homogeneous equation $\partial_t \bar{\Sigma} = \lambda \bar{\Sigma}$

$$\tau(t_n) = (1 - 2\alpha)\, O(\Delta t) + (3\alpha(\alpha - 1) + 1)\, O(\Delta t^2) + O(\Delta t^3) \qquad \square$$

Together, stability and consistency (i.e. $k \geq 0$) are sufficient requirements for convergence (e.g. Hughes, 1987).

The relative local truncation error in the i-th modal component can be written more explicitly as

$$\frac{\tau(t_n)}{\bar{\Sigma}} = \frac{(1-2\alpha)}{2} \lambda^2 \cdot \Delta t + \frac{(3\alpha(\alpha-1)+1)}{6} \lambda^3 \cdot \Delta t^2 + O(\lambda^4 \cdot \Delta t^3)$$

Note that for $\alpha = \frac{1}{2}$ the modal accuracy is optimal.

A further important notion is that of the *oscillation limit*. The amplification factor

$$A^i = \frac{1 + \Delta t(1-\alpha)\lambda^i}{1 - \Delta t \alpha \lambda^i}$$

becomes zero if $\lambda^i \Delta t = -1/(1-\alpha)$. If $\lambda^i \Delta t$ is less, A is negative and the sign of A^n changes in each time step. To prevent oscillatory behavior of the highest modes (the ones with the largest eigenvalues) the time step should be

$$\Delta t \leq \frac{1}{(1-\alpha)\,\lambda_{\max}}$$

(5) Upper bound to maximum eigenvalues

Estimates of critical time step sizes related to the stability, the oscillation limit and the relative modal truncation error all involve the largest eigenvalue of the eigenvalue problem (A3.3). For $\alpha \neq 0$ the eigenvalues depend on both $\bar{\Sigma}_n$ and $\bar{\Sigma}_{n+1}$. Therefore, the criteria that have been developed can not be used as a priori time step restrictions in general. In this section we estimate upper bounds to the maximum eigenvalue from the constitutive equations.

Melosh and Raefsky (1980) propose the following constitutive equations for nonlinear visco-elasticity

$$\left.\begin{aligned}
\dot{\varepsilon}_{xx} &= \frac{(1+\nu)}{E}[(1-\nu)\dot{\sigma}_{xx} - \nu\dot{\sigma}_{zz}] + \frac{(\sigma_E/\eta_{eff})^{n-1}}{4\eta_{eff}}[\sigma_{xx} - \sigma_{zz}] \\
\dot{\varepsilon}_{zz} &= \frac{(1+\nu)}{E}[(1-\nu)\dot{\sigma}_{zz} - \nu\dot{\sigma}_{xx}] - \frac{(\sigma_E/\eta_{eff})^{n-1}}{4\eta_{eff}}[\sigma_{xx} - \sigma_{zz}] \\
\dot{\varepsilon}_{xz} &= \frac{(1+\nu)}{E}\dot{\sigma}_{xz} + \frac{(\sigma_E/\eta_{eff})^{n-1}}{2\eta_{eff}}\sigma_{xz}
\end{aligned}\right\} \quad \text{(A5.1)}$$

where

$$\sigma_E = \left[\left(\frac{\sigma_{xx} - \sigma_{zz}}{2}\right)^2 + \sigma_{xz}^2\right]^{\frac{1}{2}}$$

σ_E is the second invariant of the stress deviator for plane stress.

The constitutive equations can be rewritten in terms of stress rates

$$\begin{pmatrix}\dot\sigma_{xx}\\ \dot\sigma_{zz}\\ \dot\sigma_{xz}\end{pmatrix}=\frac{E}{(1+\nu)(1-2\nu)}\begin{pmatrix}(1-\nu)&\nu&0\\ \nu&(1-\nu)&0\\ 0&0&(1-2\nu)\end{pmatrix}\left\{\begin{pmatrix}\dot\varepsilon_{xx}\\ \dot\varepsilon_{zz}\\ \dot\varepsilon_{xz}\end{pmatrix}-\frac{(\sigma_E/\eta_{eff})^{n-1}}{4\eta_{eff}}\begin{pmatrix}1&-1&0\\ -1&1&0\\ 0&0&2\end{pmatrix}\begin{pmatrix}\sigma_{xx}\\ \sigma_{zz}\\ \sigma_{xz}\end{pmatrix}\right\}$$

$$=\begin{pmatrix}\lambda+2\mu&\lambda&0\\ \lambda&\lambda+2\mu&0\\ 0&0&\mu\end{pmatrix}\left\{\begin{pmatrix}\dot\varepsilon_{xx}\\ \dot\varepsilon_{zz}\\ \dot\gamma_{xz}\end{pmatrix}-\frac{(\sigma_E/\eta_{eff})^{n-1}}{4\eta_{eff}}\begin{pmatrix}1&-1&0\\ -1&1&0\\ 0&0&4\end{pmatrix}\begin{pmatrix}\sigma_{xx}\\ \sigma_{zz}\\ \sigma_{xz}\end{pmatrix}\right\}$$

Lamé parameters $\lambda = E\nu/(1-2\nu)(1+\nu)$ and $\mu = E/2(1+\nu)$. This can be rewritten

$$\dot{\boldsymbol{\sigma}} = \boldsymbol{D}(\dot{\boldsymbol{\varepsilon}} - \dot{\boldsymbol{\varepsilon}}^{vp})$$

where

$$\dot{\boldsymbol{\varepsilon}}^{vp} = \boldsymbol{\beta}(\boldsymbol{\sigma}) = \frac{(\sigma_E/\eta_{eff})^{n-1}}{4\eta_{eff}}\begin{pmatrix}1&-1&0\\ -1&1&0\\ 0&0&4\end{pmatrix}\begin{pmatrix}\sigma_{xx}\\ \sigma_{zz}\\ \sigma_{xz}\end{pmatrix} \tag{A5.2}$$

The above formulation avoids problems related to maintaining incompressibility during viscous flow; at any moment $(\dot\sigma_{xx} + \dot\sigma_{zz}) = (\dot\sigma^0_{xx} + \dot\sigma^0_{zz})$.

The advantage of the above formulation becomes clear when we re-write power law relations in terms of the effective viscosity

$$\eta_{eff} = (2A)^{-\frac{1}{n}} \exp\left(\frac{Q}{nRT}\right) \tag{A5.3}$$

so that the effective viscosity in a given material depends solely on temperature.

The Jacobian of the stress-strain rate matrix $\boldsymbol{\beta}$ can be explicitly written

$$\frac{\partial\boldsymbol{\beta}}{\partial\boldsymbol{\sigma}} = \left(\frac{\partial}{\partial\sigma_{xx}}, \frac{\partial}{\partial\sigma_{zz}}, \frac{\partial}{\partial\sigma_{xz}}\right)^T (\beta_{xx}, \beta_{zz}, \beta_{xz})$$

$$= \frac{(\sigma_E/\eta_{eff})^{n-1}}{4\eta_{eff}}\begin{pmatrix} 1+(n-1)\left(\frac{\sigma_{xx}-\sigma_{zz}}{2\sigma_E}\right)^2 & -\left[1+(n-1)\left(\frac{\sigma_{xx}-\sigma_{zz}}{2\sigma_E}\right)^2\right] & (n-1)\frac{\sigma_{xx}-\sigma_{zz}}{\sigma_E^2}\sigma_{xz} \\ -\left[1+(n-1)\left(\frac{\sigma_{xx}-\sigma_{zz}}{2\sigma_E}\right)^2\right] & 1+(n-1)\left(\frac{\sigma_{xx}-\sigma_{zz}}{2\sigma_E}\right)^2 & -(n-1)\frac{\sigma_{xx}-\sigma_{zz}}{\sigma_E^2}\sigma_{xz} \\ (n-1)\frac{\sigma_{xx}-\sigma_{zz}}{\sigma_E^2}\sigma_{xz} & -(n-1)\frac{\sigma_{xx}-\sigma_{zz}}{\sigma_E^2}\sigma_{xz} & 4\left[1+(n-1)\left(\frac{\sigma_{xz}}{\sigma_E}\right)^2\right] \end{pmatrix} \tag{A5.4}$$

To estimate the maximum eigenvalue belonging to (A3.3) we can as well consider the equation

$$(\bar{L}_{n+\alpha}\bar{S} - \lambda^i)(\bar{L}_{n+\alpha}\boldsymbol{\phi}^i) = \mathbf{0}$$

(note that the eigenvectors are different, however). Replacing L by $C\Gamma$, and dropping the time indices, the eigenvalue problem becomes

$$(\bar{C}\bar{\Gamma}\bar{S} - \lambda^i)\phi' = 0 \tag{A5.5}$$

From (A5.2) we observe that the local $\bar{\Gamma}$-matrix is symmetric positive definite, so that since the integration weights c_i are positive, $\bar{C}\bar{\Gamma} = \bar{\Gamma}\bar{C} > 0$. Since $\bar{S}$ is a symmetric semi-negative definite matrix, eigenvalues of (A5.5) are negative or zero. If we rewrite the eigenvalue problem

$$(\bar{S})\phi' = \lambda(\bar{C}^{-1}\bar{\Gamma}^{-1})\phi'$$

for which we can derive the Rayleigh quotient for a vector $\bar{X}$:

$$Q(\bar{X}) = \frac{\bar{X}^T\bar{S}\bar{X}}{\bar{X}^T\bar{C}^{-1}\bar{\Gamma}^{-1}\bar{X}} \leq 0$$

from which we can get the magnitude of the maximum eigenvalue

$$\lambda = \max_{\bar{X}} |Q(\bar{X})|$$

Expanding $\bar{S}$ we have

$$\lambda = \max_{\bar{X}}\left[\frac{\bar{X}^T\bar{D}\bar{C}^{-1}\bar{X}}{\bar{X}^T\bar{C}^{-1}\bar{\Gamma}^{-1}\bar{X}} - \frac{\bar{X}^T\bar{D}\bar{B}\bar{K}^{-1}\bar{B}^T\bar{X}}{\bar{X}^T\bar{C}^{-1}\bar{\Gamma}^{-1}\bar{X}}\right]$$

As the second term is positive

$$\lambda \leq \max_{\bar{X}} \frac{\bar{X}^T\bar{D}\bar{C}^{-1}\bar{X}}{\bar{X}^T\bar{C}^{-1}\bar{\Gamma}^{-1}\bar{X}}$$

which is the Rayleigh coefficient of the related eigenvalue problem (λ, ϕ^*) defined by

$$(\bar{D})\phi^* = \lambda(\bar{\Gamma}^{-1})\phi^*$$

or of the alternative problem (with the same eigenvalues, but different eigenvectors)

$$(\bar{D}\bar{\Gamma})\phi^* = \lambda\phi^*$$

so that, due to the block diagonal structure of both $\bar{\Gamma}$ and $\bar{D}$

$$\begin{aligned}\lambda &\leq \max_{i=1,\ldots,G}\left(\max_{v}\frac{v^T\Gamma_i v}{v^T D_i^{-1} v}\right)\\ &\leq \max_{i=1,\ldots,G}\left(\frac{\lambda_{\max}(\Gamma_i)}{\lambda_{\min}(D_i^{-1})}\right)\end{aligned}$$

which comes down to

$$\lambda \leq \max_{i=1,\ldots,NUMEL} \left(\frac{E(\sigma_E/\eta_{eff})^{n-1}}{(1+\nu)(1-2\nu)\eta_{eff}} \right) \tag{A5.6}$$

As expected, the strongest time step constraints (largest eigenvalues) come from elements with the lowest effective viscosities.

(6) Minimum viscosity

Given the estimate for the largest eigenvalue (A5.6), equations (A4.1) and (A4.2) can be used to set the viscosity minimum at a given time step size Δt. In case of a Crank-Nicholson scheme ($\alpha = 0.5$), if a modal error percentage $\theta = \tau/\bar{\Sigma}$ is required, we can write

$$\lambda_m = (24\theta/\Delta t^2)^{\frac{1}{3}}$$

From the oscillation limit (A4.2) we get

$$\lambda_o = \frac{2}{\Delta t}$$

and

$$\frac{\lambda_m}{\lambda_o} = (3 \cdot \theta \cdot \Delta t)^{\frac{1}{3}}$$

Typically, Δt will be of the order of thousands of years ($O(10^{10}$seconds)) and $\theta < 0.1$, so that $\lambda_m > \lambda_o$. The strongest constraint on the minimum viscosity therefore comes from the oscillation limit. Equation (A5.6) can be used to relate λ_o to $\eta_{\min}$:

$$\eta_{\min} = \frac{E}{(1-\nu)(1-2\nu)\lambda_o}$$

REFERENCES

Braun, J., Styles of continental extension: results from numerical experiments, *unpublished Ph.D. thesis*, pp. 352, Dalhousie University, Halifax, Nova Scotia, 1988.

Byerlee, J. D., Friction of rocks, *Pageoph, 116*, 615-626, 1978.

Cormeau, I., Numerical stability in quasi-static elasto/visco-plasticity, *Int. J. Numer. Meth. Eng., 9*, 109-127, 1975.

Darot, M., and Y. Gueguen, High-temperature creep of forsterite single-crystals, *J. Geophys. Res., 86*, 6219-6234, 1981.

Desai, C. S., and J. F. Abel, *Introduction to the finite element method. A numerical method*

for engineering analysis, 477 pp., NY, Cincinnatti, Toronto, 1972.

Durham, W. B., and C. Goetze, Plastic flow of oriented single crystals of olivine. 1. Mechanical data, *J. Geophys. Res., 82*, 5737-5753, 1977.

Goetze, C., The mechanisms of creep in olivine, *Phil. Trans. Roy. Soc. London, A288*, 99-119, 1978.

Franssen, R.C.M.W., and C.J. Spiers, Deformation of polycrystalline salt in compression and in shear at 250-350 °C, in *Deformation Mechanisms, Rheology and Tectonics*, edited by Knipe, R.J., and E.H. Rutter, pp. 201-213, Geological Society of London Special Publication, 45, London, 1990.

Hughes, T. J. R., *The finite element method*, Prentice-Hall, Englewood Cliffs, N.J., 1987.

Hughes, T. J. R., and R. L. Taylor, Unconditionally stable algorithms for quasi-static elasto/visco-plastic finite element analysis, *Comput. Struct., 8*, 169-173, 1978.

Jaeger, J. C., and N. G. W. Cook, *Fundamentals of Rock Mechanics*, Chapman and Hall, London, 1976.

Koch, P. S., J. M. Christie, and R. P. George, Flow law of "wet" quartzite in the α-quartz field, *Trans. Am. Geophys. Un., 61*, 376, 1980.

Kusznir, N. J., Lithosphere response to externally and internally derived stresses: a viscoelastic stress guide with amplification, *Geophys. J. R. astr. Soc., 70*, 399-414, 1982.

Kusznir, N. J., and R. G. Park, The extensional strength of the continental lithosphere: its dependence on geothermal gradient, and crustal composition and thickness, in *Continental extensional tectonics, 28*, edited by M. P. Coward, J. F. Dewey and P. L. Hancock, pp. 35-52, Geological Society Special Publication, 1987.

Melosh, H. J., and A. Raefsky, The dynamical origin of subduction zone topography, *Geophys. J. R. Astr. Soc., 60*, 333-354, 1980.

Melosh, H. J., and A. Raefsky, Anelastic response of the earth to dip slip earthquakes, *J. Geophys. Res., 88*, 515-526, 1983.

Ranalli, G., *Rheology of the Earth: Deformation and Flow Processes in Geophysics and Geodynamics*, Allen and Unwin, London, 1987.

Shelton, G., and J. Tullis, Experimental flow laws for crustal rocks, *EOS Trans. Am. Geophys. Un., 62*, 1111, 1981.

Williams, C. A., and R. M. Richardson, A rheologically layerd three-dimensional model of the San Andreas Fault in Central and Southern California, *J. Geophys. Res., 96*, 16,597-16,623, 1991.

Zienkiewicz, O. C., *The Finite Element Method (3rd ed.)*, McGraw-Hill, Maidenhead, Berkshire, England, 1977.

Zienkiewicz, O. C., I. C. Cormeau, Visco-plasticity, plasticity, and creep in elastic solids - a unified numerical solution approach, *Int. J. Num. Meth. Eng., 8*, 821-845, 1974.

Chapter 4

Initiation of Lithosphere Scale Faults: Extension of Stable Continental Lithosphere †

R. Govers and M.J.R. Wortel

ABSTRACT

Extension of continental lithosphere and basin formation, in some regions of the world, appears to be reasonably well described by the pure shear model. The kinematics of continental extension beneath other basins seems to be rather well described by the simple shear model. Geological evidence suggests that, once lithosphere-scale zones of localized deformation have been formed, they tend to stay operative in subsequent tectonic phases. We focus on the stages in the evolution of continental lithosphere when these weak zones are initiated. Lithosphere-scale faults may grow at lateral material discontinuities, but there is no evidence that these weak zones are always initiated along material boundaries. It is the purpose of this paper to investigate the physical conditions that control the initiation of weak zones in continental lithosphere which is laterally fairly homogeneous.

Once they have been initiated, faults and shear zones that cut strong layers in the lithosphere will have a major influence on the evolution during extension. We investigate the physical conditions for strain localization in the upper mantle directly beneath the Moho. Based on extrapolated experimental flow laws, this region represents the strongest part of the continental lithosphere. Strain localization in the shallow upper mantle is therefore expected to have a pronounced effect on the response of the lithosphere during extension.

Low viscosities in the lower crust decouple the crust mechanically from the upper mantle. Causes for strain localization must therefore be sought in the mantle it-

---

† This chapter has been submitted for publication as: R. Govers and M.J.R. Wortel, Extension of Stable Continental Lithosphere and the Initiation of Lithosphere Scale Faults, *Tectonics*, 1993.

self. In this study we investigate whether boudinageing and strain weakening lead to localized deformation in the upper mantle. We focus on the evolution of thermo-mechanical models of continental lithosphere that initially are close to mechanical and thermal equilibrium. In-plane forces resulting from plate boundary processes generate intraplate stresses that are transmitted to interior parts of the continental plate.

We conclude that boudinageing does not evolve from small-scale perturbations during continental extension. Boudinageing as a mechanism to localize strain in the upper mantle is therefore discarded. The weakening effect of a deformation mechanism transition from dislocation creep to diffusion creep is several orders of magnitude. Our modeling results suggest that strain localization as a result of strain weakening will not occur in stable continental lithosphere. Initiation of lithosphere-scale faults in continental lithosphere which is laterally fairly homogeneous and which is mechanically and thermally close to equilibrium is concluded to be unlikely.

INTRODUCTION

The lithospheric stretching model that was originally proposed by Artemjev and Artyushkov (1971) and analyzed by McKenzie (1978) and the simple shear model of Wernicke (1981; 1985) represent end-members of a range of models that describe the kinematics of continental extension. With these models, and intermediate derivatives from them (Royden and Keen, 1980; Kusznir and Egan, 1989; Lister and Davis, 1989), it appeared very well possible to describe the first order kinematics of extending continental lithosphere. Interpretations are not always unique; in the North Sea basin, for instance, both the simple shear and the pure shear stretching model are advocated (Gibbs, 1984; Beach, 1986; Gibbs, 1987; Klemperer and White, 1989; White, 1989; Latin and White, 1990). In some basins the pure shear model seems a reasonable description of the extensional strain of the underlying lithosphere, whereas the simple shear model is a reasonable description of the kinematics of other basins. Thus, the problem of lithospheric extension is to understand what conditions determine the mode of extension.

Once lithosphere-scale zones of localized deformation have been formed they tend to stay operative in subsequent tectonic phases (White *et al.*, 1986). Lister and Davis (1989) argue that weak zones cutting rheologically strong layers control the evolution of extending lithosphere. Therefore, one of the central issues related to the problem of lithospheric extension is to understand under what conditions lithosphere-cutting faults initiate. One possibility is that these weak zones grow along lateral material discontinuities, which may for instance be the result of accretion

processes. There is, however, no compelling evidence that rifting and basin formation always occur along pre-existing lateral inhomogeneities. Localized strain in mantle peridotites which might be related to lithosphere-scale faults, is not associated with lateral inhomogeneities (R.L.M. Vissers, personal communication). In this chapter we, therefore, investigate the conditions for strain localization in the upper mantle of stable continental lithosphere. We define stable lithosphere as lithosphere which thermally and mechanically is close to equilibrium, meaning that the geothermal gradient is constant and strain rates are lower than $3 \cdot 10^{-16}\ s^{-1}$ (1% strain in 100 milion year (Ma)). It is clear that lithosphere which has been subject to a recent thermal and/or tectonic event is not stable, since stresses have not yet equilibrated to the new boundary conditions and temperatures are transient. We put special emphasis on the region just beneath the Moho because the upper mantle has the largest load bearing capacity (Kirby and Kronenberg, 1987, and references therein); localization of strain in upper mantle rocks undoubtly will have the most prominent effects on the evolution of the extending lithosphere. Causes for breaking the strong sub-Moho layers must be sought in the mantle itself, since the upper mantle and lower crust are expected to be mechanically decoupled by low viscosities in normal lower crust. We investigate two mechanisms that have been proposed for strain localization in continental lithosphere; boudinage and strain softening.

Theoretical studies predict that (parts of) the lithosphere will boudinage during extension (Fletcher and Hallet, 1983; Zuber *et al.*, 1986; Ricard and Froidevaux, 1986; Martinod and Davy, 1992; Fleitout *et al.*, 1993). Boudinageing has been put forward to explain observations of structures that exhibit spatial periodicity, both in oceanic (Moriceau and Fleitout, 1989) and continental lithosphere (Fletcher and Hallet, 1983; Ricard and Froidevaux, 1986). The inhomogeneous deformation associated with pinch and swell structures could be relevant in the context of initiating lithosphere-scale faults. We will therefore investigate a large deformation model of continental extension under conditions which are predicted to be favorable for the development of boudinage.

Large deformation models of continental extension (Houseman and England, 1986; Braun and Beaumont, 1987; Braun and Beaumont, 1989a; 1989b; Dunbar and Sawyer, 1989; Bassi, 1991; Christensen, 1992) are based upon steady state flow laws that relate composition, strain rate, temperature and stress at a constant microstructure. The assumption of constant microstructure, i.e. that material parameters like grain size, preferred orientation and metamorphic phase are constant, is very important. In large strain models, the effect of variations in microstructure become prominent because a strain-induced change of deformation mechanism is likely to occur. (White, 1973; White, 1976; Karato *et al.* 1986; Brodie and Rutter

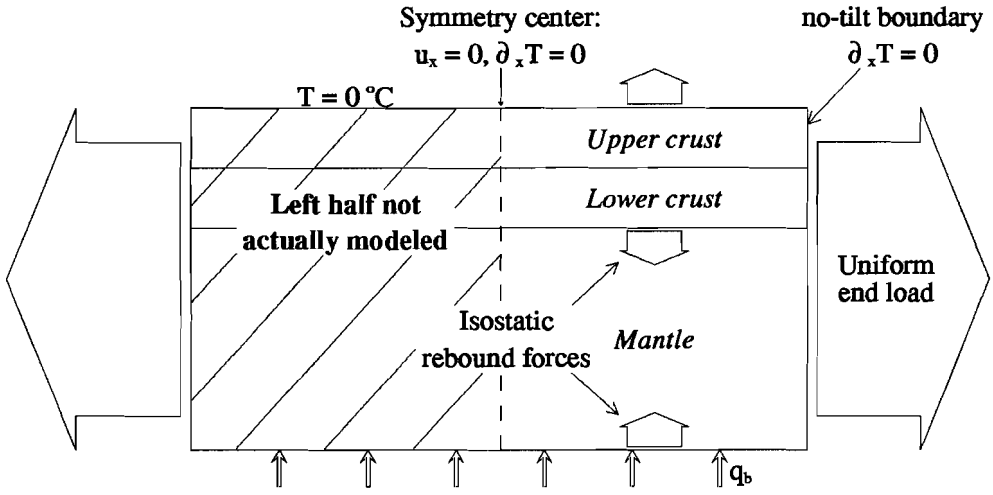

Fig. 1. *Generalized model of continental lithosphere. For economy reasons only the right half is modeled. Mechanical and thermal boundary conditions on the left side reflect symmetry. The model is assumed to continue to the right infinitely. This is reflected in the mechanical and thermal boundary conditions of no-tilt and no horizontal heat flow. The top of the lithosphere is at 0°C, and a constant basal heat flow q_b is applied to the lower boundary. Isostatic rebound forces act on density interfaces and a uniform force is applied to the right boundary. See text for explanation.*

1987; Rutter and Brodie 1988; Handy, 1989; Drury *et al.*, 1991). One especially important consequence of a non-constant microstructure could be that deformation localizes in pervasive zones. In this case, the continuum deformation approach that is adopted in lithosphere deformation models breaks down as the overall lithospheric strength and deformation behavior is controlled by "fault zones" that constitute only a minor part of the total volume. We use a numerical method to investigate whether strain localizes when a dramatic rheological weakening occurs due to a change in deformation mechanism from dislocation creep to diffusion creep.

THERMO-MECHANICAL MODEL AND FINITE ELEMENT APPROACH

To model large deformation continental extension, we employ a finite element method to obtain solutions to the coupled differential equations that control the mechanical and thermal evolution of the lithosphere. The selected mechanical finite element code, TECTON, developed by Melosh and Raefsky (1980) (see also Melosh and Raefsky, 1981; Melosh and Raefsky, 1983; Melosh and Williams, 1989), solves the mechanical equilibrium equations for nodal displacements by lin-

ear shape functions using an implicit time stepping scheme. We have supplemented the code with a thermal finite element program that solves for nodal temperatures by linear shape functions on the same grid with an implicit scheme to forward the solutions with time.

We will assume plane strain, i.e. that the horizontal extent of our models perpendicular to the cross-sectional plane is large compared to the scale of the model in the plane of the figures. The models are symmetric around a vertical axis on the left hand boundary of the model; for economy reasons calculations are only performed in the right hand side of the model (Figure 1). Mechanical and thermal boundary conditions (b.c.) on the left hand boundary are formulated to reflect the symmetry: horizontal displacements and horizontal heat flux are zero on this side. In our figures we will only show the results in the right hand side of the model.

We use the "density-stripping" method (Braun, 1988; Williams and Richardson, 1991) to calculate the isostatic restoring pressures at density interfaces and to obtain the uplift of the surface. This method is a good approximation to solving the full mechanical equations (including gravity) in the absence of strong horizontal density gradients (Braun, 1988). A small density inversion of 50 kg/m^3 is modeled on the lithosphere/asthenosphere boundary. Thermal b.c.'s on horizontal interfaces are zero ^oC temperature at the surface and a constant basal heat flux on the lower boundary of the model. The b.c.'s on the right hand side of the model reflect the assumption that the plate continues to the right; the horizontal heat flow is zero and mechanically this is a no-tilt boundary.

In this study we apply a horizontal in-plane force -constant in time and uniform with depth- to the right hand boundary of the model. This force b.c. is used to model boundary conditions associated with plate boundary forces (e.g. slab pull, trench resistance) and body forces (e.g. ridge push, density moment distributions) which are transmitted to interior parts of the continental plate. Geological data from compressive regions suggest that the rate of axial shorting decreases with time. Wdowinski and O'Connell (1990) conclude therefore that in-plane force b.c.'s are more appropriate than constant velocity b.c.'s. A constant strain rate b.c. does also imply a decreasing indentation velocity with time, but this b.c. is more difficult to implement in a displacement based finite element procedure. For continental extension, Sawyer (1985) shows that constant velocity and constant strain rate b.c.'s are equivalent to an end load that decreases with time. She shows that both b.c.'s can cause continental breakup. It is therefore to be expected that a constant in-plane force b.c. will lead to rifting and oceanization.

Table 1a. Rheological data.

		n_{pl}	Q_{pl} kJ/mole	A_{pl} $Pa^{-n}s^{-1}$
Upper crust	Wet quartzite[1)]	3.1	135	$7.7621 \cdot 10^{-26}$
Lower crust	Granulite[2)]	3.1	243	$9.5534 \cdot 10^{-21}$
Mantle	Wet olivine[3)]	3	420	$8.5746 \cdot 10^{-15}$

[1)] Paterson and Luan [1990], [2)] Wilks and Carter [1990], [3)] Rutter and Brodie [1988]

		n_{dc}	Q_{dc} kJ/mole	A_{dc} $Pa^{-n}s^{-1}$
Mantle	Wet olivine[3)]	1	240	0.6253

Table 1b. Thermal data.

	H_{60} $\mu W/m^3$	k_{60} $Wm^{-1}K^{-1}$	C_p $Jkg^{-1}K^{-1}$	α K^{-1}
Upper crust	1.37	2.56	1300	$3.2 \cdot 10^{-5}$
Lower crust	0.45	2.60	1300	$3.2 \cdot 10^{-5}$
Mantle	0.02	3.20	1300	$3.2 \cdot 10^{-5}$

Composition, temperatures and rheology

The continental lithosphere is modeled as a three layer system; upper crust, lower crust and mantle. Mechanically, the model lithosphere is a continuum which can achieve permanent strain by thermally activated viscous flow or by plastic failure, which is selected to approximate Byerlee's (1978) yield strength. The rheology is elastic, viscous or plastic depending on the composition, pressure, stress and temperature. In the upper crust we assume a "wet" quartzite viscous rheology (Paterson and Luan, 1990), in the lower crust a "wet" granulite rheology (Wilks and Carter, 1990) and in the mantle a "wet" olivine rheology (Rutter and Brodie, 1988). The rheological data are given in Table 1a. The steady state flow laws we adopt are the result of extrapolation of empirical results, and should therefore be considered as first order estimates of the stresses at specific strain rates. For calculation of (initially steady state) geotherms we use the thermal parameters suggested by Chapman (1986). Pressure and temperature dependence of the upper crustal conductivity is included by selecting average conductivities that are a function of the initial surface heat flow.

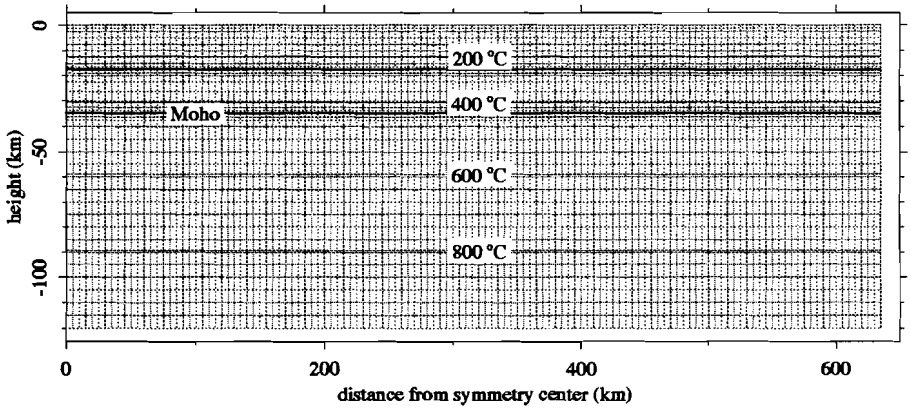

Fig. 2. *Initial finite element grid and isotherms of boudinage model. Filled thick lines indicate density interfaces below the upper and lower crust.*

BOUDINAGE

Theoretical studies based upon linear stability analysis, predict that periodic instabilities (mainly boudinage) can develop in laterally homogeneous continental lithosphere in extension (Fletcher and Hallet, 1983; Zuber *et al.*, 1986; Ricard and Froidevaux, 1986; Martinod and Davy, 1992). It is argued that heterogeneous deformation often is energetically more favorable than uniform stretching. The theoretical models are based upon visco-plastic rheologies and neglect the elastic strength of the lithosphere. The linear stability analysis is valid only for small strains. Martinod and Davy (1992) use viscosities derived from powerlaw flow laws to predict geothermal gradients at which boudinage would take place.

Boudinageing is potentially important for the problem of continental extension and, therefore, we will investigate whether boudinage actually develops in large deformation models. Martinod and Davy (1992) predict that two types of periodic instabilities can develop in continental extension: boudinage "of opposite phase" and crustal boudinage. In the "opposite phase" mode of boudinage both the upper crust and the upper mantle immediately beneath the Moho are boudinaged, with a pinch and swell variation of opposite phases, i.e. if there is a pinch in the upper crust, there is a swell in the mantle and *vice versa*. Crustal boudinage solely affects the upper crust, and is therefore considered less relevant for strain localization in the upper mantle.

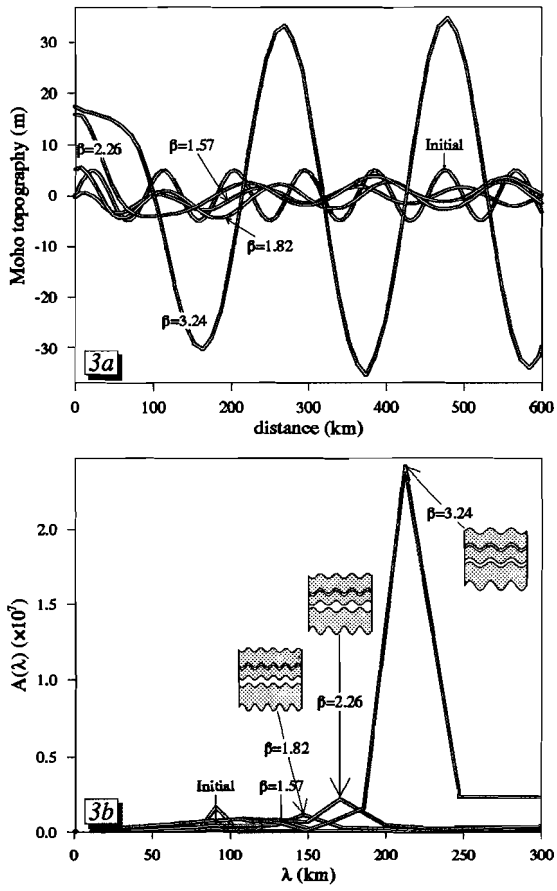

Fig. 3. *Results of the boudinage model. (a) Moho topography as a function of amount of stretching, β. Initially, the initial topography decreases. At $\beta = 2.26$ Moho amplitudes begin to increase slowly. (b) Wavelength spectra as a function of β. The "pac-man" inset figures give greately exaggerated impressions of the mode of deformation. Grey layers in these inset figures represent brittle zones deforming by plasticity. Light layers are deforming by nonlinear ductile creep. The bottom of the inset figures reflects the level in the mantle below which all deformation is ductile. Up to $\beta = 1.82$ the mode of deformation is mantle buckling, i.e. Moho and lower mantle boundary are in opposite phase. At $\beta = 2.26$ we observe an intermediate mode; lower crustal buckling. At $\beta = 3.24$ the final mode of deformation, whole lithosphere buckling has been established.*

Boudinage model

The parameters in the finite element model are selected to enable boudinage "of opposite phase", according to Martinod and Davy (1992). Figure 2 shows the finite element mesh and initial steady state temperature distribution, which has been calculated for a surface heat flow of 50 mW/m^2. For a weak crust and a geotherm consistent with a Moho temperature 439 °C Martinod and Davy predict a boudinage wavelength of approximately 100 km. According to Martinod and Davy, initial depth perturbations of the Moho would be amplified by a factor $\exp(5[\beta - 1])$ where β is the extension factor in the definition of McKenzie (1978). To facilitate initiation of pinch and swell structures we give the Moho an initial harmonic depth variation with a 91 km wavelength and 5 meter amplitude. A uniform in-plane

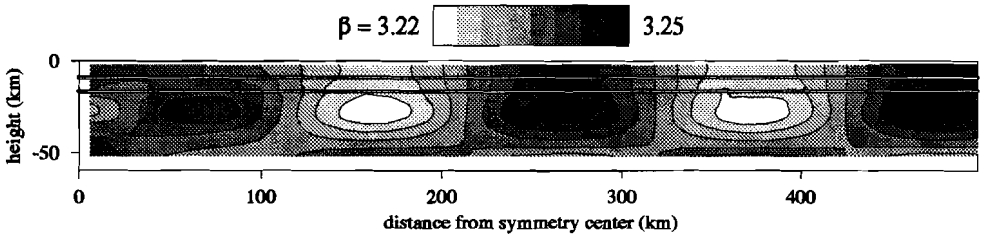

Fig. 4. *Deformed boudinage model, 60 Ma after loading. Note that stretching is close to homogeneous; β-factors in light and dark zones differ by 0.03 only. Horizontal grey lines in the Figure show the Moho and the upper-lower crust transition.*

force is applied to the right boundary. Initially this boundary is at a distance of 635 km from the center of the model. This is far enough to ensure that the depth distribution of the force has no influence on the results near the center. The in-plane force is linearly increased with time between 0 and 1 Ma to $1.2 \cdot 10^{13}$ N/m and kept constant onward. This force is equivalent to an in-plane stress of 100 MPa which is uniformly distributed over the lithospheric thickness. In Chapter 2 of this thesis we show that stresses on the order of hundreds of MPa's are consistent with stress magnitudes derived from seismicity data.

In Figure 3a the Moho topography as a function of the average stretching factor is displayed. At $t = 48$ Ma ($\beta = 1.57$), the initial Moho amplitudes have been attenuated. The style of deformation up to $\beta = 1.82$ (at 52 Ma time) is boudinage of the mantle, as schematically shown in Figure 3b. After a rapid phase shift of the Moho topography, the deformation style at 56 Ma ($\beta = 2.26$) has changed to boudinage of the viscous lower crust. However, this is only an intermediate stage in the development of the final style of deformation, which has developed at $\beta = 3.24$, after 60 Ma. Buckling of the whole model is a style of deformation which allows the Moho topography to grow. The vertical growth rate of this mode is slow; at $\beta = 6.2$ ($t = 64$ Ma, not shown in the Figure) topography amplitudes are 60 meters only.

In the initial stage of extension the harmonic Moho depth perturbation generates small lateral temperature perturbations, which cause preferential thinning below thicker crust. The lithosphere/asthenosphere boundary rises slightly more below thicker regions, causing the boudin-like mantle structure. Ongoing deformation attenuates the Moho depth perturbations and stretches the boudin wavelength with time.

Figure 4 shows the deformed model, 60 Ma after the end force was applied. The most important observation is that extension is almost uniform. Deviations from the average stretching factor $\beta = 3.24$ are small. The figure shows regularly spaced

zones where extension is smaller and larger than average. None of the conclusions of Martinod and Davy (1992) are supported by our modeling; we do not observe boudinage of "opposite phase" and exponential growth of pinch and swell structures. Preferential amplification of specific wavelengths is not supported by our modeling. We find that dominant wavelengths increase with β, and are not constant even if we correct for the amount of stretching. The late-stage uniform buckling mode of extension cannot operate to localize deformation; not only are the amplitudes too small, but also the wavelengths are too large to cause strain localization. We infer that boudinageing is not an effective mechanism for localizing strain.

STRAIN WEAKENING

Hobbs *et al.* (1990) note that "it is a prominent theme in both the materials and the geological literature that strain softening ... is a necessary and sufficient condition for localization of deformation". This statement is not undisputed since it has been noted that strain softening is not a sufficient condition for shear localization by others (see discussion and references in Drury *et al.*, 1991). In this section we investigate whether strain softening in the mantle portion of stable continental lithosphere leads to localized deformation.

Strain localization mechanisms

Drury *et al.* (1991) give an overview of mechanisms that could lead to localized deformation. In the context of this chapter, we will not consider shear localization induced by the imposed physical conditions -i.e. boundary conditions or material properties- during experimental deformation of rocks. Localization resulting from imposed mechanical boundary conditions could potentially be important, but the amount of experimental evidence is limited. Non-coaxial deformation experiments by Franssen and Spiers (1990) indicate, however, that this effect may be significant. We will review only the localization mechanisms known as "intrinsic", i.e. mechanisms that even lead to localized deformation in rigidly confined, materially and thermally homogeneous and isotropic rocks.

The most well known localization mechanism is brittle failure. The importance of brittle failure in the lithosphere as a strength limiting mechanism is generally acknowledged. The large number of brittle faults in especially continental lithosphere makes that brittle failure can well be approximated by continuum deformation on a lithosphere-scale in most cases.

Deeper in the lithosphere, at elevated temperatures, materials deform by crystal plastic or diffusion processes. Here, the strain can become localized as a result of decreasing viscosities with increasing strain ("strain softening"). Strain softening

mechanisms can be divided into five main classes (i) thermal softening as a result of shear heating, (ii) reaction softening, resulting from a (metamorphic) phase transformation, (iii) geometric softening due to changes in the crystallographic fabric (the average orientation and shape of crystals that constitute a rock), (iv) brittle softening, induced by a combination of brittle and ductile processes, (v) structural softening, induced by changes in microstructure (see Drury *et al.*, 1991, and references therein).

A distinction can be made between mechanisms that lead to localization of deformation and mechanisms that are required to keep ongoing deformation localized. In the absence of phase transformations, thermal softening typically is a mechanism to keep deformation localized; in the absence of localized deformation shear heating is negligible in typical tectonic processes.

Syntectonic reactions, either as pure phase transformations or as chemical reactions, probably are a very efficient means to localize deformation (e.g. Tullis and Yund, 1985; Handy, 1989; Drury *et al.*, 1991). We are not aware of any experiments in which quantitative estimates are made of the amount of weakening due to syntectonic reactions, so that reaction weakening cannot be modeled.

Wenk *et al.* (1991) estimate the effect of geometric softening on viscosities to be less than a factor of ten. Geometric softening is therefore considered irrelevant for large scale modeling.

Hobbs *et al.* (1990) and Tullis *et al.* (1990) discuss localization due to brittle processes in rocks in which the bulk deformation occurs by ductile mechanisms. It is conceivable that brittle softening does occur in the brittle-ductile transition zone, but again, quantitative estimates are not available.

Diffusion creep

Various papers (e.g. Rutter and Brodie, 1988; Handy, 1989) address the issue of strain localization due to a change of deformation mechanism. It is especially the experimental work of Karato *et al.* (1986), Brodie and Rutter (1987) and Rutter and Brodie (1988) which is important, in that some quantitative relations are established for the weakening behavior of olivine with a controlled grain size. In Figure 5 the effects of grain size, strain (or time), and temperature on the steady state flow stress are shown. If it is assumed that the starting material initially has a grain size of 1 cm and a temperature of 600 °C, it is clear from Figure 5a that recovery-controlled dislocation creep is the controlling mode of deformation at geologically significant strain rates (10^{-12}-10^{-16} s^{-1}). The flow stress does not depend on the grain size in this field, but creep polygonization, rotation recrystallization and possibly migration recrystallization (Drury *et al.*, 1991) lead to a reduction of grain size with increasing strain. After "some strain" the grain size has been reduced suf-

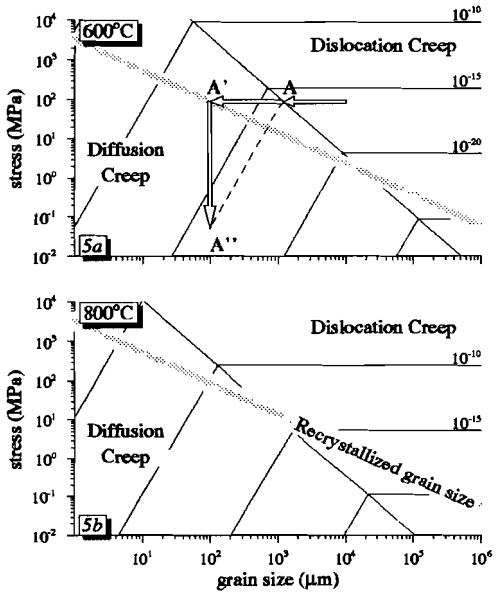

Fig. 5. *Strain weakening upon a deformation mechanism change from dislocation creep to diffusion creep in wet olivine (after Rutter and Brodie (1988)). The thin line at which constant-strain-rate lines (labeled 10^{-10}, 10^{-15}, etc.) kink, separates domains where diffusion creep and dislocation creep mechanisms prevail. At low stress and small grain sizes, deformation occurs by diffusion creep. At high stress and large grain sizes dislocation creep is the dominant mechanism of deformation. The grey line in the figures represents the paleopiezometric grain size relation. See text for explanations. (a) At temperature of 600 °C, (b) At temperature of 800 °C.*

ficiently, and the deformation mechanism changes to diffusion creep, i.e. diffusion of vacancies controls the rate of deformation.

The grey line in Figure 5 is the recrystallized grain size as a function of stress. This empirical relationship between grain size and stress is fairly well calibrated, because it is considered as one of the basic tools for measuring the flow stress magnitude from deformed rock. Dynamic recrystallization is driven by the elastic strain energy stored in dislocations and is therefore confined to the dislocation creep field. The average grain size is generally reduced by dynamic recrystallization. In the diffusion creep field, however, the surface energy provides a driving mechanism for grain growth. Although his model is definitively not undisputed (see, for instance Poirier, 1985), Twiss (1977) argues that the piezometric grain size relation represents a dynamic balance between stress-driven dislocation processes and surface energy driven grain growth processes. Based upon these arguments, it is therefore to be expected that the recrystallized grain size line coincides with the transition between dislocation creep and diffusion creep fields. The fact that this is not the case may reflect uncertainties in the underlying flow laws and piezometric relations (C.J. Spiers, personal communication, 1992). Also, monomineralic rocks with a uniform grain size are hardly ever observed outside the laboratory. The transition between the dislocation and diffusion creep fields in natural rocks is therefore not a sharp line, but a gradual transition in which both mechanisms are opera-

tive. According to Twiss' argument the empirical recrystallized grain size line falls within this range. Other models (e.g. Derby and Ashby, 1987), however, do predict piezometric and mechanism regime boundaries which are distinct.

Within the grain size sensitive field the stress drop can be estimated if we consider the following rheological path (Rutter and Brodie, 1988), in which the relation between strain and the volume fraction of recrystallized material is based upon the experiments of White *et al.* (1985) (A-A'-A'' in Figure 5). Recrystallization continues at elevated strain rates within the diffusion creep field until the flow stress is in equilibrium with the grain size. Then, diffusion creep involves a stress drop until the original steady state strain rate has been re-established. Handy (1989) discusses alternative rheological paths, but no quantitative estimates for the stress drop can be made from these.

It is clear from Figure 5b that the stress drop is considerably less at 800 °C; rates of dislocation climb and grain growth increase rapidly with temperature, shifting the paleopiezometric grain size line towards the dislocation creep field. At low strain rates ($< 10^{-12}\ s^{-1}$) a change of dislocation creep to diffusion creep will never occur since the equilibrium grain size lies well in the dislocation creep field.

In their experiments on fabric softening, White *et al.* (1985) observed that the weakening was complete at 40% natural strain. Rutter and Brodie (1988) therefore assume that strain weakening resulting from a mechanism transition to diffusion creep is complete at 40% too. It is clear that this observation depends on the initial grain size distribution within the aggregate. We introduce two parameters, ϵ_0 and ϵ_1, that describe the uncertainties in the initial grain size and in the "hardness" of the transition. ϵ_0 is the natural strain at which weakening starts (point A' in Figure 5) and ϵ_1 is the natural strain at which the stress drop is completed (point A'' in Figure 5). If ϵ_0 is small, the initial grain size was small and weakening commences soon after deformation starts. The hardness of the transition is defined by $(\epsilon_1 - \epsilon_0)$; a decrease in the transition hardness increases the rapidness of the weakening.

Strain weakening model

To investigate the effect of strain weakening in mantle lithosphere we designed a finite element model at conditions that enable a dramatic and rapid decrease in viscosity due to straining. Initially the model is close to mechanical equilibrium, i.e. stresses are so close to hydrostatic that strain rates are very low (of the order of $10^{-20}\ s^{-1}$ or less). A slight deviation from mechanical equilibrium occurs in the transition zone between 50 and 75 km from the vertical symmetry center (Figure 6). The Moho thickness varies from 40 km, left from the transition zone, to 35 km, right from the transition zone. Recent papers (Kruse *et al.*, 1991; Bird, 1991) em-

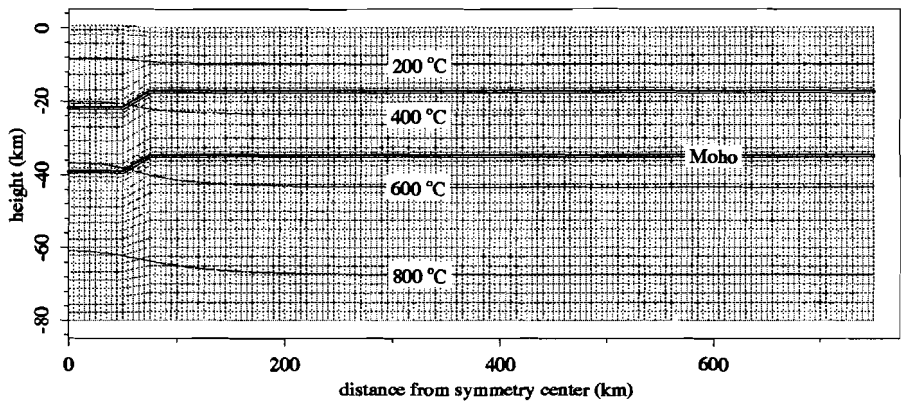

Fig. 6. *Initial finite element mesh and geotherms in model with thickenned crust.*

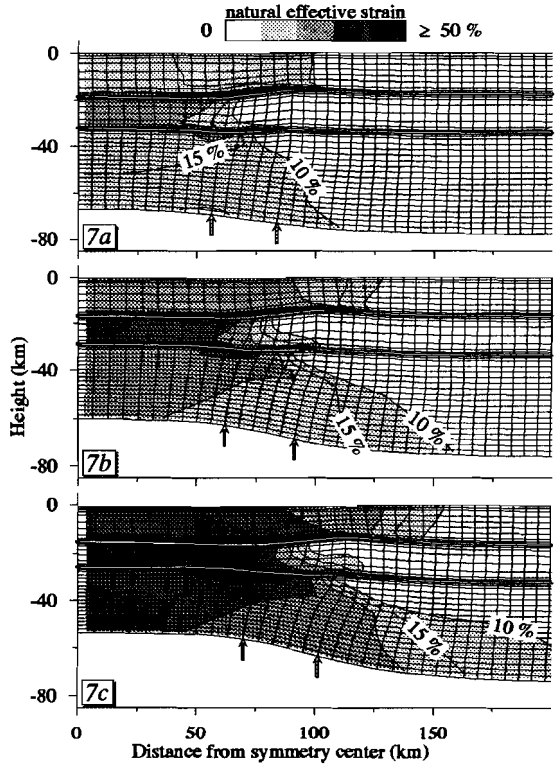

Fig. 7. *Deformed mesh and contours of natural effective strain in the strain weakening model with a thickened crust. The limit at which weakening starts,* $\epsilon_0 = 10\%$*, and the natural strain at which weakening is complete,* $\epsilon_1 = 15\%$*, are indicated in the figure. Arrows below the lower model boundary indicate the position of the transition zone. (a)* $t = 0.38$ *Ma. (b)* $t = 0.63$ *Ma. (c)* $t = 0.88$ *Ma.*

phasize that the lower crust, because of its low viscosities, is very efficient in attenuating strong lateral density gradients. Relatively mild Moho depth gradients, like in our model, can be expected in continental lithosphere that mechanically is close to equilibrium.

Initially the model is in thermal equilibrium. The surface heat flow varies from 63 mW/m^2 near the symmetry center to 58 mW/m^2 at the right. The Moho temperature ranges from 626 °C at the base of the thicker crust to 529.3 °C at the base of the thinner crust. The stress drop due to a change in deformation mechanism to diffusion creep is at least three orders of magnitude at these temperatures. In the current model we set the lower limit for strain weakening in the mantle to $\epsilon_0 = 10\%$. At $\epsilon_1 = 15\%$ weakening is completed and all deformation occurs by diffusion creep. This transition is much more rapid than was found by White *et al.* (1985). We take a high value for the transition hardness to obtain an upper limit to the localization potential due to strain weakening. We assume a grain size distribution that initially is uniform in the mantle.

A uniform force of $8 \cdot 10^{12}$ N/m is linearly added between 0 and 0.1 Ma to the right hand boundary of the model and kept constant onward.

Strain weakening in the upper mantle starts at $\approx$ 0.2 Ma. Figure 7a displays the finite element grid and contours of the effective natural strain at 0.38 Ma. Weakening front and weakening end contours are labeled 10% and 15% respectively. Low viscosity regions in the upper and lower crust are more strained in the transition zone. With time, (0.63 Ma in Figure 7b and 0.88 Ma in Figure 7c), the lower crust acts as a low viscosity channel that accommodates most of the thinning. After 0.63 Ma, the deformation mechanism change, to diffusion creep in the mantle, has been completed below the thickened crust. Migration of the softening front into the transition zone and reference lithosphere proceeds much more slowly, at a velocity that is mainly controlled by slow deformation in the strong sub-Moho region.

The total effective strain rate ($\dot{\varepsilon_E} = 1/2 \dot{\varepsilon_{ij}}' \dot{\varepsilon_{ij}}'$) at 0.38 Ma, 0.63 Ma and 0.88 Ma is shown in Figures 8a, 8b and 8c respectively. Maximum strain rates are attained in the most fluid parts of the lower and upper crust and strain rates are more than two orders of magnitude lower in reference lithosphere. The total extension rate increases upon weakening, but the strain rate distribution in the mantle is rather insensitive to the passing weakening front. The main effect of strain weakening is a drop of flow stresses, which is most dramatic in the strong region directly beneath the Moho.

The total strain rate gradient is an indicator for strain localization. In Figure 9 we show the horizontal strain rate gradient, defined by

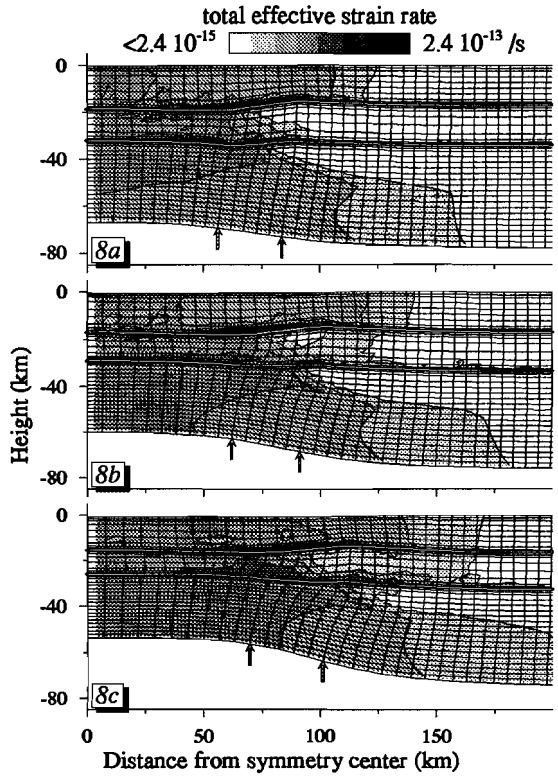

Fig. 8. *Total effective strain rates $\dot{\varepsilon}_E$ as a function of time in the thickened crust model. (a) $t=0.38$ Ma. (b) $t=0.63$ Ma. (c) $t=0.88$ Ma.*

$$\partial_x \dot{\varepsilon_E} = l_x \cdot \frac{\partial(^{10}\log \dot{\varepsilon_E})}{\partial x}$$

l_x is what a geologist would refer to as "the scale of observation"; strain can be homogeneous on a large scale, but strongly heterogeneous on a smaller scale. The (minimum) scale of observation in our models is a single element. The proposed measure for strain localization has the property of giving order of magnitude strain rate gradients; a two orders of magnitude change in strain rate on the scale of observation yields $\partial_x \dot{\varepsilon_E} = 2$. The conspicuous dipping zone in the upper mantle indicates that there is some tendency for strain localization below the transition zone at all time steps. The maximum strain rate gradient however is less than half an order of magnitude, so that the localization is only minor.

As the local element size enters the analysis via the "scale of observation" parameter, we ran the model at twice the mesh density to find that our conclusions are not affected by the spatial discretization. Another model calculation for an initial

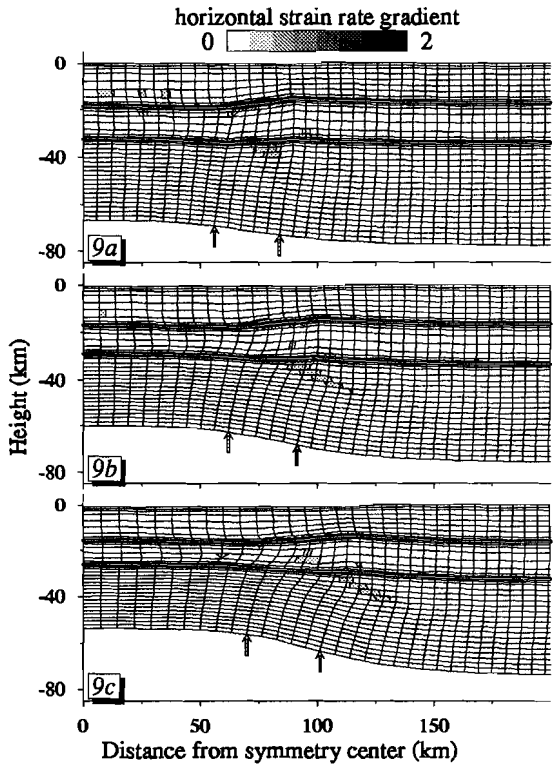

Fig. 9. *Horizontal strain rate derivative* $\partial_x \dot{\varepsilon}_E$ *as a function of time in the thickened crust model. Although there is some tendency to localized deformation, the magnitude of the sub-Moho grey region is too low to initiate a shear zone. (a)* $t = 0.38$ *Ma. (b)* $t = 0.63$ *Ma. (c)* $t = 0.88$ *Ma.*

thermal gradient corresponding to a surface heat flow of 40 mW/m^2 did give different time scales, but our basic conclusion that no strain localization occurs is supported. Calculations at higher geothermal gradients than the one considered here are unnecessary, because increased Moho temperatures decrease the effect of softening (Figure 5). We selected parameters in our modeling to promote softening and strain localization. Thus, although we did not conduct a full investigation of the parameter space, we are confident that strain localization due to a deformation mechanism switch to diffusion creep is unlikely in stable continental lithosphere that is subject to in-plane forces.

Figure 10 displays the surface topography and upper and lower crustal stretching factors as a function of time. The topographic bulge developing above the reference lithosphere results from isostatic rebound forces in the thickened lithosphere that are flexurally supported (Vening Meinesz, 1950; Beaumont *et al.*, 1982; Braun and Beaumont, 1989c). This result is consistent with the mechanism for flexural uplift of rift shoulders that was proposed by Braun and Beaumont (1989c). They recognized that if the lithosphere retains a finite strength during extension, vertical up-

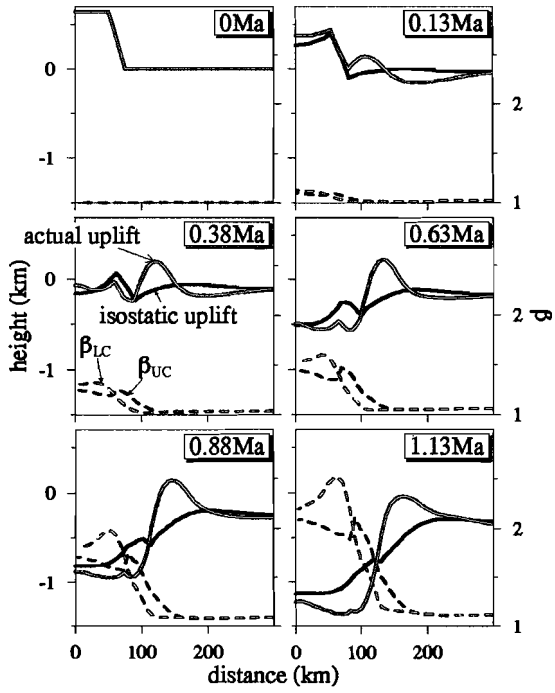

Fig. 10. *Surface uplift, isostatic surface uplift, upper crustal stretching factor β_{UC} and lower crustal stretching factor β_{LC} of the strain weakening model with thickened crust. There is no signal from the dramatic weakening at 0.20 Ma that is clearly separable from the signal due to stretching.*

lifts of the surface are flexurally supported. Consequently, Weissel and Karner (1989) introduced a new parameter in their kinematic stretching model, the necking depth, which is a measure of the deviation of the thinned lithospheric column from local isostasy. By visual inspection of Figure 10 it is clear that the long wavelength component of the actual uplift differs very little from the isostatic long wavelength uplift. The flexural outer bulge of approximately 200 km wavelength is necessarily supported by strong levels in the crust only after onset of mantle weakening at 0.20 Ma. No surface uplift signal, clearly distinct from the surface signal due to thinning, is generated by the dramatic weakening of the sub-Moho mantle.

DISCUSSION AND CONCLUSIONS

Based upon empirical ductile flow laws and realistic geotherms, a strength maximum can be expected in the sub-Moho mantle. Strain localization in this region would undoubtedly have prominent effects on the evolution of extending lithosphere as a whole. Low viscosities in the lower crust decouple the mantle and crust mechanically so that causes for strain localization must be found in the mantle itself. In this chapter we, therefore, focused on mechanisms that may lead to strain localization in the upper mantle. We consider two potential causes for localization;

inhomogeneous deformation as a result of a) boudinageing and b) strain localization due to a deformation mechanism change from dislocation creep to diffusion creep.

Our modeling of extensional boudinage has mainly been motivated by the results of Martinod and Davy (1992). Their model is based upon a linear stability analysis at small strains and they employ a plastic/viscous rheology. Our model is more general in that it can accommodate larger strains and more realistic rheologies: elastic, plastic or viscous, depending on temperature, stress and pressure. Parameters in our finite element model are selected to promote development of "boudinage of opposite phase". None of the findings of Martinod and Davy (1992) are supported by our results. Instead, we find that deformation is homogeneous up to moderate strains. We therefore conclude that geometric instabilities are not effective in localizing deformation. This finding is in accordance with the results of Bassi and Bonnin (1988a; 1988b) and Bassi (1991), who find that no preferred boudinage wavelength emerges during continental extension. In our opinion, the discrepancy between our results and the conclusions from theoretical studies is caused by a difference in employed rheologies. All theoretical studies (Fletcher and Hallet, 1983; Zuber *et al.*, 1986; Ricard and Froidevaux, 1986; Martinod and Davy, 1992) neglect the flexural (elastic) strength of the lithosphere. Physically, boudinageing is caused by the destabilizing effect of large strength contrasts. In the absence of density inversions, buoyancy forces have a stabilizing effect on lithospheric deformation. Elasticity also has a stabilizing effect, especially in lithosphere in tension, in that it opposes (local) vertical motions. Further theoretical work is required on boudinageing in lithosphere that does have have a flexural strength. Pinch and swell structures might well develop at wavelengths close to or greater than the flexural wavelength of lithospheric layers. In the context of initiating lithosphere-scale faults these wavelengths are probably to large to be relevant.

Rheological instabilities resulting from strain localization can be triggered by strain softening processes. Quantitative estimates of strain weakening are available for few of the dozen weakening processes. From recent experiments (Karato *et al.*, 1986; Brodie and Rutter, 1987), the weakening effect resulting from a transition of deformation mechanism from dislocation creep to diffusion creep can be estimated. In our modeling we have incorporated this specific strain weakening law. The results show that, although weakening is dramatic, no strain localization occurs in stable continental lithosphere that is subject to in-plane forces. We consider the use as synonyms of "weakening" and "localization" in geological literature therefore unwarranted. The mechanical and thermal boundary conditions play an equally important role in determining whether localization occurs as do the rheological properties.

A conclusion we draw from our work is that, for the strain softening mechanism we studied, lithosphere scale localization is difficult to establish in the strong sub-Moho region of stable continental lithosphere. Initiation of whole lithosphere cutting faults/shear zones is therefore not very likely in this setting, unless it occurs due to causes not incorporated in the present approach. Reaction softening and brittle softening are potentially relevant causes for shear localization which have not been incorporated in the present analysis since quantitative laws are not available. In Chapter 5 of this thesis we will focus on initiation of lithosphere-scale faults in continental lithosphere that is, or has been, subject to recent orogeny. In this case, the lithosphere is no longer in mechanical and/or thermal equilibrium and is subject to different kind of boundary conditions.

Acknowledgments

Jay Melosh of the Lunar and Planetary Lab and Department of Geosciences in Tucson, Arizona, is gratefully acknowledged for sharing his mechanical finite element code. Constructive reviews of an early version of this paper by Martyn Drury and Reinoud Vissers are greatly appreciated. With Chris Spiers we had a very interesting discussion on shear localization in relation to strain weakening. During this research, R.G. was financially supported by AWON, the Earth Science branch of the Netherlands Organization for Scientific Research (NWO). M.J.R.W. was partially supported by the Netherlands Organization for Scientific Research (NWO) through the Pionier project PGS 76-144.

REFERENCES

Artemjev, M.E., and E.V. Artyushkov, Structure and isostasy of the Baikal rift and the mechanism of rifting, *J. Geophys. Res., 76,* 1,197-1,211, 1971.

Derby, B., and M.F. Ashby, On dynamic recrystallization, *Scripta Metall., 21,,* 879-884, 1987.

Bassi, G., Factors controlling the style of continental rifting: insights from numerical modelling, *Earth Planet. Sci. Lett., 105,* 430-452, 1991.

Bassi, G., and J. Bonnin, Rheological modelling and deformation instability of lithosphere under extension, *Geophys. J., 93,* 485-504, 1988a.

Bassi, G., and J. Bonnin, Rheological modelling and deformation instability of lithosphere under extension - II. Depth-dependent rheology, *Geophys. J., 94,* 559-565, 1988b.

Beach, A., A deep seismic reflection profile across the northern North Sea, *Nature, 232,* 53-55, 1986.

Beaumont, C., C.E. Keen, and R. Boutilier, A comparison of foreland and rift margin sedimentary basins, *Phil. Trans. R. Soc. London (A), 305,* 295-317, 1982.

Bird, P., Lateral extrusion of lower crust from under high topography, in the isostatic limit,

J. Geophys. Res., 96, 10,275-10,286, 1991.

Braun, J., Styles of continental extension: results from numerical experiments, *unpublished Ph.D. thesis,* pp. 352, Dalhousie University, Halifax, Nova Scotia, 1988.

Braun, J., and C. Beaumont, Styles of continental rifting: results from dynamical models of lithospheric extension, in *Sedimentary basins and basin-forming mechanisms, 12,* edited by C. Beaumont and A.J. Tankard, pp. 241-258, Can. Soc. Petrol. Geol. Mem., 1987.

Braun, J., and C. Beaumont, Dynamical models of the role of crustal shear zones in asymmetric continental extension, *Earth Planet. Sci. Lett., 93,* 405-423, 1989a.

Braun, J., and C. Beaumont, Contrasting styles of lithospheric extension: implications for differences between Basin and Range Province and rifted continental margins, *Am. Ass. Petr. Geol. Mem., 46,* 53-79, 1989b.

Braun, J., and C. Beaumont, A physical explanation of the relation between flank uplifts and the breakup unconformity at rifted continental margins, *Geology, 17,* 760-764, 1989c.

Brodie, K.H., and E.H. Rutter, Deep crustal extensional faulting in the Ivrea zone Northern Italy, *Tectonophysics, 140,* 193-212, 1987.

Byerlee, J.D., Friction of rocks, *Pageoph., 116,* 615-626, 1978.

Chapman, D.S., Therman gradients in the continental crust, in *The nature of the lower continental crust, 24,* edited by J.B. Dawson, D.A. Carswell, J. Hall and K.H. Wedepohl, pp. 63-70, Geological Society of London Special Publication, 1986.

Christensen, U.R., An Eulerian technique for thermomechanical modeling of lithospheric extension, *J. Geophys. Res., 97,* 2,015-2,036, 1992.

Drury, M.R., R.L.M. Vissers, D. van der Wal, and E.H. Hoogerduijn Strating, Shear localization in upper mantle peridotites, *Pageoph., 137,* 439-460, 1991.

Dunbar, J.A., and D.S. Sawyer, How preexisting weaknesses control the style of continental breakup, *J. Geophys. Res., 94,* 7,278-7,292, 1989.

Fleitout, L., M.P. Doin and C. Froidevaux, Formulation for boudinage with depth dependent mechanical properties: Application to the origin of Pacific geoid lineations, *Earth Planet. Sci. Lett., in press,* 1993.

Fletcher, R.C., and B. Hallet, Unstable extension of the lithosphere: a model for Basin-and-Range structure, *J. Geophys. Res., 88,* 7,457-7,466, 1983.

Franssen, R.C.M.W., and C.J. Spiers, Deformation of polycrystalline salt in compression and in shear at 250-350 °C, in *Deformation Mechanisms, Rheology and Tectonics,* edited by Knipe, R.J., and E.H. Rutter, pp. 201-213, Geological Society of London Special Publication, 45, London, 1990.

Gibbs, A.D., Structural evolution of extensional basin margins, *Geol. Soc. London J., 141,* 609-620, 1984.

Gibbs, A.D., Linked tectonics of the northern North Sea basins, in *Sedimentary basins and basin-forming mechanisms, 12,* edited by C. Beaumont and A.J. Tankard, pp. 163-171, Can. Soc. Petrol. Geol. Mem., 1987.

Handy, M.R., Deformation regimes and the rheological evolution of fault zones in the lithosphere: the effect of pressure, temperature, grain size and time, *Tectonophysics, 163,* 119-152, 1989.

Hobbs, B.E., H.-B. Mülhaus, and A. Ord, Instability, softening and localization of deformation, in *Deformation Mechanisms, Rheology and Tectonics,* edited by R. Knipe and E.H.

Rutter, pp. 143-165, Geol. Soc. London Special Publication, 1990.
Houseman, G.A., and P.C. England, A dynamical model of lithosphere extension and sedimentary basin formation, *J. Geophys. Res., 91,* 719-729, 1986.
Karato, S.-I., M.S. Paterson, and J.D. Fitzgerald, Rheology of synthetic olivine aggregates: influence of grain size and water, *J. Geophys. Res., 91,* 8,151-8,176, 1986.
Kirby, S.H., and A.K. Kronenberg, Rheology of the lithosphere: selected topics, *Rev. Geophys., 25(6),* 1,219-1,244, 1987.
Klemperer, S.L., and N.J. White, Coaxial stretching or lithospheric simple shear in the North Sea? Evidence from deep seismic profiling and subsidence, *Am. Ass. Petr. Geol. Mem., 46,* pp. 511-522, 1989.
Kruse, S., M. McNutt, J. Phipps-Morgan, and L. Royden, Lithospheric extension near Lake Mead, Nevada: a model for ductile flow in the lower crust, *J. Geophys. Res., 96,* 4,435-4,456, 1991.
Kusznir, N., and S.S. Egan, Simple-shear and pure-shear models of extensional sedimentary basin formation: application to the Jeanne d'Arc, Grand Banks of Newfoundland, *Am. Ass. Petr. Geol. Mem., 46,* 305-322, 1989.
Latin, D., and N. White, Generating melt during lithospheric extension: pure shear vs. simple shear, *Geology, 18,* 327-331, 1990.
Lister, G.S., and G.A. Davis, The origin of metamorphic core complexes and detachment faults formed during Tertiary continental extension in the northern Colorado River region, U.S.A., *J. Struct. Geol., 11,* 65-94, 1989.
Martinod, J., and P. Davy, Periodic instabilities during compression or extension of the lithosphere 1. Deformation modes from an analytical perturbation method, *J. Geophys. Res., 97,* 1,999-2,014, 1992.
McKenzie, D., Some remarks on the development of sedimentary basins, *Earth Planet. Sci. Lett., 40,* 25-32, 1978.
Melosh, H.J., and A. Raefsky, The dynamical origin of subduction zone topography, *Geophys. J. R. astron. Soc., 60,* 333-354, 1980.
Melosh, H.J., and A. Raefsky, A simple and efficient method for introducing faults into finite element computations, *Bull. Seismol. Soc. Am., 71(5),* 1,391-1,400, 1981.
Melosh, H.J., and A. Raefsky, Anelastic response of the earth to dip slip earthquakes, *J. Geophys. Res., 88,* 515-526, 1983 stablity of split nodes.
Melosh, H.J., and C.A. Williams, Mechanics of graben formation in crustal rocks: a finite element analysis, *J. Geophys. Res., 94,* 13,961-13,973, 1989.
Moriceau, C., and L. Fleitout, A directional analysis of the small wavelength geoid of the Pacific Ocean, *Geophys. Res. Lett., 16,* 251-254, 1989.
Paterson, M.S., and F.C. Luan, Quartzite rheology under geological conditions, in *Deformation Mechanisms, Rheology and Tectonics, 54,* edited by R.J. Knipe and E.H. Rutter, pp. 299-307, Geological Society of London Special Publication, London, 1990.
Poirier, J.-P., Creep of Crystals, *Earth Science Series,* pp. 260, Cambridge University Press, Cambridge, MA, 1985.
Ricard, Y., and C. Froidevaux, Stretching instabilities and lithospheric boudinage, *J. Geophys. Res., 91,* 8,314-8,324, 1986.
Royden, L., and C.E. Keen, Rifting processes and thermal evolution of the continental margin of eastern Canada determined from subsidence curves, *Earth Planet. Sci. Lett., 51,*

343-361, 1980.

Rutter, E.H., and K.H. Brodie, The role of tectonic grain size reduction in the rheological stratification of the lithosphere, *Geol. Rund., 77*, 295-308, 1988.

Sawyer, D.S., Brittle failure in the upper mantle during extension of continental lithosphere, *J. Geophys. Res., 90*, 3,021-3,025, 1985.

Tullis, J., and R.A. Yund, Dynamic recrystallization of feldspar: a mechanism for ductiles-hear zone formation, *Geology, 13*, 238-241, 1985.

Tullis, J., L. Dell'Angelo, and R.A. Yund, Ductile shear zones from brittle precursors in feldspatic, *Geophysical Monograph, 56*, 67-81, 1990.

Twiss, R.J., Theory and applicability of a recrystallized grain size paleopiezometer, *Pageoph., 115*, 227-244, 1977.

Vening Meinesz, F.A., Les grabens Africain résultant de compression ou de tension dans la crôute terrestre, *Colonial Institute of Amsterdam Bulletin, 21*, 539-552, 1950.

Weissel, J.K., and G.D. Karner, Flexural uplift of rift flanks due to mechanical unloading of the lithosphere during extension *J. Geophys. Res., 94*, 13,919-13,950, 1989.

Wdowinski, S., and R.J. O'Connell, On the choice of boundary conditions in continuum models of continental deformation., *Geophys. Res. Lett., 17*, 2,413-2,416, 1990.

Wenk, H.-R., K. Bennet, G.R. Canova, and A. Molinari, Modelling plastic deformation of peridotite with the self-consistent theory, *J. Geophys. Res., 96*, 8,337-8,349, 1991.

Wernicke, B., Low-angle normal faults in the Basin and Range Province: nappe tectonics in an extending orogen, *Nature, 291*, 645-648, 1981.

Wernicke, B., Uniform-sense normal simple shear of the continental lithosphere, *Can. J. Earth Sci., 22*, 108-125, 1985.

White, N.J., The nature of lithospheric extension in the North Sea, *Geology, 17*, 111-114, 1989.

White, S.H., Syntectonic recrystallization and texture development in quartz, *Nature, 244*, 276-278, 1973.

White, S.H., The effects of strain on the microstructures fabrics and deformation mechanisms in quartzites, *Phil. Trans. R. Soc. London (A), 283*, 69-86, 1976.

White, S.H., M.R. Drury, S.E. Ions, and F.J. Humphreys, Large strain deformation studies using polycrystalline magnesium as a rock analogue. Part 1: grain paleopiezometry in mylonite zones, *Phys. Earth Planet. Interiors, 40*, 201-207, 1985.

White, S.H., P.G. Bretan, and E.H. Rutter, Fault-zone reactivation: kinematics and mechanisms, *Phil. Trans. R. Soc. London (A), 317*, 81-97, 1986.

Wilks, K.R., and N.L. Carter, Rheology of some continental lower crustal rocks, *Tectonophysics, 182*, 57-77, 1990.

Williams, C.A., and R.M. Richardson, A rheologically layerd three-dimensional model of the San Andreas Fault in Central and Southern California, *J. Geophys. Res., 96*, 16,597-16,623, 1991.

Zuber, M.T., E.M. Parmentier, and R.C. Fletcher, Extension of continental lithosphere: a model for two scales of Basin-and-Range deformation, *J. Geophys. Res., 91*, 4,826-4,838, 1986.

Chapter 5

Initiation of Asymmetric Extension in Continental Lithosphere †

R. Govers and M.J.R. Wortel

ABSTRACT

The physical conditions are investigated under which the lithospheric scale style of extension is pure shear or simple shear. We focus on the initial stages of continental extension to monitor how symmetric or asymmetric modes of extension evolve from specific tectonic conditions. Continental collision, magma intrusions and interaction between the lithosphere and the underlying mantle are investigated as sources for extension. We use a finite element method to model the thermomechanical evolution of continental lithosphere. Experimental flow laws are used to model the elastic, brittle, power law creep or diffusion creep rheology of lithospheric rocks. Our results indicate that if in-plane forces change from compressive to tensile immediately after a rapid mountain building phase, initiation of a lithosphere scale detachment fault is possible. We find a strong dependence of the extensional style on the distribution with depth of residual stresses from the collision phase. This result is consistent with observations of gravitational collapse in regions, like the Aegean and the Basin and Range Province, where detachment faults have exhumed lower crustal rocks. The predicted dip direction of the fault also agrees with observations in these areas. Intrusion of magma into continental lithosphere, which is subject to in-plane tensile forces, will cause localization of pure shear deformation. The style of deformation resulting from mantle plumes impinging to the base of the lithosphere is symmetric. Delamination of lithospheric mantle may initiate detachment faults if delamination occurs at the end of a collision

---

† This chapter has been submitted for publication as: R. Govers and M.J.R. Wortel, Initiation of Asymmetric Extension in Continental Lithosphere, *Tectonophysics*, 1993.

phase, when in-plane forces change sign from compressive to tensile. This result also strongly depends on the assumed residual stress distribution. If delamination occurs during the mountain building phase, the style of deformation will be pure shear. Another interesting outcome from our modeling is that dramatic strain weakening as a result of a deformation mechanism change from dislocation creep to diffusion creep, reduces the tendency to strain localization.

INTRODUCTION

A large volume of the published work on continental extension has been concentrated on quantifying the stretching factor β of the pure shear model of McKenzie (1978a). In some basins it was found that the kinematics of deformation could be more accurately described by depth-dependent stretching factors (Royden and Keen, 1980), which introduced asymmetry near basin edges. In the simple shear model of Wernicke (1981; 1985), the asymmetry is complete as continental extension occurs along a lithosphere cutting detachment fault ("fault" is used here in a loose way to describe a high degree of localized deformation accommodated by an unspecified deformation mechanism). In terms of asymmetry, the pure shear and simple shear models represent end-members of a spectrum of models for continental extension that allow non-homogeneous deformation in some depth range (Royden and Keen, 1980; Hellinger and Sclater, 1983; Rowley and Sahagian, 1986; Gans, 1987; Kusznir and Egan, 1989; Lister and Davis, 1989). These papers motivated work to investigate what geological or geophysical data allow the models to be discriminated (e.g. Furlong and Londe, 1986; Ruppel *et al.*, 1988; Buck *et al.*, 1988; Latin and White, 1990). Additionally work has been done to determine the overall style of extension in sedimentary basins and passive margins (e.g. Sclater and Christie, 1980; Le Pichon and Sibuet, 1981; Barton and Wood, 1984; Beach, 1986; Lister *et al.*, 1986; White, 1989; Latin and Waters, 1991).

Surprisingly, a realistic assessment of the physical conditions which determine the style of continental extension is made in a few papers only. In interior parts of the continental lithosphere total strain rates tend to be uniform with depth, independent of the exact nature of the plate boundary forces (e.g. slab pull) that drive extension (Kusznir and Bott, 1977; chapter 3 of this thesis). Equivalently, the normal mode of intraplate deformation as a result of in-plane forces alone is pure shear. In chapter 4 of this thesis we show that initiation of lithosphere scale detachment faults is unlikely in continental lithosphere which, mechanically and thermally, is in equilibrium. It is concluded that in-plane forces alone do not suffice to generate asymmetric deformation in lithosphere not containing pre-existing weak zones. Initiation of shallow dipping lithosphere-scale faults therefore has to occur under different circumstances. Braun and Beaumont (1989a) and Dunbar and Sawyer

(1989) investigate the style of extension in continental lithosphere containing offset pre-existing weaknesses in the crust and mantle. They conclude that the weak lower crust can act as a level of decollement between crust and mantle, along which the horizontally offset mantle and crustal weaknesses may link up.

Pre-existing weaknesses might control the initiation of detachment faults, but there is no evidence that this is always so. Also, an explanation of detachment faults in terms of pre-existing weaknesses disregards the possible relation between a pre-extension thickening period and subsequent asymmetric extension, as was suggested by Coney (1987) for the Basin and Range Province. Yin (1987; 1989) and Spencer and Chase (1989) show that stress trajectories in elastic plate-like continua which are subject to combinations of boundary conditions, agree with the low-angle nature of detachment faults. Their choice for an elastic rheology is motivated by the large deviatoric stresses which can be supported near the upper crustal brittle-ductile transition. For a more realistic rheology it can be expected that, at specific geothermal gradients, the upper crust, lower crust and mantle are decoupled to some degree by weak zones. In these cases, the results of Yin (1987; 1989) and Spencer and Chase (1989) can be interpreted to apply to these layers individually. The relevance of their models in the context of whole lithosphere deformation is, however, more difficult to determine.

In a model with a simplified rheology, Melosh (1990) shows that principal stress trajectories flatten out in a low-viscosity layer beneath a strong layer containing a (steeply dipping) normal fault. It is argued that Yin (1989) and Spencer and Chase (1989) need to invoke boundary conditions which derive from hidden sources, but in his model, Melosh (1990) invokes an ad hoc end load; basically, he assumes that the upper and lower crust ride along on an extending upper mantle. It is therefore clear from the onset that shear between crust and mantle is required. For intraplate regions, the results of Kusznir and Bott (1977) and chapter 3 of this thesis show that a uniform in-plane force boundary condition is a more realistic approximation of the end load resulting from plate boundary processes. In Melosh's (1990) model it is assumed that the dip of the fault plane in strong layers is rather steep. It has been proposed (Jackson, 1987; Wernicke and Axen, 1988) that fault planes form in steep orientations, and rotate to shallow dips during extension. However, the large areal extent of denuded footwalls and relatively constant metamorphic grade of exposed footwall rocks in the Basin and Range Province of western North America (Lister and Davis, 1989), is an argument against the theory that low-angle normal faults originally formed in steeper orientations. Melosh's model is therefore considered not relevant in the context of initiation of an asymmetric mode of extension.

Typically, the overall style of deformation is symmetric, except when specific causes for asymmetric deformation exist. Our approach is to identify the physical

conditions which lead to asymmetric deformation and to focus on the whole-lithosphere simple shear end-member. Requirements for initiation of detachment faults can be formulated as that the overall style of deformation is asymmetric and that strain is localized in a zone of finite width. It is important to realize that localization of strain is not a sufficient requirement for asymmetric extension since, in most cases, strain will localize along conjugate fault systems and induce an overall symmetric style of extension. We, therefore, consider the boundary conditions which induce asymmetric extension as primary causes for localization. In the present chapter we investigate processes which lead to conditions which are favorable for initiation of asymmetrical extension other than pre-existing weaknesses (in the following, processes which lead to conditions which are favorable for initiation of asymmetrical extension will be loosely referred to as "causes for initiation of asymmetrical extension"). We consider continental lithosphere which is not in mechanical and/or thermal equilibrium, i.e. the lithosphere recently has been subject to a tectonic and/or thermal event. Three causes for mechanical and thermal instability of continental lithosphere will be examined. The first two causes result in mechanical and thermal initial and boundary conditions within the lithosphere itself: lithospheric thickening and intrusions. The third cause results from mechanical and/or thermal interaction between the lithosphere and the underlying mantle.

ASYMMETRIC EXTENSION: POSSIBLE CAUSES

Şengör and Burke (1978) recognize two end-members of rifting: "active" rifting, in which rifting is a result of mantle convection/lithosphere interaction, and "passive" rifting, in which rifting is a response to processes occurring in the lithosphere itself. A feature common to most rifts is volcanism, and Şengör and Burke (1978) identify the expected sequence of events for active rifting as doming-volcanism-extension, and as rifting-volcanism for passive rifting. They conclude that, at present, passive rifting is "by far more widespread" than active rifting. Continental thickening as a cause for subsequent extension is a purely passive mechanism. Thermo-mechanical interaction between mantle plumes and the overlying lithosphere is a purely active mechanism. All other causes of continental extension we consider are intermediate between passive and active mechanisms.

The potential energy contrast of regions of isostatically compensated thickened crust relative to normal continental lithosphere may generate tensile stresses (Love, 1911; Artyushkov, 1973). Continental thickening as a cause for subsequent extension has been proposed for the Altiplano in the Andes (Dewey, 1988), for the Tibetian Plateau in the Himalayas (England and McKenzie, 1982; Mercier *et al.*, 1987), the Aegean Sea in the Mediterranean (McKenzie, 1972; Berckhemer, 1977; Le Pichon, 1983) and for the Basin and Range Province (Coney, 1987; Wernicke *et*

al., 1987; Sonder *et al.*, 1987). Given the evidence for major low angle normal faults in the Aegean Sea (e.g., Lister *et al.*, 1984; Lee and Lister, 1992) and in the Basin and Range Province (e.g., Wernicke, 1981; Davis, 1983; Wernicke, 1985) this mechanism must be considered a serious candidate for initiating lithosphere scale faults.

Continental extension is commonly associated with intrusions and sometimes with volcanism. It is mostly unclear whether magmatism is caused by passive upwelling of thinning lithosphere or whether magma intrusions play an initiating role in continental extension. Active magmatism and intrusions may play an important role in localizing extensional deformation in pre-stressed lithosphere. We will investigate to what extent intrusions may lead to asymmetrical deformation.

The category of sub-lithospheric causes for detachment faults generates mechanical and/or thermal boundary conditions on the lower lithosphere boundary. Examples are lithospheric mantle delamination (detachment), rising or sinking plumes and buoyant subducted slabs. McKenzie (1978b) proposed that (parts of) lithospheric mantle may delaminate during thickening and sink into the mantle. Supportive evidence for this mechanism was found from numerical experiments by Houseman *et al.* (1981). Relative to the continental mantle, the asthenosphere is buoyant as a consequence of higher asthenospheric temperatures. In the delamination model, this density inversion causes (parts of) the mantle to detach from the overlying lithosphere during or after thickening. The delaminated mantle sinks into the asthenosphere and is replaced by material of asthenospheric temperatures, consequently generating isostatic uplift pressures and a drastic change in the lower thermal boundary condition.

Quantitative estimates of the effects of mantle convection on the overlying plates necessarily derive from indirect observations. Topographic swells in oceanic basins with up to 1000 meter amplitude are commonly attributed to mantle-lithosphere interaction. Crough (1978) found that the surface heat flow over these swells is 20-25% higher than in "normal" oceanic lithosphere and subsidence after the plate passed over the "hot spot", and can be well explained by conductive cooling of a rejuvenated lithosphere. These observations strongly indicate that oceanic topographic swells are at least in part thermally supported. More recent studies do, however, not support these findings. Another effect of rising mantle plumes could be that a normal stress is applied to the base of the lithosphere (McKenzie, 1977). Dynamical pressures have an immediate effect on the surface uplift from the time a plume starts to impinge onto the base of the lithosphere, whereas a time comparable to the thermal time constant of the lithosphere is required for the thermal mechanism to generate substantial uplifts. It is difficult to separate thermal and dynamical contributions to topographic swells in oceanic plate interiors (Nakiboglu and

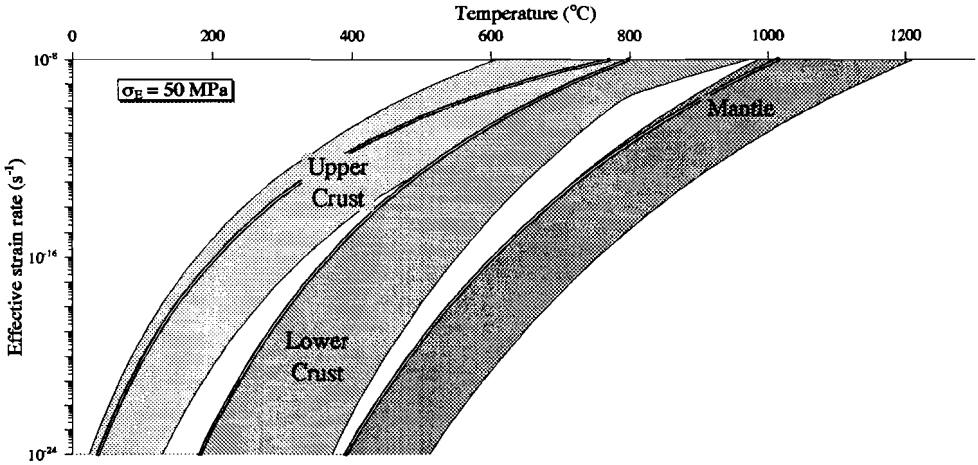

Fig. 1. *Spectrum of upper crustal, lower crustal and mantle rock rheologies and the selected flow laws.*

Lambeck, 1985).

It is as yet not clear whether, mechanically, sub-continental mantle resembles sub-oceanic mantle (see, for instance, Anderson (1989)) and whether inferences on mantle plumes, made from observations in oceanic plate interiors, can be translated to continental lithosphere (e.g. Houseman and England, 1986). Amplitudes of oceanic swells give the only observational constraints on mantle-lithosphere interaction, however. In the context of continental extension resulting from mantle plumes, the models of Sleep (1971) and Houseman and England (1986) can be regarded as end-member models, as the former assumes a completly thermal origin and the latter a completly dynamic origin for basin formation. We consider the thermal effects of mantle plumes less relevant for the initiation of asymmetric extension; even if a mantle plume could have sharp vertical boundaries creating a step change in boundary conditions along the base of the lithosphere, thermal diffusion would smear out buoyancy forces over a broader zone, making asymmetric deformation less probable. Our model therefore resembles the model of Houseman and England (1986) in that the boundary condition reflecting the plume-lithosphere interaction is completely dynamic.

It is not our purpose to present a full study of the model parameter space. Instead, we select a few models which could lead to asymmetrical extension for each of the mechanical or thermal instability causes discussed above. Our aim is to investigate whether fairly common tectonic processes may lead to lithosphere detachment faults and asymmetric deformation. In chapters 6 and 7 of this thesis, mecha-

Table 1a. Powerlaw creep parameters adopted for the lithosphere and diffusion creep parameters for the lithospheric mantle.

		n_{pl}	Q_{pl} kJ/mole	A_{pl} $Pa^{-n}s^{-1}$
Upper crust	Wet quartzite[1)]	3.1	135	$7.7621 \cdot 10^{-26}$
Lower crust	Granulite[2)]	3.1	243	$9.5534 \cdot 10^{-21}$
Mantle	Wet olivine[3)]	3	420	$8.5746 \cdot 10^{-15}$
		n_{dc}	Q_{dc} kJ/mole	A_{dc} $Pa^{-n}s^{-1}$
Mantle	Wet olivine[3)]	1	240	0.6253

[1)] Paterson and Luan (1990), [2)] Wilks and Carter (1990),
[3)] Rutter and Brodie (1988)

Table 1b. Thermal data. H_{60} and k_{60} are heat production and conductivity at a steady state geotherm with a surface heat flow of 60 mW/m^2. C_p and α are the specific heat and volumetric expansion coefficient respectively.

	H_{60} $\mu W/m^3$	k_{60} $Wm^{-1}K^{-1}$	C_p $Jkg^{-1}K^{-1}$	α K^{-1}
Upper crust	1.37	2.56	1300	$3.2 \cdot 10^{-5}$
Lower crust	0.45	2.60	1300	$3.2 \cdot 10^{-5}$
Mantle	0.02	3.20	1300	$3.2 \cdot 10^{-5}$

nisms which look promising for initiating lithosphere scale faults will be considered in more detail.

MODELING APPROACH

Continental rock rheology

Various deformation mechanisms contribute to the strain of continental rocks which are subject to stresses. The rate and relative importance of these deformation mechanisms depends mainly on temperature, pressure and composition. The rheologies which are usually considered most important in the context of whole lithosphere deformation are elasticity, brittle failure and steady-state ductile flow. Isotropic linear elastic behavior is a good approximation of recoverable strains at

low stresses (usually below one third of the uniaxial yield stress). Permanent strain at low temperatures is mainly achieved by brittle deformation. From laboratory experiments, the differential stress magnitude which is required to overcome the frictional resistance along fault planes, was found by Byerlee (1978) to be rather insensitive to rock type. This relation is not undisputed and geological and geophysical observations indicate that Byerlee's law provides an upper limit -perhaps significantly overestimated- to differential stresses at depths greater than 5 km. It is, however, one of the few quantitative relations available and we adopt Byerlee's law to determine the yield strength in brittle rocks, which is modeled using a visco-plastic rheology.

At higher temperatures, rocks respond by creep to applied differential stresses. In our rheological model we neglect transient creep and, based upon laboratory experiments, assume that power law dislocation creep laws provide a first order description of the strain rate at a given temperature, stress and composition. These empirical flow laws are the result of extrapolation of strain rates over many orders of magnitude and should therefore be considered as first order estimates at best. A second deformation mechanism which may be important at high temperatures is diffusion creep. Rutter and Brodie (1988) propose a quantitative deformation path along which a material that initially deforms by power law creep moves towards the diffusion creep field with progressive strain and becomes weaker. Chapter 4 of this thesis gives a more elaborate discussion on strain weakening mechanisms.

We assume that the development of specific types of continental extension can be studied in structures which are essentially two dimensional, in the sense that the geometry and boundary conditions hardly vary in the third out-of-plane horizontal dimension ("plane strain" assumption). In this case the constitutive equations can be summarized as

$$\left.\begin{aligned}
\dot{\varepsilon}_{xx} &= \frac{(1+\nu)}{E}\left[(1-\nu)\dot{\sigma}_{xx} - \nu\dot{\sigma}_{yy}\right] + \frac{(\sigma_E/\eta_{eff})^{n-1}}{4\eta_{eff}}\left[\sigma_{xx} - \sigma_{yy}\right] \\
\dot{\varepsilon}_{yy} &= \frac{(1+\nu)}{E}\left[(1-\nu)\dot{\sigma}_{yy} - \nu\dot{\sigma}_{xx}\right] - \frac{(\sigma_E/\eta_{eff})^{n-1}}{4\eta_{eff}}\left[\sigma_{xx} - \sigma_{yy}\right] \\
\dot{\varepsilon}_{xy} &= \frac{(1+\nu)}{E}\dot{\sigma}_{xy} + \frac{(\sigma_E/\eta_{eff})^{n-1}}{2\eta_{eff}}\sigma_{xy}
\end{aligned}\right\}$$

(c.f. Melosh and Raefsky, 1980) where $\dot{\varepsilon}_{ij}$ denote deviatoric strain rate components, ν and E are the elastic Poisson ratio and Young's modulus, and σ_{ij} are stress tensor components. A dot indicates differentiation with respect to time. η_{eff} is the effective viscosity selected to approximate the relation between effective strain rate and stress for a specific deformation mechanism, material, temperature and pres-

sure. σ_E, the effective stress, is the second invariant of the stress tensor for plane strain:

$$\sigma_E = \left[\left(\frac{\sigma_{xx} - \sigma_{yy}}{2} \right)^2 + \sigma_{xy}^2 \right]^{\frac{1}{2}}$$

In this formulation incompressibility is automatically maintained during viscous flow; isotropic stresses only affect the elastic volumetric strain, viscous volumetric strains are always zero. Other useful parameters are the effective strain and effective total deviatoric strain rate. The definitions for effective strain and strain rate are similar to the definition of the effective stress. The second invariants of the stress tensor, strain tensor and strain rate tensor are useful measures of the magnitude of the deviatoric tensor. In what follows, total strain rate is referred to as "strain rate".

We model the continental lithosphere as a three layer system; upper crust, lower crust and lithospheric mantle. In the upper crust we assume a wet quartzite power law rheology (Patterson and Luan, 1990), the lower crust is modeled using the Adirondack granulite rheology of Wilks and Carter (1990) and in the mantle we employ the wet olivine power law and diffusion creep rheologies from Rutter and Brodie (1988). From Figure 1 it is clear that the selected rheologies are at the low-viscosity end of the spectrum of upper crustal, lower crustal and mantle rheologies.

Numerical model

The above constitutive equations are incorporated in a finite element code, TECTON, developed by Melosh and Raefsky (1980; 1981; 1983) and Melosh and Williams (1989). A displacements based finite element method is used to solve the mechanical equilibrium equation

$$\nabla \cdot \sigma + X = 0$$

for body force X. We have adapted TECTON to solve the transient heat conduction equation as a function of time t

$$\rho C_p \frac{\partial T}{\partial t} = \nabla \cdot (k \nabla T) + H$$

by a finite element method for temperatures T, density ρ, specific heat C_p, thermal conductivity k and heat production H. Overlapping thermal and mechanical finite element grids are used to solve the heat and mechanical equilibrium equations sequentially. The differential equations are coupled via the effective viscosity and via thermal stresses and buoyancy forces. Table 1 gives parameter values which are adopted in this chapter.

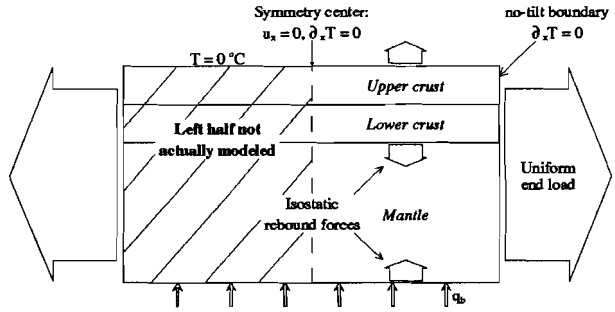

Fig. 2. *Generalized model of continental lithosphere. For economy reasons only the right half is modeled. Mechanical and thermal boundary conditions on the left side reflect symmetry. The model is assumed to continue to the right infinitely. This is reflected in the mechanical and thermal boundary conditions of no-tilt and no horizontal heat flow. The top of the lithosphere is at 0°C, and a constant basal heat flow q_b is applied to the lower boundary. Isostatic rebound forces act on density interfaces and a uniform force is applied to the right boundary. See text for explanation.*

Boundary conditions

To calculate vertical surface uplifts we employ the "density stripping method" (Braun, 1988; Williams and Richardson, 1991). In this method it is assumed that gravity pre-stresses are hydrostatic and that the slope of density interfaces is small. Initial gravity body forces do not enter the system of partial equations and buoyancy forces are replaced by restoring pressures on density interfaces. Changes in density resulting from thermal expansion are included as body forces. We assume that the asthenosphere has a slightly (50 kg/m^3) lower density than the overlying lithospheric mantle, as a result of higher asthenospheric temperatures.

Relative to normal continental lithosphere, continental lithosphere that has been thickened under isostatic conditions is very often in an average state of tension. The magnitude of the average differential stress can be calculated by comparing the density moment of two lithospheric columns (Artyushkov, 1973). In these calculations, it is implicitly assumed that force contributions from sub-lithospheric mantle processes to stresses in thickened and normal lithospheric columns have equal magnitudes. This assumption is justified if the normal and thickened columns are proximate, since most mantle processes occur on large length scales and horizontal gradients of sub-lithospheric forces are, therefore, small. We calculate the average differential stress of thickened continental lithosphere relative to normal continental lithosphere. The resulting average differential stresses are included as uniformly distributed pre-stresses in thickened lithosphere. Smaller wavelength buoyancy

contributions, for instance resulting from delamination or secondary convection, can be included by separate basal pressures.

The finite element models are symmetric about a vertical axis (Figure 2), and thus the calculations are performed only in the right hand side of the model. Boundary conditions at the left side of the actual model are formulated to reflect this symmetry; horizontal displacements and heat flux are zero on this side. We will display the results in the right half of the model only. In the following, we will discuss the style of extension of the finite element models in terms of "symmetric" and "asymmetric". We recognize that this classification might be misleading, since the models are completely symmetric around $x=0$, as just explained. With "asymmetric extension" we intend to describe deformation on one symmetry side of the model, which is predominantly localized along a fault or shear zone with a uniform sense of shear.

Boundary conditions on the right hand side of the models reflect the assumption that the model continues to the right; the horizontal heat flow is zero and mechanically this is a no-tilt boundary. In some of the models a uniform in-plane force is applied on the right hand side. These forces are assumed to derive from plate boundary forces (ridge push, slab pull, etc.) which are transmitted as stresses to plate interiors. Based upon observations of depths of oceanic intraplate earthquakes, Govers *et al.*, (1992) show that in-plane stress magnitudes of the order of hundreds of MPa's are possible. Their study confirms model calculation results of the intraplate stress field in the Indo-Australian plate (Cloetingh and Wortel, 1985). In-plane stress magnitudes in our models are less than or equal to $1 \cdot 10^{13}$ N/m, which is equivalent to 100 MPa averaged over a 100 km thick lithosphere. The upper surface is held at 0 °C. We assume that a continental keel continues below the lithosphere (Anderson, 1989) in most models. The sub-lithospheric mantle is therefore part of the thermal boundary layer and a heat flux lower boundary condition is considered more appropriate than a constant temperature lower boundary condition.

EXTENSION OF THICKENED LITHOSPHERE

As it is our aim to investigate common geological processes which may lead to lithosphere scale asymmetric deformation, we select model parameters which promote this type of extension. In this section we study a few models of thickened continental lithosphere (TCL; nomenclature taken from Braun and Beaumont, 1989b).

The initial steady-state geotherm in the reference continental lithosphere (RCL) has been calculated for the average continental surface heat flow of 60 mW/m^2. The initial crustal thickness is 35 km, the Moho temperature is 548 °C. Elevations

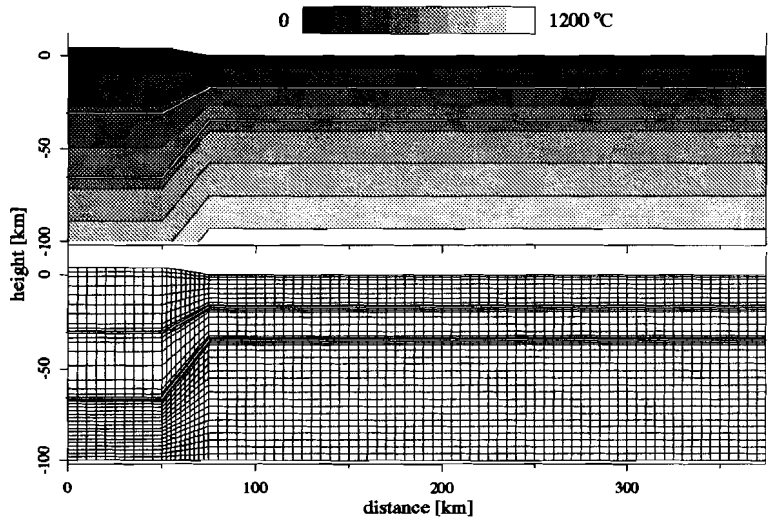

Fig. 3. *Initial grid and geotherms of thickened lithosphere model.*

are relative to the initial RCL surface.

The TCL results from instantaneous thickening of the RCL to produce a maximum laterally inhomogeneous structure. We adopt a uniform crustal thickening factor $\beta^{-1}=2$, which is the upper limit of thickening factors found in the Himalayas. To maximize the potential energy contrast of the TCL relative to the RCL without invoking additional tectonic mechanisms such as mantle delamination, we assume that the lithospheric mantle has not been thickened and has passively been depressed. After thickening, isotherms in the thickened lithosphere are unstable for two reasons. First, heat producting elements are concentrated in the upper crust and thickening of the crust eventually leads to a higher geothermal gradient. A second reason for thermal instability is that advective heat transport has occurred during the thickening phase. The surface elevation of the TCL relative to the RCL is calculated from local isostatic balance. Although we do not actually model the mantle beneath the TCL at depths greater than 100 km, the continental mantle is assumed to continue to greater depths.

The TCL is bounded by a transition region across which the crustal thickness returns to the reference value of 35 km. To promote lateral inhomogeneity, we select a 25 km width for the transition zone, which we consider a minimum, given that the topography of the TCL is more than 4 km (c.f. Davis *et al.*, 1983). Figure 3 displays the initial grid and geotherms.

The strain in the models we consider in this chapter will be shown to be laterally

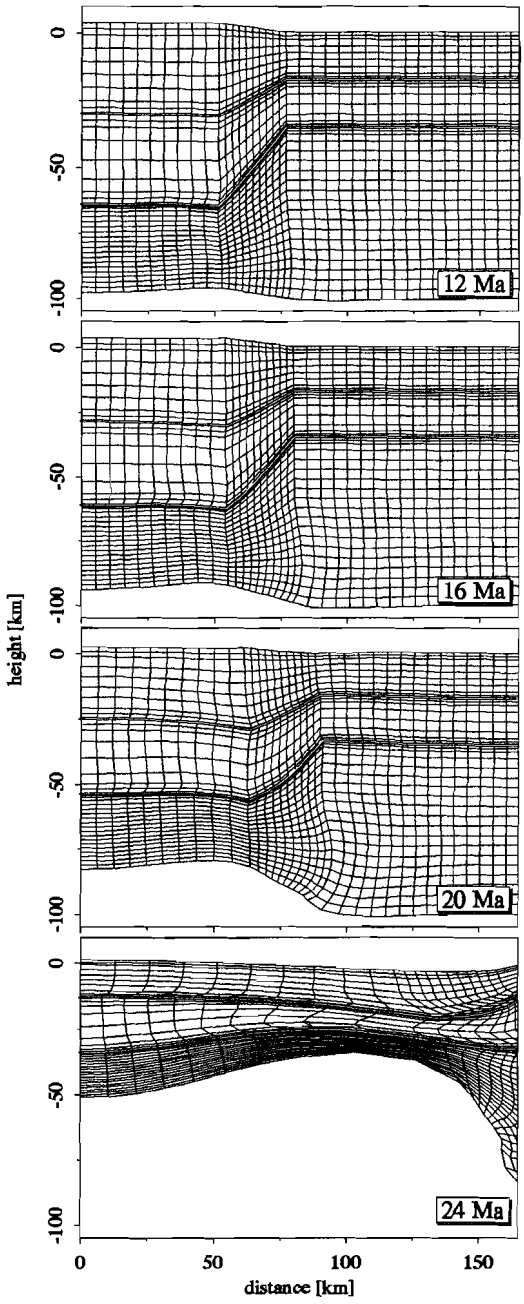

Fig. 4. *Model 1 (Gravitational collapse model). Evolution of lithosphere model.*

inhomogenous. In the following discussion, we classify the strain in extended models as either symmetric or asymmetric on a rather arbitrary basis from inspection of the deformed finite element grid, and distributions of strain and strain rate. Thusfar, an objective criterion which adequately describes the overall style of extension has not been found. Our approach to classifying the style of extension is to look for lithosphere scale asymmetries and, if the evidence for asymmetric behavior is vague or absent, to classify the style of extension as "pure-shear-like" or symmetric. Through figures of deformed model grids, we allow the reader to judge the symmetry or asymmetry of extension and weigh our classification. This approach obviates the problem that, although we might classify the style of extension on the scale of the lithosphere as symmetric, readers interested in the upper crust may decide for themselves that a specific mechanism leads to asymmetries in their region of interest. Anyway, would we have designed some objective criterion, it would not have been sufficient to present our results by merely classifying the style of extension on the basis of that criterion. The arbitrariness of prefering one criterion above another would be reflected in the fact that, in the grey area between

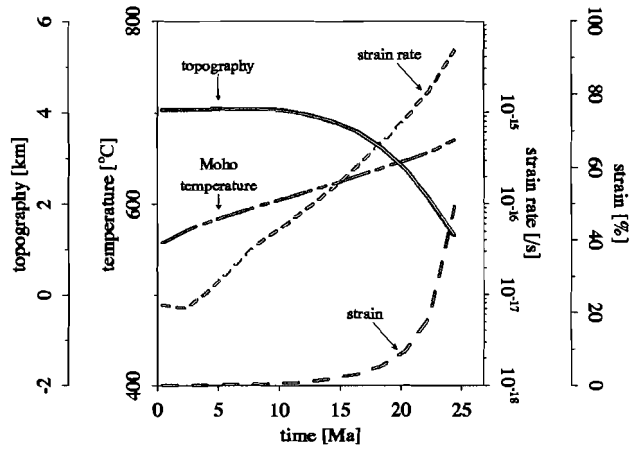

Fig. 5. *Model 1 (Gravitational collapse model). Surface topography, Moho temperature, average effective strain rate and average effective strain at symmetry center.*

pure symmetry and pure asymmetry, one criterion would classify a model as symmetric, while the other would classify it as asymmetric.

Model 1. Gravitational collapse model

In this model, the compressive in-plane force which thickened the crust is removed at $t=0$. Figure 4 shows the evolution of the model lithosphere. The potential energy stored in the TCL does not suffice to cause significant extension in the first 10 Ma. Heating of the TCL has the combined effect of creating buoyancy forces and decreasing viscosities. This increases the rate of thinning which, in turn, increases the rate of mantle heating. It is therefore conceivable that, after approximately 20 Ma, extension accelerates to lead finally to complete rifting. Figure 5 displays surface topography, Moho temperature, strain and strain rate in the symmetry center ($x=0$) as a function of time. The top panel of Figure 6 shows contours of effective strain after 22 Ma. Contours of the logarithm of effective strain rates after 22 Ma are displayed in the bottom panel. As a result of lateral heat conduction, heating is most pronounced near the transition zone. Strain and strain rate maxima occur in the weak upper and lower crust near the transition zone. It is clear that the strain and strain rates are not homogeneous, a result which is hardly surprising in a laterally strongly varying structure. However, no clear asymmetry has developed and we consider the style of deformation, therefore, as essentially symmetric. Gravitational collapse can well be described by depth dependent uniform stretching beneath the previously thickened region.

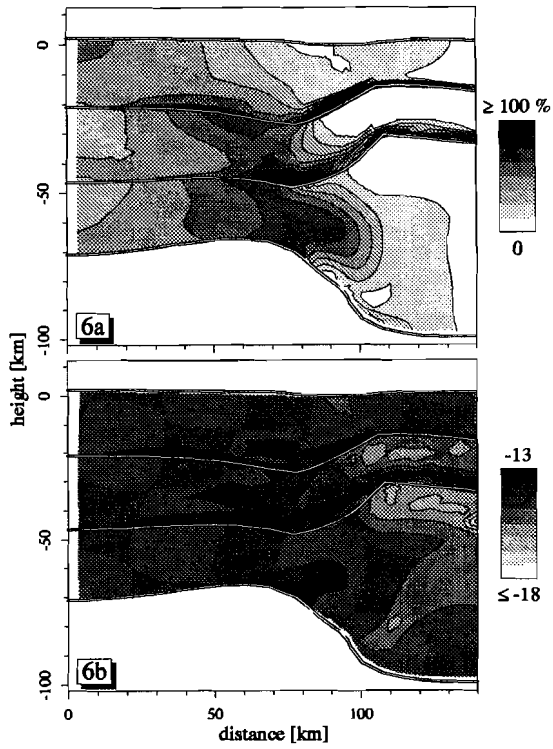

Fig. 6. *Model 1 (Gravitational collapse model). (a) Contours of effective strain after 22 Ma. (b) Contours of logarithmic effective strain rates after 22 Ma.*

Assuming different rheologies or a different initial geotherm would alter the time constants of our modeling but not the overall style of deformation. Compared to vertical heat conduction, lateral heat conduction is relatively unimportant in heating the TCL and, consequently, heating is rather uniform. Both the driving load for thinning and changes in the viscosity structure derive from heating of the TCL and, therefore, thinning occurs mainly by pure shear. Thickening of the lithospheric mantle by the same amount as the crust would focus the heating and deformation more within the crust, but it would again be fairly uniform. Although a complete investigation of the parameter space would be required to make conclusive statements, gravitational collapse is probably not relevant for initiation of a lithosphere scale asymmetrical mode of extension. This finding is in accordance with the results of Braun and Beaumont (1989b).

Model 2. Immediate extension of thickened continental lithosphere

In the previous model we removed the in-plane compressive force immediately after the thickening phase. In Model 2 the in-plane force changes sign from compressive to $5 \cdot 10^{12}$ N/m tension at $t = 0$. This force is equivalent to an in-plane

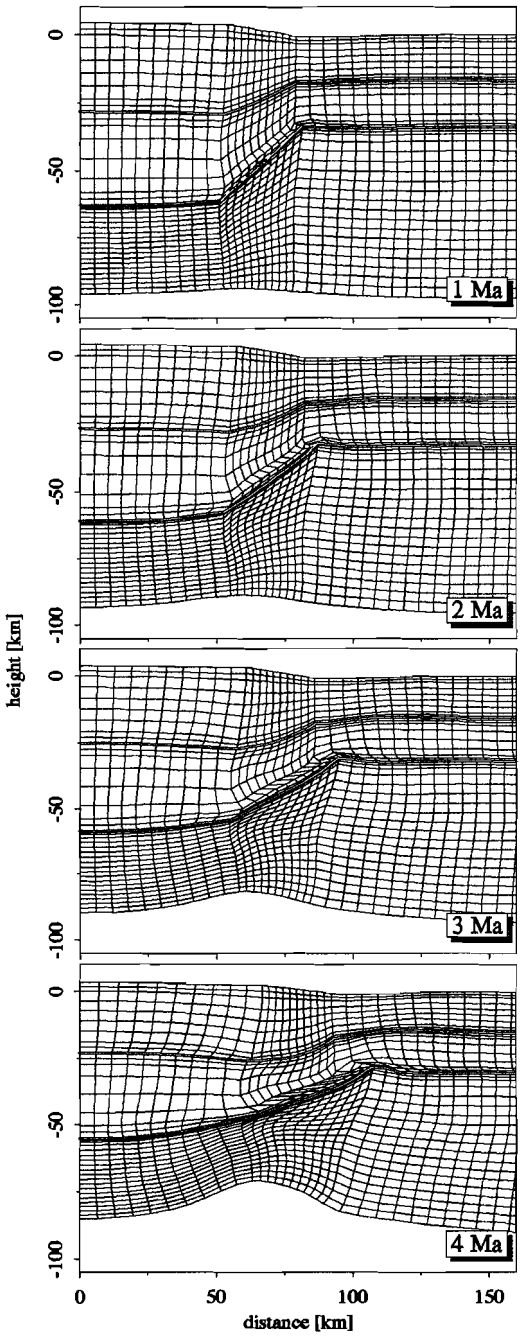

Fig. 7. *Model 2 (Extending TCL model). Evolution of deforming grid.*

stress of 50 MPa and is held constant from $t = 0$ onward.

Figure 7 shows the evolution of the extending lithosphere. The time scale of deformation is considerably shorter than in the previous model and after 4 Ma the lower crustal deformation is so large that the results are becoming inaccurate. The deep lower crust acts as a detachment level and the cold TCL mantle is pulled from underneath the thickened crust. Some 3 Ma after in-plane forces switched from compressive to tensile (Figure 8), a dipping zone of elevated strains and strain rates cuts the whole continental lithosphere. This asymmetric structure develops in the mantle and upper crust in the downdip direction of the lower crustal shear zone. The conjugate zone (Figure 8a), which develops in the TCL as a consequence of moment balance, displays more distributed strain rates (Figure 8b) and more uniform deformation. Localized deformation along a fault dipping beneath the TCL is clearly preferred.

Localized thinning of the crust generates a foredeep (Figure 9) which is partly flexurally supported. Braun and Beaumont (1989c) recognized that thinning may lead to buoyancy forces working on lithosphere with a finite flexural strength. They invoke this mechanism to give an explanation for

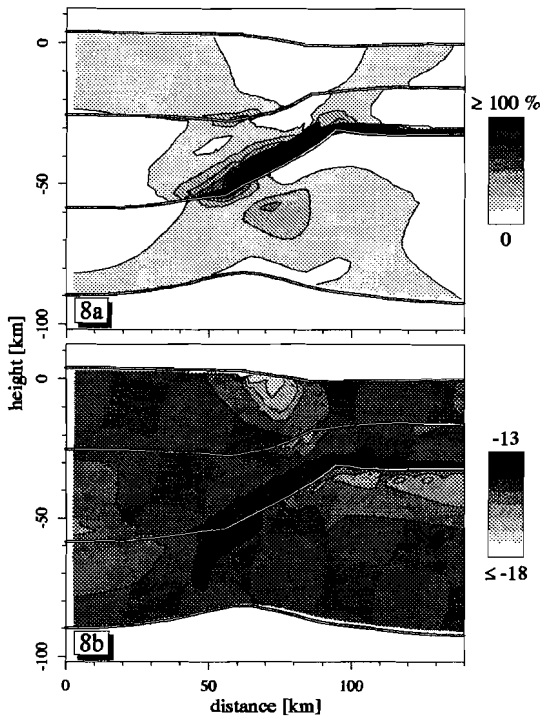

Fig. 8. *Model 2 (Extending TCL model) after 3 Ma. (a) Contours of effective strain. (b) Contours of logarithmic effective strain rate.*

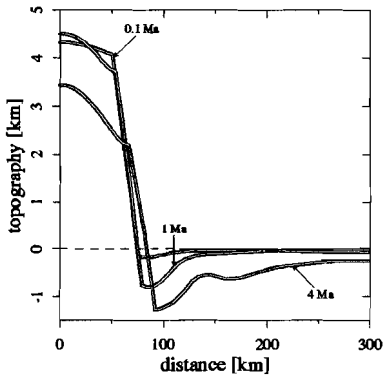

Fig. 9. *Model 2 (Extending TCL model). Surface topography at 0.1, 1 and 4 Ma.*

flank uplifts in rift zones. Likewise, crustal thinning in our model generates downward directed buoyancy forces which cause an upwarp in the RCL (shown by the change in slope of the surface topography at 4 Ma between 120 and 150 km) and a more significant flexural uplift of the TCL.

Model 3. Strain weakening in thickened lithosphere in extension

In this model we incorporate a strain-induced transition in the rheology of the mantle from dislocation creep to diffusion creep. Depending upon ambient temperature and strain rate, the effect of a switch to diffusion creep can induce a drop in viscosity of several orders of magnitude. As such, a deformation mechanism change from dislocation creep to diffusion creep is viewed as a reason for shear localization in the mantle (Poirier, 1980; see also references in Drury *et al.*, 1991). Let us assume that strain weakening in the mantle starts soon after thickening, at 5% natural strain. Following Rutter and Brodie (1988) we assume that the transi-

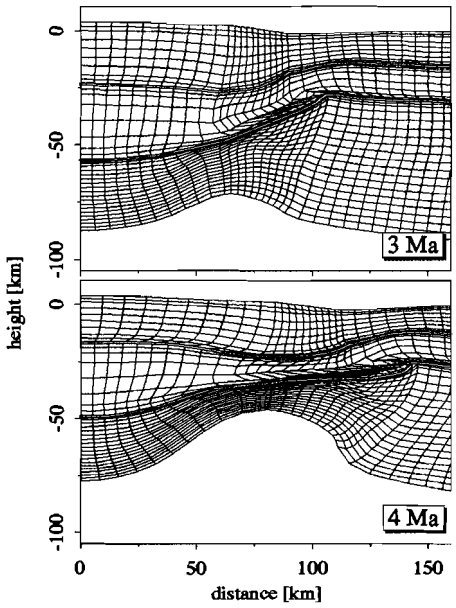

Fig. 10. *Model 3 (Extending TCL model with mantle weakening). Evolution of deforming grid.*

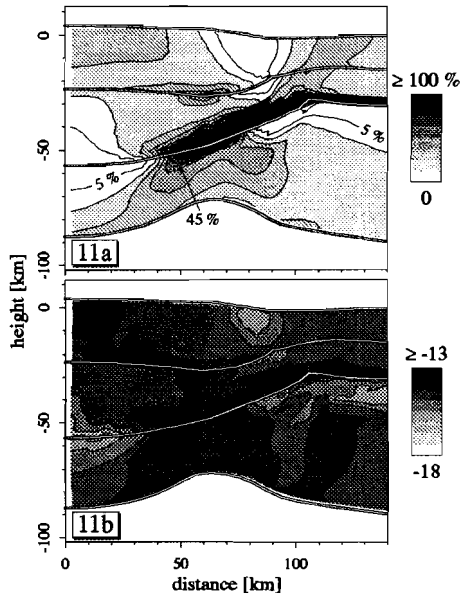

Fig. 11. *Model 3 (Extending TCL model with mantle weakening) after 3 Ma. (a) Contours of effective strain. Weakening front (5% natural strain) and weakening tail (45% natural strain) lines are indicated. (b) Contours of effective strain rate. The high strain rates zone in the mantle is much wider than in the case without weakening (Figure 8).*

tion to complete diffusion creep occurs over a strain interval of 40%, i.e. strain weakening is complete at a natural strain of 45%. Model 3 only differs in this aspect from the previous model. An in-plane tensile force, equivalent to a stress of 50 MPa which is uniformly distributed over the RCL thickness, starts extending the TCL immediately after thickening.

Figure 10 shows a few snapshots of the deforming lithosphere model. Mantle weakening starts after approximately 2 Ma. Comparison of Figures 7 and 10 shows that at 3 Ma, the Model 3 mantle has been stretched more in the TCL near the transition zone. Prior to weakening, mantle strains are highest in this region and consequently, this is the region where strain weakening starts. After 4 Ma the transition to diffusion creep is nearly complete in the mantle of the TCL. Weakening acceler-

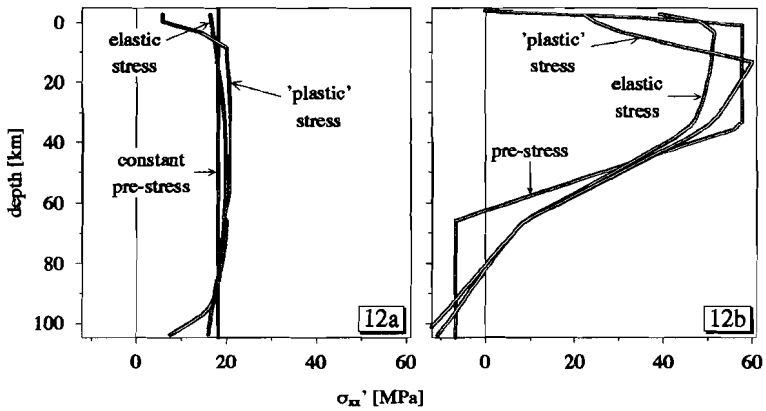

Fig. 12. *(a) Uniform pre-stress. (b) Depth-dependent pre-stress.*

ates the overall rate of extension, and beyond 4 Ma the elements is are strongly deformed and our results are no longer accurate.

The differences in style of deformation between the models with (Figure 11) and without mantle weakening (Figure 8) are significant. In Figure 11a the weakening front (5%) and weakening tail (45%) contours are indicated. Before weakening starts (at 2 Ma) the style of deformation is identical to that of Model 2, i.e. a lithosphere scale fault grows from the shearing lower crust. After the weakening front starts sweeping the mantle, the style of deformation is better described by pure shear. The dipping zone in Figure 11a is a relict of the pre-weakening strain. The strain rates give an impression of the current style of deformation, which is pure shear at 3 Ma. At first sight this result is surprising, as strain weakening is called upon as a mechanism for localization. In the absence of weakening, shear deformation in the lower crust controls the style of deformation in the mantle beneath. After weakening has occurred the mechanical coupling between lower crust and mantle disappears and the mantle flows by pure shear in response to in-plane tensile stresses.

We recognize that the conclusions we draw from this model do not apply to all strain weakening mechanisms and that, even for the mechanism change to diffusion creep we do model, various assumptions were required to arrive at a suitable flow law (Rutter and Brodie, 1988). It is, however, clear from our modeling that strain weakening and shear localization are not synonymous. This conclusion is in accordance with results from a strain weakening model of continental lithosphere which has been not been subject to orogenic events and which, therefore, is close to thermal and mechanical equilibrium (chapter 4 of this thesis).

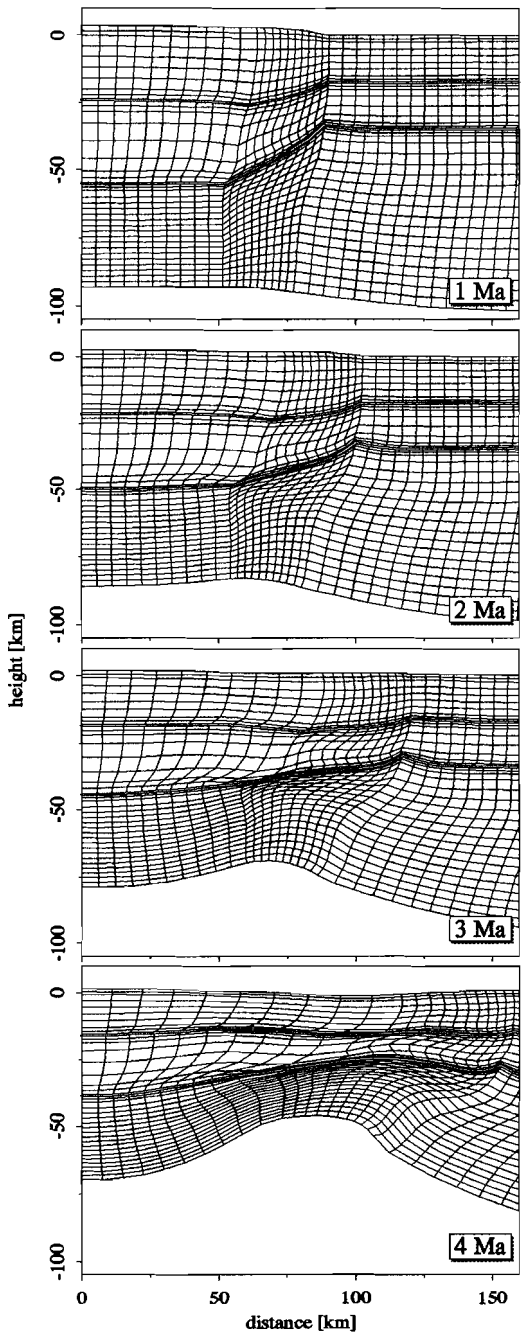

Fig. 13. *Model 4 (Extending TCL model with depth-dependent pre-stress). Evolution of deforming grid.*

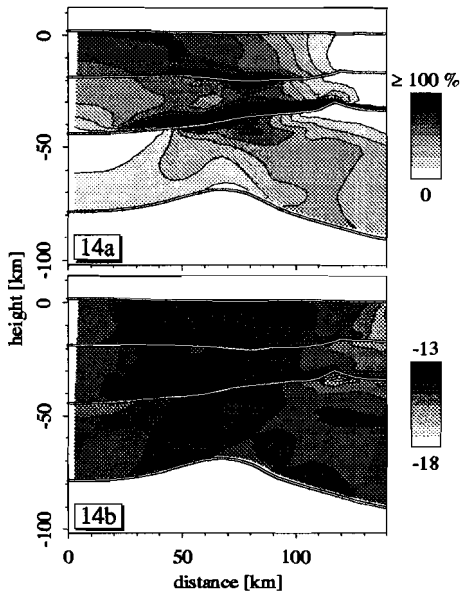

Fig. 14. *Model 4 (Extending TCL model with depth-dependent pre-stress) after 3 Ma. (a) Contours of effective strain. (b) Contours of logarithmic effective strain rate.*

Model 4. Influence of thickening pre-stress

It will be the subject of chapter 6 of this thesis to present a more detailed investigation of model parameters and assumptions that are involved in our analysis. In the context of this chapter, we need to comment upon the assumption of uniform thickening pre-stress, since it affects the results of Model 2 significantly.

By comparing the density moment of the TCL to that of RCL, the average differential stress between thickened and reference lithosphere is calculated (Artyushkov, 1973; England and McKenzie, 1982; Braun and Beaumont, 1989b). In the previous models, we incorporated this average differential stress as pre-stresses which are uniformly distributed. Figure 12a shows the initial (uniform) pre-stress at the symmetry center. Figure 12a also displays the elastic solution to the equilibrium equation, i.e. the pre-stresses in balance with gravity body forces. The 'plastic' stress, indicated in Figure 12a, represents the horizontal deviatoric stress after brittle deformation (chiefly in the upper crust) and viscous deformation in low-viscosity parts of the lithosphere has occurred.

An alternative way to incorporate thickening pre-stress is to directly compare the pressure at some depth in the thickened column to the pressure at the same depth in the reference column, and to infer a stress difference from this (Le Pichon, 1983). This yields the deviatoric pre-stress as a function of depth. Figure 12b shows the resulting pre-stress distribution. Averaged over the lithospheric column, this pre-stress versus depth is the same as in Figure 12a. It is, however, important that tensile stresses in the crust are higher, and that mantle pre-stresses are compressive in this case. It is clear from the elastic stresses in Figure 12b that the pre-stresses exert an up-bending moment on the lithosphere. From the 'plastic' stresses we infer that the upper 15 km (measured from the top of the RCL) are in brittle failure.

Model 4 is identical to Model 2, with the exception that we replaced the uniform pre-stress by a depth-dependent pre-stress. Figure 13 shows the evolution of the finite element grid, and should be compared with Figure 7. Figure 14 shows the strain and strain rate after 3 Ma, for comparison with Figure 8. In Model 2, the mantle is pulled from beneath the TCL, with the lower crust in the transition zone acting as a detachment. The combination of higher tensile pre-stress in the crust, and small tensile and compressive pre-stress in the mantle, shifts the focus of extension in Model 4 to the crust. Crustal deformation leads to more rapid attenuation of the Moho in Model 4. The overall style of deformation is therefore much more pure-shear-like (Figure 14).

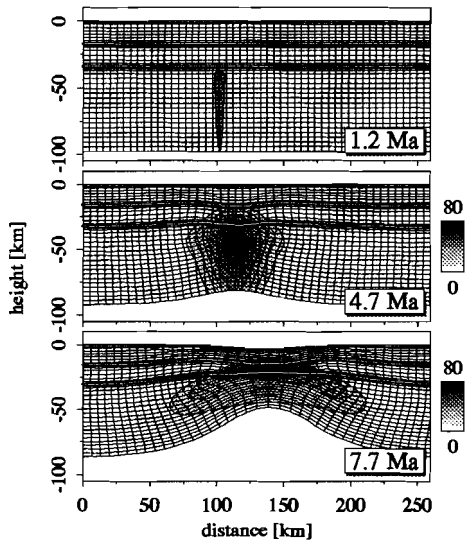

Fig. 15. *Model 5 (Intrusion model). Evolution of thermal anomaly and grid. In the top panel (1.2 Ma) intrusion has just occurred. The dark contoured indicates where the temperature change relative to the initial geotherm is greater than 450 °C. The lower two panels (4.7 and 7.7 Ma) also display contours of the temperature change since* $t = 0$.

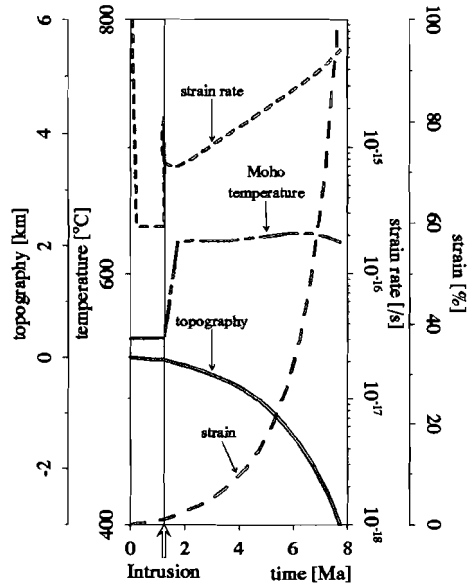

Fig. 16. *Model 5 (Intrusion model). Topography, Moho temperature, average effective strain rate and average effective strain at intrusion.*

INTRUSION IN EXTENDING LITHOSPHERE

Model 5. Instantaneous intrusion

Let us consider the RCL with a steady-state initial geotherm and a surface heat flow of 60 mW/m^2. An in-plane tensile force is applied to the right hand side of the model which is equivalent in magnitude to a 50 MPa stress, distributed evenly over the 100 km lithosphere thickness. This force is kept constant from $t = 0$ onward, and stresses are allowed to redistribute with depth. At $t = 1.2$ Ma asthenosphere material instantaneously intrudes the lower 60 km of continental lithosphere. Effectively the mantle material in this column is replaced by the asthenospheric material, which has the same material properties as the mantle and which has a temperature of 1350 °C.

The top panel of Figure 15 displays the finite element grid at 1.2 Ma and the 450

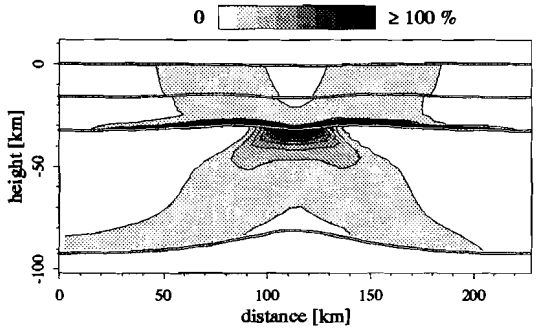

Fig. 17. *Model 5 (Intrusion model). Contours of effective strain after 4.7 Ma.*

°C temperature anomaly contour. The topography of the surface above the intrusion (Figure 16) at 1.2 Ma is negligible; the asthenospheric material penetrating the mantle up to 5 km below the Moho generates buoyancy forces which are flexurally supported mainly by the upper mantle. Tensile fiber stresses (175 MPa) supported by the upper mantle, oppose vertical motions of the Moho and the surface. The average strain rate in the intruded column increases by nearly an order of magnitude due to thermal stresses and buoyancy forces. The intruded material cools (and solidifies) very rapidly, however, and the average strain rate drops to a value which is higher than the pre-intrusion strain rate. The topography of the Moho at 4.7 Ma (Figure 15) is a consequence of localized extension of the intruded lithospheric column and widening of the thermal anomaly in the surrounding mantle; thinning of the intruded column causes subsidence and downward isostatic restoring forces, heating of mantle surrounding the intrusion generates buoyancy forces. It is clear from Figures 15 and 16 that the intrusion serves to localize deformation and leads to complete lithospheric failure at the constant in-plane force boundary condition which is applied in this model.

From the contours of effective strain at 4.7 Ma (Figure 17) it is clear that, to conserve torque balance, two conjugate systems of enhanced shear develop in the lithosphere. The system is perfectly symmetric and neither of the two conjugate systems will develop preferentially. The overall style of deformation can therefore best be described by a pure shear model. The results of Braun and Beaumont (1989a) and Dunbar and Sawyer (1989) show that if some offset material weakness is added to the system, preferential development of one of the branches is promoted. A model with the intrusion occurring at 25 km from the symmetry center ($x=0$) gives slightly asymmetrical results; as a consequence of the mechanical boundary conditions (Figure 2), the slope of horizontal interfaces in the symmetry center is zero. Consequently, the flexural behavior on either sides of the intrusion is

different, but the effects of this asymmetry on the style of deformation are minor.

In the absence of offset weak zones or other causes for asymmetrical behavior any model of vertical intrusions will illustrate the tendency of the lithosphere to overall pure shear deformation. We consider it very likely that if, at some stage, a fault (in the sense of a zone of intensely localized deformation) would develop on one branch in Figure 17 along which shear deformation occurs, the tendency to moment conservation would generate stresses on the other system to also initiate a fault. Based upon these arguments and our model results we consider intrusions alone, i.e. not in combination with causes for preferential development of one of the deformation branches, not relevant for initiating lithosphere scale asymmetrical structures.

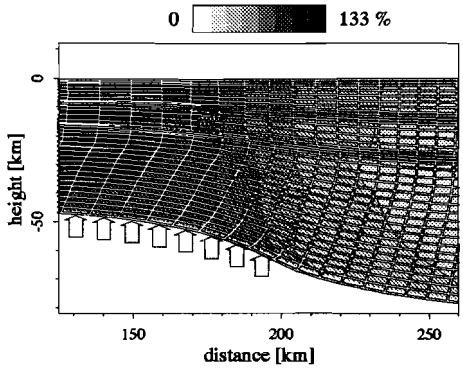

Fig. 18. *Model 6 (Mantle plume model). Contours of effective strain and deformed grid at 10 Ma. Arrows indicate where the plume is applied.*

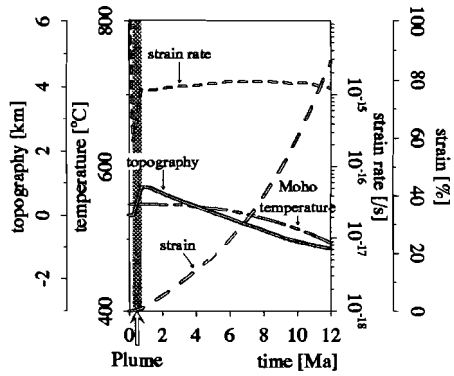

Fig. 19. *Model 6 (Mantle plume model). Surface topography, Moho temperature, average effective strain rate and average effective strain at symmetry center ($x=0$). The grey column indicates the interval in which the plume is linearly increased to its full magnitude.*

MANTLE-LITHOSPHERE INTERACTION

Model 6. Mantle plume

In this model we investigate asymmetric deformation caused by mantle plumes impinging to the base of the continental lithosphere. As discussed in the introduction, we consider the mechanical effects of mantle plumes only. A basal pressure is used to model the (mechanical) effect of a rising plume (Figure 18). The plume is applied between $t=0.2$ Ma and $t=0.7$ Ma, and kept constant onward, to a 100 km

wide zone left and right from the symmetry center ($x=0$). The basal pressure ends abruptly at 100 km to create the maximum possible lateral pressure gradient. The magnitude of the basal pressure is derived from the observation of 1000 meter amplitude oceanic swells; assuming that the swells are in local isostatic equilibrium and that uplifts are completely dynamically supported, yields a pressure of 32 MPa. The model is subject to a constant in-plane tensile force equivalent to 50 MPa, which is left to redistribute with depth before the mantle plume is applied.

Figure 19 shows the strain rate, surface topography, Moho temperature and strain at the symmetry center as a function of time. The surface topography resulting from the mantle plume is close to 1000 meter immediately after the plume is applied to the base of the lithosphere. The width of the mantle plume is larger than the flexural wavelength of the continental lithosphere and the system is close to isostatic equilibrium near the symmetry center. 4 Ma after the plume was applied the surface subsides below sea level as a result of crustal thinning. From Figure 18 it is clear that the style of deformation can well be described by pure shear. We conclude that mantle plumes are irrelevant for initiating an asymmetric mode of deformation.

Model 7. Delamination during thickening of continental lithosphere

In this model we assume that delamination occurs during a compression phase which uniformly thickened the crust by $\beta^{-1}=2$ and which passively pushed down the undeformed mantle (c.f. Model 1). The lower 35 km of the mantle are assumed to detach from the lithosphere beneath the thickened region and to be replaced by asthenosphere material. We assume that sinking of the detached mantle will maintain a back flow of asthenospheric material, inhibiting downward cooling and "mantle healing". This assumption is reflected in a constant 1350 °C temperature boundary condition beneath the TCL in our modeling. Like in Model 1, we use pre-stresses to model the potential energy difference between TCL and RCL. In-plane compressive forces are applied to balance the pre-stresses and to maintain the topography. Isostatic forces resulting from delamination are included as pressures working on the base of the TCL.

The combined effect of mantle heating and isostatic pressures is clear in Figure 20, which displays the finite element grid and strain 2.1 Ma after delamination has occurred. After about 3 Ma the mantle has become so deformed that the finite element results are inaccurate. Figure 20 shows the onset of a "asthenospheric diapir" that rapidly "eats" its way through the continental mantle. The crust hardly deforms due to the in-plane containment forces. Effectively, the style of deformation is symmetric as a consequence of a non-deforming lower crust.

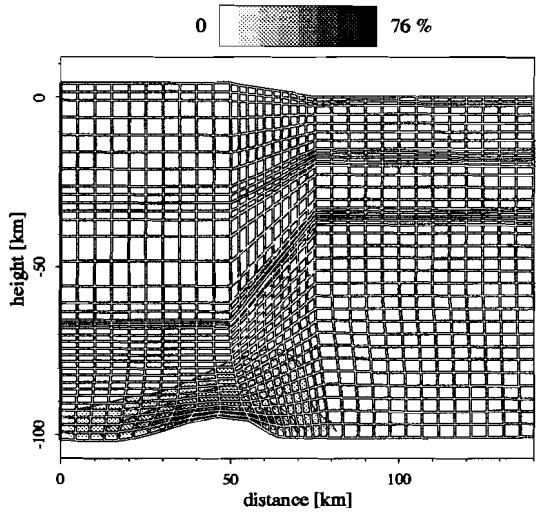

Fig. 20. *Model 7 (Delamination during thickening model). Contours of effective strain and deformed grid at 2.1 Ma.*

Model 8. Delamination after thickening of continental lithosphere

The difference between this model and Model 7 is that delamination occurs at the end of the thickening phase, which is characterized by a switch of the in-plane forces from compressive to a tensile force which is equivalent to an average stress of 50 MPa. Figure 21 shows the deformed grid, the strain and strain rates at 2.1 Ma after delamination occurred and stretching started. A zone of intense deformation has developed from the lower crust which dips into the mantle. The style of deformation near the base of the lithosphere is pure shear. As the lithosphere-asthenosphere boundary rises the strain maxima link up (Figure 22) to a lithosphere scale detachment fault.

The dependence of the results from Model 8 on the distribution of thickening pre-stresses is, like in the case of Models 2 and 4, significant. In chapter 7 of this thesis we present a detailed investigation of factors which control the symmetry or asymmetry of extension after continental thickening and delamination. We show that the style of extension is much more symmetric when residual stresses from thickening are distributed non-uniformly with depth.

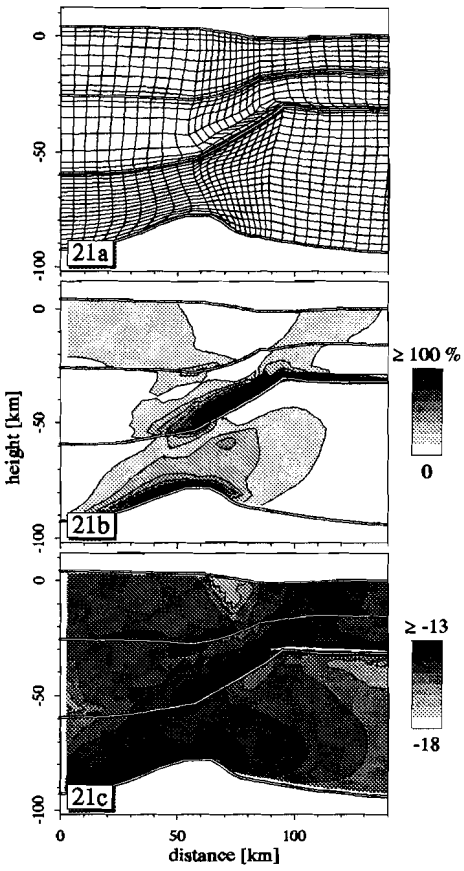

Fig. 21. *Model 8 (Delamination and in-plane pull after thickening model) after 2.1 Ma. (a) Deformed finite element grid. (b) Contours of effective strain. (c) Contours of effective strain rate.*

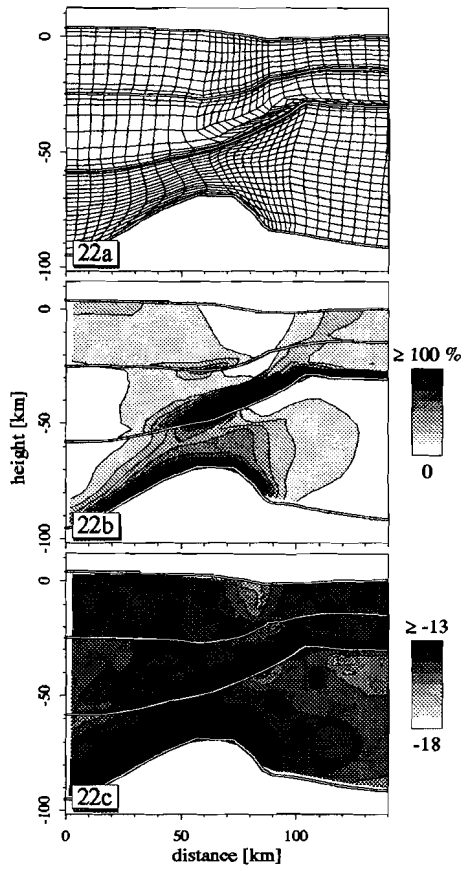

Fig. 22. *Model 8 (Delamination and in-plane pull after thickening model) after 2.4 Ma. (a) Deformed finite element grid. (b) Contours of effective strain. (c) Contours of effective strain rate.*

DISCUSSION

In intraplate regions, there is a strong tendency for total strain rates to develop which are uniform with depth (Kusznir and Bott, 1977; Kusznir, 1982; chapter 3 of this thesis; chapter 4 of this thesis), or equivalently, the normal mode of intraplate deformation is pure shear. Initiation of shallow dipping lithosphere-scale faults therefore has to occur under special circumstances. Pre-existing weaknesses might control the initiation of detachment faults, but there is no evidence that strain al-

ways localizes along mechanical discontinuities. Mechanisms for initiation of translithospheric detachments based upon pre-existing weaknesses lithosphere, disregard the possible relation between continental thickening and subsequent asymmetric extension. We have investigated physical conditions which may lead to initiation of asymmetric extension. In this study we have considered three classes of causes for initiation of asymmetrical extension on lithosphere scale faults; continental collision, magma intrusions and causes resulting from lithosphere-mantle interaction.

We find that development of detachment faults is likely in the transition zone of continental lithosphere which has been thickened very rapidly compared to the thermal time constant of the lithosphere, i.e. on the order of a few Ma. A second requirement is that the in-plane compressive force causing continental thickening, switches to in-plane tension rapidly (again compared to the thermal time constant). The fault zone is predicted to dip under the thickened continental lithosphere, consistent with observations in the Aegean (Lee and Lister, 1992) and in the Basin and Range (Wernicke, 1981). Our models predict a normal sense of shear along a dipping zone of localized deformation which evolves from the dipping lower crust. Any delay in either the mountain building or the sign switch of in-plane force will result in thermal relaxation, generating diffusely distributed buoyancy forces which tend to decrease the slope of the Moho. Since Moho depth gradients appear to be crucial for initiating dipping fault zones, thermal relaxation will thus, decrease the tendency of the lithosphere to asymmetric deformation. We show that our results are sensitive to the pre-stress distribution in our modeling.

A vertical magma intrusion into the lithosphere alone cannot initiate large scale asymmetric deformation. Two conjugate systems of localized strain evolve, but none of them develop preferentially. It is clear that the orientation of the intrusion influences the symmetry of extension. We did not actually model intrusions in more gently dipping orientations, since the results would be very similar to the findings of Braun and Beaumont (1989a) and Dunbar and Sawyer (1989), who study the style of extension of offset pre-existing weak zones in the crust and mantle. These authors show that if a cause for preferential development of one of the two conjugate branches is added (in their case an offset crustal weak zone), the system will evolve asymmetrically.

Mantle plumes are probably not relevant for initiating detachment faults.

Our model study indicates that mantle delamination resulting from continental thickening is a likely mechanism for initiating detachment faults if delamination occurs at the end of the compression phase and if in-plane tensile forces are applied to the thickened system immediately after compression. Model experiments not reported here indicate that this result is sensitive to the way thickening pre-stresses

are applied in the modeling. A particular feature of the delamination model is that an asthenospheric diapir evolves, which will generate melt as a result of its rapid ascent and decompression. Latin and White (1990) argue that melt generation is unlikely in simple shear deformation. If, however, delamination precedes simple shear extension, this is not necessarily so.

Another interesting result from our modeling is that dramatic strain weakening in the mantle decreases the tendency for localized asymmetrical deformation. Lithosphere scale detachment faulting is promoted in a layered rheological system with a weak lower crust overlying a strong mantle. Weakening of the mantle mechanically decouples the deformation behavior of the lower crust from the mantle, which subsequently deforms by pure shear.

It is important to realize that some mechanisms, which are concluded not to generate lithosphere-scale faults, do predict crustal scale detachments. Based upon experimental flow laws and realistic geotherms, the lower crust should be very weak and, therefore, represent an excellent level for decoupling the crust from the mantle. In general, crustal detachments will lead to mixed-mode extension. However, more can be learned about the controlling physical mechanisms by studying end-members of the extension models spectrum. Given the tendency to pure shear extension in intraplate deformation, we have, therefore, focussed on the physical mechanisms which are relevant in the evolution of whole-lithosphere asymmetric features. This chapter intends to give insight in the overall conditions which determine the initiation of lithosphere scale faults. We did not conduct a full parameter study but selected a few models of fairly common geological processes. Combinations of the above causes for asymmetrical deformation may occur, but are considered less likely. In chapters 6 and 7 of this thesis we investigate how parameters of the continental thickening mechanism affect the tendency to initiation of lithospheric detachment faults.

Acknowledgments

Jay Melosh of the Lunar and Planetary Lab and Department of Geosciences in Tucson, Arizona, is gratefully acknowledged for sharing his mechanical finite element code. During this research, R.G. was financially supported by AWON, the Earth Science branch of the Netherlands Organization for Scientific Research (NWO). M.J.R.W. was partially supported by the Netherlands Organization for Scientific Research (NWO) through the Pionier project PGS 76-144.

REFERENCES

Anderson, D.L., *Theory of the Earth,* 366 pp., Blackwell Scientific Publications, Boston, 1989.

Artyushkov, E.V., Stresses in the lithosphere caused by crustal thickness inhomogeneities, *J. Geophys. Res., 78,* 7,675-7,708, 1973.

Barton, P., and R. Wood, Tectonic evolution of the North Sea basin: crustal stretching and subsidence, *Geophys. J. R. astron. Soc., 79,* 987-1,022, 1984.

Beach, A., A deep seismic reflection profile across the northern North Sea, *Nature, 232,* 53-55, 1986.

Berckhemer, H., Some aspects of the evolution of marginal seas deduced from observations in the Aegean region, in *International symposium on the structural history of the Mediterranean basins, Split (Yugoslavia),* edited by B. Biju-Duval and L. Montadert, pp. 303-313, Technip, Paris, 1977.

Braun, J., Styles of continental extension: results from numerical experiments, *unpublished Ph.D. thesis,* pp. 352, Dalhousie University, Halifax, Nova Scotia, 1988.

Braun, J., and C. Beaumont, Dynamical models of the role of crustal shear zones in asymmetric continental extension, *Earth Planet. Sci. Lett., 93,* 405-423, 1989a.

Braun, J., and C. Beaumont, Contrasting styles of lithospheric extension: implications for differences between Basin and Range Province and rifted continental margins, *Am. Ass. Petr. Geol. Mem., 46,* 53-79, 1989b.

Braun, J., and C. Beaumont, A physical explanation of the relation between flank uplifts and the breakup unconformity at rifted continental margins, *Geology, 17,* 760-764, 1989c.

Buck, W.R., F. Martinez, M.S. Steckler, and J.R. Cochran, Thermal consequences of lithospheric extension: pure and simple, *Tectonics, 7,* 213-234, 1988.

Byerlee, J.D., Friction of rocks, *Pageoph., 116,* 615-626, 1978.

Cloetingh, S., and R. Wortel, Regional stress field of the Indian plate, *Geophys. Res. Lett., 12,* 77-80, 1985.

Coney, P.J., The regional tectonic setting and possible causes of Cenozoic extension in the North Americal Cordillera, in *Continental extensional tectonics, 28,* edited by M.P. Coward, J.F. Dewey and P.L. Hancock, pp. 177-186, Geological Society of London Special Publication, 1987.

Crough, S.T., Thermal origin of mid-plate hot spot swells, *Geophys. J. R. astron. Soc., 55,* 451-469, 1978.

Davis, D., J. Suppe, and F.A. Dahlen, Mechanics of fold-and-thrust belts and accretionary wedges, *J. Geophys. Res., 88,* 1,153-1,172, 1983.

Davis, G.H., Shear zone model for the origin of metamorphic core complexes, *Geology, 11,* 342-347, 1983.

Dewey, J.F., Extensional collapse of orogens, *Tectonics, 7,* 1,123-1,139, 1988.

Drury, M.R., R.L.M. Vissers, D. van der Wal, and E.H. Hoogerduijn Strating, Shear localization in upper mantle peridotites, *Pageoph., 137,* 439-460, 1991.

Dunbar, J.A., and D.S. Sawyer, How preexisting weaknesses control the style of continental breakup, *J. Geophys. Res., 94,* 7,278-7,292, 1989.

England, P.C., and D.P. McKenzie, A thin viscous sheet model for continental deformation,

Geophys. J. R. astron. Soc., 70, 295-321, 1982.
Furlong, K.P., and M.D. Londe, Thermal-mechanical consequences of Basin and Range extension, *Geol. Soc. Am. Bull., 208,* 23-30, 1986.
Gans, P.B., An open-system, two-layer crustal stretching model for the eastern Great Basin, *Tectonics, 6,* 1-12, 1987.
Govers, R., M.J.R. Wortel, S.A.P.L. Cloetingh, and C.A. Stein, Stress magnitude estimates from earthquakes in oceanic plate interiors, *J. Geophys. Res., 97,* 11,749-11,759, 1992. (Chapter 2 in this thesis)
Hellinger, S.J., and J.G. Sclater, Some comments on two-layer extension models for the evolution of sedimentary basins, *J. Geophys. Res., 88,* 8,251-8,269, 1983.
Houseman, G.A., and P.C. England, A dynamical model of lithosphere extension and sedimentary basin formation, *J. Geophys. Res., 91,* 719-729, 1986.
Houseman, G.A., and D.P. McKenzie, Convective instability of a thickened boundary layer and its relevance for the thermal evolution of continental convergent belts, *J. Geophys. Res., 86,* 6,115-6,132, 1981.
Jackson, J.A., Active normal faulting and crustal extension, in *Continental extensional tectonics, 28,* edited by M.P. Coward, J.F. Dewey and P.L. Hancock, pp. 3-18, Geological Society of London Special Publication, 1987.
Kusznir, N.J., Lithosphere response to externally and internally derived stresses: a viscoelastic stress guide with amplification, *Geophys. J. R. astron. Soc., 70,* 399-414, 1982.
Kusznir, N.J., and M.M.P. Bott, Stress concentration in the upper lithosphere caused by underlying visco-elastic creep, *Tectonophysics, 43,* 247-256, 1977.
Kusznir, N., and S.S. Egan, Simple-shear and pure-shear models of extensional sedimentary basin formation: application to the Jeanne d'Arc, Grand Banks of Newfoundland, *Am. Ass. Petr. Geol. Mem., 46,* 305-322, 1989.
Latin, D., and F.G. Waters, Melt generation during rifting in the North Sea, *Nature, 351,* 559-562, 1991.
Latin, D., and N. White, Generating melt during lithospheric extension: pure shear vs. simple shear, *Geology, 18,* 327-331, 1990.
Le Pichon, X., Land-locked oceanic basins and continental collision: the eastern Mediterranean as a case example, in *Mountain building processes,* edited by K. Hsü, pp. 201-211, Acad. Press, London, 1983.
Le Pichon, X., and J.-C. Sibuet, Passive margins: a model of formation, *J. Geophys. Res., 86,* 3,708-3,720, 1981.
Lee, J., and G.S. Lister, Late Miocene ductile extension and detachment faulting, Mykonos, Greece, *Geology, 20,* 121-124, 1992.
Lister, G.S., and G.A. Davis, The origin of metamorphic core complexes and detachment faults formed during Tertiary continental extension in the northern Colorado River region, U.S.A., *J. Struct. Geol., 11,* 65-94, 1989.
Lister, G.S., G. Banga, and A. Feenstra, Metamorphic core complexes of Cordilleran type in the Cyclades, Aegean Sea, Greece, *Geology, 12,* 221-225, 1984.
Lister, G.S., M.A. Etheridge, and P.A. Symonds, Detachment faulting and the evolution of passive continental margins, *Geology, 14,* 246-250, 1986.
Love, A.E.H., *Some problems of geodynamics,* Cambridge Univ. Press, London, 1911.
McKenzie, D.P., Active tectonics of the Mediterranean region, *Geophys. J. R. astron. Soc.,*

30, 109-185, 1972.
McKenzie, D.P., Surface deformation, gravity anomalies and convection, *Geophys. J. R. astron. Soc., 48*, 211-238, 1977.
McKenzie, D., Some remarks on the development of sedimentary basins, *Earth Planet. Sci. Lett., 40*, 25-32, 1978a.
McKenzie, D.P., Active tectonics of the Alpine-Himalayan belt: the Aegean Sea and surrounding regions, *Geophys. J. R. astron. Soc., 55*, 217-254, 1978b.
Melosh, H.J., Mechanical basis for low-angle normal faulting in the Basin and Range province, *Nature, 343*, 1990.
Melosh, H.J., and A. Raefsky, The dynamical origin of subduction zone topography, *Geophys. J. R. astron. Soc., 60*, 333-354, 1980.
Melosh, H.J., and A. Raefsky, A simple and efficient method for introducing faults into finite element computations, *Bull. Seismol. Soc. Am., 71(5)*, 1,391-1,400, 1981.
Melosh, H.J., and A. Raefsky, Anelastic response of the earth to dip slip earthquakes, *J. Geophys. Res., 88*, 515-526, 1983.
Melosh, H.J., and C.A. Williams, Mechanics of graben formation in crustal rocks: a finite element analysis, *J. Geophys. Res., 94*, 13,961-13,973, 1989.
Mercier, J.-L., R. Armijo, P. Tapponier, E. Carey-Gailhardis, and H.T. Lin, Change from Late Tertiary compression to Quaternary extension in southern Tibet during the India-Asia collision, *Tectonics, 6*, 275-304, 1987.
Nakiboglu, S.M., and K. Lambeck, Thermal response of a moving lithosphere over a mantle heat source, *J. Geophys. Res., 90*, 2,985-2,994, 1985.
Paterson, M.S., and F.C. Luan, Quartzite rheology under geological conditions, in *Deformation Mechanisms, Rheology and Tectonics, 45*, edited by R.J. Knipe and E.H. Rutter, pp. 299-307, Geological Society of London Special Publication, London, 1990.
Poirier, J.P., Shear localization and shear instability in the ductile field, *J. Struct. Geol., 2*, 135-142, 1980.
Rowley, D.B., and D. Sahagian, Depth-dependent stretching: a different approach, *Geology*, 32-35, 1986.
Royden, L., and C.E. Keen, Rifting processes and thermal evolution of the continental margin of eastern Canada determined from subsidence curves, *Earth Planet. Sci. Lett., 51*, 343-361, 1980.
Ruppel, C., L. Royden, and K.V. Hodges, Thermal modeling of extensional tectonics: application to pressure-time histories of metamorphic rocks, *Tectonics, 7*, 947-957, 1988.
Rutter, E.H., and K.H. Brodie, The role of tectonic grain size reduction in the rheological stratification of the lithosphere, *Geol. Rund., 77*, 295-308, 1988.
Sclater, J.G., and P.A.F. Christie, Continental stretching: an explanation for the post-Mid-Cretaceous subsidence of the central North Sea Basin, *J. Geophys. Res., 85*, 3,711-3,739, 1980.
Şengör, A.M.C., and K. Burke, Relative timing of rifting and volcanism on earth and its tectonic implications, *Geophys. Res. Lett., 5*, 419-421, 1978.
Sleep, N.H., Thermal effects of the formation of Atlantic continental margins by continental break up, *Geophys. J. R. astron. Soc., 24*, 325-350, 1971.
Sonder, L.J., P.C. England, B.P. Wernicke, and R.L. Christiansen, A physical model for Cenozoic extension of western North America, in *Continental extensional tectonics, 28*, edited by M.P. Coward, J.F. Dewey and P.L. Hancock, pp. 187-201, Geological Society

of London Special Publication, 1987.

Spencer, J.E., and C.G. Chase, Role of crustal flexure in initiation of low-angle normal faults and implications for structural evolution of the Basin and Range Province, *J. Geophys. Res., 94,* 1,765-1,775, 1989.

Wernicke, B., Low-angle normal faults in the Basin and Range Province: nappe tectonics in an extending orogen, *Nature, 291,* 645-648, 1981.

Wernicke, B., Uniform-sense normal simple shear of the continental lithosphere, *Can. J. Earth Sci., 22,* 108-125, 1985.

Wernicke, B., and G.J. Axen, On the role of isostasy in the evolution of normal fault systems, *Geology, 16,* 848-851, 1988.

Wernicke, B., R.L. Christiansen, P.C. England, and L.J. Sonder, Tectonomagmatic evolution of Cenozoic extension in the North American Cordillera, in *Continental extension tectonics, 28,* edited by M.P. Coward, J.F. Dewey and P.L. Hancock, pp. 203-221, Geological Society of London Special Publication, 1987.

White, N.J., The nature of lithospheric extension in the North Sea, *Geology, 17,* 111-114, 1989.

Wilks, K.R., and N.L. Carter, Rheology of some continental lower crustal rocks, *Tectonophysics, 182,* 57-77, 1990.

Williams, C.A., and R.M. Richardson, A rheologically layered three-dimensional model of the San Andreas Fault in Central and Southern California, *J. Geophys. Res., 96,* 16,597-16,623, 1991.

Yin, A., Origin of regional, rooted low-angle normal faults: a mechanical model and its tectonic implications, *Eos Trans. AGU, 68,* 1,449, 1987.

Yin, A., Origin of regional, rooted low-angle normal faults: a mechanical model and its tectonic implications, *Tectonics, 8,* 469-482, 1989.

Chapter 6

Conditions controlling the style of post-thickening extension

INTRODUCTION

In chapter 5 of this thesis we discussed various causes for initiation of lithosphere scale faults. It was concluded that continental thickening, with or without delamination of lithospheric mantle, may lead to asymmetric extension. The relevance of these results in the context of continental extension and rifting is discussed in chapter 1. Earlier studies on the response in extension of continental lithosphere containing offset crustal and mantle weak zones (Braun and Beaumont, 1989a; Dunbar and Sawyer, 1989) showed that these may link up into a single asymmetric system along which extension is accommodated. In the case of the continental thickening mechanism, creation of dipping weak zones and subsequent large scale asymmetric extension are integral parts of one single process.

It is the purpose of this chapter to present an investigation of parameters which affect the symmetry or asymmetry of post-thickening extension. Extension after mantle delamination will be the subject of chapter 7. It is impossible to present the results of a full parameter space investigation, first, because we did not do it, and second, because there is little benefit to be gained. Instead, we will try to develop some understanding of the mechanisms which control the style of extension. The insight, thus gained, should be the basis for assessing the evolution for parameter settings we did not actually model, at least in a qualitative way.

The chapter is divided into two parts, based upon the distribution with depth of residual stresses (pre-stresses) from the mountain building phase. In the first part we study the evolution of lithosphere in which residual stresses are distributed uniformly with depth. In the second part, results will be shown in which pre-stresses vary with depth. This approach is motivated by the fact that most studies on post-thickening extension adopt the simplified assumption of uniform pre-stress (England and McKenzie, 1982; Houseman and England, 1986; Sonder *et al.*, 1987; Braun and Beaumont, 1989b). It is therefore relevant to compare results obtained with a uniform pre-stress assumption with results based upon depth-dependent pre-stresses. Also, the physical mechanism(s) controlling the style of extension are

Table 1. Model parameters.

Asthenosphere temperature	T_m	1350	°C
Asthenosphere density	ρ_a	3253	$kg \cdot m^{-3}$
Young's modulus	E	10^{11}	Pa
Poison's ratio	ν	0.25	
Sediment flux coefficient	K_{sed}	$6 \cdot 10^{-6}$	$m^2 \cdot s^{-1}$
Sediment density	$\overline{\rho_s}$	2800	$kg \cdot m^{-3}$
Gravity acceleration	g	9.8	$m \cdot s^{-2}$
Specific heat	C_p	1300	$J \cdot kg^{-1} \cdot K^{-1}$
Thermal expansion coefficient	α_v	$3.2 \cdot 10^{-5}$	K^{-1}

most easily analyzed in the context of uniform pre-stress models. We will show that the distribution of residual stresses from the collision phase plays an important role in controlling the style of subsequent extension.

Each of the two parts of this chapter is subdivided into three sub-parts. In the first sub-part, we investigate the effects on the style of extension of parameters that are related to the period before thickening started, like the initial composition and initial geotherm. The second sub-part deals with the influence of syn-thickening parameters, such as the geometry of the collision belt and the duration of the mountain building period. In the third sub-part, the impact of post-thickening assumptions is analyzed. Mountain building is assumed to have occurred as a result of a compressive in-plane force, and the end of this orogenic phase signifies that there is either a balance between this in-plane force and the tendency to gravitational spreading of the thickened lithosphere, or that the magnitude of the in-plane force has decreased. In the third sub-part, we will therefore investigate various scenarios in which the in-plane force remains constant, or changes in magnitude and/or sign at some instant.

MODELING APPROACH

Governing equations

The mechanical evolution of continental lithosphere on million year (Ma) time scales is governed by the equilibrium equation

$$\nabla \cdot \boldsymbol{\sigma} + \rho \boldsymbol{X} = 0$$

where $\boldsymbol{\sigma}$ is the Cauchy stress tensor, ρ mass density and $\boldsymbol{X}$ body force. A more suitable form of the equilibrium equation is found when it is supplemented with constitutive equations. We model the rheology of continental lithosphere as a combination of elasto-visco-plasticity and non-linear visco-elasticity (c.f. chapter 3). To include the buoyancy effects due to thermal expansion and to incorporate the strong non-linear dependence of rock rheologies on temperature, combined solution of the heat equation is required

$$\rho C_p \frac{\partial T}{\partial t} = \nabla \cdot (\boldsymbol{k} \nabla T) + H + \boldsymbol{\sigma} \cdot \dot{\boldsymbol{\varepsilon}}$$

where C_p is the specific heat at constant pressure, T is temperature, t is time, $\boldsymbol{k}$ the conductivity tensor, H the heat production per unit volume and $\dot{\boldsymbol{\varepsilon}}$ the strain rate tensor. The mechanical equilibrium equation and heat equation are solved sequentially using a two-dimensional finite element procedure. We refer to chapter 3 for a more elaborate discussion of the basic equations and solution procedures. The boundary conditions (b.c.) we employ are identical to the ones in chapter 5.

Erosion and sedimentation

Relative to the previous chapters, a new feature in our finite element calculations is that we incorporate the effects of erosion and sedimentation. It has long been recognized that sedimentation and erosion can have significant tectonic influence since, mechanically, erosion and sedimentation cause a lateral migration of surface loads. To incorporate the effects of erosion and sedimentation on the evolution of continental lithosphere we use a diffusion equation (Culling, 1960)

$$\frac{\partial h}{\partial t} = K_{sed} \cdot \nabla^2 h$$

where h is elevation, K_{sed} is a mass flux coefficient and ∇^2 is the spatial Laplace operator. Although there is no sound physical basis for using a diffusion equation for all possible kinds of sediment transport, Flemings and Jordan (1989) give arguments in support of this approach. Probably, on the scale of the lithosphere, the diffusion equation is a first order description of mass transport as a result of erosion

Table 2. RCL parameters for $q_0 = 60\text{mW/m}^2$

Upper crust			
Rheology	Wet quartzite (Patterson and Luan, 1990)		
	Q_{pl}	135	$kJ \cdot mole^{-1}$
	A_{pl}	$7.76 \cdot 10^{-26}$	$Pa^{-3.1} \cdot s^{-1}$
	n_{pl}	3.1	
Density	$\overline{\rho_{uc}}$	2872	$kg \cdot m^{-3}$
Geotherm	k_{uc}	2.56	$W \cdot m^{-1} \cdot K^{-1}$
	H_{uc}	1.37	$\mu W \cdot m^{-3}$
Thickness		17.5	km
Lower crust			
Rheology	Adirondack granulite (Wilks and Carter, 1990)		
	Q_{pl}	243	$kJ \cdot mole^{-1}$
	A_{pl}	$9.55 \cdot 10^{-21}$	$Pa^{-3.1} \cdot s^{-1}$
	n_{pl}	3.1	
Density	$\overline{\rho_{lc}}$	2872	$kg \cdot m^{-3}$
Geotherm	k_{lc}	2.55	$W \cdot m^{-1} \cdot K^{-1}$
	H_{lc}	0.45	$\mu W \cdot m^{-3}$
Thickness		17.5	km
Lithospheric mantle			
Rheology	Wet olivine (Rutter and Brodie, 1988)		
	Q_{pl}	420	$kJ \cdot mole^{-1}$
	A_{pl}	$8.57 \cdot 10^{-15}$	$Pa^{-3} \cdot s^{-1}$
	n_{pl}	3	
Density	$\overline{\rho_{ma}}$	3297	$kg \cdot m^{-3}$
Geotherm	k_{ma}	3.20	$W \cdot m^{-1} \cdot K^{-1}$
	H_{ma}	0.02	$\mu W \cdot m^{-3}$
Thickness		70	km

and sedimentation. Related to the problem of the physical process(es) controlling the large scale erosion and sedimentation, is the problem of determining the mass flux coefficient K_{sed}. Depending on the geomorphological environment, numbers ranging between $3 \cdot 10^{-11}$ m^2/s and $2 \cdot 10^{-2}$ m^2/s have been found (Flemings and Jordan, 1989). In our modeling we chose an average value of $K_{sed} = 6 \cdot 10^{-6}$ m^2/s (Table 1).

The mechanical effects of lateral mass transfer as a result of erosion and sedimentation are included as nodal forces in our finite element code. Mass conservation is implicitly included in the diffusion equation, meaning that sediment flux in-

Table 3. Models which are discussed in this chapter.

Uniform pre-stress models	
U1	Rheology: low-viscosity upper crust, lower crust and mantle. Geothermal gradient: $q_0 = 60\ \mathrm{mW/m^2}$. Thickening: instantaneous, $\beta_c^{-1}=2$, $\beta_m^{-1}=1$. Transition zone width 25 km. Inplane tensile force: applied immediately after thickening, equivalent to a uniform 50 MPa inplane stress. Subsequent models are identical to this model, except for the indicated deviation.
U2	Strong upper crust model.
U3	Viscous lower crust model.
U4	Strong mantle model.
U5	Cold initial geotherm model.
U6	Hot initial geotherm model.
U7	Duration of thickening period 5 Ma.
U8	Duration of thickening period 20 Ma.
U9	Uniform thickening model.
U10	Wide transition zone model.
U11	Gravity collapse model.
U12	Inplane force starts acting after 20 Ma.
U13	Twice inplane force magnitude.
Non-uniform pre-stress models	
N1	Identical to model U1, except for initial stress distribution.
N2	Viscous lower crust model. Subsequent models are identical to this model, except for the indicated deviation.
N3	Viscous upper crust model.
N4	Strong mantle model.
N5	Cold initial geotherm model.
N6	Hot initial geotherm model.
N7	Duration of thickening period 5 Ma.
N8	Duration of thickening period 20 Ma.
N9	Uniform thickening model.
N10	Wide transition zone model.
N11	Gravity collapse model.
N12	Inplane force starts acting after 15 Ma.
N13	Twice inplane force magnitude.

to or out of the model is excluded. Sediment compaction and thermal effects of erosion or blanketing are not included into the modeling.

It can easily be shown that the solution of the diffusion equation in symmetric models in two dimensions is the sum of Fourier components

$$h(x,t) = \sum_{n=0}^{\infty} A_n \cos\left(\frac{n\pi x}{L}\right) \exp\left(-K_{sed}\left(\frac{n\pi x}{L}\right)^2 t\right)$$

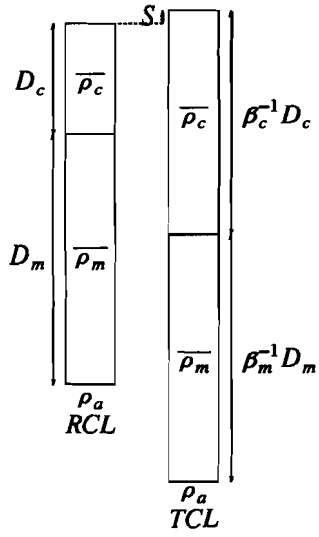

Fig. 1. *Definition of geometrical parameters. Thickening of the crust and lithospheric mantle is quantified using uniform stretching parameters* β_c *and* β_m.

for model length L. Note that short wavelength components ($\lambda_n = L/2n$) have very short decay times ($\tau_n = L^2/n^2\pi^2 K_{sed}$). We checked our finite element solutions against these analytical solutions and found a good agreement.

Residual stress from thickening

Relative to normal lithosphere, continental lithosphere that has been thickened under local isostatic conditions is in a state of stress (Love, 1911). In this chapter, we adopt two different approaches to incorporating these residual stresses. In the first approach, the average stress difference between thickened and normal columns of continental lithosphere is calculated. In our finite element models, these stresses are incorporated as pre-stresses which are distributed uniformly with depth in the thickened lithosphere. This uniform pre-stress approach is basically identical to the method used by other workers (England and McKenzie, 1982; Houseman and England, 1986; Sonder *et al.*, 1987; Braun and Beaumont, 1989b). In the second approach, pre-stresses in the thickened continental lithosphere are calculated by comparing the pressures in different columns at the same depth (Le Pichon, 1983; see also, Fleitout and Froidevaux, 1982). Conceptually, the depth-dependent pre-stress approach is more simple and therefore it will be discussed first.

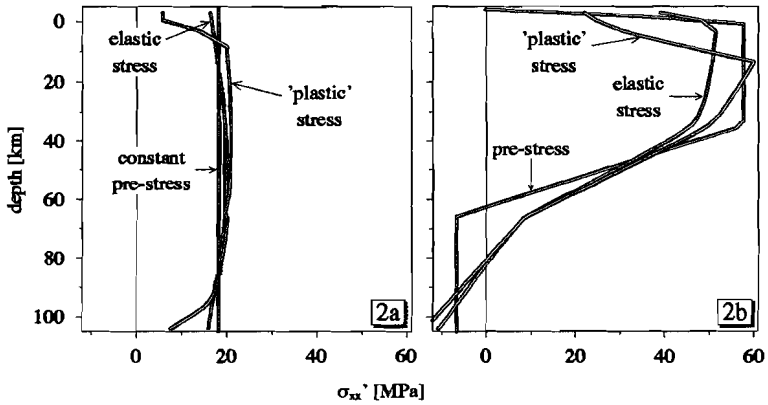

Fig. 2. *Pre-stress resulting from isostatic thickening. (a) Depth-dependent residual stresses. The line labeled "pre-stress" shows a typical distribution with depth of pre-stresses in the TCL. The elastic equilibrium response to the pre-stress input is labeled "elastic stress". The "plastic stress" line displays the stress distribution after relaxation of elastic stresses by brittle deformation. (b) Shows the stress distributions for uniformly distributed pre-stresses.*

Depth-dependent pre-stress

In the absence of tectonic contributions, the horizontal stress σ_{xx} at depth z is approximately equal to the overburden pressure (pressure negative)

$$\sigma_{xx}(z) = -g\int_{S}^{z}\rho(z')\mathrm{d}z'$$

where S represents surface elevation. In our simple lithospheric model, the isostatic surface elevation in the thickened continental lithosphere (TCL), relative to the reference continental lithosphere (RCL), is

$$S = D_c\left(\frac{1}{\beta_c}-1\right)\left(\frac{\rho_a-\overline{\rho_c}}{\rho_a}\right)+D_m\left(\frac{1}{\beta_m}-1\right)\left(\frac{\rho_a-\overline{\rho_m}}{\rho_a}\right)$$

for RCL crustal thickness D_c, RCL mantle thickness D_m, crustal stretching factor β_c, mantle stretching factor β_m, crustal average density $\overline{\rho_c}$, mantle average density $\overline{\rho_m}$ and asthenospheric density ρ_a (Figure 1). We adopt the original definition of the stretching factor β to describe homogenous thinning. In this definition, the inverse stretching factor β^{-1} is the homogeneous thickening factor. The average densities depend on composition and initial geotherm. In the following, we will refer to the lithospheric mantle as "the mantle". The mantle beneath the lithosphere will

be referred to as "the asthenosphere". The stress difference between the TCL and RCL at some depth is obtained by a straightforward comparison of horizontal stresses in the respective columns

$$\Delta\sigma_{xx}(z) = g\int_S^z \rho^{TCL}(z')\mathrm{d}z' - g\int_S^z \rho^{RCL}(z')\mathrm{d}z'$$

Figure 2a shows a typical pre-stress distribution in the TCL. The "elastic stress" line shows the stress distribution, after the pre-stresses have balanced with buoyancy forces. The "plastic stress" line indicates the stress distribution after relaxation of brittle overshoot stresses. It is clear from Figure 2a that, as a result of depth-dependent pre-stresses, a net torque is exerted on the TCL. In vertical planes cutting the TCL, a net shear stress is therefore required to maintain equilibrium. Basically, this is inconsistent with our initial assumption of local isostasy, which requires that lithospheric columns are able to move freely, i.e. that no shear stresses are supported between them.

Average residual stresses from thickening

The above inconsistency does not occur in the second approach, in which the average stress difference between RCL and TCL columns is calculated. The horizontal mechanical equilibrium equation in two dimensions

$$\frac{\partial\sigma_{xx}}{\partial x} + \frac{\partial\sigma_{xz}}{\partial z} = 0$$

may be integrated from the surface down to the isostatic compensation depth d_c:

$$\begin{aligned} 0 &= \int_S^{d_c} \frac{\partial}{\partial x}\sigma_{xx}\mathrm{d}z + \int_S^{d_c} \frac{\partial}{\partial z}\sigma_{xz}\mathrm{d}z \\ &= \frac{\partial}{\partial x}\int_S^{d_c} \sigma_{xx}\mathrm{d}z + \sigma_{xz}(d_c) - \sigma_{xz}(S) \end{aligned}$$

if $\partial S/\partial x$ and $\partial d_c/\partial x$ are negligible. Implicitly it is assumed here that sublithospheric stress contributions are absent. Shear stresses at the free upper surface are zero. We assume that shear stresses at the compensation depth are also negligible as a result of low viscosities. In this case, the shear stress terms drop from the equations, and the horizontal force is constant

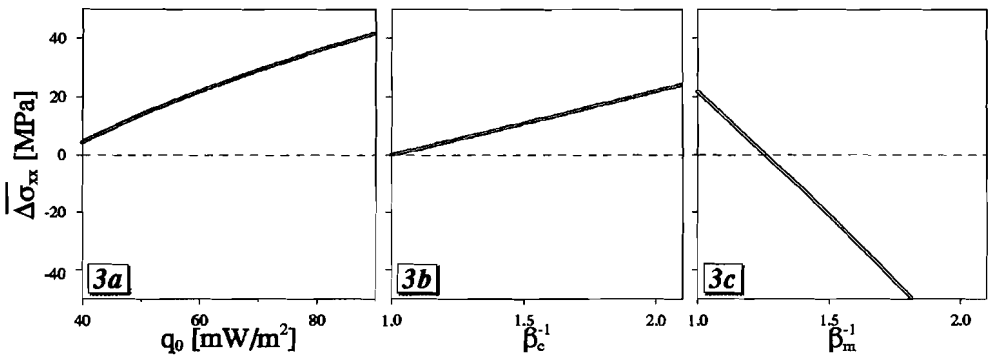

Fig. 3. *Dependence of average pre-stress magnitude on initial geotherm (parameterized by q_0), crustal thickening factor β_c^{-1} and mantle thickening factor β_m^{-1}.*

$$F_x = \int_S^{d_c} \sigma_{xx} dz$$

Like before, we assume that the horizontal stress is equal to the overburden pressure, to arrive at the following expression for the horizontal force in a lithospheric column

$$F_x = -g \int_S^{d_c} \int_S^{z} \rho(z') dz' dz \tag{1}$$

The depth-averaged horizontal stress $\overline{\Delta\sigma_{xx}}$ between a TCL column and a RCL column is defined by

$$\overline{\Delta\sigma_{xx}} = \frac{F_x^{RCL} - F_x^{TCL}}{d_c}$$

At this stage we can relax the assumption that sub-lithospheric forces are negligible; for calculation of $\overline{\Delta\sigma_{xx}}$ we use the difference between the horizontal forces in respective lithospheric columns. Processes in the mantle beneath the continental lithosphere probably occur on large length scales. It is, therefore, sufficient if the lithospheric columns are proximate so that the mantle contribution to both columns is the same. Calculation of the average horizontal stress of continental columns relative to an oceanic column (Braun and Beaumont, 1989b) is therefore considered less realistic.

Figure 2b shows the uniformly distributed pre-stress in the TCL. The resulting

elastic stress distribution is very similar to the input pre-stress. Stress relaxation due to brittle deformation in the upper crust and little ductile deformation in the lower crust and mantle is evident in the "plastic stress" line in Figure 2b.

Figure 3 displays $\overline{\Delta\sigma_{xx}}$ as a function of initial surface heat flow q_0, β_c^{-1} and β_m^{-1}. The results are based on a model of TCL with an initial steady state geotherm with a surface heat flow of 60mW/m^2, $\beta_c^{-1}=2$ and $\beta_m^{-1}=1$. Average crustal and mantle densities depend on the geotherm and the isostatic surface elevation S varies as a function of q_0. The compensation depth d_c in (1) is set at the 1350°C isotherm. Therefore, both the integration limits and the density terms in (1) depend on the geothermal gradient, and from Figure 3a it is clear that the average stress difference depends on q_0 in a non-linear fashion. Figure 3b shows the effect of variations in crustal thickening at a constant geotherm and without mantle thickening. It has been noted by several authors (e.g. Fleitout and Froidevaux, 1982) that the average pre-stress in TCL with a thickened mantle root may be compressive. This is clear in Figure 3c.

UNIFORM PRE-STRESS MODELS

Model U1

Model U1 In the first part of this chapter we consider models of post-thickening extension in which residual stresses from the thickening phase are distributed uniformly with depth. The first model is identical to Model 2 in chapter 5, with the exception of sediment loads which are included in the current model. Our finite element models are symmetric around a vertical axis and actual calculations are performed in the right hand side of the complete model only. The left hand vertical boundary therefore is a symmetry axis and mechanical and thermal boundary conditions are selected to reflect this symmetry; horizontal displacements and horizontal heat flow are zero on this side. Boundary conditions on the right hand vertical model boundary are based upon the assumption that the model continues infinitely, or at least very far, to the right. In chapter 3 it was concluded that vertical gradients in horizontal strain rates are negligible at a few hundred kilometers from a vertical boundary where non-rotative end loads are applied. Mechanically, the left model boundary is therefore a no-tilt boundary and the boundary is thermally insulated. Temperatures at the free upper surface are zero °C. A uniform heat flow applies to the lower model boundary. The lithosphere-asthenosphere boundary is modeled as a small density inversion, with a magnitude which depends on the initial geotherm via the average lithospheric mantle density. Parameter settings which have been used throughout this chapter are shown in Table 1.

The initial steady state geotherm in the RCL has been calculated for a surface

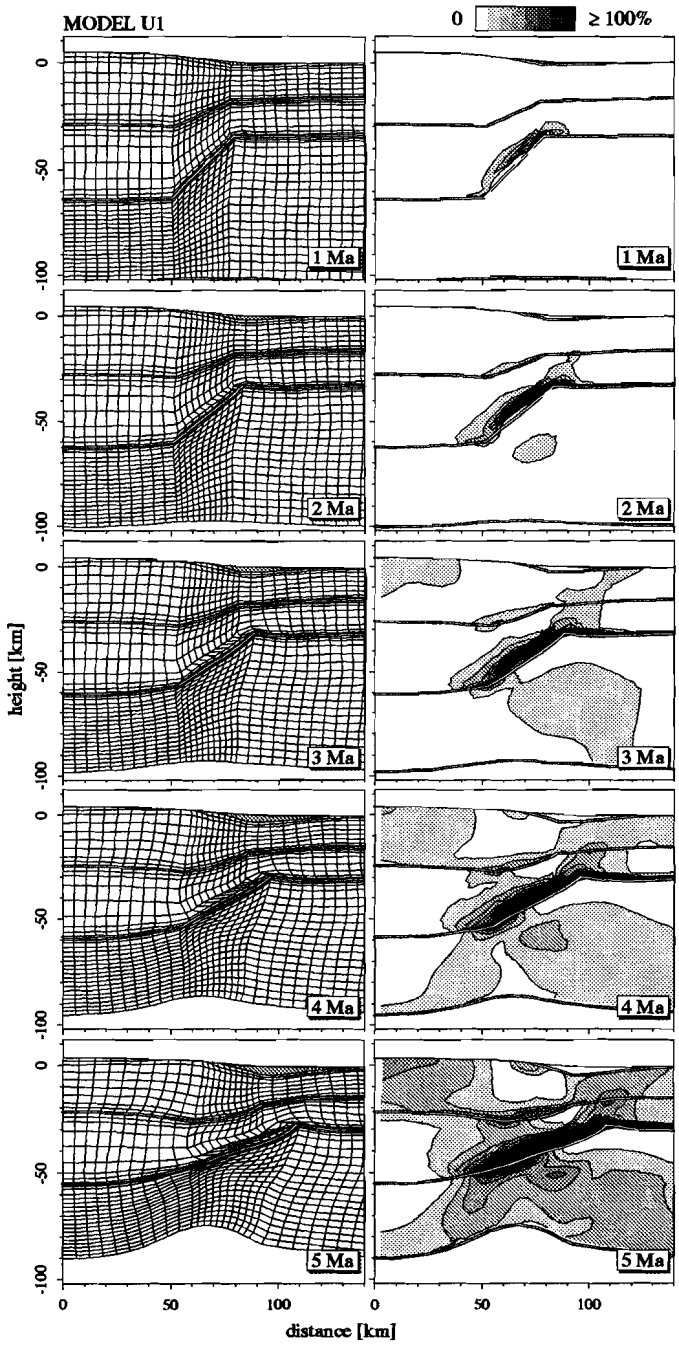

Fig. 4. *Evolution of Model U1. Left column shows finite element grid, right column contours of effective strain. Sediment deposition and erosion is apparent from infill and truncation patterns near the TCL/RCL boundary.*

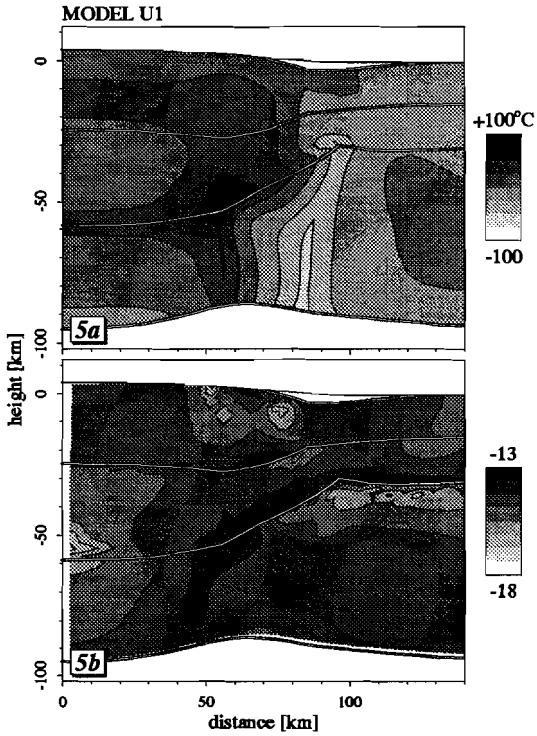

Fig. 5. *Model U1 after 4 Ma. (a) Temperature change since $t=0$. (b) Contours of logarithmic effective strain rate.*

heat flow of 60 mW/m^2. Table 2 shows layer parameters which are specific for Model U1. The crustal thickness of the RCL is 35 km. In our models, the thickness of the RCL is controlled by the minimum viscosity which can be handled by the finite element method. The TCL results from instantaneous thickening of RCL by a factor $\beta_c^{-1}=2$ in the crust. The TCL mantle has not been thickened and has been passively pushed down. Preliminary experiments with non-flat lower model boundaries indicated that the topography of the lower boundary controlled the evolution of the overlying lithosphere, as a result of instabilities which developed near this interface. The finite element method we employ is not very suited for modeling fluid-flow like processes which occur near the lithosphere- asthenosphere boundary. Therefore, in order to minimize the influence of the initial shape of the lower model boundary on the lithosphere model, the lower boundary is flat and the TCL mantle portion which has been depressed below the RCL thickness is not explicitly modeled. Heat production in the lithospheric mantle is very low, so that applying the heat flow b.c. to the flat TCL lower boundary, instead of applying it to the bottom of the depressed mantle, gives nearly identical temperatures in the overlying lithosphere. Mechanically, not modeling the depressed mantle is equivalent to

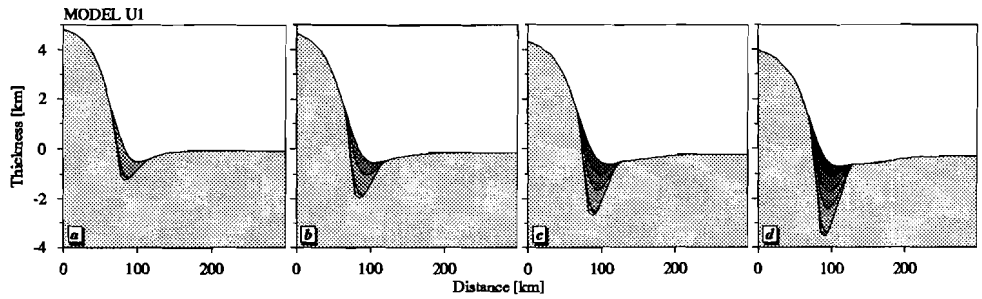

Fig. 6. *Sediment thicknesses of material eroded between 0 and 1 Ma, between 1 and 2 Ma, between 2 and 3 Ma, and between 3 and 4 Ma. (a) After 1 Ma. (b) After 2 Ma. (c) After 3 Ma. (d) After 4 Ma.*

assuming that straining this low-viscosity part of the mantle has a negligible effect on the deformation of the overlying lithosphere.

In Model U1, the width of the transition zone between TCL and RCL is 25 km (c.f. Figure 3 of chapter 5). At $t=0$, the in-plane compressive force that caused lithospheric thickening and mountain building, changes into a tensile force equivalent to 50 MPa, distributed uniformly over the lithospheric thickness.

Figure 4 shows the evolution of the lithosphere model and contours of effective strain (c.f. definition in chapter 5). Compared to the results of the model without sedimentation (Figure 7 in chapter 5), little has changed. Slight differences occur as a result of the fact that, in the current initial model, the lithospheric mantle is 5 km thicker than the mantle in the previous model. Heating of the TCL mantle from below is therefore slower. The timing of onset of asymmetric extension in the mantle is somewhat delayed, but it is apparent from Figures 4 and 5 that the overall style of extension is identical to that of Model 2 in chapter 5. The upper sedimentary/erosional surface of the panels in Figure 4 show that material is transported from the TCL to the foot of the mountains.

Figure 6 shows the synthetic stratigraphy at various instants during extension. As a result of the vertical exaggeration in the Figure, angular relations between various sediment beds are distorted. It was noted before that small wavelength morphological features are removed very rapidly. The initial sharp edge of the TCL has eroded away after 1 Ma (Figure 6a) and sediment deposition has smoothed out the RCL edge near the transition zone. Uplift of exhumed rocks and subsidence of sediment loaded basement occurs, producing a continued transport of sediment material from the TCL to the basin. With time, the surface gets smoother, and the basin depocenter migrates outward. The total sediment thickness after 4 Ma is close to 3 km.

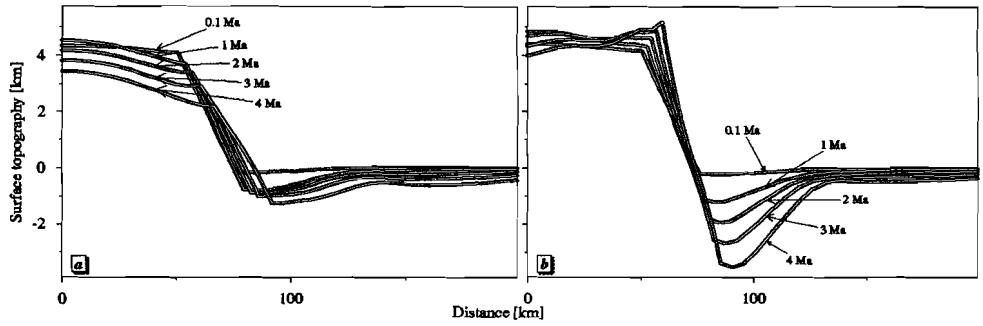

Fig. 7. *Topography of uneroded surface at 0.1 Ma, 1 Ma, 2 Ma, 3 Ma and 4 Ma. (a) Topography in model without sedimentary transport (Model 2 of Chapter 5). (b) Topography of Model U1.*

It was already observed from Figures 4 and 5 that the overall style of deformation is little affected by the effects of erosion and sedimentation. Differences are most clearly seen by comparing the surface topography of the model without sediment transport (Model 2 of chapter 5) and the (uneroded) basement topography of Model U1 (Figure 7). Like in Figure 6, the effects of unloading due to erosion and loading as a result of sediment deposition are clear in Figure 7b.

Figure 8 is a very schematic view of the lithosphere, which we use to identify the physical mechanisms controlling the onset of asymmetric extension. The top panel shows the initial TCL-RCL geometry, to which a uniform end force is applied. It has been shown in chapter 3 and by Kusznir and Park (1987) that stresses redistribute rapidly in strong layers of the lithosphere. This is shown in the middle panel of Figure 8. The strongest part of the lithosphere is the mantle directly beneath the Moho, and consequently, most of the load is supported here. The effect of extending the TCL-RCL system may be compared with stretching a piece of crooked rubber band. Stretching the rubber band will straighten it out, and likewise, tensile loads on the sub-Moho lithosphere will generate vertical forces. Shear in the lower crust of the model is required by the initial geometry. Namely, the length of the horizontal line between points *a* and *b* is less than the the length measured along the Moho line between the same points. Therefore, extension and flattening out of the Moho must be accompanied by shear strain. This shear occurs in the relatively weak lower crust.

It remains to explain why shear in the lower crust links up with the strong mantle, as these layers are mechanically partially decoupled by the low viscosities of the lower crust. Basically, this is caused by the initial thermal field of the thickened lithosphere. Thermally, the TCL is unstable as a result of the thicker crust

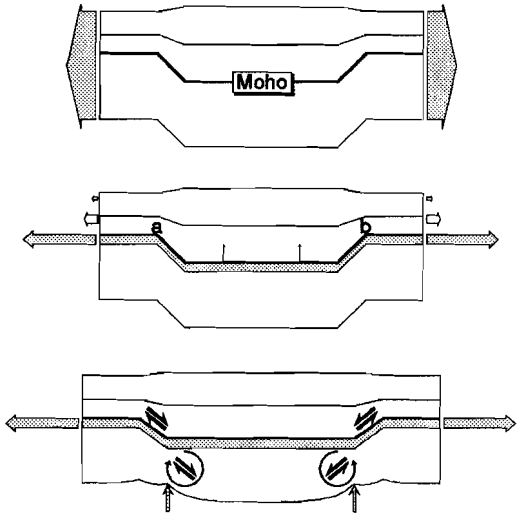

Fig. 8. *Mechanisms controlling the style of extension. Top panel:a uniform in-plane end load is applied to the TCL/RCL system. Middle panel: most of the stresses are supported in strong layers of the lithosphere, notably in the mantle directly beneath the Moho. Lower panel: the combination of straightening out of the Moho and buoyancy forces in the lithospheric mantle is the cause of an overall asymmetric style of extension.*

which overlies it, and because it has been advected very rapidly. The mantle beneath the TCL is relatively cold initially, and starts to heat up by thermal conduction. Near the transition zone, thermal conduction occurs both vertically and laterally and heating is therefore more rapid than in other parts of the TCL mantle (c.f. Figure 5a). Thermal expansion and buoyancy forces, together with a strong decrease in effective viscosities, are the reason for a rather localized region where thinning occurs and the asthenosphere starts to rise. Rising light asthenospheric material exerts an upward force (see Figure 8, bottom panel). The combined effect of a net moment exerted by the rising asthenosphere and shear in the lower crust, causes preferential development of the shear system in the mantle that dips beneath the TCL.

The finite element results of Model U1 and the analysis presented above, will serve as a frame of reference for the uniform pre-stress models we will examine next.

Variations in pre-thickening parameters

Model U1 was the result of a three-stage evolution; (1) a period before thickening, in which the composition and initial geotherm of the RCL were defined, (2) an instantaneous syn-thickening phase, with crustal thickening by a factor of 2 and no mantle thickening, and (3) the post-thickening period which starts at $t=0$. In this sub-part we investigate the influence of pre-thickening parameters on the style of extension after $t=0$. The models we consider next differ from Model U1 in one

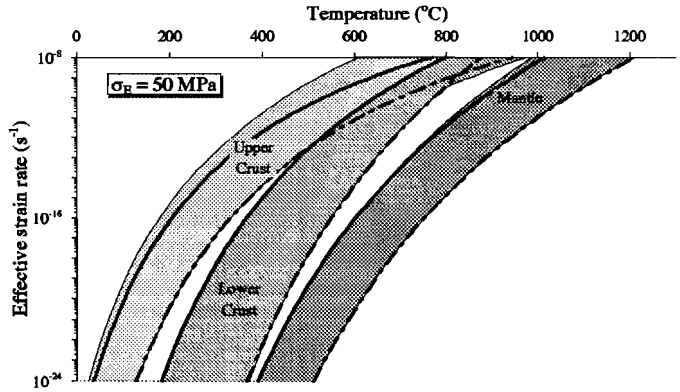

Fig. 9. *Rheologies for upper crust, lower crust and mantle. Grey colored areas show strength ranges derived from rheological parameters in the literature. Solid lines indicate the rheologies used in most of the models of this Chapter. Dashed lines show rheologies used in Models U2, U3 and U4 (see text for further explanation).*

single parameter only. Table 3 shows in which parameter the models are different from Model U1.

Composition

Figure 9 shows that experimental flow laws for upper crustal, lower crustal and mantle materials predict orders of magnitude differences in strain rate for different rocks. It is clear that the rheologies we adopted in Model U1 (thick lines in Figure 9) are relatively weak. In this section we investigate the influence of selecting more viscous materials on the style of extension (dashed lines in the Figure).

Model U2 In Model U2 we retain the parameter settings of Model U1, with the exception of the upper crustal rheology, for which we select dry quartzite ($Q_{pl} = 184.1$ kJ/mole, $A_{pl} = 2.20 \cdot 10^{-22}$ $Pa^{-2.8} \cdot s^{-1}$, $n_{pl} = 2.8$) (Jaoul *et al.*, 1984).

The results (Figure 10) show that extension of the lithosphere occurs at a slower rate than in Model U1. Obviously, the higher strength of the upper crust relative to that of Model U1 decreases the extension rate. A comparison of the strain at 6 Ma with the strain in Model U1, shows that the style of extension is basically identical, i.e. asymmetric extension occurs predominantly along a localized zone which dips from the RCL under the TCL. Asymmetric deformation in the lower crust and mantle will therefore link up with the free surface, irrespective of the upper crustal rheology. This result is in agreement with the conceptual model of Figure 8, in which the strength of the upper crust does not play a relevant role.

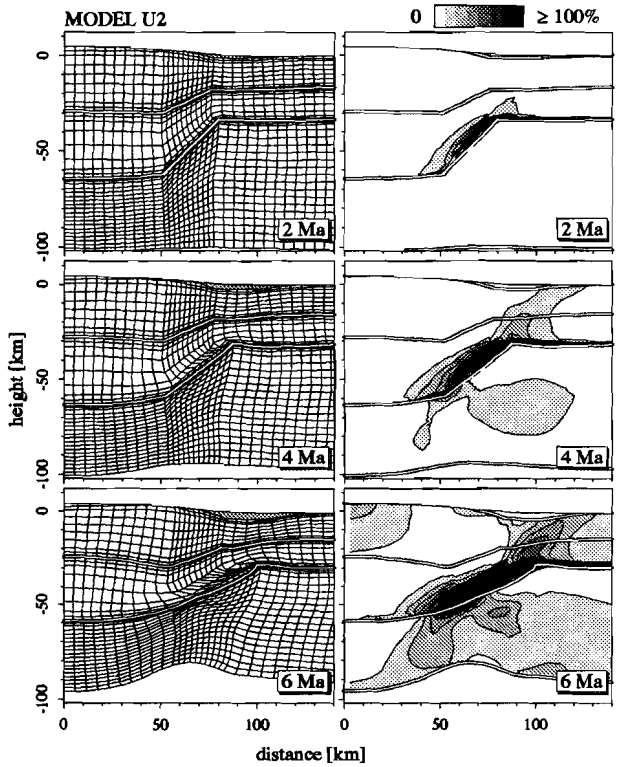

Fig. 10. *Evolution of strong upper crust Model U2.*

Model U3 The next model, Model U3, differs from Model U1 in that the viscosity of the lower crust is higher. Lower crustal rocks are assumed to have a Pikwitonei granulite rheology ($Q_{pl}=445$ kJ/mole, $A_{pl}=7.68\cdot 10^{-21}$ $Pa^{-4.2}\cdot s^{-1}$, $n_{pl}=4.2$) (Wilks and Carter, 1990).

Figure 11 shows the evolution of the model lithosphere. Compared to Model U1, the model evolves significantly slower. Shear in the transition zone lower crust is negligible. After 25 Ma, the TCL has heated to induce a sufficient viscosity drop and an increase in the extension rate. It is interesting to note that the relatively weak upper crust in the transition zone takes on the role the lower crust had in Model U1; sinistral shear deformation along the sloping upper-lower crust interface occurs in order to flatten out the Moho. After 28 Ma, deformation in the upper crust has linked up with the lower crust. Deformation in the TCL mantle is rather homogeneous, and consequently, a lithosphere scale fault will not develop. Referring to our conceptual model in Figure 8, this result is not unexpected; we already noted that the weak lower crust plays a fundamental role in our uniform pre-stress model

for asymmetric extension.

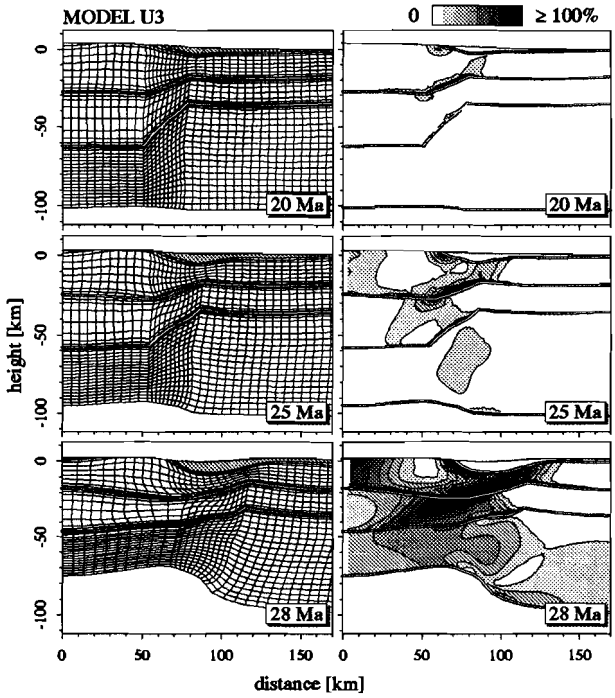

Fig. 11. *Evolution of strong lower crust Model U3.*

Model U4 The influence of mantle rheology is investigated in Model U4. Again, all parameters are identical to Model U1, except that a dry olivine flow law is adopted in the mantle (Q_{pl} = 510 kJ/mole, $A_{pl} = 7 \cdot 10^{-14}$ Pa$^{-3} \cdot s^{-1}$, $n_{pl} = 3$) (Kirby, 1983).

The results (Figure 12) show that the evolution of the extending lithosphere is slower than in Model U1. The high strength of the mantle at first inhibits significant extension of the TCL. After 15 Ma, however, the lower TCL mantle has heated sufficiently (T > 900°C) to cause a drop in viscosities below 10^{21} Pa · s. The combined effect of in-plane tensile stresses resulting from the end load and buoyancy forces associated with thermal expansion of the lower TCL mantle cause thinning and uplift of the lower mantle. Lateral heat conduction warms the TCL mantle of the transition zone more rapidly than the mantle beneath the TCL and cools the RCL side of the transition zone. Consequently, preferential rising and sinking of the transition zone mantle occurs, causing an indentation next to a bulge in the mantle. The sharpness of the indentation of the lower boundary at 20 Ma is an

artefact of the numerical procedure. As a result of fluid flow processes which start occurring near the model bottom at 20 Ma, our finite element approach gives inaccurate results and was therefore stopped. Up to 20 Ma, the style of deformation is markedly different from the style of extension of Model U1, as the strong mantle inhibits straightening out of the Moho and shear deformation in the lower crust does not occur. The results of Model U4 indicate that an increase of the mantle strength decreases the tendency to lithosphere scale asymmetric deformation, in accordance with the conceptual model of Figure 8.

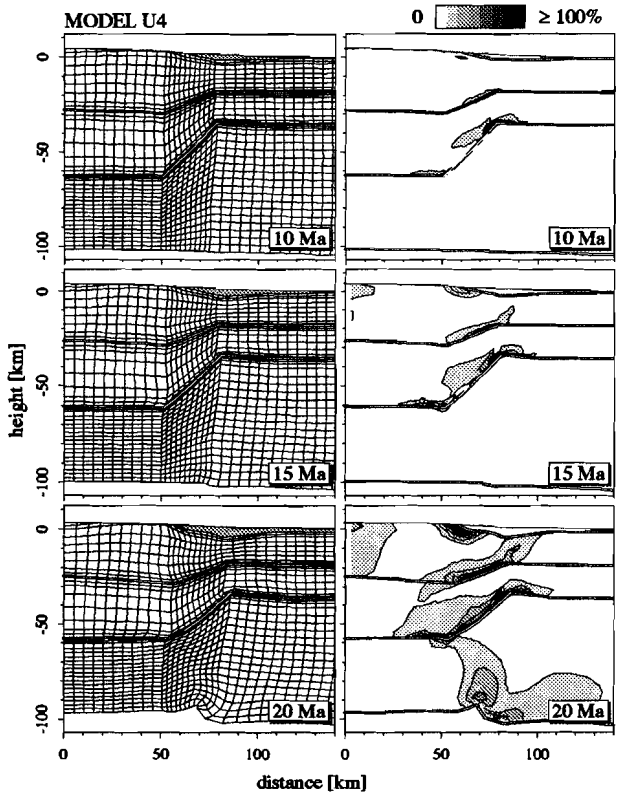

Fig. 12. *Evolution of strong mantle Model U4.*

Geotherm

The pre-thickening steady state geotherm in Model U1 was calculated for a surface heat flow of 60 mW/m^2. In this section we investigate the influence of the initial geothermal gradient on the style of extension.

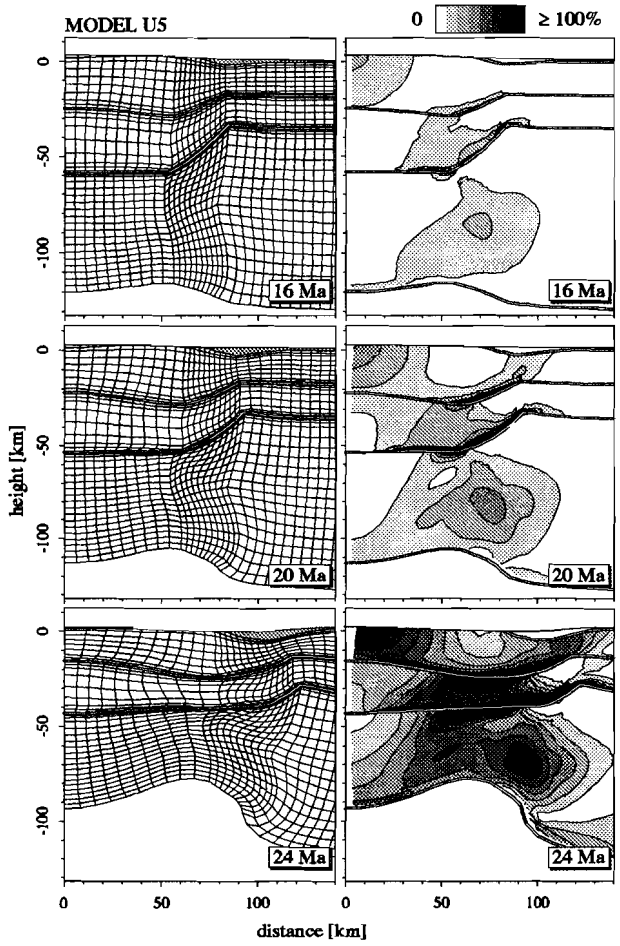

Fig. 13. *Evolution of cold lithosphere Model U5.*

Model U5 Before thickening, Model U5 has a steady state geotherm with a surface heat flow of 50 mW/m^2. This model represents a rather unusual situation, in which the geothermal gradient prior to mountain building is colder than average ($\approx$ 60 mW/m^2). The thickness of the lithosphere in our models is defined by the depth at which the TCL viscosity drops to the lower limit that can be handled by our finite element code at a specific time step size (c.f. Appendix of chapter 3), with a minimum of 100 km. The lithospheric thickness is therefore, via the exponential dependence of viscosities on temperature, a function of the initial geotherm. As a result, Model U5 lithosphere is thicker (130 km) than in Model U1 (105 km). Like in Model U1, the in-plane tensile force at $t=0$ is 50 MPa, uniformly distributed

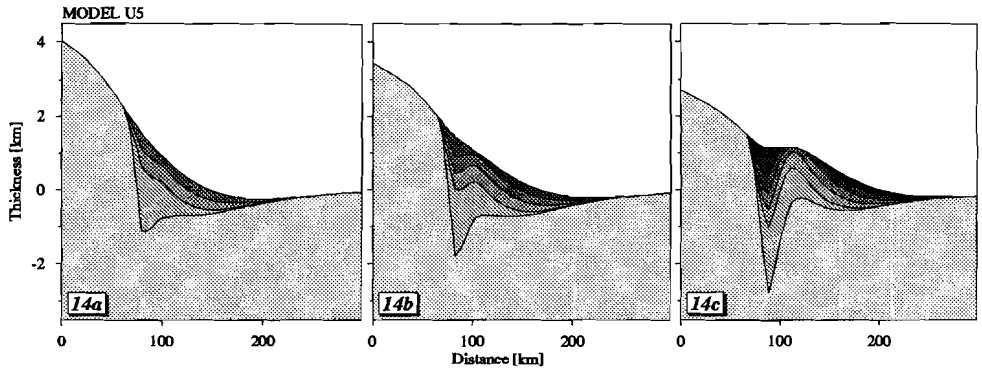

Fig. 14. *Stratigraphy of cold lithosphere Model U5 of material eroded between 0 and 4 Ma, between 4 and 8 Ma, between 8 and 12 Ma, between 12 and 16 Ma and between 16 and 20 Ma. (a) After 12 Ma. (b) After 16 Ma. (c) After 20 Ma.*

over the lithospheric thickness.

Figure 13 shows the evolution of the cold lithosphere model. Compared to Model U1, Model U5 evolves slower. Significant deformation starts occurring 16 Ma after the collision phase has ended. Compared to Model U1, shear deformation in the lower crust is limited, and pure-shear-like thinning of the TCL side of the transition zone becomes the dominant mode of deformation after 16 Ma. The foreland basin is wider than in Model U1 (Figure 14) as a result of the greater flexural strength of the colder lithosphere. Thinning of the lithosphere after 16 Ma is expressed as a shift towards the model symmetry center of the basin depocenter.

Differences between Model U5 and Model U1 can be understood in the light of their different viscosity structures. As a result of lower temperatures, Model U5 is stronger than Model U1 and responds more slowly to an end load of the same magnitude. The tendency of the Moho to straighten out (c.f. Figure 8) is less in Model U5, which explains why there is less shear deformation between crust and mantle of the transition zone in this model. Therefore, the style of deformation is rather symmetric. The time required for the mantle to heat up to cause a sufficient reduction in viscosities is about 16 Ma, after which thinning of the TCL side of the transition zone commences. Like in previous models, lateral heat conduction has warmed this particular part of the mantle faster. Therefore, thinning starts on the TCL side of the transition zone, which in turn increases the rate of heating of this region.

Model U6 In Model U6 we investigate the effect of a pre-thickening geothermal gradient which is higher than in Model U1. The surface heat flow initially is 70 mW/m^2, and the lithosphere thickness is 100 km. All other parameters are identical

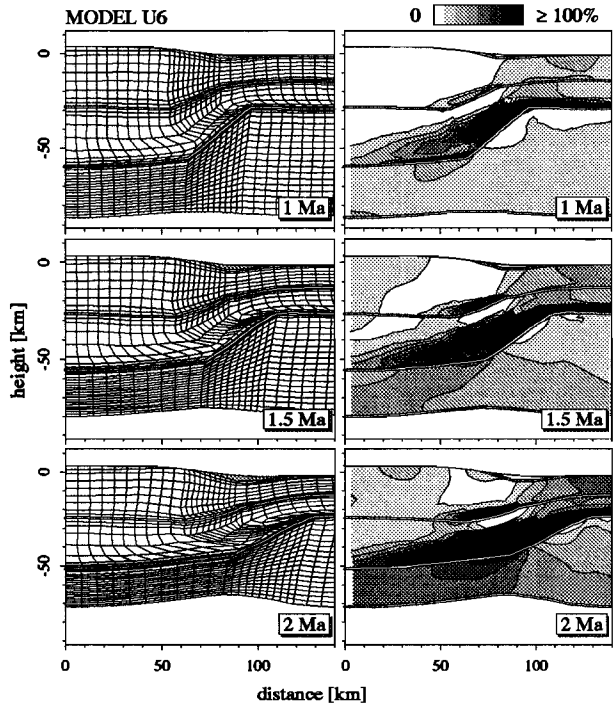

Fig. 15. *Evolution of hot lithosphere Model U6.*

to Model U1.

The hot lithosphere model evolves more rapidly than Model U1 (Figure 15). After 3 Ma only, the lithosphere has been stretched by a factor greater than 3 and, although our modeling does no longer produce accurate results at this time, it is clear that complete rifting and oceanization will follow. A zone of high shear deformation evolves in the lower crust and in the TCL mantle which is wider than in Model U1. The overall style of deformation in Model U6 is clearly asymmetric. The sediment deposition pattern (Figure 16) is similar to that of Model U1 with the exception that, as a result of higher extension rates, the basin is more sediment starved. In Model U6, the whole lower crust in the transition zone is sheared to attenuate the Moho topography, instead of the lower part of the lower crust only in Model U1. A higher geothermal gradient therefore not only increases the rate of extension at the same end load, but produces also wider dipping zones of elevated strain.

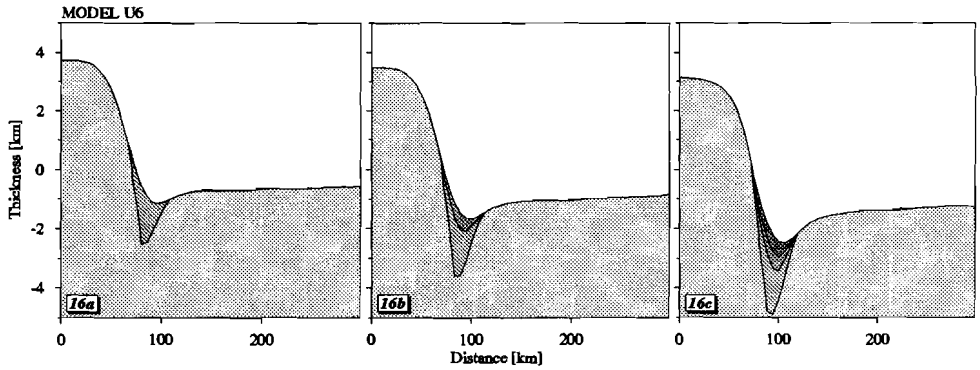

Fig. 16. *Stratigraphy of hot lithosphere Model U6 of material eroded between 0 and 1 Ma, between 1 and 1.5 Ma and between 1.5 and 2 Ma. (a) After 1 Ma. (b) After 1.5 Ma. (c) After 2 Ma.*

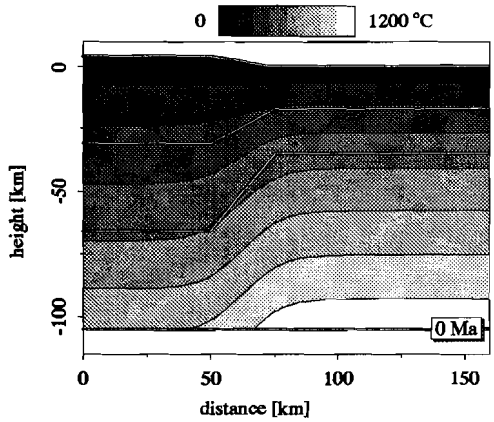

Fig. 17. *Temperatures at $t=0$ of Model U7, in which the duration of mountain building is 5 Ma.*

Variations in syn-thickening parameters

Finite thickening period

The results of the previous models are based on the assumption that thickening of the TCL occurred instantaneously, or at least on a timescale which is short compared to the time required for significant thermal diffusion. We also assumed that complete isostatic compensation had occurred within this short timespan. These assumptions are rather unrealistic, and in this sub-section we will investigate the effect of a thickening period of finite duration on the subsequent style of extension.

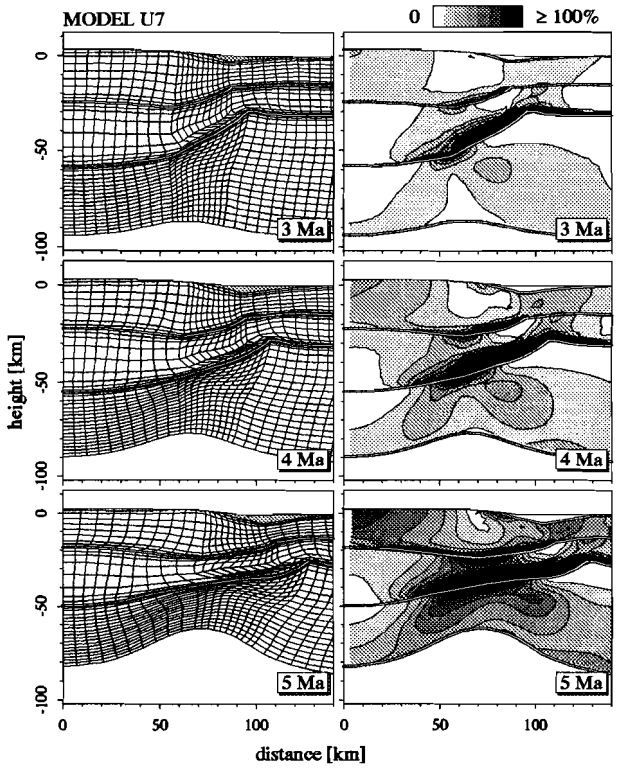

Fig. 18. *Evolution of 5 Ma thickening Model U7.*

Model U7 In Model U7 we investigate the influence of a finite thickening period of 5 Ma. For a mountain belt of 50 km half-width, this is equivalent to a relative horizontal velocity of 2 cm/yr, which is relatively slow. Apart from its initial thermal field, Model U7 is identical to Model U1. Figure 17 displays the geotherms at $t = 0$, when thickening ends and extension starts. The initial thermal field was calculated by solving the heat equation on a finite element grid with prescribed nodal velocities.

The evolution of the deforming lithosphere (Figure 18) is similar to the evolution of Model U1. The strain increases more rapidly than in Model U1 as a result of lower initial viscosities in and near the transition zone. The overall style of extension after 4 Ma closely resembles the extensional style after 5 Ma in Model U1. Upper crustal deformation beneath the foreland basin after 5 Ma is partially controlled by sediment loading, and a detachment system develops which soles out onto the upper-lower crust interface.

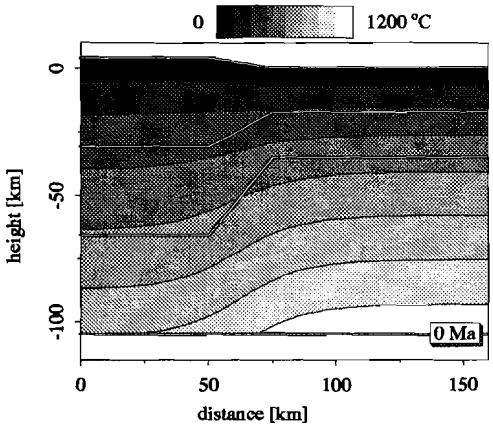

Fig. 19. *Temperatures at $t=0$ of Model U8, in which the duration of mountain building is 20 Ma.*

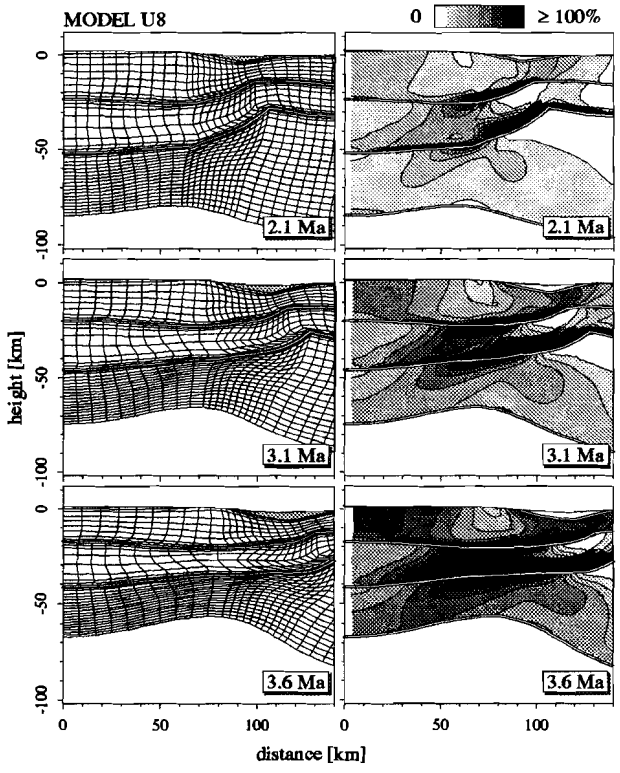

Fig. 20. *Evolution of 20 Ma thickening Model U8.*

Model U8 Continental thickening may result from a sequence of tectonic pulses or, equivalently, the thermal field in the part of the lithosphere that was thickened to the TCL may not have been in steady state prior to thickening. The next model, Model U8, is designed to model these scenarios and extension starts after a 20 Ma thickening period. The thermal field at the end of the thickening phase is shown in Figure 19.

Figure 20 shows the post-thickening evolution of the extending lithosphere. The rate of overall extension is significantly greater than in Model U1. The style of deformation is not very much different from Model U1 in the initial stages of extension, when shear in the lower crust prevails. Potentially important to the surface geology is a stronger tendency for shear deformation in the deep upper crust of the transition zone, which would be observed as a normal fault which flattens out on the upper-lower crust interface. After 3 Ma, deformation in the TCL lower crust and mantle becomes more uniform and symmetric than in Model U1. Lateral viscosity variations in the transition zone mantle are less pronounced than in Model U1 and, as a result, thinning occurs in a broader mantle region. We conclude that the duration of the thickening period is not critical to the style of extension, but that an increase of the duration of collision does decrease the tendency to asymmetric extension.

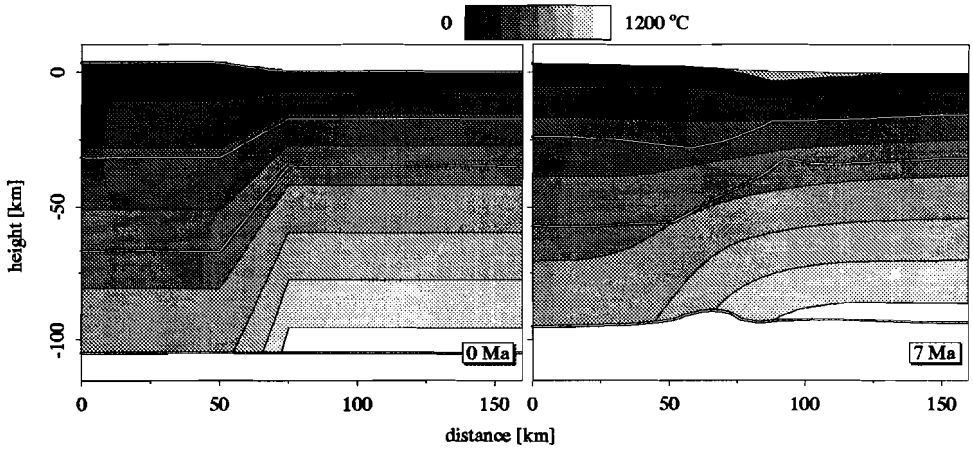

Fig. 21. *Geotherms in uniform thickening Model U9 at t = 0 and t = 7 Ma.*

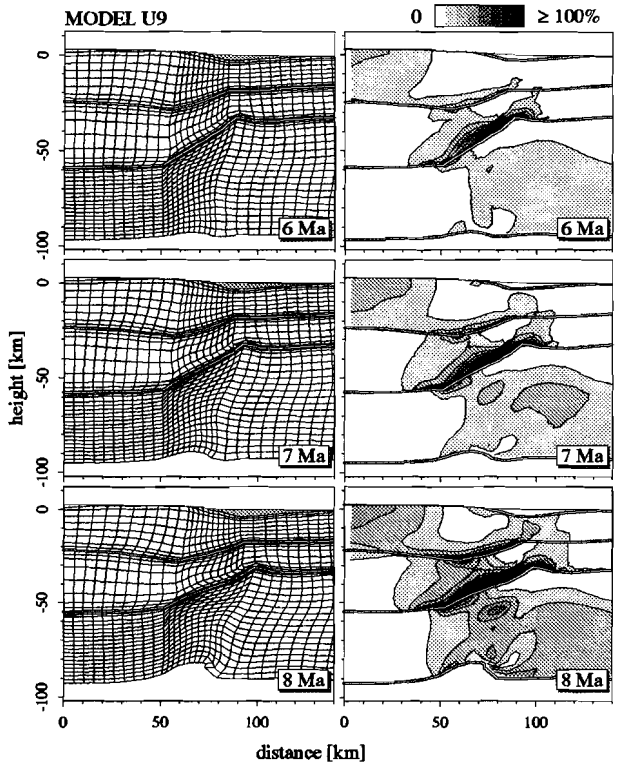

Fig. 22. *Evolution of uniform thickening Model U9.*

Thickening geometry

Model U9 In order to model tectonic thickening processes, in which overthrusting of crustal nappes is the predominant cause of mountain building, we choose to select crustal and mantle thickening factors of $\beta_c^{-1} = 2$ and $\beta_m^{-1} = 1$ in Model U1. In Model U9 we investigate how strongly this assumption affects the post-thickening style of extension by selecting uniform thickening of crust and mantle by a factor of 2. Recall that the TCL mantle below the depth of the RCL lower boundary is not actually modeled, and the initial model geometry is identical to Model U1. The initial geotherm in the TCL (Figure 21a) is, however, clearly distinct from that of Model U1. To incorporate the thermal effects of the TCL mantle below the flat lower model boundary, the heat flow b.c. acting on the flat lower model boundary is lower by a factor 2 in Model U9.

Figure 22 shows the finite element grid and effective strain at 6 Ma, 7 Ma and 8 Ma after extension has started. Compared to Model U1, the transition zone and the

TCL initially is more viscous and deformation in the mantle proceeds more slowly. Through the heat flow b.c., the cold mantle below the modeled TCL has a strong impact on the rate of heating of the TCL mantle. It is apparent from Figure 21b that the relative importance of horizontal heat conduction from the RCL to the transition zone and TCL is great compared to vertical heat conduction. A significant drop in viscosities therefore only occurs in the transition zone, where thinning localizes after 6 Ma. No deformation occurs in the TCL mantle and, as a result, shear deformation and localization is confined to upper and lower crustal layers of the transition zone. The cold TCL mantle effectively blocks asymmetric extension. Referring to Figure 8, this results confirms that (preferential) thinning of the TCL mantle is an essential ingredient for initiating asymmetric extension of the scale of the whole lithosphere.

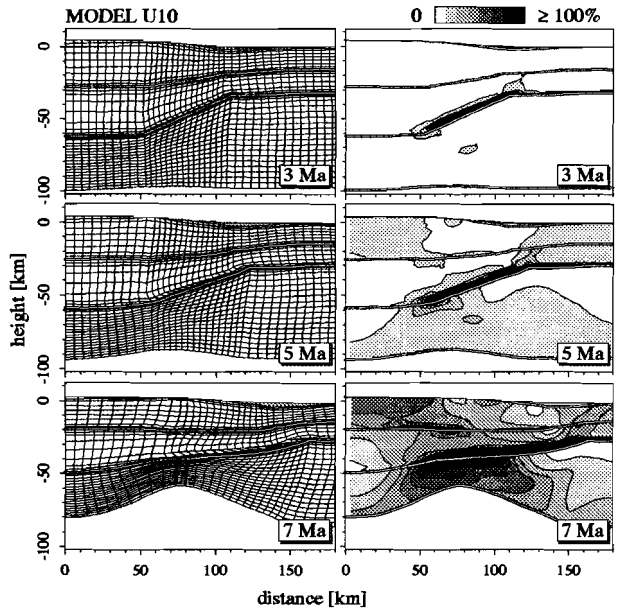

Fig. 23. *Evolution of wide transition zone Model U10.*

Model U10 Since the slope of the Moho appears to be a key element in the conceptual model in Figure 8, the importance of establishing the dependence of the style of extension on the width of the transition zone is apparent. In the next model, Model U10, we consider the influence of the width of the transition zone on the style of extension. Model U10 has a 50 km wide transition zone, i.e. twice the width of Model U1.

Figure 23 shows the evolution of the finite element grid and effective strain. The shear zone in the lower crust again develops and links up with the free surface and mantle zone of preferential thinning and uplift. At 7 Ma, the lower mantle connects offset zones of thinning in the mantle and upper crust and a lithosphere scale asymmetric zone has developed. Sediment loading of the foreland basin appears to influence the breakthrough of lower crustal deformation to the free surface. Sedimentary loads amplify normal sense of shear deformation along the fault dipping under the TCL. It is clear that the width of the transition zone does not significantly influence the mode of extension.

Variations in post-thickening parameters

Gravitational collapse

Model U11 Post-thickening extension is to a large extent controlled by the timing and magnitude of the in-plane end load. In Model U1, the compressive end load which was responsible for the mountain building phase, switched to a tensile load equivalent to 50 MPa at $t=0$. In Model U11 we investigate the response of the lithosphere when the in-plane compressive force is set to zero at $t=0$. This gravitational collapse model is similar to Model 1 of chapter 5, with the exception of sediment loads, which are included in Model U11 and were not in Model 1 of chapter 5.

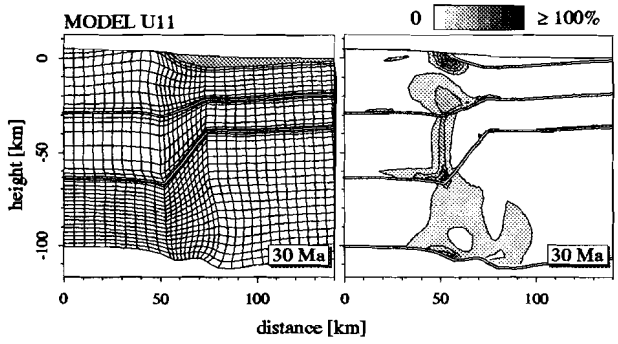

Fig. 24. *Grid and effective strain after 30 Ma in gravity collapse Model U11.*

Figure 24 shows the finite element grid and effective strain at 30 Ma after thickening has ended. The results confirm the conclusion from chapter 5 that gravitational collapse does not lead to asymmetric extension. The effect of sediment transport produces a marked difference in the amount of extension, however. In Model 1 of chapter 5, the model calculations stopped at 22 Ma, when thinning of the TCL

became very large. In Model U11 virtually no extension occurs. Erosion of the TCL produces compressive stresses in the TCL which balance tensile pre-stresses in Model U11. The depth of the foreland basin after 30 Ma is nearly 5 km, and the weight of sediment load depresses the RCL side of the transition zone. Including the effects of sediment transport in this case has a strong influence on the deformation of the lithosphere.

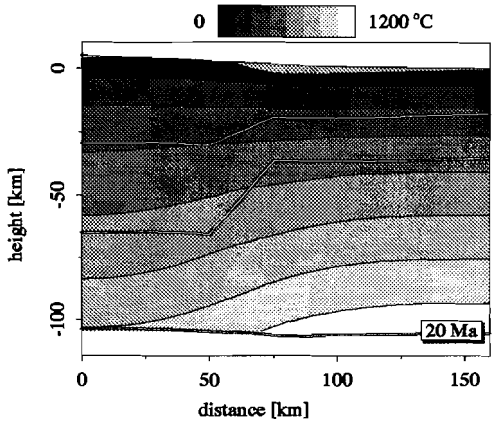

Fig. 25. *Temperatures after 20 Ma in delayed pull Model U12.*

Delayed in-plane end load

Model U12 In Model U12, an in-plane force equivalent to 50 MPa starts acting 20 Ma after thickening has ended. In the intermediate period, the in-plane load is zero. Comparing the thermal field after 20 Ma (Figure 25) with the temperatures of the Model U8 (Figure 19), we see that the TCL of Model U12 is hotter and geotherms are smoother. This difference in thermal field is caused by the fact that Model U12 results from instantaneous thickening and subsequent thermal re-equilibration, whereas the initial temperatures in Model U8 are a consequence of a 20 Ma thickening period. Therefore, the TCL of Model U12 has been exposed to a thickened crust for a longer period than Model U8. As a result of the fact that most of the heat producing radioactive elements reside in the crust, Model U12 has been heated more after 20 Ma than Model U8.

Figure 26 shows the finite element grid and effective strain after 20 and 21 Ma. After 21 Ma, the effective strain rate at the model symmetry center is $2 \cdot 10^{-14}\ s^{-1}$ and accelerates rapidly. The style of extension is pure shear. Differences between the results of Model U12 and Model U8 are mainly caused by distinctions in the thermal field at the onset of extension. Shear in the lower crust does occur, but does not link up into a lithosphere scale asymmetric zone. Compared to Model U1, the result of delayed pull is that the style of extension is more rapid and more sym-

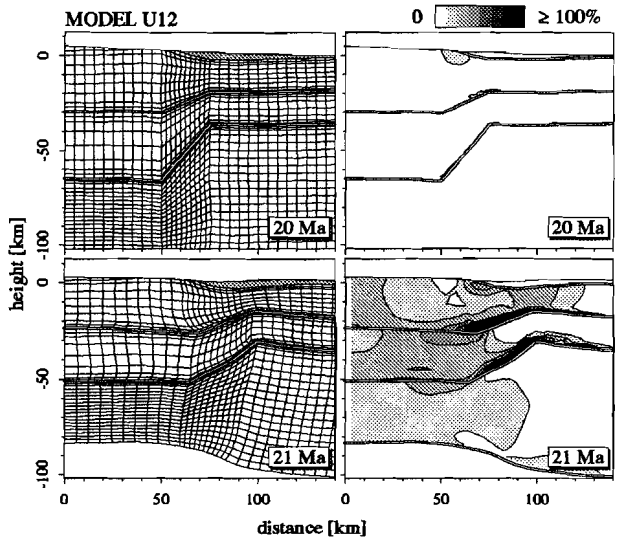

Fig. 26. *Evolution of delayed pull Model U12.*

metric. In accordance with the cartoon of Figure 8, lateral variation of TCL mantle viscosities are a requisite for lithosphere scale asymmetric extension to develop.

End load magnitude

Model U13 Model U13 is again identical to Model U1, with exception of the in-plane end load, which is twice as large in magnitude.

It should not come as a surprise that Model U13 extends more rapid than Model 1 (Figure 27). Shear deformation in the lower and upper crust evolves into a dipping zone which accommodates asymmetric extension. In the mantle, strains indicate that the broad conjugate zone, which dips from the TCL under the RCL, is more active than the system parallel to the dipping lower crust. After 1.5 Ma, strain rates in the mantle (not shown in the Figure) are rather homogeneous. An increase in the end load magnitude appears to decrease the tendency to lithosphere scale asymmetric deformation. Referring to Figure 8, more uniform mantle deformation can be understood as a result of a lack of time for lateral heat transfer and lateral viscosity contrasts to develop.

At this point we refer to the discussion and conclusions section at the end of this chapter for a summary of the results of the uniform pre-stress models.

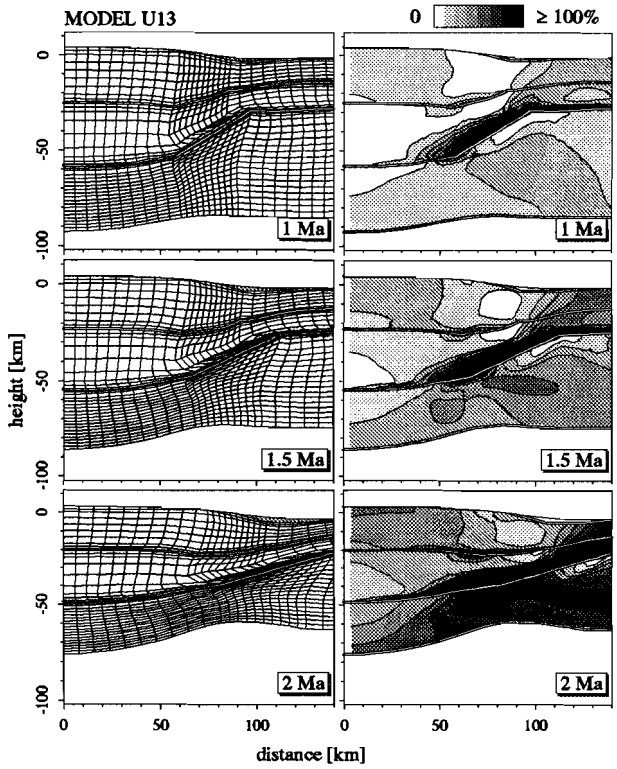

Fig. 27. *Evolution of Model U13, in which the in-plane end load is twice as large as in Model U1.*

NON-UNIFORM PRE-STRESS MODELS

Model N1

Model N1 The basic canvas in the second part of this chapter is identical to the tectonic history we considered before. The left part of a RCL, which initially is in thermal equilibrium, is instantaneously thickened by a factor 2 in the crust. The TCL mantle is passively pushed down, without thickening. The TCL is in local isostatic equilibrium. The difference with respect to the previous part is that we now assume that residual stresses are a function of depth. At $t=0$ the mountain building phase ends and extension commences as a response to an in-plane tensile load.

The first model, Model N1, is identical to Model U1, with exception of the pre-stress distribution. Figure 28 shows the evolution of the extending lithosphere and effective strains at subsequent timesteps. As a result of high tensile pre-stresses in

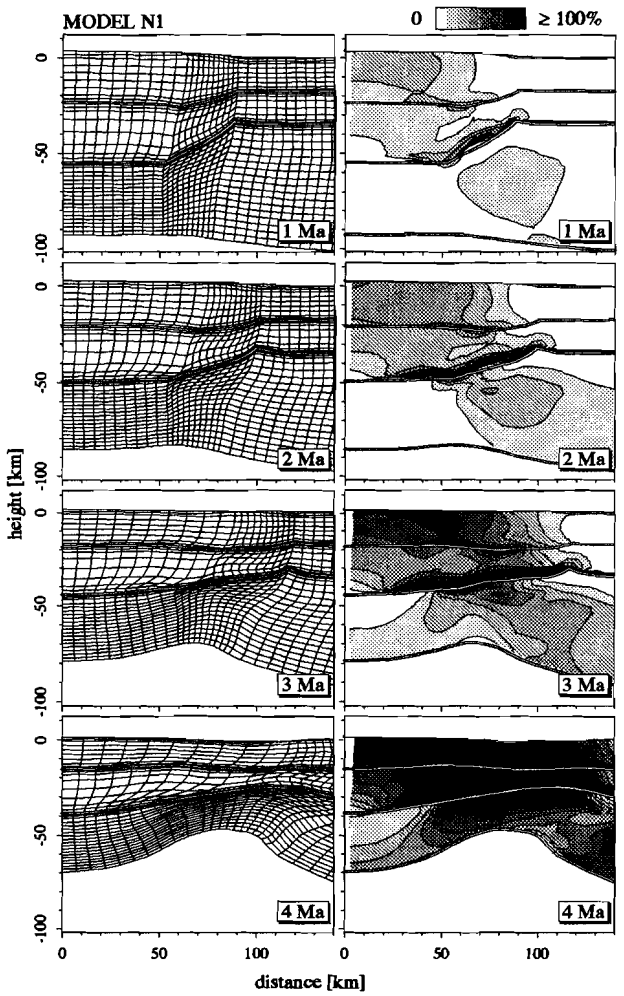

Fig. 28. *Evolution of non-uniform pre-stress Model N1.*

the TCL crust, crustal attenuation and extension is more rapid in Model N1 than in Model U1. This result is in accordance with the findings from Model 4 of chapter 5. Compared to Model U1, the style of extension in Model N1 is very different. In Model N1, strain localizes in a zone which dips from the TCL to the RCL, i.e. dipping in a direction *opposite* to the direction in which lithosphere scale shear zones developed in the uniform pre-stress models. A closer look at the deformed grid in Figure 28 shows that the sense of shear in the upper crust and most of the lower crust is dextral normal. The TCL side of the transition zone mantle also shows evidence of dextral shear deformation. In the lower crust of the transition zone near

the Moho, sinistral normal shear occurs on the conjugate branch.

To understand the reason for the different style of extension we refer to the lower right panel of Figure 4, in which the effective strain at 5 Ma of Model U1 is displayed. The high strain zone dipping from the RCL under the TCL clearly has developed preferentially, but it is interesting to notice that the conjugate system, which dips from the TCL under the RCL, is present too. It was already noted in chapter 5 that conjugate systems develop as a result of the tendency of the lithosphere to conserve moment. Deformation with a normal sense of shear on either conjugate fault system has the effect of attenuating the topography of the Moho. Referring to the bottom panel of Figure 8, preferential thinning of the TCL mantle near the transition zone provided the extra moment which was necessary for a lithosphere scale normal fault to develop in the uniform pre-stress models. In the non-uniform pre-stress approach, a net moment is exerted which is opposite to the moment induced by the lower crustal shear in the transition zone (Figure 29). Development of the fault dipping under the TCL is therefore impeded, and the conjugate fault system develops preferentially, at least in the upper crust and most of the lower crust.

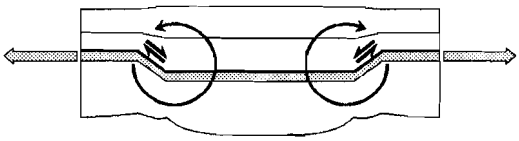

Fig. 29. *The effect of a non-uniform pre-stress distribution is that a net moment is exerted, acting clockwise on the right hand side and anti-clockwise on the left hand side of the TCL.*

Thusfar, model studies on post-thickening extension have adopted a uniform pre-stress assumption (England and McKenzie, 1982; Houseman and England, 1986; Sonder *et al.*, 1987; Braun and Beaumont, 1989b). Notably, Braun and Beaumont (1989b) investigated plane strain models of cross-sections of continental mountain belts, like we do. The focus of their work was more on overall rates of extension in relation to the mountain building process than on the style of internal deformation of the lithosphere. Since the rate of extension is also significantly affected by the pre-stress distribution, the time constants they derive should be looked upon with care. This argument obviously is also important to plan view models of the lithosphere, in which the properties of the lithosphere are approximated by their vertical averages.

In the remaining part of this chapter we present the same type of investigation of pre-, syn-, and post-thickening parameters as we did for the uniform pre-stress models.

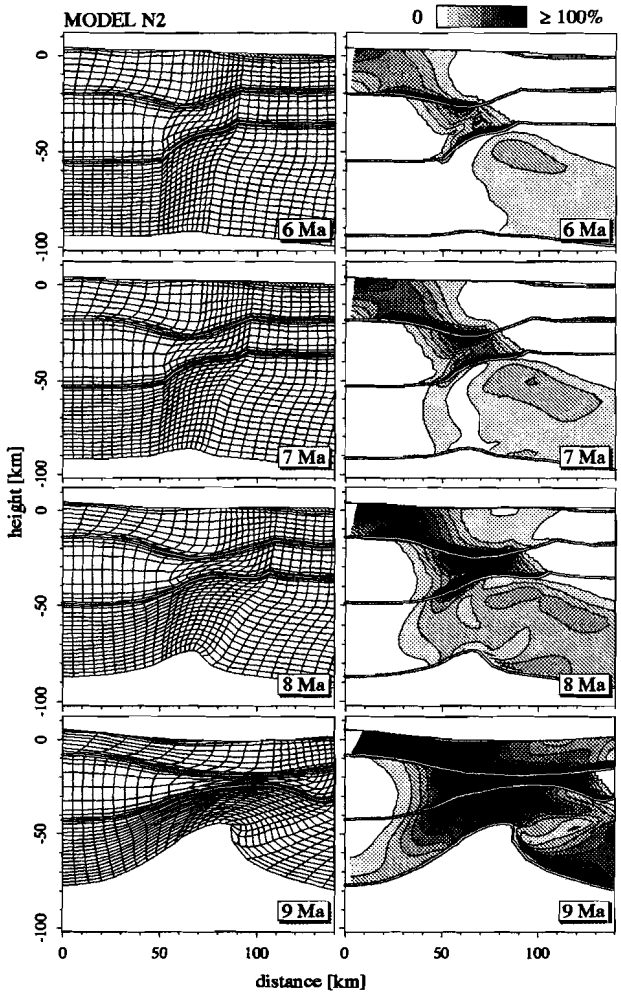

Fig. 30. *Evolution of strong lower crust Model N2.*

Variations in pre-thickening parameters

Composition

Model N2 Model N2 has a a Microgabbro rheology in the lower crust ($Q_{pl}=497$ kJ/mole, $A_{pl}=1.12\cdot10^{-10}$ $Pa^{-3.4}\cdot s^{-1}$, $n_{pl}=3.4$) (Wilks and Carter, 1990), and is notably more viscous than model N1. All other parameters of Model N1 and Model N2 are identical.

Figure 30 shows the evolution of the lithosphere model and effective strain. At 6

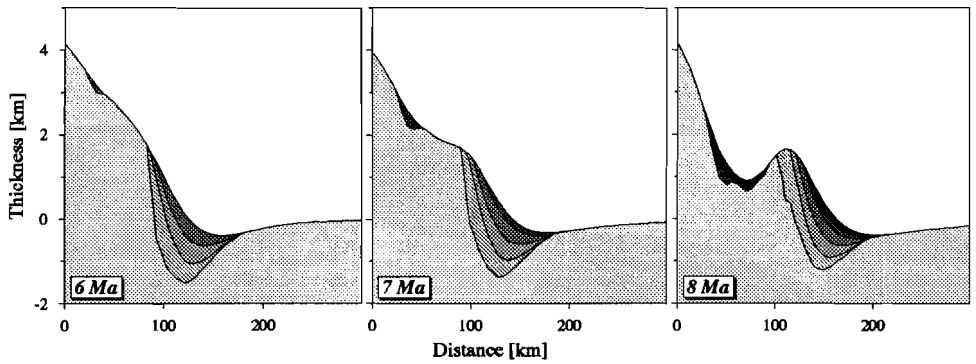

Fig. 31. *Stratigraphy of strong lower crust Model N2 of material eroded between 0 and 2 Ma, between 2 and 4 Ma, between 4 and 6 Ma, between 6 and 7 Ma, and between 7 and 8 Ma.*

Fig. 32. *Net surface uplift of the symmetry center of strong lower crust Model N2.*

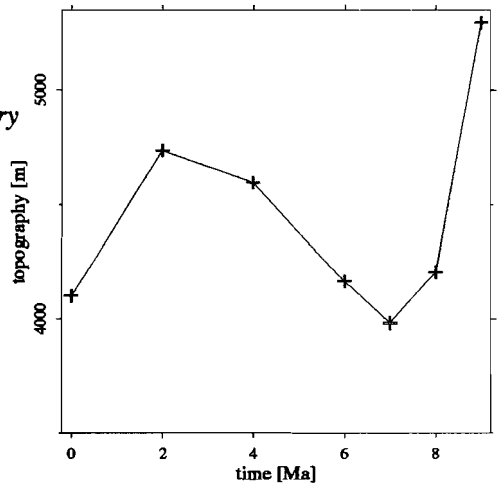

Ma, strain in the upper crust and lower crust is localized in a band dipping from the TCL to the RCL. Although we do not model faults explicitly, it is considered likely that the surface geology is dominated by dextral normal faults which sole out in either the lower upper crust or into the lower crust. In the early stages of extension, the strong sub-Moho mantle of the TCL is hardly deformed. Heating of the sub-Moho mantle occurs preferentially near the Moho edge on the transition from TCL to the transition zone (c.f. Figure 5a). Driven by the thermally induced drop in viscosities, the mantle in this region starts thinning after 6 Ma. The sense of shear in the TCL mantle is dextral with a reverse vertical component. Deformation therefore

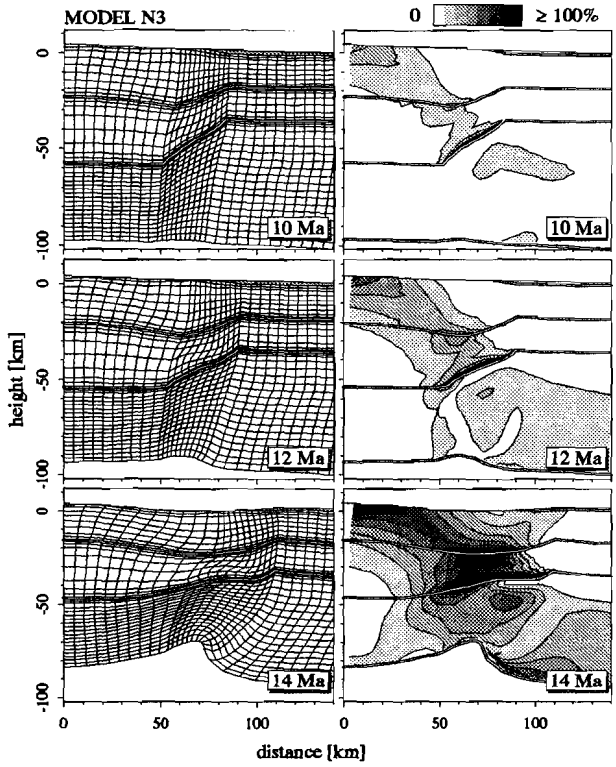

Fig. 33. *Evolution of strong upper crust Model N3.*

has evolved in an asymmetric fashion after 9 Ma. Effectively, this results in an asymmetric deformation pattern characterized by a large discrepant zone. The onset of deformation in the TCL mantle is expressed in the sedimentation pattern (Figure 31). After 6 Ma a foreland basin has evolved with a sediment thickness of approximately 1.5 km. The onset of mantle thinning is accompanied by a jump towards the model symmetry center of the thinning, which is evident from the sediment starved basin evolving after 6 Ma. An interesting feature is the net surface uplift, i.e. the uplift of rocks minus the thickness of eroded material. Figure 32 shows the net surface uplift of the symmetry center as a function of time. In the first 2 Ma following collision, the symmetry center surface is uplifted as a consequence of redistribution of surface loads associated with erosion and sedimentation. Crustal thinning results in subsidence of the surface at $x = 0$. After 6 Ma, with the onset of mantle thinning, the locus of thinning jumps towards the symmetry center. Subsidence as a result of thinning occurs within the TCL region, thereby steepen-

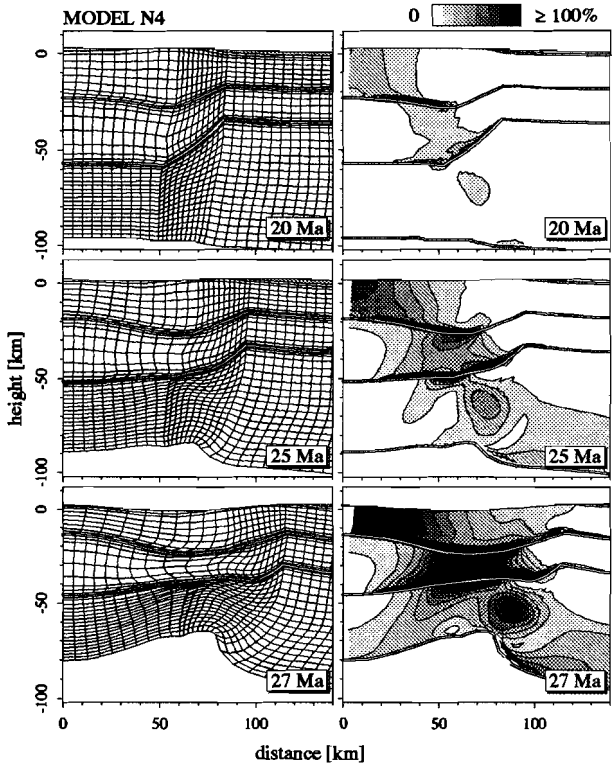

Fig. 34. *Evolution of strong mantle Model N4.*

ing the surface near the symmetry center and increasing the erosion and sedimentation rate. Erosion leads to repeated uplift; after 8 Ma, the net surface uplift rate of the symmetry center is 1 mm/yr.

Compared to Model N1, the strong lower crust Model N2 deforms more slowly. The effect of the weak lower crust in Model N1 is that more dextral shear deformation is accommodated in the crust and consequently, the style of deformation in the mantle is more symmetric than in Model N2. As stated before, the natural mode of deformation of continental lithosphere is pure shear. Since it is our aim to study causes for large scale asymmetric behavior we will use Model N2 as a reference for the non-uniform pre-stress models we present in the second part of this chapter.

Model N3 The next model, Model N3, is identical to Model N2, except for the rheology of the upper crust, for which we use dry quartzite ($Q_{pl} = 184.1$ kJ/mole, $A_{pl} = 2.20 \cdot 10^{-22}$ Pa$^{-2.8} \cdot s^{-1}$, $n_{pl} = 2.8$) (Jaoul *et al.*, 1984).

The evolution of the lithosphere model is depicted in Figure 33. The main dif-

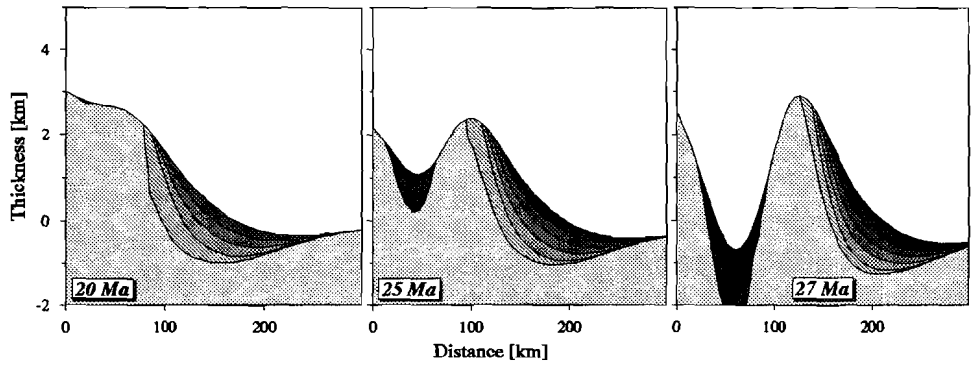

Fig. 35. *Stratigraphy of strong mantle Model N4 of material eroded between 0 and 5 Ma, between 5 and 10 Ma, between 10 and 15 Ma, between 15 and 20 Ma, between 20 and 25 Ma, and between 25 and 27 Ma.*

ference between Model N2 and Model N3 is a delay in the onset of extension. Little deformation occurs until, 12 Ma after thickening has ended, heating has induced a drop in transition zone mantle viscosities and mantle thinning commences. Relative to Model N2, shear deformation in the upper crust is limited, and the crust responds more like a single unit. The tendency of upper crustal faults to sole out into the upper-lower crust interface is therefore clearly less prominent in Model N3. The locus of dextral shear deformation is shifted to the relatively weak TCL mantle, in which a reverse dextral shear zone evolves after 14 Ma. The overall style of deformation is not very different from the style of Model N2.

Model N4 The influence of mantle rheology is investigated in Model N4. Again, all parameters are identical to Model N2, except that a dry olivine flow law is adopted in the mantle ($Q_{pl}=510$ kJ/mole, $A_{pl}=7\cdot 10^{-14}$ Pa$^{-3}\cdot s^{-1}$, $n_{pl}=3$) (Kirby, 1983).

The evolution of the viscous mantle Model N4 is shown in Figure 34. Apart from creating a wide basin (Figure 35), which reflects the high flexural strength of the system, virtually nothing happens in the first 20 Ma after thickening has ended. The overall style of extension is not very different from the style of Model N2. The main difference as a result of a strong lithospheric mantle rheology is the delay before extension starts.

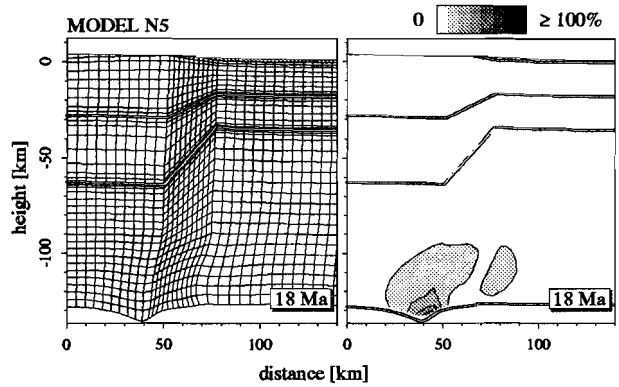

Fig. 36. *Finite element grid and effective strain after 18 Ma in cold lithosphere model N5.*

Geotherm

Model N5 In Model N5 we investigate the effects of a colder pre-thickening steady state geotherm which produces a surface heat flow of 50 mW/m^2.

Figure 36 shows the finite element grid and contours of effective strain after 18 Ma. In the TCL, the horizontal deviatoric stress is compressive as a consequence of depth-dependent pre-stress. Preferential heating of the TCL mantle near the transition zone generates a local viscosity minimum, and a mantle drip is squeezed from the mantle after 18 Ma. The drip is gravitationally unstable since it is colder and therefore more dense than the asthenosphere below. Eventually, the droplet will detach from the lithosphere and sink. Unfortunately, our finite element approach does not allow us to accurately track the evolution of the lower boundary after 18 Ma. We can therefore draw no conclusions about the style of extension at relatively low thermal gradients. A different approach to the numerical problem is required to resolve if shedding of lithospheric drips controls the evolution of relatively cold lithosphere, or if these are merely transient processes which have a minor impact on the evolution of the lithosphere as a whole.

Model N6 Compared to Model N2, the thermal field of Model N6 prior to thickening is hotter. The heat flow in the thermally stable RCL is 70 mW/m^2.

Figure 37 shows that the lithosphere model extends readily as a result of the end load equivalent to 50 MPa. The upper and lower crust are effectively decoupled by low viscosities in the deep upper crust. As a result, the upper crust is sheared over the lower crust. Normal faults developing in the upper crust will therefore not penetrate the lower crust. Lateral viscosity contrasts are small in the mantle, and mantle deformation is well described by pure shear. The style of deformation in litho-

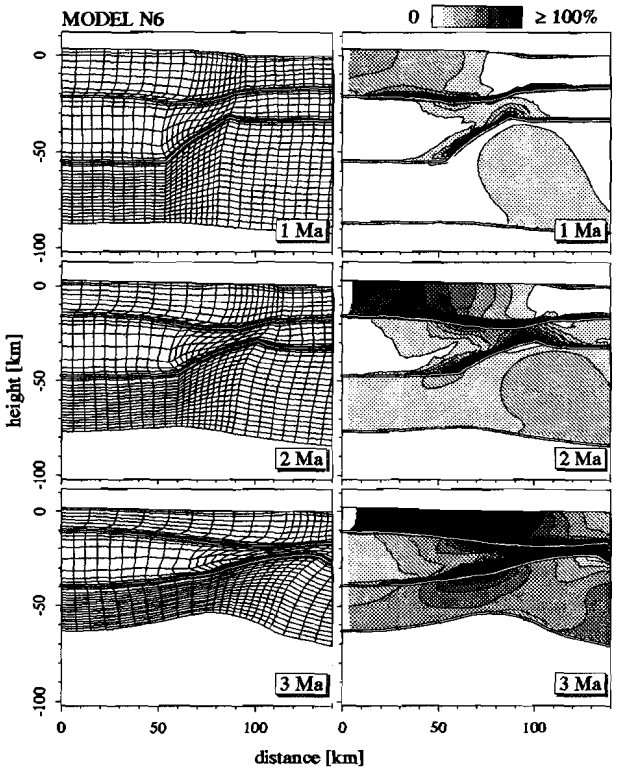

Fig. 37. *Evolution of hot lithosphere Model N6.*

sphere with a higher initial gradient is asymmetric in the crust and symmetric in the mantle below it.

Variations in syn-thickening parameters

Finite thickening period

Model N7 The TCL of Model N7 results from isostatic thickening of RCL during a period of 5 Ma. Figure 38 shows the evolution of the grid and strain following mountain building. The onset of mantle thinning occurs slightly sooner than in Model N2. The final deformation in the mantle is more symmetric than in Model N2, which is a result of the smoother initial temperature field.

Model N8 In Model N8, we investigate the style of extension after a 20 Ma thickening period. As a result of lower viscosities, the lithosphere model deforms more

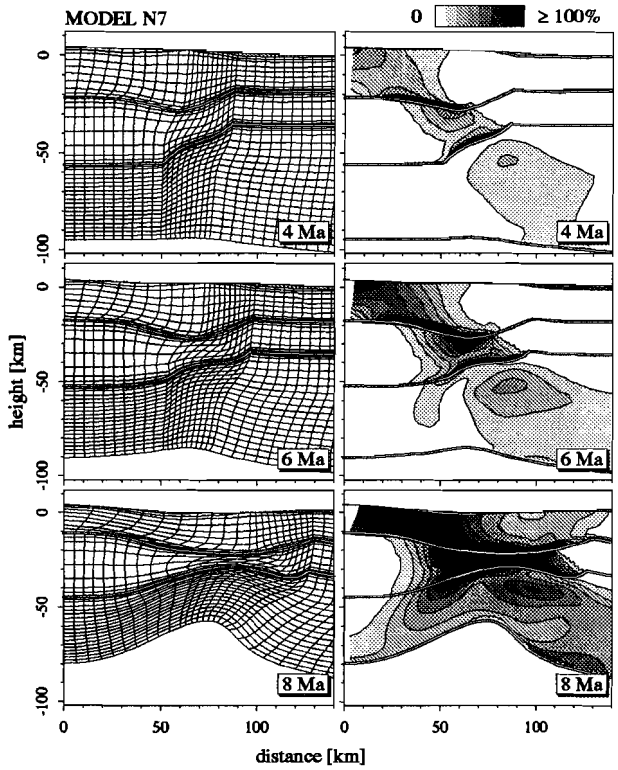

Fig. 38. *Evolution of 5 Ma thickening Model N7.*

rapidly than Models N2 and N7 (Figure 39). Strain contours are broader and smoother than in Model N2 and deformation in the mantle is more symmetric. Crustal asymmetric extension is insensitive to the duration of thickening. The style of extension in the mantle becomes more homogeneous with the duration of the collision phase. The results after 8 Ma resemble the kinematic model for continental extension proposed by Kusznir and Mathews (1988) and Lister and Davis (1989), in which a crust deforming by simple shear overlies a mantle deforming by pure shear.

Thickening geometry

Model N9 The influence of uniform $\beta_c^{-1} = \beta_m^{-1} = 2$ thickening on the style of post-thickening extension is investigated in Model N9. Figure 40 shows the lithosphere model and contours of effective strain after 7 Ma. A drip-like feature has evolved in the lower boundary of the transition zone. Like in Model N5, destabi-

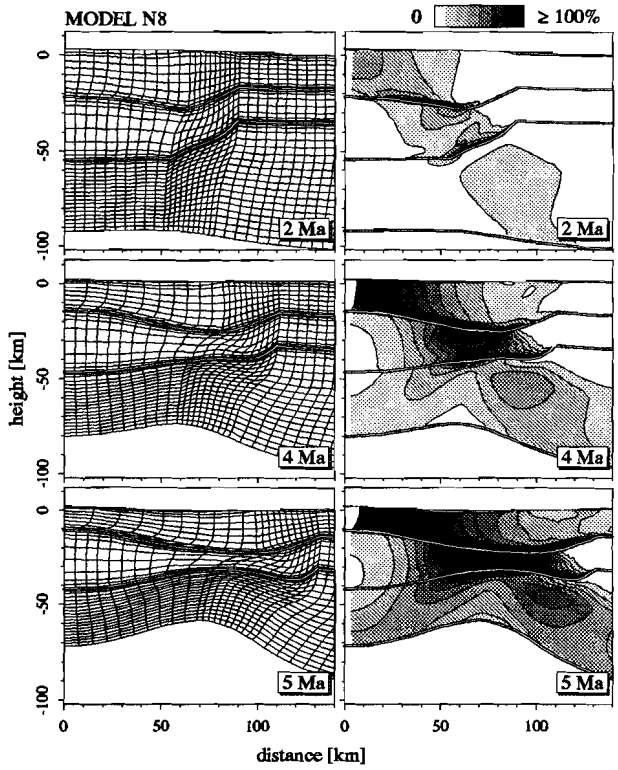

Fig. 39. *Evolution of 20 Ma thickening Model N8.*

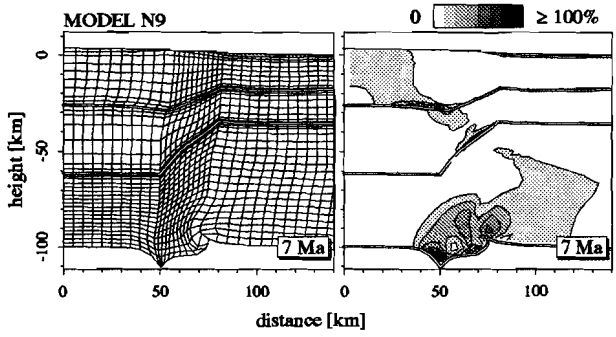

Fig. 40. *Grid and effective strain of uniform thickening Model N9 after 7 Ma.*

lization of the lower boundary forces us to stop the model.

Model N10 In our reference model, the width of the transition zone between the RCL and the TCL was 25 km. To investigate the influence of this assumption, we consider a model in which the transition zone width is 50 km.

The results of this model, Model N10, are displayed in Figure 41. Compared to Model N2, an interesting difference occurs in the timing of the onset of significant extension; as a result of the wider transition zone, horizontal temperature gradients are smaller. Heating of the TCL mantle directly beneath the Moho is therefore slower and onset of extension is delayed by 4 Ma. As a consequence of smaller lateral viscosity gradients, the style of mantle extension is more symmetric in Model N10 than in Model N2.

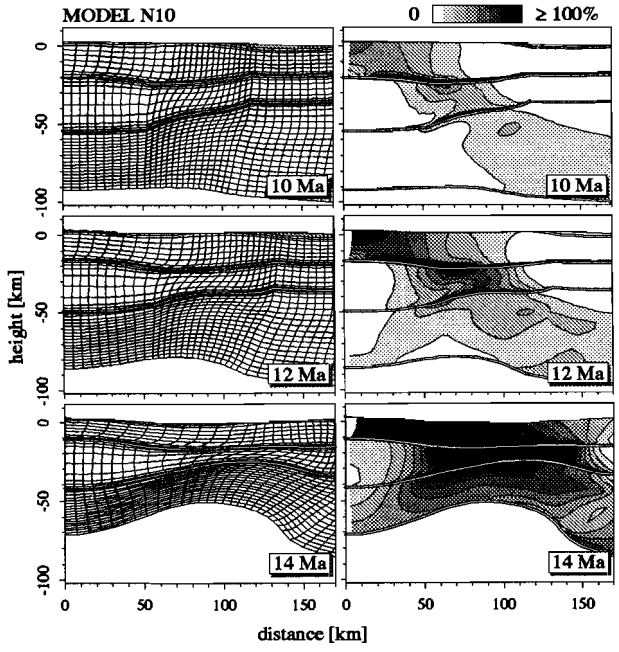

Fig. 41. *Evolution of wide transition zone Model N10.*

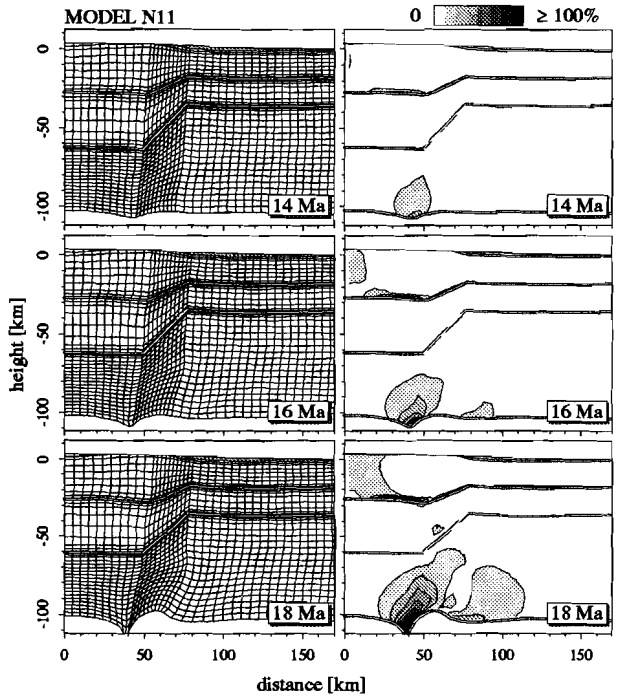

Fig. 42. *Evolution of gravity collapse Model N11.*

Variations in post-thickening parameters

Gravitational collapse

Model N11 In Model N11 we investigate the response of the model lithosphere to pre-stresses alone, i.e. the in-plane end load which thickened the lithosphere is removed at $t = 0$.

The model results (Figure 42) show that lithosphere hardly deforms until, after 18 Ma, a mantle drop has developed and the model is halted. Aided by a thermally induced decrease in viscosities, compressive pre-stresses in the TCL lower mantle squeeze out a droplet. In the first 18 Ma, near surface horizontal strain rates vary between 10^{-15} s^{-1} and 10^{-16} s^{-1}.

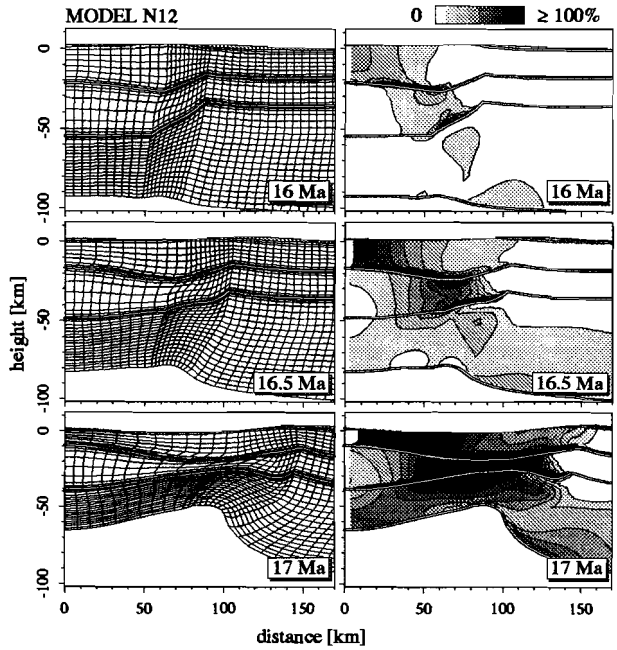

Fig. 43. *Evolution of delayed pull Model N12.*

Delayed in-plane end load

Model N12 In Model N12, the in-plane end load equivalent to 50 MPa, starts acting on the lithosphere model from 15 Ma onward.

Up to 15 Ma, the evolution of the model is identical to Model N11, i.e. a mantle drip has started to develop. Figure 43 displays the model evolution after application of the in-plane force. The rate of extension after 15 Ma is higher than in Model N2. Thermal reequilibration has heated the TCL at the onset of extension and the style of extension in the mantle is more symmetric than in model N2.

End load magnitude

Model N13 With the last model of this chapter, Model N13, we investigate the influence of the end load magnitude on the style of extension. The in-plane force is $10.5 \cdot 10^{12}$ N/m, which is equivalent to 100 MPa uniformly distributed over the lithospheric thickness.

The lithosphere extends more than twice as fast as Model N2 (Figure 44). Dextral strain in the upper crust, lower crust and mantle links up into a lithosphere scale fault dipping from the TCL under the RCL.

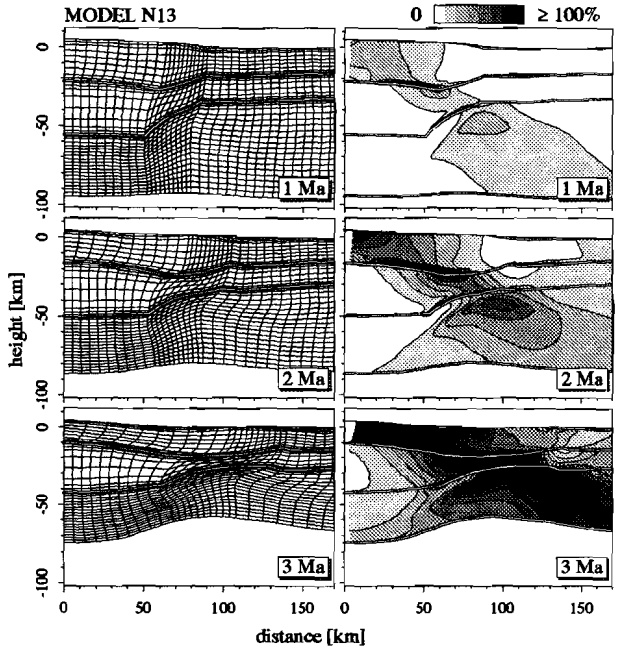

Fig. 44. *Evolution of Model N13, in which the in-plane end load is twice as large as in Model N2.*

CONCLUSIONS

In the first part of this chapter we consider models of thickened continental lithosphere in which pre-stresses are distributed uniformly with depth. The conceptual model of Figure 8 indicates the most important mechanisms controlling the style of extension in this case. Within the framework of uniform pre-stress models, a lithosphere scale "fault" dipping from the RCL under the TCL develops, provided that (1) the lower crust and mantle have weak rheologies, (2) the pre-thickening temperature field is not colder than a steady state geotherm with a surface heat flow of 60 mW/m^2, (3) mountain building results from thickening of the crust alone, (4) a tensile in-plane force starts acting on the thickened lithosphere shortly after thickening has ended. An increase in the duration of the thickening phase may affect the style of extension through the deformation in especially the upper crust, where development is promoted of sinistral faults which sole out onto the upper-lower crust interface. In this case, the overall style of extension remains asymmetric, but strain is no longer localized along a single dipping zone.

The results from the models with a depth-dependent pre-stress distribution are

remarkably different from the uniform pre-stress results. The extension rate is higher than in the uniform pre-stress models and the style of deformation is different. As a result of the moment which is exerted by a non-uniform thickening pre-stress, deformation is localized along a fault zone which dips from the TCL beneath the RCL. In most cases, this fault zone will not cut the whole lithosphere but will sole out into the upper or lower crust. Deformation in the mantle can be asymmetric with a shear zone dipping from the Moho of the transition zone under the TCL. A higher initial temperature gradient, an increase in the duration of the mountain building phase or a delay between the end of thickening and the moment when the in-plane force is applied, will result in more symmetric mantle thinning. A lithosphere cutting fault system is predicted to evolve only in the last model, Model N13.

A noteworthy feature of most of the non-uniform pre-stress models is that they predict a distinct jump in the locus of extension. In contrast, the uniform pre-stress models predict a smooth inward shift of the basin depocenter. In principle, sedimentary data could therefore be used to discriminate between uniform and non-uniform pre-stress models.

REFERENCES

Braun, J., and C. Beaumont, Dynamical models of the role of crustal shear zones in asymmetric continental extension, *Earth Planet. Sci. Lett., 93*, 405-423, 1989a.

Braun, J., and C. Beaumont, Contrasting styles of lithospheric extension: implications for differences between Basin and Range Province and rifted continental margins, in *Extensional tectonics and stratigraphy of the North Atlantic Margins*, edited by A.J. Tankard and H.R. Balkwill, pp. 53-79, Am. Ass. Petr. Geol. Mem. 46, 1989b.

Braun, J., and C. Beaumont, A physical explanation of the relation between flank uplifts and the breakup unconformity at rifted continental margins, *Geology, 17*, 760-764, 1989c.

Culling, W.E., Analytical theory of erosion, *J. Geology, 68*, 336-344, 1960.

Dunbar, J.A., and D.S. Sawyer, How preexisting weaknesses control the style of continental breakup, *J. Geophys. Res., 94*, 7,278-7,292, 1989.

England, P.C., and D.P. McKenzie, A thin viscous sheet model for continental deformation, *Geophys. J. R. astron. Soc., 70*, 295-321 B, 1982.

Fleitout, L., and C. Froidevaux, Tectonics and topography for a lithosphere containing density heterogeneities, *Tectonics, 1*, 21-56, 1982.

Flemings, P.B., and T.E. Jordan, A synthetic stratigraphic model of foreland basin development, *J. Geophys. Res., 94*, 3,851-3,866, 1989.

Houseman, G.A., and P.C. England, A dynamical model of lithosphere extension and sedimentary basin formation, *J. Geophys. Res., 91*, 719-729, 1986.

Jaoul, O., J. Tullis, and A. Kronenberg, The effect of varying water contents on the creep

behavior of Heavitree quartzite, *J. Geophys. Res., 89,* 4,298-4,312, 1984.
Kirby, S.H., Rheology of the lithosphere, *Rev. Geophys. Space Phys., 21,* 1458-1487, 1983.
Kusznir, N., and D.H. Mathews, Deep seismic reflections and the deformational mechanisms of the continental lithosphere, *J. Petrol., Special Lithosphere Issue,* 63-87, 1988.
Kusznir, N.J., and R.G. Park, The extensional strength of the continental lithosphere: its dependence on geothermal gradient, and crustal composition and thickness, in *Continental extensional tectonics, 28,* edited by M.P. Coward, J.F. Dewey and P.L. Hancock, pp. 35-52, Geological Society Special Publication, 1987.
Le Pichon, X., Land-locked oceanic basins and continental collision: the eastern Mediterranean as a case example, in *Mountain building processes,* edited by K. Hsü, pp. 201-211, Acad. Press, London, 1983.
Lister, G.S., and G.A. Davis, The origin of metamorphic core complexes and detachment faults formed during Tertiary continental extension in the northern Colorado River region, U.S.A., *J. Struct. Geol., 11,* 65-94, 1989.
Love, A.E.H., *Some problems of geodynamics,* Cambridge Univ. Press, London, 1911.
Paterson, M.S., and F.C. Luan, Quartzite rheology under geological conditions, in *Deformation Mechanisms, Rheology and Tectonics, 45,* edited by R.J. Knipe and E.H. Rutter, pp. 299-307, Geological Society of London Special Publication, London, 1990.
Rutter, E.H., and K.H. Brodie, The role of tectonic grain size reduction in the rheological stratification of the lithosphere, *Geol. Rund., 77,* 295-308, 1988.
Sonder, L.J., P.C. England, B.P. Wernicke, and R.L. Christiansen, A physical model for Cenozoic extension of western North America, in *Continental extensional tectonics, 28,* edited by M.P. Coward, J.F. Dewey and P.L. Hancock, pp. 187-201, Geological Society of London Special Publication, 1987.
Wernicke, B., Uniform-sense normal simple shear of the continental lithosphere, *Can. J. Earth Sci., 22,* 108-125, 1985.
Wilks, K.R., and N.L. Carter, Rheology of some continental lower crustal rocks, *Tectonophysics, 182,* 57-77, 1990.

Chapter 7

Conditions controlling the style of extension after mantle delamination

In chapter 5 of this thesis it was concluded that continental thickening, with or without delamination of the mantle of the thickened lithosphere, may lead to asymmetric extension on the scale of the lithosphere. In chapter 6 we discussed the conditions which affect the style of extension following continental thickening. Extension following continental thickening and mantle delamination will be the subject of the present chapter. In contrast to other possible causes for asymmetric extension which have been discussed in this thesis, delamination of continental mantle is a hypothetical mechanism. In this chapter, we will assume that delamination of continental mantle occurs to investigate its consequences on the style of extension.

INTRODUCTION

McKenzie (1978) proposed that (parts of) the lithospheric mantle may detach from continental lithosphere and sink into the less dense asthenosphere below. In McKenzie's view, the cold root of a thickened lithosphere was the most viable candidate for delamination. Based on numerical convection experiments, Houseman *et al.* (1981) found evidence in support of this hypothesis and, although no observations have unequivocally established that mantle delamination actually occurs, this mechanism has been put forward by various authors to explain observations of rapid uplift and rapid heating. For the Basin and Range Province, mantle delamination following thickening was put forward by Sonder *et al.* (1987) to explain the onset of extension after the Laramide orogeny. Surface observations in the Tibetan Plateau indicate that the upper crust is in a state of tension. England and Houseman (1989) note that their thin sheet models of the Tibetan Plateau fail to match this observation and conclude, therefore, that mantle delamination should have occurred. Obviously, by neglecting the possible depth-variation of thickening prestresses -which is implicit in their method since it treats the continental lithosphere by vertical averages-, England and Houseman (1989) disregard the consequence of their approach that it does not predict the evolution of the free surface. Instead, the results of a thin sheet model indicate how *some curved reference surface at depth*

evolves with time. The discrepancy between their previous model results and surface observations should, therefore, not be used as an argument for mantle delamination. The radial pattern of deformation and P-T-*t* data in the Betic Cordillera lead Platt and Vissers (1989) to hypothesize that mantle delamination has occurred beneath the Alboran Sea.

The proposed relation between delamination and the onset of asymmetric extension in the Basin and Range Province and the Alboran Sea, led us to investigate the style of extension after mantle delamination in chapter 5 of this thesis. It was concluded that lithosphere cutting faults may initiate if residual stresses from thickening are distributed uniformly with depth in the thickened continental lithosphere and if delamination occurs at the end of an orogenic period. In this chapter we present a systematic investigation of the conditions which control the onset of asymmetric extension after mantle delamination. The end of continental thickening can either signify that in-plane compressive forces are balanced by gravitational spreading forces or that a "drop" occurs in the magnitude of in-plane compressive forces. Since it was concluded in chapter 5 that delamination does not lead to asymmetric extension while a compressive in-plane load acts on the TCL, we focus on models in which delamination occurs at the end of the collision period. We investigate models in which the in-plane force drops to zero at the end of the thickening period ($t=0$), and models in which the in-plane force is tensile from $t=0$ onward.

An important previous study of the style of extension following mantle delamination was done by Braun and Beaumont (1989b). Their approach is, however, different from ours in that they consider the mechanical effects of mantle delamination only, i.e. they neglect the influence of replacement of the foundered and sunken mantle by hotter asthenospheric material. The models of Braun and Beaumont (1989b) evolve therefore very slowly, i.e. on timescales of 50 to 100 million years (Ma), whereas our models mostly evolve on timescales of a few Ma. The distribution of residual stresses in the models of Braun and Beaumont (1989b) is assumed to be uniform with depth. In fact, most dynamic models in the contemporary literature, in which the effects of continental thickening are investigated, invoke a uniform pre-stress assumption (e.g., England and McKenzie, 1982; Houseman and England, 1986; Sonder *et al.*, 1987; Braun and Beaumont, 1989b). Therefore, we consider it relevant to compare results obtained with a uniform pre-stress approach, with results from models in which the residual stresses from thickening are a function of depth.

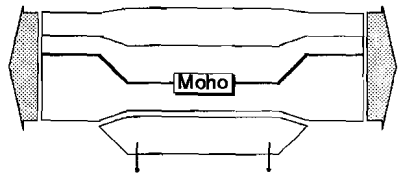

Fig. 1. *The model for mantle delamination which is adopted in this chapter. The mantle of the thickened lithosphere detaches instantaneously at the end of the collision phase. The delaminated mantle sinks intothe asthenosphere and is mechanically completely uncoupled from the lithosphere. Hot asthenosphere material replaces the detached mantle, thus exposing the lower lithosphere boundary to a temperature of 1350* °C.

UNIFORM PRE-STRESS MODELS

In the first part of this chapter we consider models of continental thickening followed by delamination, in which residual stresses from the thickening phase are uniformly distributed with depth. Initial conditions and boundary conditions (b.c.) are identical to the initial and boundary conditions in the models of chapter 6, except for the boundary conditions related to detachment. We do not specifically model the detachment process and we assume that a part of the TCL mantle detaches from the overlying lithosphere (Figure 1). In our models, delamination removes that part of the TCL mantle which was depressed below the depth of the lower boundary of the reference continental lithosphere (RCL). It is assumed that, mechanically, the detached mantle is instantaneously and completely uncoupled from the TCL. The magnitude of isostatic rebound forces which result from delamination depend on the initial geothermal gradient, through the temperature dependence of the density. Flow of asthenospheric material immediately replaces the foundered lithospheric mantle. Thus, the lower boundary is instantaneously exposed to asthenospheric mantle temperatures. For reasons of consistency, a temperature b.c. is applied to the complete lower boundary of the model; beneath the TCL the temperature is 1350 °C, beneath the RCL the lower boundary temperature is 1148 °C in the models with an initial surface heat flow of 60 mW/m^2. We assume a linear variation of the temperature at the lower boundary of the transition zone.

Uniform pre-stress Model Ud1

Model Ud1 Parameter settings in Model Ud1 are identical to Model U1 of chapter 6 (Model 6.U1[1]). We refer to tables 6.1 and 6.2 for the relevant parameter values. Model Ud1 is identical to Model 5.8, with the exception of the effects due

Table 1. Uniform pre-stress models which are discussed in this chapter.

Ud1	Rheology: low-viscosity upper crust, lower crust and mantle. Geothermal gradient: $q_0 = 60$ mW/m^2. Thickening: instantaneous at $t=0$, $\beta_c^{-1}=2$, $\beta_m^{-1}=1$. Transition zone width 25 km. Delamination: instantaneous at $t=0$. Inplane tensile force: applied immediately after thickening, equivalent to a uniform 50 MPa inplane stress. Subsequent models are identical to this model, except for the indicated deviation.
Ud2	Strong upper crust model.
Ud3	Viscous lower crust model.
Ud4	Strong mantle model.
Ud5	Cold initial geotherm model.
Ud6	Hot initial geotherm model.
Ud7	Duration of thickening period 5 Ma.
Ud8	Duration of thickening period 20 Ma.
Ud9	Uniform thickening model.
Ud10	Wide transition zone model.
Ud11a	Gravity collapse model with pre-thickening steady state geotherm with surface heat flow of 60 mW/m^2.
Ud11b	Gravity collapse model with pre-thickening steady state geotherm with surface heat flow of 50 mW/m^2.
Ud11c	Gravity collapse model with pre-thickening steady state geotherm with surface heat flow of 70 mW/m^2.
U12	Twice inplane force magnitude.

erosion and sedimentation, which are included in Model Ud1.

The geometry and thermal structure of Model Ud1 -and of all other models we consider in this chapter- is the result of a four-stage evolution; (1) a pre-thickening period, (2) a syn-thickening period, (3) a delamination period and (4) a post-thickening/post-delamination period. Before thickening, the composition of the crust and mantle is defined. The initial geothermal gradient is in steady state everywhere in the model. Before thickening, therefore, the complete model is a RCL. In the thickening period, a 100 km wide mountain belt is built by instantaneous and uniform thickening of the crust near the symmetry center. The width of the transition zone between TCL and RCL is 25 km. The RCL (initially) is unaffected by the thickening event. In the third phase, partial delamination of the TCL mantle occurs instantaneously. At $t=0$, i.e. after delamination has occurred, the compressive inplane load which acted on the model lithosphere during the thickening and delami-

1. In this chapter, figures, tables and model names from other chapters will be referred to as "ChapterNo.FigureNo", "ChapterNo.TableNo" and "ChapterNo.ModelNo" respectively. For example, Figure 3.2 is Figure 2 from chapter 3 of this thesis.

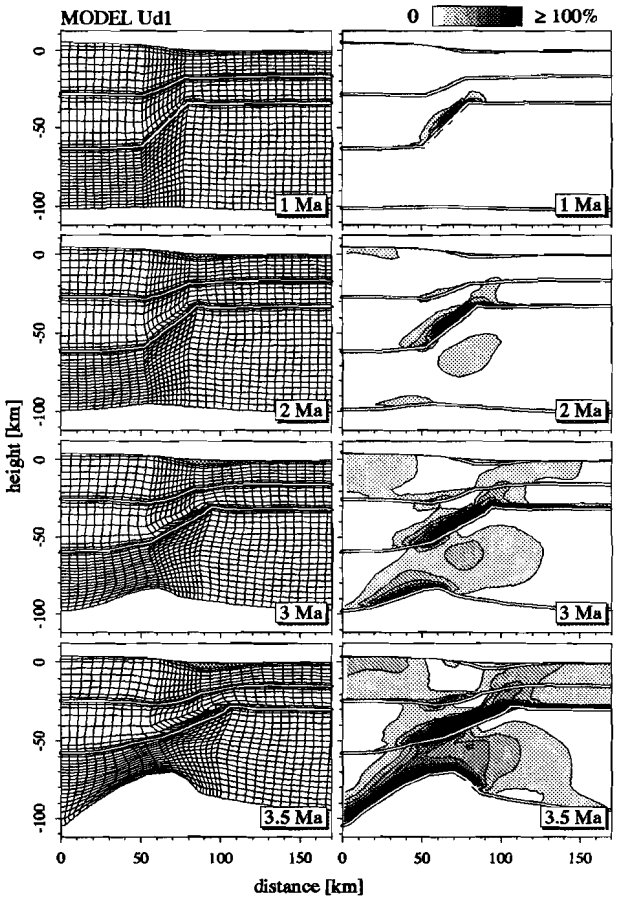

Fig. 2. *Evolution of Model Ud1. In this model, pre-stresses are uniformly distributed with depth. The left column shows the finite element grid, the right column contours of effective strain.*

nation phases, either drops to zero or becomes tensile.

Figure 2 shows the evolution of the model lithosphere and contours of effective strain (see definition in chapter 5 of this thesis). Compared to Model 5.8, Model Ud1 evolves slower. The clockwise moment, which is exerted on Model Ud1 as a result of erosion and sedimentation, decreases the rate of extension but does not completely hinder extension along the zone dipping from the RCL underneath the TCL. Eventually, after 3.5 Ma, a lithosphere cutting fault has developed. The results from Model Ud1 therefore support the conclusion from Model 5.8 that extension after mantle delamination may lead to the development of lithosphere cutting faults and asymmetric extension.

The thermal effects of delamination are apparent from Figure 3, which displays

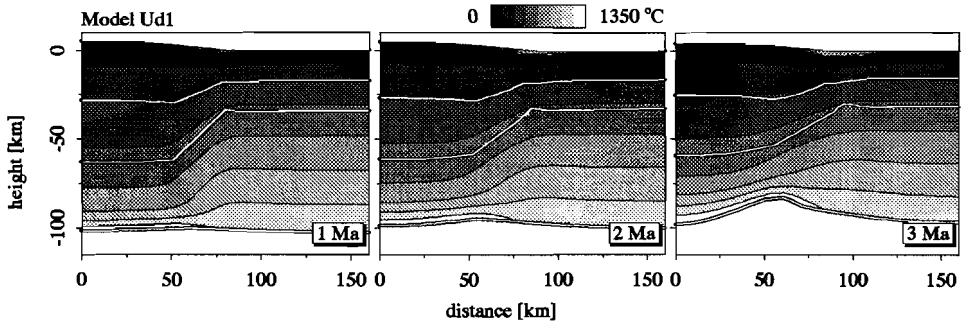

Fig. 3. *Temperatures of Model Ud1. Delamination clearly has a strong heating effect on the lower TCL boundary.*

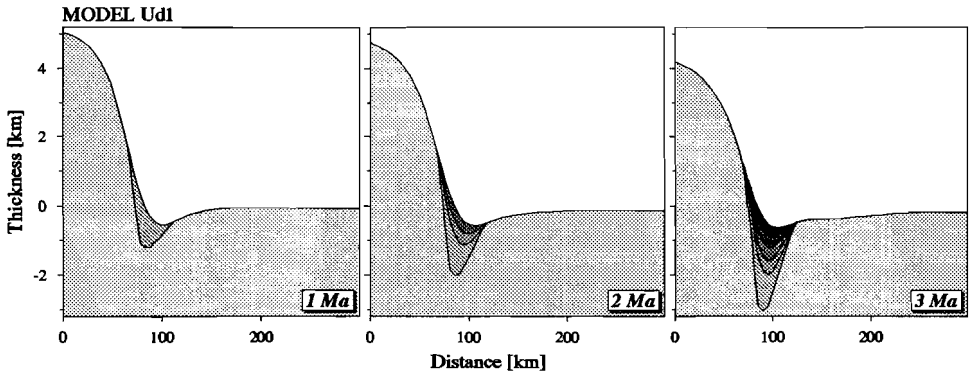

Fig. 4. *Net surface topography and sediment thicknesses of material eroded between 0 and 1 Ma, between 1 and 1.5 Ma, between 1.5 and 2 Ma, between 2 and 2.5 Ma and between 2.5 and 3 Ma.*

the temperature field at subsequent times. Figure 4 shows the evolution of the erosion surface and sedimentation. A comparison with the sedimentation pattern of the same model without delamination (Model 6.U1 and Figure 6.6) shows that the large-scale sedimentation pattern is hardly affected by mantle delamination. Compared to Model 6.U1, the net surface topography[2] at the model symmetry center is slightly larger in Model Ud1, as a result of the isostatic response to delamination. In the first Ma, the net surface uplift rate of the symmetry center of Model Ud1 is 0.9 mm/yr (Figure 5). The mechanisms which are responsible for the initiation of a

2. Net surface topography: tectonic surface topography minus the thickness of material that has been eroded off

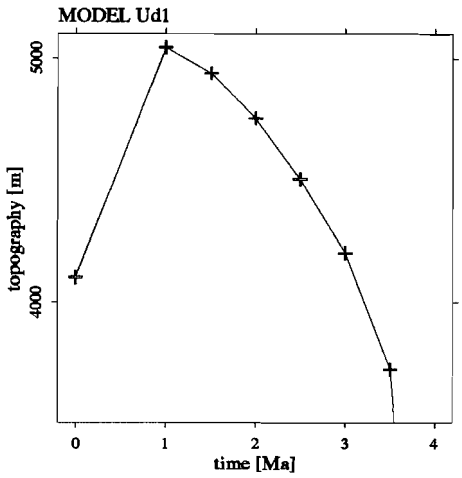

Fig. 5. *Net surface topography of the symmetry center as a function of time. The initial uplift rate resulting from isostatic rebound and flexural unloading due to sediment transport is 0.9 mm/yr.*

lithosphere scale fault are basically identical to the mechanisms driving asymmetric extension in Model 6.U1. Dextral shear deformation in the lower crust, resulting from the tendency of the strong sub-Moho mantle to straighten out, links up with dextral shear deformation in the mantle of the TCL which is caused by preferential thinning of this part of the mantle. A more elaborate discussion of the mechanisms underlying initiation of asymmetric extension is given in chapter 6.

Model Ud1 serves as a reference for models we consider in the following sub-parts. The models we consider below are, therefore, identical to Model Ud1, with the exception of one single parameter. The parameters in which these models are different are classified into sub-parts according to the evolutionary period they apply to. Table 1 lists the various models and the parameter in which they are different from the reference model.

Variations in pre-thickening parameters

Composition

Model Ud2 The upper crustal rheology we employ in Model Ud1 is at the low-viscosity end of the range of upper crustal powerlaw creep rheologies available from the contemporary literature (c.f. Figure 6.9). Model Ud2 is identical to Model Ud1, except for the upper crustal rheology, which is more viscous in Model Ud2 (dry quartzite, $Q_{pl} = 184.1$ kJ/mole, $A_{pl} = 2.20 \cdot 10^{-22}$ Pa$^{-2.8} \cdot s^{-1}$, $n_{pl} = 2.8$) (Jaoul *et al.*, 1984).

Compared to Model Ud1, Model Ud2 deforms slightly slower (Figure 6). The

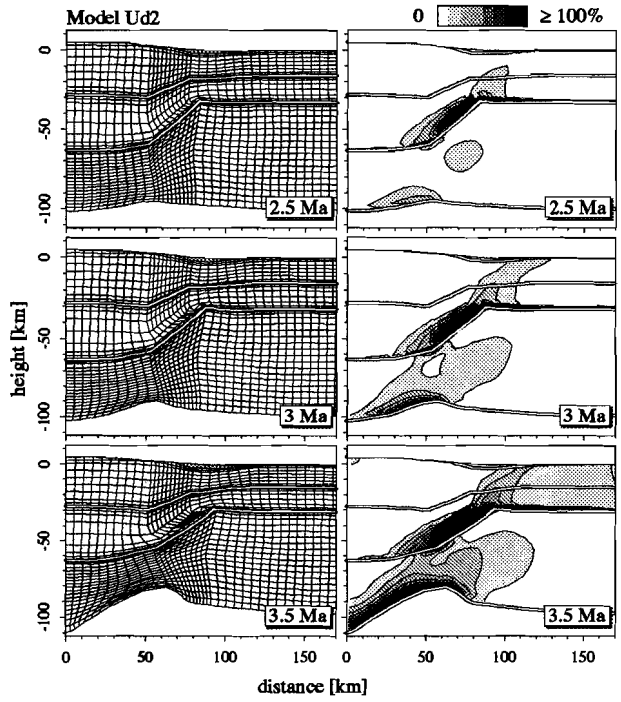

Fig. 6. *Evolution of Model Ud2. Compared to Model Ud1, Model Ud2 has a more viscous upper crustal rheology. The left column shows the finite element grid, the right column contours of effective strain.*

upper crust of the TCL is clearly less strained than in Model Ud1, but the overall style of deformation is hardly different. We conclude that the style of extension is insensitive to the upper crustal rheology, in agreement with the conclusion from Model 6.U2.

Model Ud3 The viscosity of the lower crust of Model Ud1 is at the low end of values reported in the literature (Figure 6.9). The next model, Model Ud3, differs from Model Ud1 in that the viscosity of the lower crust is higher. Lower crustal rocks are assumed to have a Pikwitonei granulite rheology ($Q_{pl}=445$ kJ/mole, $A_{pl}=7.68\cdot 10^{-21}$ $Pa^{-4.2}\cdot s^{-1}$, $n_{pl}=4.2$) (Wilks and Carter, 1990).

Figure 7 shows the evolution of Model Ud3. The strong lower crust inhibits shear deformation in the transition zone and extension of the TCL. Heating and thermal expansion generate buoyancy forces in the TCL mantle which initiate an "asthenospheric diapir". Mass is transported towards the model symmetry center and towards the relatively cool and viscous RCL. As a result, mantle "drips" are

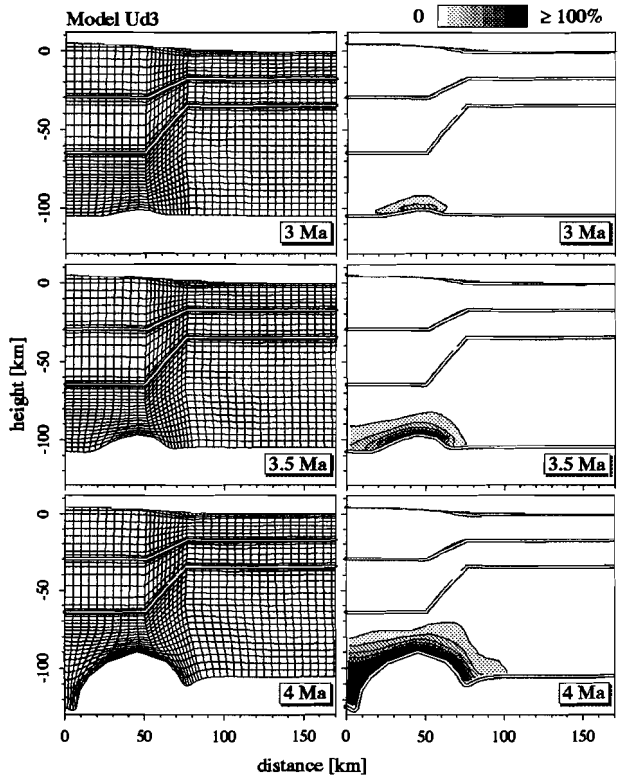

Fig. 7. *Evolution of Model Ud3. The lower crust is more viscous compared to Model Ud1. The deformed finite element grid is displayed in the left column, the right column shows contours of effective strain.*

created which, eventually, will detach and sink into the asthenosphere. Processes near the lithosphere-asthenosphere boundary control the evolution of the lithosphere when the lower crust is very viscous.

The results of Model Ud3 give insight in the evolution of mantle delamination itself. In our model, the thickness of the foundered TCL mantle is selected on an rather arbitrary basis. This approach is motivated by the inability of the finite element method we employ to deal with fluid-like processes. The results of Model Ud3 indicate that, in fact, the delamination process still goes on through shedding of mantle droplets. Possibly, the complete delamination process occurs by peeling off mantle drips. In this case, a rhythmic surface uplift signal would be observed. Once initiated, delamination will continue until the complete TCL mantle has been removed, unless asthenospheric temperatures decrease as a result of cooling by the

sinking mantle blobs. As such, the mantle delamination process is critically dependent on the thermal boundary condition imposed by the asthenosphere. Model Ud3 therefore might represent a transient stage in the delamination process. In this transient stage, extension is insignificant and processes near the lower TCL boundary control the evolution of the lithosphere system.

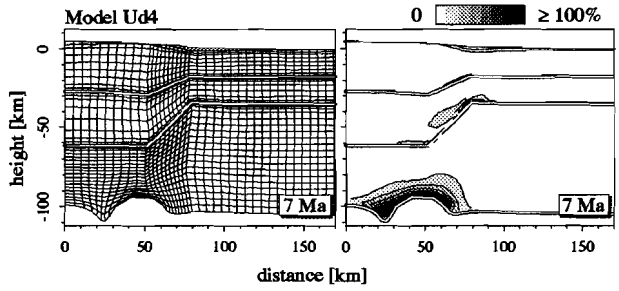

Fig. 8. *Model Ud4: deformed model lithosphere and effective strain after 7 Ma. Compared to Model Ud1, the mantle in this model is more viscous.*

Model Ud4 In Model Ud4, the low viscosity end-member mantle rheology of Model Ud1 is replaced by the high viscosity end-member (Figure 6.9). Again, all parameters are identical to Model Ud1, except that a dry olivine flow law is adopted in the mantle ($Q_{pl}=510$ kJ/mole, $A_{pl}=7\cdot10^{-14}$ $Pa^{-3}\cdot s^{-1}$, $n_{pl}=3$) (Kirby, 1983).

Figure 8 shows the deformed grid and strains after 7 Ma, when the lower TCL mantle has started destabilizing. Like in Model Ud3, the relative significance of extensional strain is limited compared by the strain related to the formation of a mantle drip. Model Ud4 therefore represents a transient stage in an ongoing delamination process.

Geotherm

Model Ud5 In Model Ud1 the geothermal gradient before thickening is a steady state geotherm with a surface heat flow of 60 mW/m^2. To investigate the influence on the style of extension of the initial temperature field, Model Ud5 initially has a steady state geotherm with a surface heat flow of 50 mW/m^2. The mechanical thickness of the lithosphere increases with a decrease in the geothermal gradient and, therefore, the thickness of the RCL of Model Ud5 (130 km) is larger than the RCL thickness of Model Ud1 (105 km). The in-plane force is, like in Model Ud1, equivalent to a 50 MPa stress which is uniformly distributed over the lithospheric thickness. Because the lithospheric thickness of Model Ud5 is larger than Model Ud1, the in-plane tensile force magnitude is larger; $6.5\cdot10^{12}$ N/m.

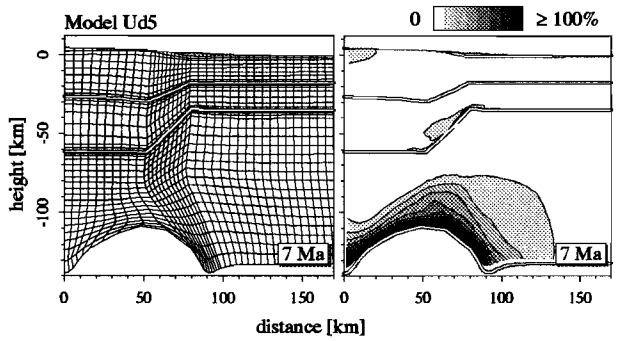

Fig. 9. *Model Ud5: the initial surface heat flow in this model is 50* $\mathrm{mW/m^2}$. *Shown are the deformed finite element grid and contours of effective strain after 7 Ma.*

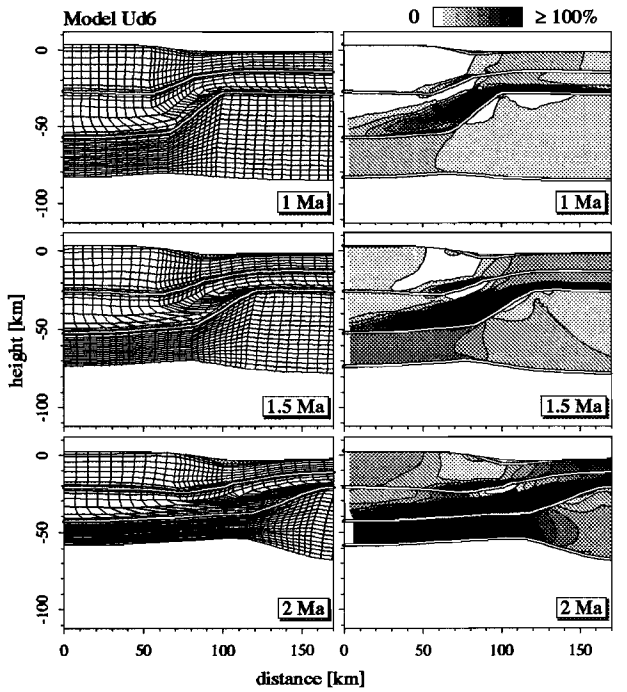

Fig. 10. *Evolution of Model Ud6. Compared to Model Ud1, Model Ud6 has a higher initial temperature gradient. The left column shows the finite element grid, the right column contours of effective strain.*

Figure 9 shows the finite element grid and contours of effective strain, 7 Ma after thickening has ended. The cold lithosphere model is more viscous than Model Ud1 and the significance of extension relative to delamination processes is therefore limited compared to Model Ud1. A mantle drip has formed near the model symmetry center and the transition zone. The location of the droplet which forms below the transition zone is determined by the initial geometry of the detachment and the resulting temperature b.c. at the lower model boundary.

Model Ud6 The next model we consider, Model Ud6, has an initial steady state geothermal gradient which is higher than in Model Ud1; the surface heat flow before thickening is 70 mW/m^2. The initial thickness of the lithosphere model is 100 km. The magnitude of the end load is equivalent to an in-plane tensile stress of 50 MPa which is uniformly distributed over the lithospheric thickness. As a result, the effective magnitude of the end load is 5% lower than in Model Ud1.

Figure 10 shows that the lithosphere model extends more rapidly than Model Ud1. Sinistral shear deformation in the lower crust of the transition zone links pure shear deformation in the TCL mantle with pure shear extension in the RCL crust. The width of the lower crustal layer where shear strain is accommodated is larger than the width of the lower crustal shear zone in Model Ud1. The style of deformation is asymmetric with a fault zone which is wider than in Model Ud1. The relative importance of delamination processes (c.f. Model Ud5) is limited in this model for two reasons; (1) the lithosphere extends more rapidly due to the thermally induced reduction in viscosities, (2) heating of the TCL mantle is slower than in colder models, since the mantle is already relatively hot.

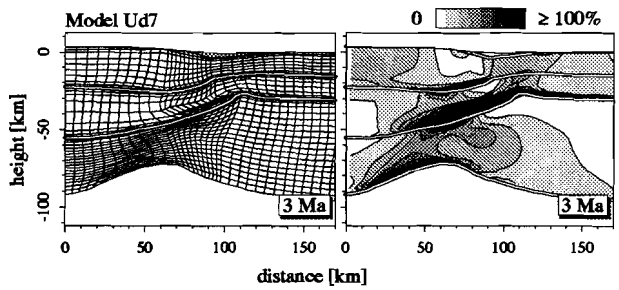

Fig. 11. *Lithosphere model and contours of effective strain after 3 Ma in Model Ud7. In Model Ud7, the duration of the thickening period is 5 Ma.*

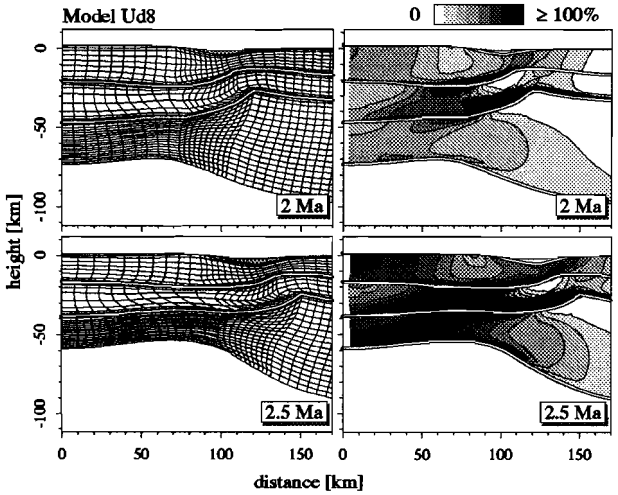

Fig. 12. *Evolution and contours of effective strain of Model Ud8. The duration of the thickening period is 20 Ma in this model.*

Variations in syn-thickening parameters

Finite thickening period

Model Ud7 In Model Ud1 we assumed that thickening of the crust occurs instantaneously, or at least very fast compared to the time required for diffusive heat transport over significant distances. For instance, the characteristic time required for thermal diffusion over a distance of 1 km is $42 \cdot 10^3$ yr (Turcotte and Schubert, 1982). Simultaneously, we assume that complete isostatic compensation of the thickened lithosphere has occurred on this short timescale. These assumptions are rather unrealistic, which is a good motivation for investigating the sensitivity of the results from Model Ud1 to the duration of the thickening period. In Model Ud7, the phase of thickening lasts 5 Ma, equivalent to an average relative horizontal velocity of 2 cm/yr in our model. At $t = 0$ the lower part of the TCL mantle detaches and the in-plane tensile force starts acting on the system.

Figure 11 shows the finite element grid and contours of effective strain after 3 Ma. Heating during thickening decreases the viscosities of the TCL, resulting in an increase in the extension rate compared to Model Ud1. More deformation occurs outside the dipping fault zone in Model Ud7, but the overall style of extension is very similar. Therefore, the style of extension is not very sensitive to the duration of the thickening period. This result is in accordance with findings from the post-

collisional extension models 6.U7 and 6.U8.

Model Ud8 With the next model, Model Ud8, we intend to investigate the evolution of continental lithosphere in which thickening results from a number of orogenic pulses during a period of 20 Ma. The initial thermal field of this model was calculated by solving the heat equation on a grid which advects with constant nodal velocities. The TCL of Model Ud8 has heated considerably (Figure 6.19) since the onset of thickening.

After 2 Ma, both the upper crust and the lower crust in the transition zone have accommodated sinistral shear (Figure 12). Therefore, instead of a single lithosphere cutting fault, two faults evolve; (1) a sinistral normal fault which soles out on the upper-lower crust interface or soles out into the lower crust and (2) a distinct lower crustal shear zone which links up with the TCL mantle. Compared with the post-thickening extension model 6.N8, the style of deformation is very similar. The main difference between these models is the rate of extension, which is higher after delamination. The overall style of extension in Model Ud8 is asymmetric, although the asymmetry is less pronounced than in Model Ud1. We conclude, therefore, that the duration of the thickening phase slightly reduces the tendency to asymmetric extension. This result confirms the findings from the uniform pre-stress models in chapter 6.

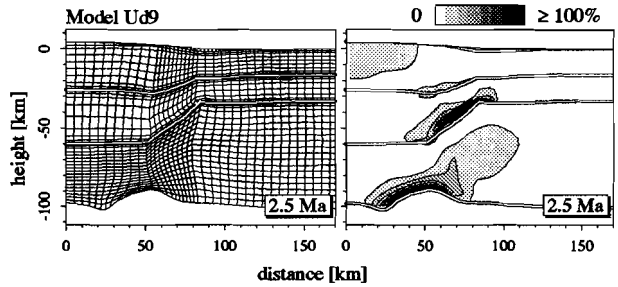

Fig. 13. *Uniform thickening model, Model Ud9. Deformed grid and effective strain after 2.5 Ma.*

Thickening geometry

Model Ud9 In Model Ud1 it is assumed that continental thickening results from thickening of the crust alone. With Model Ud9 we investigate the sensitivity of the style of extension to the thickening distribution by assuming uniform thickening, i.e. $\beta_c^{-1} = \beta_m^{-1} = 2$.

In the first Ma, the net surface uplift rate is more than 1.5 mm/yr. The thickness of the delaminated mantle is larger than in Model Ud1 and, therefore, the isostatic

restoring forces are larger. After 2.5 Ma, the model lower boundary starts destabilizing (Figure 13). This difference in style of deformation between Model Ud1 and Model Ud9 results from the much cooler initial thermal structure of Model Ud9; asthenospheric heating is more rapid in a cool mantle and extension of the more viscous TCL is slower. The relative amount of extensional strain is therefore limited at the onset of the mantle drip.

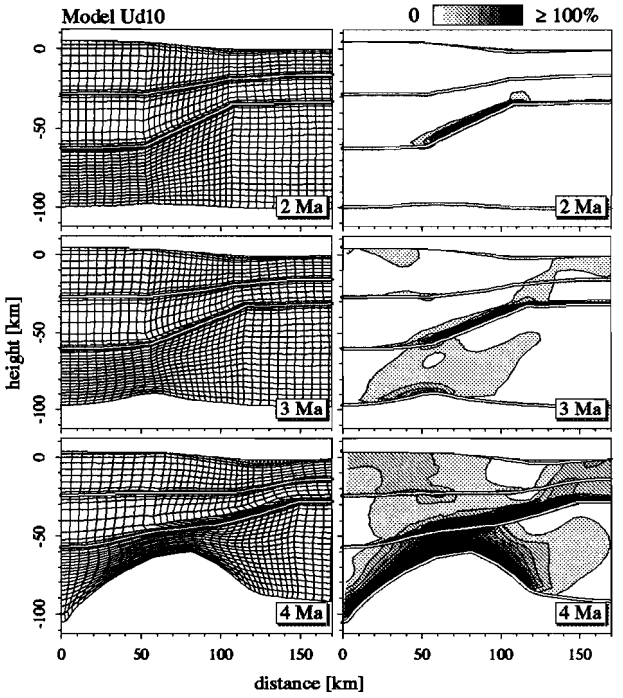

Fig. 14. *Evolution and contours of effective strain of Model Ud10. The width of the transition zone is 50 km in this model.*

Model Ud10 The sensitivity of the results of Model Ud1 to the width of the transition zone is tested in Model Ud10, which has a transition zone width of 50 km.

Compared to Model Ud1, Model Ud10 evolves slightly slower (Figure 14). Sinistral shear in the lower crust of the transition zone links up with deformation zones in the upper crust of the RCL and the mantle of the TCL. As a result of the wider transition zone, loci of upper crustal and mantle deformation are offset further, and the lithosphere scale style of deformation is more pronounced asymmetric than in Model Ud1. After 4 Ma, a mantle drip has evolved near the model symmetry center, but the relative importance of extensional strain in this stage is greater

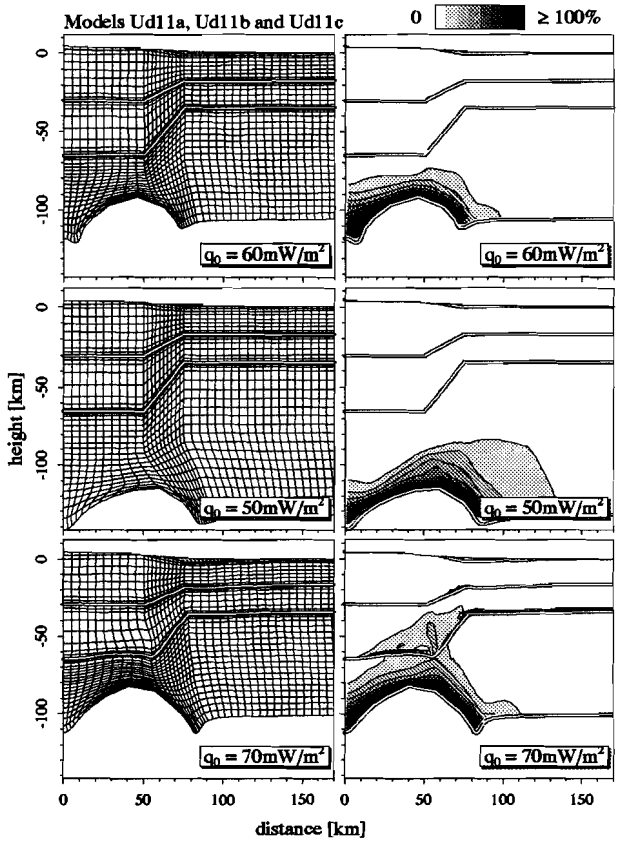

Fig. 15. *Finite element grid and effective strain (top row) Model Ud11a after 4 Ma: initial surface heat flow 60* mW/m^2*, (middle row) Model Ud11b after 4 Ma: initial surface heat flow 50* mW/m^2 *and (bottom row) Model Ud11c after 5 Ma: initial surface heat flow 70* mW/m^2.

than the strain associated with the drop.

Variations in post-delamination parameters

Gravitational collapse

Models Ud11 It was concluded in chapter 5 of this thesis that lithosphere scale asymmetric extension will occur if delamination occurs simultaneously with a switch in the in-plane force from compressive to tensile. Delamination during the compression phase was concluded to destabilize the lower boundary and would not

lead to significant extension. In this section we investigate whether significant extension will result from delamination during a drop in the in-plane force magnitude to zero. The initial surface heat flow of Models Ud11a, Ud11b and Ud11c respectively is 60 mW/m^2, 50 mW/m^2 and 70 mW/m^2. With these models, we intend to investigate gravitational collapse after thickening and delamination of average, cold and hot continental lithosphere.

Figure 15 shows the deformed lithosphere and strain in Model Ud11a, 4 Ma after delamination (top row), Model Ud11b after 4 Ma (middle row) and in Model Ud11c after 5 Ma (bottom row). It is clear that the initial geothermal gradient is insignificant for the resulting deformation style. In all three models, a lithospheric drip evolves near the model symmetry center and in the transition zone. Partial delamination and subsequent gravity collapse leads to continued delamination without producing significant amounts of extensional strain. Figure 16 shows the net surface topography of the model symmetry center for the three gravitational collapse models. The dependence of the flexural strength of the lithosphere on the geothermal gradient is reflected in the magnitude of the uplift. The temporal evolution of the three models is similar; the free surface of the symmetry center is initially uplifted resulting from isostatic restoring forces, followed by rapid subsidence associated with the onset of mantle drips. The timing of onset of the mantle drips is a function of the initial geotherm; the process of heating and subsequent destabilization occurs more rapidly in a cold than in a hot mantle.

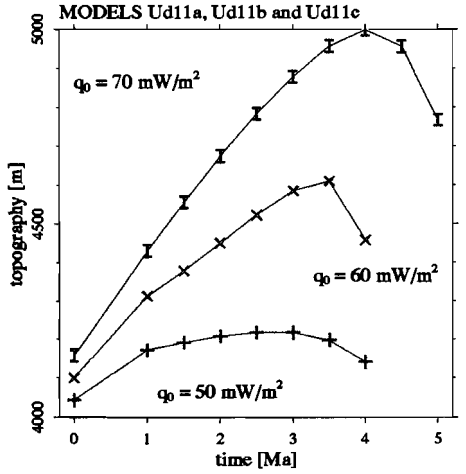

Fig. 16. *Net surface topography of model symmetry center of gravitational collapse models Ud11a, Ud11b and Ud11c.*

Sonder *et al.* (1987) consider gravitational collapse models of continental thick-

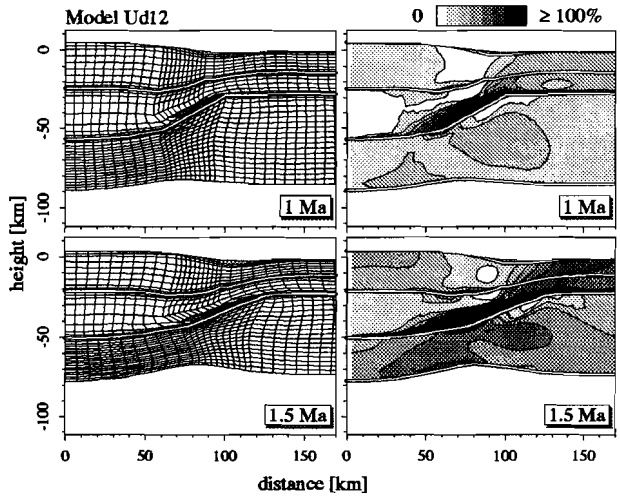

Fig. 17. *Deformed lithosphere model and contours of effective strain of Model Ud12. In this model, the in-plane end load is equivalent to a stress of 100 MPa which is uniformly distributed over the thickness of the lithosphere.*

ening followed by delamination. In their opinion, it ".. is a reasonable first approach .." to ".. neglect the .." ".. effects of lateral variations in strain and consider the thermal and mechanical evolution of a single column of lithosphere ..". The one-dimensional models are integrated in their method, and they consider vertical averages of stress, rheology and strain in continental lithosphere which has been uniformly thickened. The rheology in their models is more viscous than the rheologies we employ and thickening pre-stresses are uniformly applied. From their models, Sonder *et al.* (1987) conclude that delays up to 100 Ma between (instantaneous) delamination and the onset of gravitational spreading may occur. The results from our modeling indicate that lateral variations do have a pronounced effect on the evolution of the lithosphere. Ongoing delamination processes and shedding of mantle drips are a likely consequence of our (and their) initial delamination model. Also, their models predict that surface elevations on the order of 4 km, are maintained during periods of 50 Ma. Erosion and sedimentation probably are very effective on these timescales and at these elevations (c.f. England and Molnar, 1990). Sonder *et al.* (1987) do, however, not consider the effects of sediment transport.

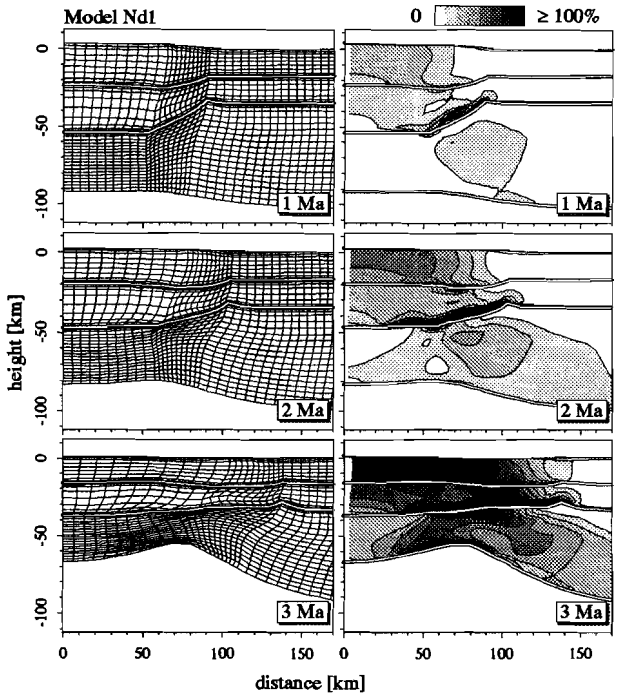

Fig. 18. *Evolution of depth-dependent pre-stress Model Nd1. The left column shows the finite element grid, the right column contours of effective strain.*

In-plane force magnitude

Model Ud12 In Model Ud12, the magnitude of the end load which starts acting on the RCL/TCL system is twice as large as in Model Ud1. The in-plane force is therefore equivalent to an in-plane stress of 100 MPa which is uniformly distributed over the thickness of the lithosphere. In chapter 2 of this thesis it is shown that average in-plane stresses with magnitudes of hundreds of MPa's are consistent with seismicity data in the Central Indian Ocean.

The extension rate of Model Ud12 is significantly larger than the rate of extension of Model Ud1 (Figure 17). Sinistral shear zones in the upper crust and mantle derive from the lower crust and a lithosphere-cutting fault develops. Because less time is available for heating in Model Ud12, deformation in the mantle is more homogeneous compared to Model Ud1. An increase in the in-plane force magnitude results in a slight decrease in the asymmetry of the system as a whole.

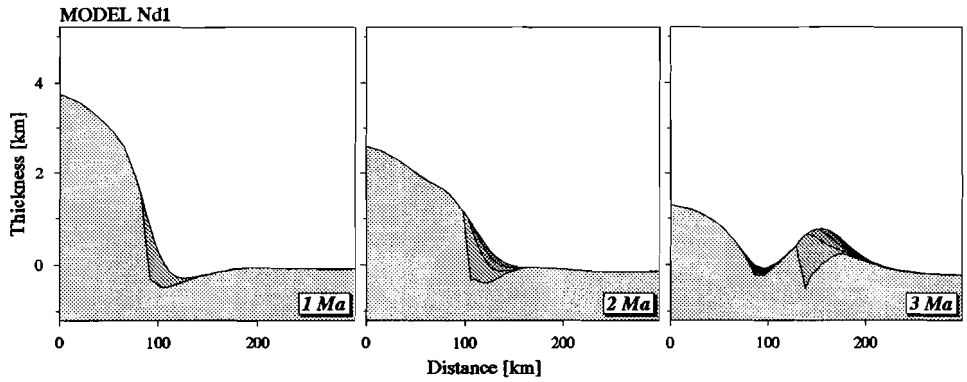

Fig. 19. *Net surface topography and sediment thicknesses of material eroded between 0 and 1 Ma, between 1 and 1.5 Ma, between 1.5 and 2 Ma, between 2 and 2.5 Ma and between 2.5 and 3 Ma.*

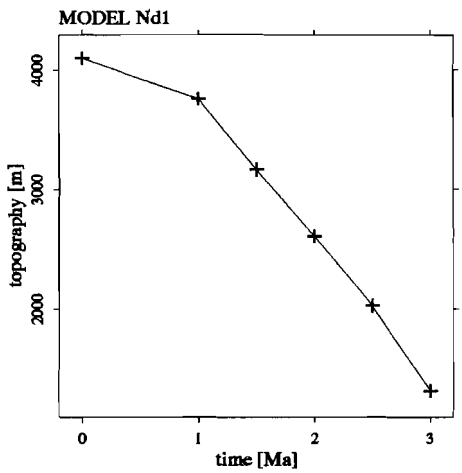

Fig. 20. *Net surface topography of the symmetry center of Model Nd1 as function of time.*

NON-UNIFORM PRE-STRESS MODELS

It was concluded in chapters 5 and 6 of this thesis that the distribution of pre-stresses in the thickened lithosphere plays a crucial role in determining the style of extension after collision. In the second part of this chapter we therefore investigate the influence of assuming a depth-dependent pre-stress distribution on the style of extension following thickening and delamination.

Table 2. Non-uniform pre-stress models which are discussed in this chapter.

Nd1	Identical to model U1, except for initial stress distribution. This model serves as a reference for subsequent models. The aspect in which the models below deviate from Model Nd1 is indicated.
Nd2	Strong upper crust model.
Nd3	Viscous lower crust model.
Nd4	Strong mantle model.
Nd5	Cold initial geotherm model.
Nd6	Hot initial geotherm model.
Nd7	Duration of thickening period 5 Ma.
Nd8	Duration of thickening period 20 Ma.
Nd9	Uniform thickening model.
Nd10	Wide transition zone model.
Nd11a	Gravity collapse model with pre-thickening steady state geotherm with surface heat flow of 60 mW/m^2.
Nd11b	Gravity collapse model with pre-thickening steady state geotherm with surface heat flow of 50 mW/m^2.
Nd11c	Gravity collapse model with pre-thickening steady state geotherm with surface heat flow of 70 mW/m^2.
N12	Twice inplane force magnitude.

Model Nd1

Model Nd1 Model Nd1 is identical to Model Ud1, with the exception of the pre-stress distribution (see tables 6.1 and 6.2 for parameter values).

Figure 18 shows the evolution of the lithosphere model and contours of effective strain. From a comparison of the results with the results of Model Ud1 it is clear that the influence of the pre-stress distribution on the style of extension is large. The clockwise moment which is exerted by the depth-dependent pre-stresses is expressed in the style of extension (Figure 6.29). In the upper crust of the TCL, dextral shear will be accommodated along brittle faults with a normal vertical component. Both dextral and sinistral shear deformation occur in the lower crust of the TCL and transition zone, and the resulting style of deformation is more symmetric. Likewise, in the mantle, no predominant asymmetry evolves. In contrast with the result of the uniform pre-stress model Ud1, in which a lithosphere cutting fault evolved, asymmetric extension in Model Nd1 is confined to the upper crust and rather symmetric below. The uniform pre-stress model deforms slower because more stress is applied to the strong upper mantle and less to the (weaker) crust (Figure 6.2). Onset of thinning in the TCL mantle is associated with subsidence of the TCL surface and a jump in the depocenter towards the mantle symmetry center (Figure 19). In chapter 6, this depocenter jump was concluded to be a characteristic feature of depth-dependent pre-stress models and possibly a diagnostic tool for

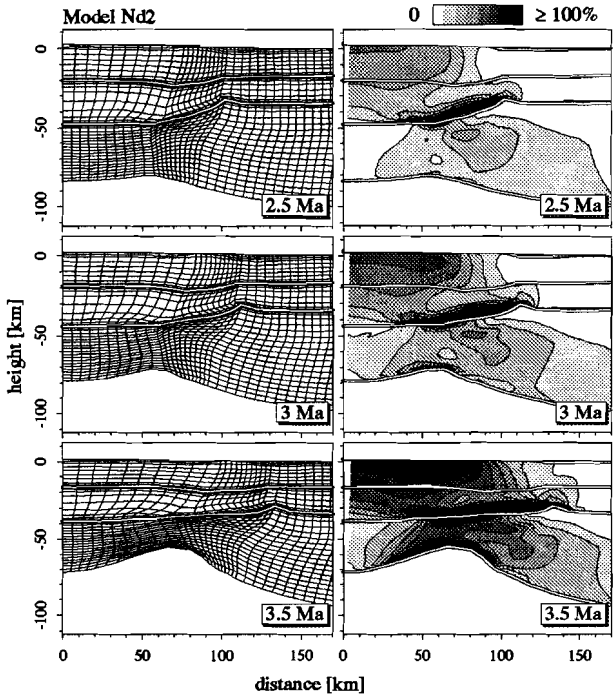

Fig. 21. *Deformed finite element grid and contours of effective strain of Model Nd2. The viscosity of the upper crust of this model is high compared to the upper crustal viscosity of Model Nd1.*

determining the thickening pre-stress distribution in extending mountain belts. Immediately after delamination, the net surface uplift rate of the symmetry center of Model Ud1 was found to be 0.9 mm/yr (Figure 9). Figure 20 shows that the symmetry center of Model Nd1 is not uplifted as a result of isostatic rebound forces associated with delamination. Instead, subsidence due to crustal thinning commences immediately after delamination has occurred.

Model Nd1 will serve as a reference for the models we consider next. The models below are identical to Model Nd1, except for one parameter (c.f. table 1).

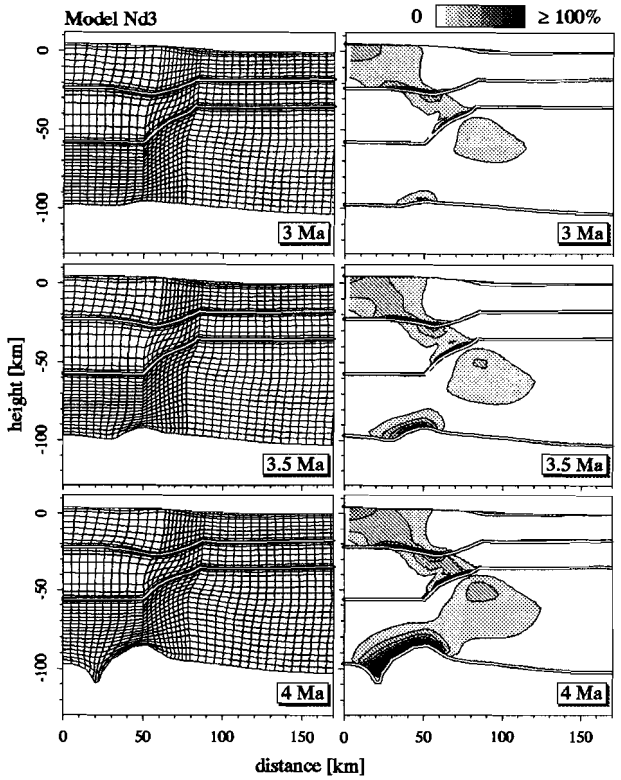

Fig. 22. *Evolution of finite element grid and contours of effective strain of viscous lower crust Model Nd3.*

Variations in pre-thickening parameters

Composition

Model Nd2 With Model Nd2 we investigate the influence of the upper crustal rheology on the style of deformation. A dry quartzite powerlaw creep flow law is adopted in the upper crust, and the upper crust is more viscous than in Model Nd1 ($Q_{pl} = 184.1$ kJ/mole, $A_{pl} = 2.20 \cdot 10^{-22}$ $Pa^{-2.8} \cdot s^{-1}$, $n_{pl} = 2.8$) (Jaoul *et al.*, 1984).

The evolution of the lithosphere model is slightly slower than in Model Nd1 (Figure 21), but the overall style of deformation is similar. The upper crust of the TCL is deformed less than in Model Nd1 and sinistral shear in the lower crust of the transition zone is more prominent. No lithosphere scale asymmetry evolves, however.

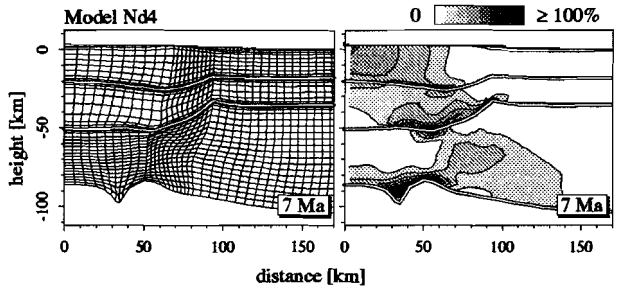

Fig. 23. *Model Nd4: compared to Model Nd1, the viscosity of the mantle in this model is significantly higher. Deformed model lithosphere and contours of effective strain after 7 Ma.*

Model Nd3 The viscosity of the lower crust is significantly higher in Model Nd3, compared to Model Nd1. The lower crust has a Pikwitonei granulite rheology ($Q_{pl}=445$ kJ/mole, $A_{pl}=7.68\cdot10^{-21}$ $Pa^{-4.2}\cdot s^{-1}$, $n_{pl}=4.2$) (Wilks and Carter, 1990).

Shedding of a lithospheric drip starts controlling the evolution of the TCL from 3.5 Ma onward (Figure 22). Compared to Model Ud3, Model Nd3 has extended more at the onset of the instability. This discrepancy is due to the high tensile pre-stresses in the crust in the depth-dependent pre-stress model. Since the crust is weak relative to the mantle, Model Nd3 therefore deforms more.

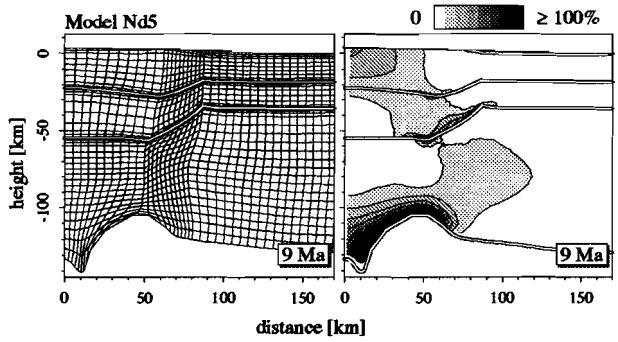

Fig. 24. *Finite element grid and contours of effective strain after 9 Ma of Model Nd5 which, initially, has a surface heat flow of 50* mW/m^2.

Model Nd4 The influence of mantle rheology is investigated in Model Nd4. Again, all parameters are identical to Model Nd1, except that a dry olivine flow law is adopted in the mantle ($Q_{pl}=510$ kJ/mole, $A_{pl}=7\cdot10^{-14}$ $Pa^{-3}\cdot s^{-1}$, $n_{pl}=3$) (Kirby, 1983).

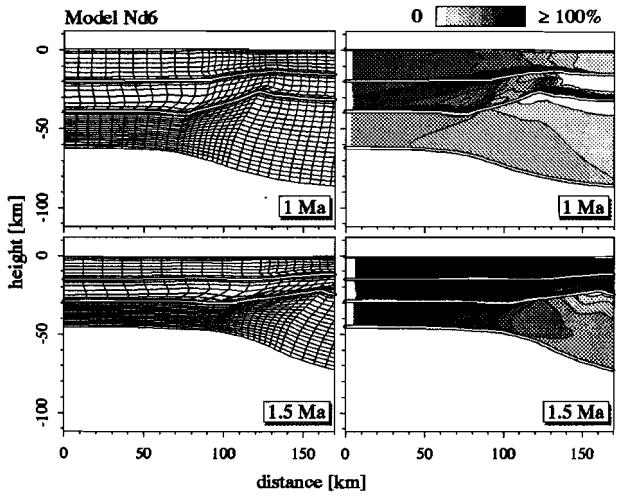

Fig. 25. *Evolution of Model Nd6. Compared to Model Nd1, the initial temperatures in this model are higher. The deformed finite element grid is displayed in the left column, the right column shows contours of effective strain.*

After 7 Ma, the lower TCL mantle destabilizes (Figure 23) when a mantle drip has formed. Like in the previous model, more extensional strain has occurred in the depth-dependent pre-stress model than in the uniform pre-stress model (c.f. Figure 8) at the onset of the drip.

Geotherm

Model Nd5 The initial temperatures of Model Nd5 are lower than in Model Nd1; before thickening the surface heat flow associated with the steady state geotherm is 50 mW/m^2.

The evolution of the cold lithosphere model is controlled by ongoing delamination processes (Figure 24). Compared to the uniform pre-stress Model Ud5, Model Nd5 is extended more and compressive pre-stresses in the TCL mantle of Model Nd5 delay the onset of the lithospheric drip.

Model Nd6 Model Nd6 has an initial surface heat flow of 70 mW/m^2 and, accordingly, the initial steady state geothermal gradient is significantly steeper than the geotherm of Model Nd1.

After 1.5 Ma, the TCL has extended by a factor greater than two (Figure 25). Strain contours in the upper and lower crust after 1 Ma indicate that the upper crust of the transition zone acts as a detachment level, along which lower crustal rocks

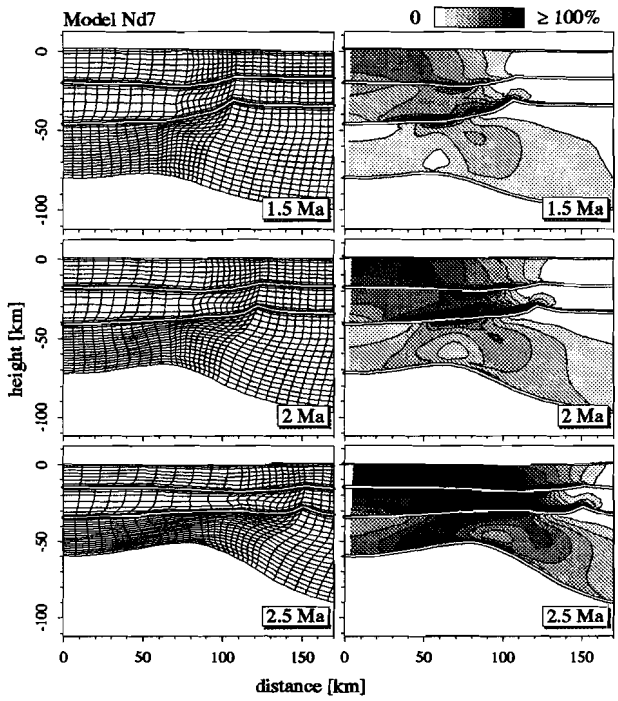

Fig. 26. *Extension following a 5 Ma thickening period and delamination. The left column displays the finite element grid of Model Nd7 and the right column shows contours of effective strain.*

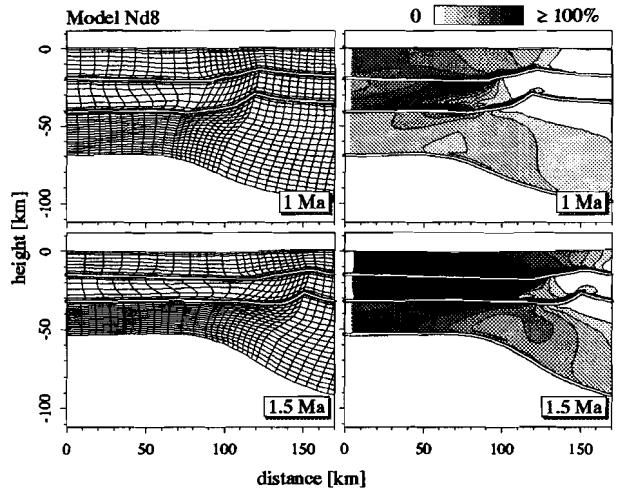

Fig. 27. *Model Nd8: extension after a 20 Ma thickening phase, followed by delamination of a part of the TCL mantle. The left column shows the deformed finite element grid and the right column contours of effective strain.*

are exhumed by sinistral normal shear. In the TCL mantle, the style of deformation is pure shear.

Variations in syn-thickening parameters

Finite thickening period

Model Nd7 In Model Nd7, thermal diffusion has occurred during the 5 Ma thickening period. For the rest, the model is identical to Model Nd1.

Thermal re-equilibration increases the rate of thinning of the TCL (Figure 26). The style of deformation, however, is hardly affected by the duration of the thickening period.

Model Nd8 The influence of an increase of the duration of the orogenic period to 20 Ma is studied in Model Nd8.

After 1.5 Ma, the average rate of extension of this model more than 3 cm/yr (Figure 27). Contours of strain after 1 Ma indicate asymmetrical deformation in the upper and lower crust. On the scale of the lithosphere however, the style of extension is symmetric.

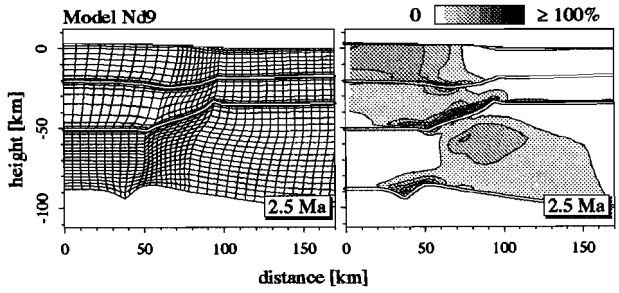

Fig. 28. *Uniform thickening Model Nd9: deformed model lithosphere and contours of effective strain after 2.5 Ma.*

Thickening geometry

Model Nd9 In Model Nd9, the lithosphere is thickened by uniform thickening of the crust and mantle by a factor of two.

After 2.5 Ma, a mantle droplet has formed in Model Nd9 (Figure 28). Like in previous cases where shedding of lithospheric droplets controls the evolution of the TCL, the depth-dependent pre-stress model extends more than the uniform pre-stress model.

Model Nd10 The width of the transition zone of Model Nd10 is 50 km, i.e. twice

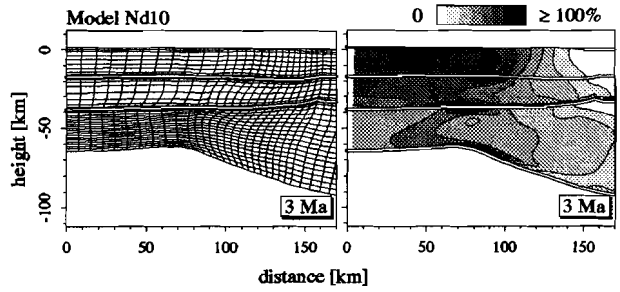

Fig. 29. *Deformed grid and contours of effective strain, 3 Ma after thickening has ended and delamination has occurred. The width of the transition zone of this model, Model Nd10, is twice as large as the transition zone width of Model Nd1.*

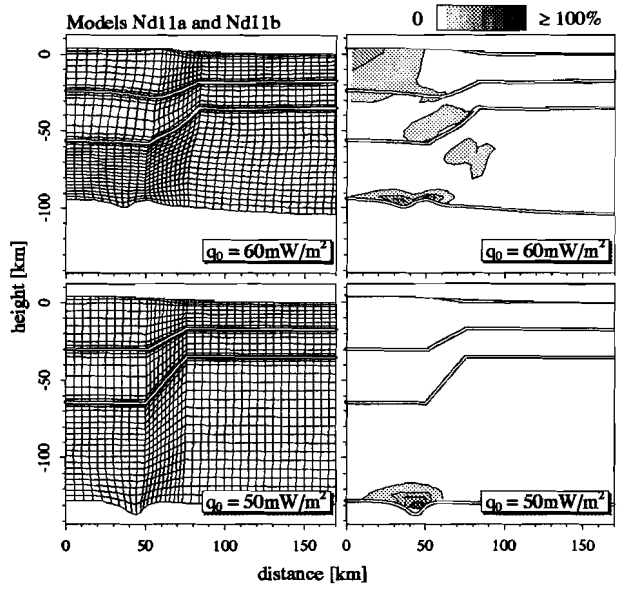

Fig. 30. *Gravity collapse models. Top row: finite element grid and strains after 4 Ma of Model Nd11a. The initial geothermal gradient of this model is identical to the geotherm of Model Nd1. Bottom row: finite element grid and strains after 4.5 Ma of "cold lithosphere" Model Nd11b.*

the transition zone width of Model Nd1.

Figure 29 shows the finite element grid and contours of effective strain, 3 Ma after delamination has occurred and the tensile end load started acting on the lithosphere. Deformation is clearly more uniform than in Model Nd1 and the style of

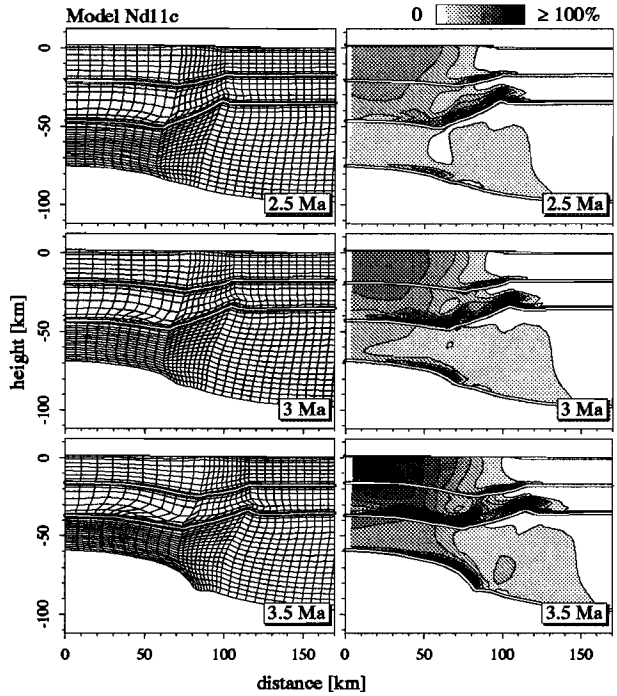

Fig. 31. *Evolution of the "hot lithosphere" gravity collapse Model Nd11c. The left column shows the finite element grid and the right column shows contours of effective strain.*

extension is well described by pure shear. An interesting discrepancy occurs with the uniform pre-stress model (Figure 14). A higher extension rate reduces the relative importance of processes occurring near the lithosphere-asthenosphere boundary.

Variations in post-delamination parameters

Gravitational collapse

Models Nd11 Gravitational collapse resulting from delamination and a drop to zero of the in-plane compressive load which caused thickening of the lithosphere, is modeled in Models Nd11a, Nd11b and Nd11c. The initial surface heat flow in these models is 60, 50 and 70 mW/m^2 respectively.

Figure 30 shows that the lower boundary of the "cold" models has destabilized and that the formation of mantle drips controls the evolution of the lithosphere.

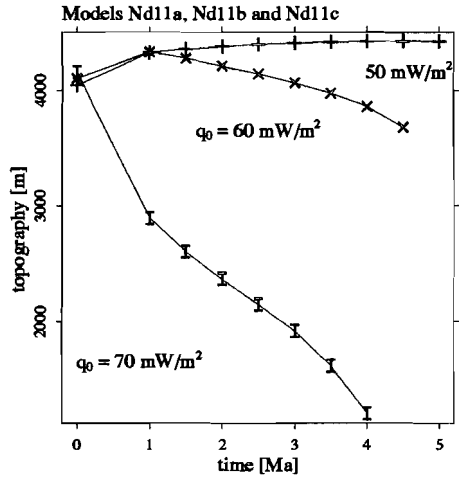

Fig. 32. *Net surface topography as function of time of the model symmetry center of gravity collapse Models Nd11a, Nd11b and Nd11c.*

Figure 31 shows that delamination of Model Nd11c, the "hot" model results in significant extension and thinning of the TCL. The style of extension of Model Nd11c initially is symmetric, but becomes more asymmetric after 3.5 Ma, when dextral normal shear zones in the upper crust, lower crust and mantle are on the verge of linking up into a lithosphere cutting system. The net surface topography of the symmetry centers of Models N11a, N11b and N11c are shown in Figure 32. Compared with the surface uplift signals of the uniform pre-stress models (Figure 16), the net surface topography of the depth-dependent pre-stress models is clearly different. A significant and somewhat surprising result of from the non-uniform pre-stress models is that delamination is not necessarily followed by surface uplift.

Magnitude of in-plane force

Model Nd12 The last model we consider is identical to Model Nd1, except that the magnitude of the in-plane force, which starts acting at $t = 0$, is twice as large, i.e. equivalent to an in-plane stress of 100 MPa which is distributed uniformly over the lithosphere thickness.

Figure 33 shows that the model lithosphere extends more rapidly than Model Nd1. After 1 Ma, sinistral shear in the lower crust of the transition zone is balanced by dextral shear in the conjugate zone which dips from the TCL underneath the RCL. Clearly, this conjugate zone is wider than the lower crustal shear zone. After 1.5 Ma, the style of deformation is symmetric.

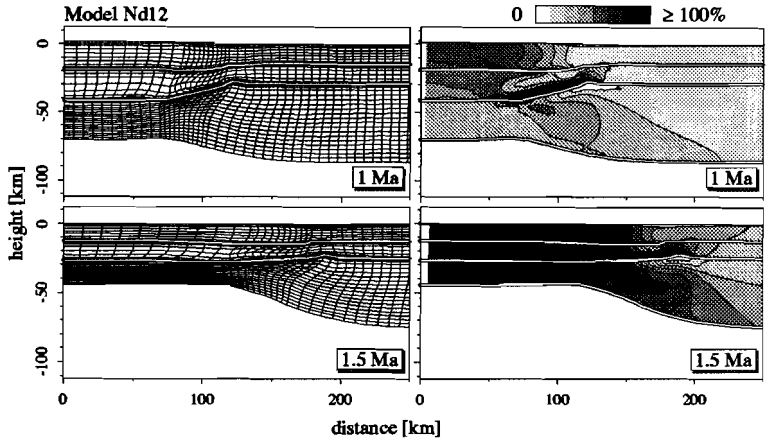

Fig. 33. *Evolution of Model Nd12. In this model, the magnitude of the in-plane end load is equivalent to an in-plane stress of 100 MPa magnitude, uniformly distributed over the thickness of the RCL, i.e.* $10.5 \cdot 10^{12}$ *N/m. Compared to Model Nd1, the in-plane force magnitude is therefore twice as large.*

DISCUSSION

In the delamination model we adopt (Figure 1) we make assumptions on the timing of delamination and on the geometry of the detached mantle. In our models, we assume that delamination occurs at the end of a mountain building phase, when in-plane forces switch from compressive to tensile. The numerical models of Houseman *et al.* (1981) show that the time at which detachment occurs depends on the intensity of mantle convection, and that detachment may occur between 0 and 100 Ma after the end of the collision phase. The motivation for investigating models in which detachment occurs immediately after thickening is that, based upon the results from chapter 5, delamination in a compressive in-plane stress field does not lead to asymmetrical extension. Since we concluded in chapter 3 of this thesis that symmetric extension is the normal deformational style of continental lithosphere, our aim is to identify the physical conditions at which the mode of deformation is asymmetric. The results of chapter 5 indicate that delamination of TCL mantle may be effective in initiating lithosphere scale faults if the in-plane compressive force has dropped to zero or has become tensile, i.e. if delamination occurs at or after the end of the collision phase. We did not investigate models in which there is a delay between the end of thickening and delamination. If the TCL extends very slowly after thinning, the effect of a delay in the onset of delamination on the style of extension after delamination will be small. If the TCL extends rapidly after thickening, and delamination has not yet occurred, delamination of the TCL

becomes less likely with time, since thinning of the TCL restores the stability of the TCL mantle.

The assumed geometry of the detachment is reflected in our models through the mechanical and thermal b.c.'s acting on the lower boundary of the remaining TCL. The more viscous and slow-deforming models appear to be sensitive to the exact nature of the boundary conditions and, therefore, to details of the delamination process itself. Mantle drips evolve in a number of these models, which will detach and sink into the asthenosphere as a result of their higher relative density. The onset of lithospheric drips is merely a transient stage in the process of convectively removing the whole TCL mantle. Once some part of the TCL mantle has been delaminated, the process is self-maintained through the destabilizing effect of asthenospheric temperatures to which the remaining mantle is exposed. The fact that transient stages of this delamination process are characterized by shedding of lithospheric drops might indicate that the complete process of delamination is controlled by droplets which fall from the TCL. Further work, based upon Eulerian techniques, is required to investigate whether the instantaneous delamination model we adopt in this chapter is an appropriate description of the underlying physical process. In such a study, it would be imperative to consider the effects of a deforming lithosphere, since deformation and thinning affects the asthenospheric flow through the time-dependent temperature boundary conditions it imposes. Finite element methods which are capable of solving the coupled thermo-mechanical equations for realistic rheologies in both the lithosphere and the asthenosphere are subjects of active research (e.g. Christensen, 1992).

CONCLUSIONS

In this chapter we have investigated the style of extension in continental lithosphere which has been subject to continental thickening, immediately followed by delamination. The end of continental thickening is signified by a drop in the in-plane end load to zero or a sign change of the in-plane force from compressive to tensile. If thickening pre-stresses are uniform with depth, an asymmetric style of extension may evolve. The style of extension is more symmetric if pre-stresses are a function of depth, based upon local pressure differences between TCL and RCL (Figure 6.2).

For the uniform pre-stress models, conditions which have a significant effect on the style of extension are;

(1) The in-plane end load. Asymmetric extension occurs if a tensile in-plane force equivalent to an in-plane stress of 50 MPa, uniformly distributed over the lithospheric thickness, is applies to the thickened lithosphere from $t=0$ onward. At smaller end load magnitudes, the relative significance of lower boundary de-

lamination processes increases at the expense of the amount of extension. At larger magnitudes, the asymmetry of extension slightly decreases.

(2) The viscosity of lower crust and mantle. At high viscosities of the lower crust and mantle, either as a result of composition and rheology or as a result of a low geothermal gradient, extension of the TCL is inhibited and the TCL mantle destabilizes.

(3) The thickening geometry. Tectonic thickening of the lithosphere leads to preferential thickening of the crust. In this case, initiation of a lithosphere scale fault is possible after delamination. If the continental lithosphere has been uniformly thickened, delamination destabilizes the TCL mantle and extension is limited. For a 25 km wide transition zone, a single lithosphere cutting fault initiates. If the transition zone is 50 km wide, asymmetric extension in the upper crust and the lower crust and mantle is uncoupled.

The style of deformation in the depth-dependent pre-stress models is more symmetric. This result is insensitive to any of the parameter variations we investigated. In models with a relatively weak upper crust, the style of deformation in the upper crust alone is asymmetric. Probably, in these cases, the surface geology will be dominated by normal faults dipping away from the TCL. In later stages of the extension, uniform pre-stress models and depth-dependent pre-stress models predict very distinct sedimentation patterns. The average extension rate of the lithosphere is significantly higher in the depth-dependent pre-stress models than in the uniform pre-stress models.

Delamination may result in uplifts on the order of 1 km and uplift rates on the order of 1 mm/yr. It is noteworthy, however, that uplift following delamination does not always occur and is a model-dependent feature.

REFERENCES

Braun, J., and C. Beaumont, Contrasting styles of lithospheric extension: implications for differences between Basin and Range Province and rifted continental margins, in *Extensional tectonics and stratigraphy of the North Atlantic Margins*, edited by A.J. Tankard and H.R. Balkwill, pp. 53-79, Am. Ass. Petr. Geol. Mem. 46, 1989.

Christensen, U.R., An Eulerian technique for thermomechanical modeling of lithospheric extension, *J. Geophys. Res., 97*, 2,015-2,036, 1992.

England, P., and G. Houseman, Extension during continental convergence, with application to the Tibetan Plateau, *J. Geophys. Res., 94*, 17,561-17,579, 1989.

England, P.C., and D.P. McKenzie, A thin viscous sheet model for continental deformation, *Geophys. J. R. astron. Soc., 70*, 295-321, 1982.

England, P., and P. Molnar, Surface uplift, uplift of rocks, and exhumation of rocks, *Geolo-*

gy, 18, 1,173-1,177, 1990.
Houseman, G.A., and P.C. England, A dynamical model of lithosphere extension and sedimentary basin formation, *J. Geophys. Res., 91,* 719-729, 1986.
Houseman, G.A., D.P. McKenzie, and P. Molnar, Convective instability of a thickened boundary layer and its relevance for the thermal evolution of continental convergent belts, *J. Geophys. Res., 86,* 6,115-6,132, 1981.
Jaoul, O., J. Tullis, and A. Kronenberg, The effect of varying water contents on the creep behavior of Heavitree quartzite, *J. Geophys. Res., 89,* 4,298-4,312, 1984.
Kirby, S.H., Rheology of the lithosphere, *Rev. Geophys. Space Phys., 21,* 1458-1487, 1983.
McKenzie, D.P., Active tectonics of the Alpine-Himalayan belt: the Aegean Sea and surrounding regions, *Geophys. J. R. astron. Soc., 55,* 217-254, 1978.
Platt, J.P., and R.L.M. Vissers, Extensional collapse of thickened continental lithosphere: a working hypothesis for the Alboran Sea and Gibraltar arc, *Geology, 17,* 540-543, 1989.
Sonder, L.J., P.C. England, B.P. Wernicke, and R.L. Christiansen, A physical model for Cenozoic extension of western North America, in *Continental extensional tectonics, 28,* edited by M.P. Coward, J.F. Dewey and P.L. Hancock, pp. 187-201, Geological Society of London Special Publication, 1987.
Turcotte, D.L., and G. Schubert, *Geodynamics: applications of continuum physics to geological problems,* 450 pp., John Wiley & Sons,, New York, 1982.
Wilks, K.R., and N.L. Carter, Rheology of some continental lower crustal rocks, *Tectonophysics, 182,* 57-77, 1990.

Chapter 8

Summary and conclusions

Much of the work on continental margins and sedimentary basins has been directed at quantifying parameters of the pure shear extension model (or stretching model) (McKenzie, 1978). This is surprising, since a sound physical basis of this kinematic model is lacking. Alternative kinematic models, like the simple shear model (Wernicke, 1981) have been proposed which, at least in some basins, explain the surface observations equally well. In terms of asymmetry, the pure shear model and the simple shear model represent end-members of a spectrum of kinematic models for continental extension (Figure 1). The central issue of this thesis is to determine -by numerical modeling- whether the pure shear model and the simple shear model are physically plausible and to gain insight in the physical conditions which control the style of extension.

In chapter 2 of this thesis we derive constraints on the magnitude of inplane stresses from focal depths of intraplate earthquakes. In this study, experimental results on the rheology of lithospheric rocks are used to relate observations of strain to stress. In fact, since the work we present focuses on aspects of the dynamics of continental extension, results derived from laboratory experiments on the rheology of rocks play a prominent role throughout this thesis. It is shown in chapter 2 that average intraplate stresses on the order of hundreds of MPa's in the Central Indian Ocean are consistent with seismicity observations. Observations of gravity highs and lows in this region have been attributed to 200-km wavelength undulations resulting from lithospheric buckling. High seismicity and buckling of the oceanic lithosphere indicate that intraplate stresses in the Central Indian Ocean are high compared to other oceanic plates. The results from chapter 2 are relevant for the numerical models we develop in subsequent chapters, since they put an upper limit on the magnitude of inplane forces which may be applied to finite element models of continental extension.

Extension of continental lithosphere which is laterally homogeneous is studied in chapter 3. Finite element models of the continental lithosphere are subject to inplane tensile end loads which may derive from plate boundary forces (e.g. slab pull and trench resistance) or body forces (e.g. ridge push and density moment distribu-

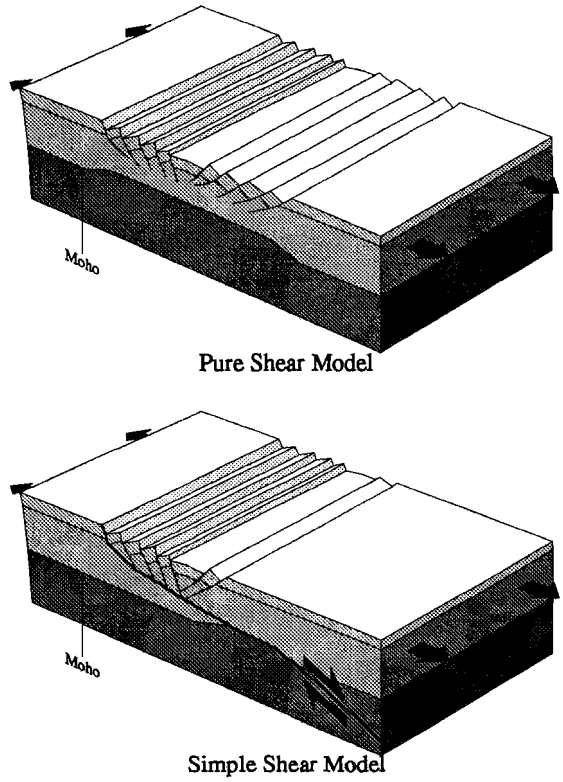

Fig. 1. Derivatives of the pure shear model and the simple shear model for describing the kinematics of extension. Both figures represent "realistic" versions of the original end-member extension models. Compared to the pure shear model *sensu stricto* (Figure 1 in chapter 1), the pure shear model in the top figure has some localized, non-coaxial deformation in the upper crust. The simple shear model in the bottom panel is more symmetric in the upper crust than the original model, (Figure 2 in chapter 1) as a result of conjugate faults which have developed.

tions). The influence of assuming different (non-rotative) distributions with depth of the end-load is tested. It is concluded that the total horizontal strain rate is uniform with depth at distances greater than 500 km from plate boundaries, independent of the assumed depth-dependence of the end load. This result, which was an assumption in the models of Kusznir (1982), is of fundamental importance in understanding the mechanisms that control the style of extension and, therefore, to subsequent chapters of this thesis. It means that extension by pure shear is the "na-

tural" response of continental lithosphere to inplane stresses, away from plate boundaries. Therefore, lithosphere-scale asymmetries in the style of extension have to be the result of either (1) lateral inhomogeneities within the continental lithosphere or (2) proximity of a plate boundary which imposes depth-dependent mechanical boundary conditions. Since lateral inhomogeneities in the continental lithosphere are well-established compared to the nature of plate boundary forces, we focus in this thesis on causes for asymmetric extension in interior parts of continental lithosphere.

Once lithosphere-scale faults have been formed, they tend to stay operative in subsequent tectonic phases. A low-angle detachment fault which is rooted in strong parts of the lithosphere will initiate an asymmetric style of extension if the mechanical boundary conditions allow the system to evolve this way. It is therefore interesting to investigate the conditions at which such faults might initiate in strong parts of the lithosphere. Pre-defined weaknesses might control the initiation of detachment faults, but there is no evidence that this is always so. Also, an explanation of detachment faults in terms of pre-defined weaknesses disregards the possible relation between a pre-extension thickening period and subsequent extension which has been found in the Basin and Range Province and in the Aegean Sea. Therefore, the work presented in chapters 4, 5, 6 and 7 aims at determining the physical conditions which control the onset of lithosphere scale asymmetries.

Two mechanisms have been proposed for initiation of lithosphere scale faults in continental lithosphere which, thermally and mechanically, is close to equilibrium, i.e. lithosphere which has not been subject to thermal and/or orogenic events for a long time. First, strain localization resulting from a strain softening has been put forward. The second mechanism involves boudinage of lithospheric layers which would lead to inhomogeneous deformation and asymmetric extension. These mechanisms are investigated in chapter 4 of this thesis and it is concluded that neither mechanism is relevant in the context of extension on the scale of the whole lithosphere. Mild deviations from lateral homogeneity are not sufficient to initiate lithosphere scale faults.

In chapter 5, we investigate various possible causes for asymmetric extension in lithosphere which is, or has recently been, subject to a tectonic and/or thermal event. We consider thickening of continental lithosphere, magma intrusions, mantle plumes and the hypothetical mechanism of delamination of the mantle of thickened continental lithosphere as possible causes for subsequent extension. We conclude that initiation of lithosphere cutting faults and asymmetric extension is possible after thickening. This result is consistent with observations of asymmetric extension in terrains that previously were subject to continental thickening, like the Basin and Range Province and the Aegean Sea. The predicted direction of dip also

agrees with observations in these areas. Mantle delamination is also found the be a feasible mechanism for asymmetric extension. Magma intrusions and mantle plumes result in a symmetric, pure-shear-like, style of extension.

The conclusions from chapter 5 motivated us to investigate the parameters which influence the style of extension following continental collision. In chapter 6 we investigate the influence of relevant parameters of this three-stage evolution, i.e. the pre-thickening period, the syn-thickening period and the post-thickening period. The physical mechanisms controlling the style of extension are identified in this chapter. It is concluded that the distribution of residual stresses (or pre-stresses) from the collision phase play a crucial role in determining the style of extension. Initiation of asymmetric extension is promoted by residual stresses which are distributed rather uniformly with depth. The rheology of the lower crust and mantle, the geothermal gradient, the amount of thickening of the mantle during the mountain building phase and the timing of onset of an inplane tensile force are concluded to control the style of extension if residual stresses are uniformly distributed with depth. If the residual stresses are modeled as function of depth, the rate of extension is higher and the style of deformation more symmetric. Lithosphere-cutting faults are predicted to evolve in case inplane forces have large magnitudes. In this single case, the predicted dip direction of the fault is opposite to the dip direction that was predicted for the uniform residual stress models. An interesting detail is that the sedimentation pattern appears to be sensitive to the distribution of residual stresses and could possibly be used to discriminate between uniform and non-uniform pre-stress models.

Based on the results of chapter 5, a more detailed investigation is presented in chapter 7 of the conditions which control the style of extension, assuming that delamination of the mantle of thickened continental lithosphere occurs. Residual stresses from the thickening phase are found to strongly influence the style of extension following delamination. Lithosphere-cutting faults and an asymmetric style of extension are initiated if pre-stresses are uniformly distributed with depth. If residual stresses from thickening are a function of depth, the style of extension is more symmetric.

Within the framework of our finite element models, we have shown in this thesis that lithosphere-scale asymmetries evolve under rather special conditions. The model results provide some basis for the inference from geological observations that lithosphere-scale asymmetric extension might have evolved from thickened continental lithosphere. More in general, specific geological observations may put constraints on conditions which have prevailed before the onset of continental extension. The modeling results we present in this thesis indicate which parameters or conditions are relevant for the style of continental extension. Reversely, the re-

sults of this thesis should be helpful in determining the type of observations that would put constraints on the physical conditions which are relevant in the context of continental extension. In present-day mountain belts, initiation of lithosphere scale asymmetries might be currently underway, and the results we present in this thesis provide a framework for interpretation of geological and geophysical observations in these areas.

REFERENCES

Kusznir, N.J., Lithosphere response to externally and internally derived stresses: a viscoelastic stress guide with amplification, *Geophys. J. R. astron. Soc., 70,* 399-414, 1982.

McKenzie, D.P., Some remarks on the development of sedimentary basins, *Earth Planet. Sci. Lett., 40,* 25-32, 1978a.

Wernicke, B., Low-angle normal faults in the Basin and Range Province: nappe tectonics in an extending orogen, *Nature, 291,* 645-648, 1981.

Samenvatting

De vorming van sedimentaire bekkens en passieve continentale marges is in veel gevallen het gevolg van extensie (uitrekking) van continentale lithosfeer. Het Noordzeebekken, de Rijnslenk en de Oost-Afrikaanse rift zone zijn voorbeelden van bekkens die door extensie zijn gevormd. Wanneer continentale lithosfeer sterk wordt opgerekt en verdund, breekt een continentale plaat doormidden en ontstaat een nieuwe oceaan.

Meer dan een decennium geleden werden twee modellen voorgesteld voor het proces van continentale extensie die nog steeds van groot belang zijn. Het eerste model werd in modelvorm geformuleerd door McKenzie (1978), en hierin werd aangenomen dat de coaxiale rek-deformatie uniform met de diepte verdeeld is (zie figuur 1 in hoofdstuk 1), d.w.z. net als een stuk kauwgum dat wordt uitgerekt. Dit zogenaamde "pure shear model" is daarom volledig symmetrisch om een verticale as. Het andere model werd voorgesteld door Wernicke (1981), waarin werd aangenomen dat de gehele lithosfeer doorsneden is door een vlak hellende breuk (figuur 2 in hoofstuk 1, zie ook figuur 1 in hoofdstuk 8). In dit zogenaamde "simple shear model" word extensie geaccomodeerd door schuifbeweging langs de breuk, waardoor de stijl van extensie sterk asymmetrisch is. Het belangrijkste nadeel van deze modellen was dat ze voornamelijk beschrijvend van aard waren en dat een grondige fysische onderbouwing vooralsnog uitbleef.

Veel (wetenschappelijke) energie is sinds het verschijnen van deze publicaties gestoken in het beschrijven van verschillende extensiegebieden in termen van het pure shear model of het simple shear model. Het bleek dat, voor zover dit op basis van observaties aan het oppervlak bepaald kon worden, het pure shear model een goede beschrijving was van de deformatie onder sommige sedimentaire bekkens en passieve marges, terwijl het simple shear model een goede beschrijving was onder andere bekkens en passieve marges. Relatief weinig aandacht werd tot nu toe besteed aan de vraag wat de fysische condities zijn die leiden tot ofwel grootschalige pure shear extensie ofwel simple shear extensie op de schaal van de hele lithosfeer. Het is met name dit aspect dat wordt belicht in mijn onderzoek naar lithosfeerdeformatie in de context van de vorming en evolutie van sedimentaire bekkens en passieve marges.

In dit proefschrift wordt uitgegaan van krachten die op continentale lithosfeer werken om, via de materiaaleigenschappen van de gesteenten waaruit de lithosfeer

is opgebouwd, de deformatie van de lithosfeer af te leiden. In hoofdstuk 2 bepalen we een bovengrens voor de aan te leggen krachten, door uit de seismiciteit in de Indo-Australische plaat de magnitudes van de aldaar heersende spanningen af te leiden. Uit observaties van hoge seismiciteit en van golvingen in de oceanische lithosfeer werd eerder afgeleid dat de spanningen in deze plaat hoog zijn vergeleken met andere oceanische gebieden. De resultaten van dit onderzoek tonen tevens aan dat de hoge spanningsmagnitudes in de Indische plaat, zoals die uit een modelstudie gevonden werden door Cloetingh en Wortel (1985), compatibel zijn met seismische observaties.

Met behulp van een eindige-elementen methode wordt de thermische en mechanische evolutie van continentale lithosfeer kwantitatief onderzocht. Hierbij worden het sterk niet-lineaire gedrag van elastische/ductiele/brosse gesteenten en de temperatuur- en drukafhankelijkheid van de materiaaleigenschappen geincorporeerd. Hoofdstuk 3 is een bondig overzicht van de belangrijkste vergelijkingen. Hier wordt uitgebreid ingegaan op details die specifiek zijn voor de modellering in de context van lithosfeerdeformatie. In dit hoofdstuk wordt geconcludeerd dat, op horizontale afstanden groter dan 500 km van plaatgrenzen, horizontale strain rates uniform met de diepte zijn. Dit resultaat is van fundamenteel belang voor het inzicht in extensieprocessen, omdat het aangeeft dat het pure shear model de "natuurlijke" wijze van extensie van continentale lithosfeer is. De implicatie is dat lithosfeer-doorsnijdende breuken en asymmetrische extensie onder relatief speciale fysische condities zouden moeten ontstaan.

Deze ideeën worden nader uitgewerkt in hoofdstuk 4, waarin wordt onderzocht of extensie van stabiele lithosfeer kan leiden tot initiatie van lithosfeerdoorsnijdende breuken en grootschalige asymmetrie. Het is bekend dat, wanneer zich reeds grootschalige zwaktezones in de lithosfeer bevinden, deze aanleiding kunnen zijn tot localisatie van de deformatie en asymmetrische extensie. In dit proefschrift worden daarom de fysische condities onderzocht die leiden tot initiatie van grootschalige zwaktezones (breuken), op de eerste plaats omdat uit geologische evidentie blijkt dat dit soort structuren niet altijd op mechanische discontinuiteiten ontstaan. Een andere reden om geen aandacht te besteden aan de invloed van reeds bestaande zwaktezones is dat er een relatie is gesuggereerd in de literatuur tussen gebergtevorming en de daarop volgende grootschalige asymmetrische extensie. Deze relatie suggereert een verband tussen de mechanische en thermische randvoorwaarden die worden geïnduceerd door gebergtevorming en de stijl van extensie en niet zozeer een verband met reeds bestaande zwaktezones.

In de literatuur worden twee mechanismen aangedragen voor initiatie van asymmetrische extensie in stabiele lithosfeer, n.l. boudinage van de korst en lithosferische mantel en localisatie van deformatie als gevolg van strain softening. Van bei-

de mechanismen wordt geconcludeerd dat ze niet effectief zijn in het initiëren van grootschalige breuken en asymmetrische extensie. De conclusie van hoofdstuk 4 is daarom dat grootschalige asymmetrische extensie niet zal beginnen in stabiele lithosfeer zonder reeds bestaande zwaktezones.

In hoofdstuk 5 van dit proefschrift wordt onderzocht of grootschalige asymmetrische extensie het gevolg kan zijn gebergtevorming, intrusies, mantel*plumes* of van delaminatie van de continentale mantel. Uit de resultaten volgt dat indien intraplaat-extensie direct volgt op een continentale verdikkingsfase, initiatie van lithosfeer-doorsnijdende breuken mogelijk is. Dit resultaat is in overeenstemming met observaties in het Egeïsch gebied (Griekenland) en de Basin and Range Province in de westelijke Verenigde Staten, waar grootschalige asymmetrische extensie voorafgegaan werd door gebergtevorming. Ook is de voorspelde hellingsrichting van het breukvlak in overeenstemming met de waarnemingen in deze gebieden. Deze bevindingen zijn echter afhankelijk van de wijze waarop voorspanningen -veroorzaakt door de verdikkingsfase- met de diepte verdeeld zijn. Een meer symmetrische stijl van extensie volgt na intrusie van asthenosferisch magma in continentale lithosfeer waarop rekspanningen aangelegd zijn. Het effect van mantel*plumes* is dat de lithosfeer op een symmetrische wijze uitrekt en verdund wordt. Delaminatie van de continentale mantel kan leiden tot grootschalige asymmetrische extensie, afhankelijk van het moment waarop delaminatie optreedt.

In de hoofdstukken 6 en 7 worden de modelparameters nader onderzocht waarvoor respectievelijk het continentale verdikkingsmechanisme en het delaminatiemechanisme voor asymmetrische extensie gevoelig zijn.

Binnen het kader van de numerieke modellen is in dit proefschrift aangetoond dat asymmetrische extensie optreedt onder redelijk specifieke fysische condities. De modelresultaten ondersteunen de gevolgtrekking uit geologische observaties dat lithosfeer-doorsnijdende breuken en asymmetrische extensie het gevolg zouden kunnen zijn van een eerdere verdikkingsfase. Meer in het algemeen kunnen bepaalde geologische observaties een indicatie geven voor de condities die geheerst hebben voordat continentale extensie optrad. De modelresultaten gepresenteerd in dit proefschrift geven aan welke parameters of condities relevant zijn voor de stijl van extensie. Omgekeerd zouden de resultaten van de modelstudies een leidraad kunnen vormen voor het type waarnemingen dat noodzakelijk is om de fysische condities tijdens extensie af te bakenen. Mogelijkerwijs is het proces van initiatie van lithosfeer-doorsnijdende breuken op het moment gaande in verschillende gebergtegordels en kunnen geologische en geofysische waarnemingen in deze gebieden beter worden begrepen tegen de achtergrond van de modellen uit dit proefschrift.

Acknowledgements/Dankbetuiging

Ik wil iedereen bedanken die op de een of andere manier heeft bijgedragen tot het tot stand komen van voorliggend proefschrift.

Mijn dank gaat in het bijzonder uit naar mijn eerste promotor en begeleider Rinus Wortel. Het was voor mij een voorrecht te mogen samenwerken met een van de meest innovatieve tectonofysici in Europa, die zijn grote kennis van het vakgebied paart aan inzicht in de relevante fysische processen. Ondanks zijn hoge werkbelasting wist Rinus op cruciale momenten steeds tijd voor me vrij te maken. Zijn plezierige manier in de omgang heeft onze samenwerking steeds op een positieve manier beinvloed.

Prof. Dr. N.J. Vlaar wil ik bedanken dat hij mij in de gelegenheid stelde het onderzoek te verrichten dat leidde tot dit proefschrift.

During the initial stages of the research, Kevin Furlong has had a great influence on the development of ideas that form the basis of this thesis.

Jay Melosh of the Lunar and Planetary Lab and Department of Geosciences in Tucson, Arizona, is gratefully acknowledged for sharing his mechanical finite element code, TECTON.

Het was bijzonder plezierig Maarten Remkes als kamergenoot te hebben. Zijn positieve en collegiale houding en nimmer aflatende bereidheid om problemen met betrekking tot de computers te verhelpen, hebben bijgedragen tot het feit dat ik terug kan zien op een prettige tijd bij de vakgroep.

Met name wil ik ook mijn collega's Paul Meijer en Bert Vermeerssen bedanken voor de vele discussies over geologie en geofysica. Marc de Jonge en Wim Spakman hebben de grafische faciliteiten toegankelijk gemaakt zonder welke dit proefschrift er absoluut anders uit zou hebben gezien.

In Chris Spiers heb ik gewaardeerd dat hij een fysische benadering van rheologische problemen combineerde met een positieve en kritische houding in de discussies die we hadden. Reinoud Vissers wil ik bedanken voor zijn enthousiaste benadering van mijn onderzoek en interessante discussies.

The finite element work reflected in this thesis has benefitted from fruitful discussions with Charles Williams.

This research was funded by AWON, the Earth Science branch of the Netherlands Organization for Scientific Research (NWO), project AWON-NWO 751.345.017.

Curriculum Vitae

June 10 1961	Born in Tilburg, The Netherlands.
September 1 1973 - May 30 1979	Atheneum B, Paulus Lyceum in Tilburg, The Netherlands.
September 1 1979 - September 20 1982	Kandidaatsexamen G4 (B.Sc. Geology with physics and mathematics).
May 30 1988	Doctoraal examen (M.Sc.) Geophysics.
June 1 1988 - April 15 1993	Research assistant at the Department of Geophysics, Utrecht University, The Netherlands.
April 16 1993 -	Post-doctoral researcher at the Department of Geophysics, Utrecht University, The Netherlands.